Form and Function:
An Ontogenetic Study of Adaptive Responses in Human Pelvic Morphology

by

Marla MacKinnon

B.A. (Honours), Queen's University, Canada, 2012
M.Sc., University College London, UK, 2013

A Dissertation Submitted in Partial Fulfillment of the
Requirements for the Degree of

DOCTOR OF PHILOSOPHY

in the Department of Anthropology

University of Victoria

We acknowledge and respect the Lək̓ʷəŋən peoples on whose traditional territory the university stands and the Songhees, Esquimalt, and W̱SÁNEĆ peoples whose historical relationships with the land continue to this day.

Form and Function:
An Ontogenetic Study of Adaptive Responses in Human Pelvic Morphology

by

Marla MacKinnon

B.A. (Honours), Queen's University, Canada, 2012
M.Sc., University College London, UK, 2013

Supervisory Committee

Dr. Helen Kurki, Supervisor
Department of Anthropology

Dr. Yin-Man Lam, Departmental Member
Department of Anthropology

Dr. Alison Murray, Departmental Member
Department of Anthropology

Dr. Lesley Harrington, Outside Member
Department of Anthropology, University of Alberta

Abstract

Human pelvic morphology has often been described in terms of an evolutionary compromise between bipedalism, encephalization, and obstetrics, however recent research has argued that the pelvis is more biologically plastic than previously thought. Variation in pelvic form exists among adult populations, but the factors influencing this variation, and when it manifests during growth, remain to be understood. The aim of this study is to investigate patterns of growth and development of the pelvis, and to consider how ecological factors, including activity, may affect this growth. Pelvic morphology was examined using a geometric morphometrics approach in an ontogenetic sample of pelvic bones from four forager populations, two of whom pursued terrestrial foraging strategies (Later Stone Age southern Africa, Indian Knoll) and two of whom pursued marine foraging strategies (Point Hope, Sadlermiut) (juvenile n=169; adult n=88). Principal components analysis shows population-based patterning in ilium morphology from birth, but a similar pattern is not apparent in the ischium. This may imply a greater degree of adaptive response in the ilium to environmental stimuli or may reflect body shape differences. Age-related changes appear to be the most prominent source of variation in ischium morphology. Cross-sectional geometric (CSG) measures of long bones (humerus, femur, and tibia), representing habitual activity patterns, were used to examine the impact of loading on pelvic morphology. No relationship was found between pelvic shape and CSG measures, suggesting that pelvic morphology is not influenced by habitual behaviours. As has been hypothesized for epiphyseal morphology, it may be that the functional significance of the pelvis has led to a form that is more canalized and less plastic than the cross-sectional parameters of long bones. Instead, it seems that group differences, which may be driven by climate-related directional selection or neutral evolutionary processes (or, most likely, a combination thereof), as well as ontogenetic allometry, are the strongest drivers of morphological variation in the ilium and the ischium during growth.

Table of Contents

List of Tables

List of Figures

Acknowledgements

I've often heard it said that it takes a lot of "brains" to complete a PhD, but I've learned throughout the course of this degree that what it actually takes is a lot of self-motivation and a staunch commitment to ~~science~~ the sunk cost fallacy. But in all seriousness, what it also takes is a strong support network, and I can say with confidence that I have got the best. First and foremost, I have to thank my supervisor, Dr. Helen Kurki, whose unwavering encouragement and enthusiasm has left me feeling supported and valued from day one of this degree. She has an incredible knack for tactfully helping turn bad ideas into good ones, and her genuine passion for learning is infectious. She is compassionate and caring, knows just how to provide the right motivation to get the job done, and is the best mentor I could have hoped for.

I've also been very fortunate to be surrounded by a supportive and thoughtful committee, and I'm grateful for the many conversations (about anthropology and not about anthropology) that I've had with Drs. Alison Murray, Lesley Harrington, and Yin-Man Lam over the past several years. Thanks are due as well to Dr. Libby Cowgill for being collaboratively minded and sharing data that contributed to some of the analyses in this thesis. I am grateful to Dr. Jeremy DeSilva for serving as my external examiner, and for the thoughtful comments and questions he brought up at my defence. Other members of the PhASE lab (Dr. Ammie Kalan, Dr. Sarah-Louise Decrausaz, Dr. Stephanie Calce, Rae Dias) have also been a constant source of social, emotional, and academic support, and I am grateful to have had the opportunity to practice conference presentations, discuss departmental drama, and everything in between with them.

A portion of this degree was undertaken during the pandemic, and I am grateful in particular to my friends of "The Whingeing Corner" (Mark, Anu, Sarah-Louise, Kyle) for being there to tackle this unprecedented global event together – sometimes remotely, sometimes physically, but always with good humour, witty insights, and a significant helping of dumb memes. I'm also grateful to my parents, family, and friends both near and far for always being up for a laugh or a cry (or sometimes both), and for not asking too many questions about my thesis topic or when I'm going to be finished grad school.

This research is based on the study of human skeletal remains, and as such I would like to thank the curators who care for the remains at the Canadian Museum of History (Gatineau), the American Museum of Natural History (New York), the University of Kentucky (Lexington), the

Albany Museum (Grahamstown), the Iziko South African Museum (Cape Town), the McGregor Museum (Kimberley), the National Museum Bloemfontein (Bloemfontein), the University of Cape Town (Cape Town), as well as the Inuit Heritage Trust. I feel very privileged to have been able to work with these collections.

I need to thank the Department of Anthropology at UVic, the Social Sciences and Humanities Research Council of Canada, the Natural Sciences and Engineering Research Council of Canada, and Drs. Helen Kurki, Lesley Harrington, and Alison Murray once again for providing various avenues of funding that have supported me throughout this degree. I also need to thank Jindra Bélanger, Cathy Rzeplinski, and Kay del Sol of the Anthropology main office for all the assistance they have given not just to me, but to all the members of our department, over the years. They truly keep our department functional and have been so welcoming and generous with their time.

Last, but certainly not least, I have to thank my partner, Stephen. He has supported me throughout the entirety of this degree and continues to be the cheerleader I didn't know I needed. I believe the acknowledgements of my Master's thesis ended by thanking Stephen for his stats help, and I would be remiss if I didn't do the same here, and also add in a thanks for the R help – a lot of the analyses in this thesis wouldn't have been possible without his programming knowledge, and I'm grateful for his patience and understanding as he helped me figure out how to make R do what I needed. This thesis truly couldn't have been completed without him!

I never thought I would be someone who took seven (and a bit) years to complete a PhD, but despite the amount of time it's taken I am very grateful for the people I've met and the lessons I've learned in this time. A lot of unexpected circumstances emerged during this period (looking at you, COVID-19), but I'm thankful that the extended time allowed me to strengthen the relationships I've made along the way. It feels important to reiterate the significant impact my strong support network has had throughout this degree, so thank you again to everyone who has been a part of this journey with me.

CHAPTER 1: INTRODUCTION

The human pelvis exhibits unique features both in form and function compared with those of other primates. Pelvic morphology has long been thought to be the product of an evolutionary trade-off between obligate bipedalism and encephalization, resulting in secondarily altricial neonates and a difficult childbirth process because of the so-called "obstetrical dilemma" (Washburn, 1960). More recently, however, researchers have shown that the pelvis is under a wider range of selective pressures than previously thought, and that ecological factors and biological plasticity likely play significant roles in the development of pelvic morphology (Wells *et al.,* 2012; Wells, 2015). Ecological and cultural attributes of foraging populations, such as diet, activity, and disease ecology, influence growth trajectories of the skeleton, and thereby affect overall bone morphology. Further, the pelvis does not appear to be more tightly constrained in terms of morphological variation in comparison to the rest of the skeleton, and actually appears highly evolvable (Betti *et al.*, 2014; Grabowski *et al.,* 2011; Kurki, 2013b; Kurki & Decrausaz, 2016). This is not to say that the human childbirth process is not difficult, or that encephalization and locomotion are not important drivers of morphological change, but that a purely selection-based explanation fails to account for the range of factors affecting pelvic morphology.

The aim of this research, therefore, is to analyse patterns of growth and development of the human bony pelvis, and to investigate how ecological factors may affect this growth. Activity patterns and foraging strategy, specifically, will be the main factors examined, with climate and latitude included as considerations. Previous research has shown that variation in pelvic form exists between populations (Betti, 2017; Kurki, 2013a), but the factors generating

this variation remain to be understood. An ontogenetic perspective can shed light on the processes that generate these patterns of morphological variation seen in adults, as well as provide information about the appearance of morphological details that may be correlated with certain early-life activities (e.g., the onset of walking, beginning of foraging activities).

Broadly, this project addresses three main research questions: (1) *What patterns of inter- and intra-population variation in pelvic growth are apparent in archaeological skeletal remains of forager populations?* (2) *When during development do these patterns appear?* and (3) *What are the ecological and cultural factors that contribute to this variation?* To answer these questions, skeletal remains from four mid- to late-Holocene forager populations were examined: Later Stone Age (LSA) foragers from southern Africa, semi-sedentary foragers from Indian Knoll in Kentucky, foragers from Point Hope in Alaska, and the Sadlermiut foragers from Tunermiut, Southampton Island in Nunavut. Both the LSA and Indian Knoll foragers pursued a terrestrial-based mode of subsistence, while the Point Hope and Sadlermiut foragers frequently exploited marine resources from open waters and are thus considered to have had a marine-based mode of subsistence. Foragers, despite their widely variable cultural features and food-procurement strategies (Kelly, 2013), typically lead highly mobile lives and thus leave more obvious markers of activity on their skeletons than sedentary populations; the prominence of these skeletal markers of activity, therefore, make foraging populations ideal candidates for observations of skeletal variation.

To consider the first two questions posed above, a geometric morphometrics analysis was used to examine pelvic shape variation both within and between the study samples; inclusion of age and size data contributed ontogenetic context to the results. The third question was addressed through examination of biomechanical signatures of habitual behaviours, both between groups to

compare sample-wide patterns of activity and in relation to the results of the analyses of pelvic shape variation. Along with contextual details derived from the archaeological record, these analyses provided insight into the influence of ecological factors (including activity and physical environment) on pelvic shape and morphological variation throughout ontogeny.

The second chapter of this dissertation will outline and review published literature relevant to these research aims, and chapters 3 and 4 will discuss the materials and methods of the study. Chapters 5 and 6 provide the results and are organized by bone, detailing results related to the ilium and the ischium, respectively. Chapter 7 then synthesizes the results into a discussion of significant findings and provides conclusions.

CHAPTER 2: LITERATURE REVIEW

2.1 Pelvic Form and Growth

The pelvic girdle is comprised of four bones: the right and left os coxae, the sacrum, and the coccyx. Each os coxa is made up of three separate bones at birth (the ilium, ischium, and pubis) which fuse to form one single bone between the ages of 11-15 years in females and 14-17 years in males (Scheuer & Black, 2000). The left and right os coxae articulate anteriorly with each other at the pubic symphysis and articulate posteriorly with the sacrum at the sacroiliac joints. The individual elements (and the pelvis as a whole) undergo complex growth processes, beginning in utero and only reaching completion in early adulthood. The pelvic girdle serves the primary function of transferring weight from the upper body to the lower body during both standing and locomotion and forms the bony portion of the birth canal in females (Verbruggen & Nowlan, 2017). A number of muscles and ligaments originate on and insert into the pelvis, contributing to its role as the stabilizing core of the skeleton. The functional significance of the pelvis means that structural integrity of the os coxae is important (Verbruggen & Nowlan, 2017). Complex growth processes of the os coxae are therefore key to shaping the morphology of the pelvis and forming this essential structure.

In utero, cartilaginous precursors of the bony pelvis begin to develop between 6 and 7 weeks and are complete by 3 months (Adair, 1918; O'Rahilly & Gardner, 1975; Verbruggen & Nowlan, 2017). Ilium ossification then begins at 2-3 months in utero, ischium ossification at 4-5 months, and pubis ossification at 6-8 months (Laurenson, 1964; Scheuer & Black, 2000; Verbruggen & Nowlan, 2017). As a result, primary ossification centres for the ilium, ischium and pubis (Figure 2.1) are already well developed at birth. From birth to three months of age the

morphology does not change drastically, but size increases quickly. Growth of the pelvic bones slows after three months, and then again at three years. This slow pace of growth is maintained until the adolescent growth spurt when secondary sex characteristics begin to manifest. At birth, the crest of the ilium demonstrates the S-shaped curve that is maintained throughout life, but the concavities/convexities of the iliac surfaces do not fully develop until approximately 2 years of age when walking becomes the primary mode of locomotion and muscle levers act more strongly on the bones (Scheuer & Black, 2000). Secondary ossification centres appear at a number of locations on the three bones within the first few years of life, including in the triradiate cartilage at the junction of the ilium, ischium, and pubis (Scheuer & Black, 2000). The presence of this multi-flanged cartilaginous centre allows for the acetabulum to expand in accordance with the growth of the femoral head.

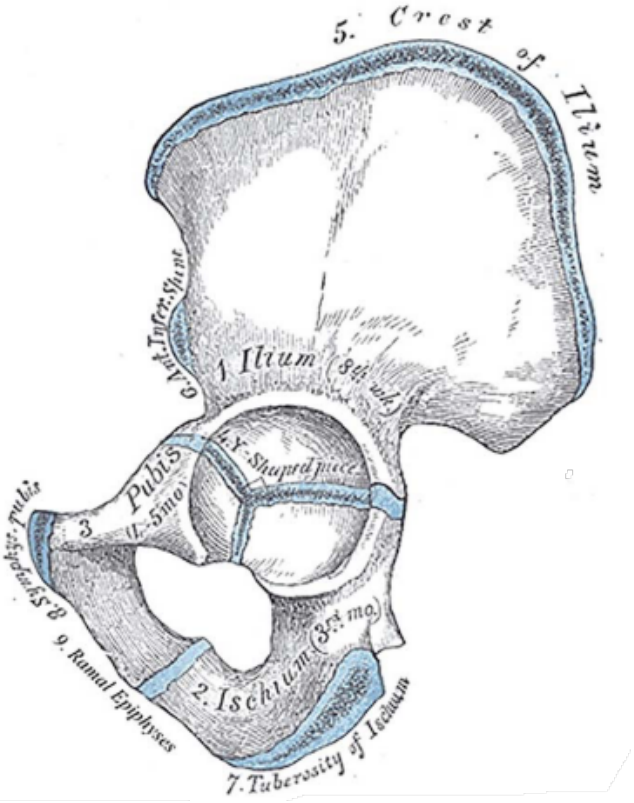

Figure 2.1 Primary (grey) and secondary (blue) ossification centres of the (1) ilium, (2) ischium, and (3) pubis. Adapted from Gray (1918) in Verbruggen & Nowlan (2017).

During growth, the most notable shape changes of the os coxa occur at the acetabulum. By 6 months of age, the ventral rim of the acetabular surface of the ilium becomes demarcated by the development of the iliopectineal line, the angle of the ischium becomes more prominent, and the pubis develops raised articular surfaces for the ilium and ischium (Verbruggen & Nowlan, 2017). By 4 to 5 years of age, the non-articular portion of the acetabular fossa has begun to develop, and by 6 years of age the sites of articulation for the pubis and ischium on the ilium have become pronounced (Verbruggen & Nowlan, 2017). Three main epiphyses form within the acetabular region, appearing between 9-14 years of age. A variable number of additional bony centres develop within the triradiate cartilage during this time, with fusion of the acetabulum reaching completion between the ages of 11-14 years in females and 14-17 years in males (Scheuer & Black, 2000).

Secondary ossification centres of the os coxae continue to develop and ossify throughout the period of adolescence and early adulthood. The last two epiphyses to fuse are the ramal portion of the ischium and the iliac crest of the ilium, with complete fusion occurring between 20-23 years of age. Throughout adulthood, features of the pubic symphysis and pubis region continue to undergo somewhat regular metamorphic changes (Scheuer & Black, 2000; Brooks & Suchey, 1990).

The pelvis is said to be the most reliably and obviously sexually dimorphic area of the human skeleton and is the preferred element to use when estimating sex from skeletal remains (Bass, 1995; Phenice, 1969; Ubelaker & Volk, 2001). Although sexual dimorphism of the pelvis may exist from an early age (Estévez *et al.,* 2017; Wilson & Humphrey, 2017), currently available methods and techniques can thus far only consistently identify sex-based differences in individuals who have undergone the adolescent pubertal growth spurt (Cardoso & Saunders,

2008; Corron, *et al.,* 2021; Klales & Burns, 2017; WEA, 1980). The main driver of sexual dimorphism in the pelvis is thought to be that the female pelvis facilitates parturition, while the male pelvis does not (Tague, 1992). This important functional difference between sexes means that the female pelvis is typically broader, with a wider sciatic notch, a wider subpubic angle, an elongated pubis, and a more rounded pelvic inlet (Bass, 1995; Phenice, 1969; Ubelaker & Volk, 2001). Dimorphic growth of the pelvis that occurs during the adolescent period is typically concentrated at the areas of the pelvis that relate to the size of the birth canal, namely the pubic length, lower iliac height, and pelvic diameter (Wood & Chamberlain, 1986).

2.2 Archaeological Studies of Growth and Development

The last two decades have seen an upsurge of interest in the study of juvenile human skeletal remains. In the past it was often the case that biological anthropologists were not interested in juvenile studies (Saunders, 2008), or, on the part of certain archaeologists, human remains in general. Becker (2006) writes that "today, no reputable scholar would trample, ignore, or throw away human remains found within tombs, which was an acceptable approach when I began work in Greece and Italy" (p.655). Although this would not be considered appropriate archaeological practice anymore, years of disinterest in juvenile studies impacts the information that anthropologists and archaeologists have to work with today. Many scholars are now bringing studies of childhood and juvenile osteology to the foreground (e.g., Beaumont *et al.,* 2020; Hillson, 2009; Lewis, 2007; Mays *et al.,* 2017; Nowell, 2021; Scheuer & Black, 2000), but the fact remains that well-preserved collections with a significant representation of juvenile individuals are often difficult to come by. Taphonomic processes, such as variability in burial practices and diagenesis, can have particular effects on the preservation of juvenile skeletal

remains and thus also affect their representation within the archaeological record. Furthermore, the delicate state of these bones means they are more susceptible to crushing by pressure from overlying sediments and can also be impacted by the pH of other decomposing organic matter in the ground (Guy *et al.*, 1997). It has been proposed that high levels of collagen present in the bones of neonates actually make for better preservation in comparison with the bones of older infants (Scott, 1999), but overall, projected population statistics of past peoples (which almost always include high infant mortality rates) frequently do not match what is recovered archaeologically.

To study growth and development in both the past and present, biological anthropologists have employed longitudinal studies, which examine growth patterns of living individuals over time, and cross-sectional studies, which look at general trends within or between populations by examining skeletal remains or living participants at a single point in time. Longitudinal studies (e.g., Denver Longitudinal Growth Study – McCammon, 1970) allow actual growth patterns of individuals to be monitored and can therefore capture information on variability in growth rate and velocity, including the adolescent growth spurt (Hoppa & FitzGerald, 1999); individual variation is emphasized, and the potential exists to correlate early life causes with later life effects (Garn & Shamir, 1958).

Longitudinal studies are not available when studying past populations, and thus cross-sectional studies are the only method available to biological anthropologists analysing human skeletal remains. Cross-sectional studies report on the averages of variation among individuals and consequently mute certain patterns – such as the adolescent growth spurt – since these kinds of studies cannot account for the velocity of changes during growth (Humphrey, 1998). As a result, data from longitudinal studies are frequently used as comparative frameworks for cross-

sectional studies (e.g., Gooderham *et al.,* 2019; Pfeiffer & Harrington, 2010; Symchych, 2016). It is important to note that the use of longitudinal data from WEIRD (Western, educated, industrialized, rich, and democratic) populations as baseline comparative samples can be problematic, since there is no universal standard for healthy growth and the growth trajectories of WEIRD populations frequently do not align with those of non-WEIRD populations (Hruschka, 2021). Nevertheless, longitudinal data can provide meaningful comparative context and it can be important to consider what differences in growth trajectories may mean. For example, it seems that early-life growth may be more indicative of environmental influences, while the adolescent growth spurt may be fuelled more by genetic mechanisms (Frisancho *et al.,* 1980; Ruff *et al.,* 2013; WHO, 1999); differences in growth trajectories of non-WEIRD samples compared to WEIRD samples could indicate different things at different points during growth.

Cross-sectional studies on their own can also prove very informative when making comparisons between populations, since the data more clearly capture population-wide patterns versus the individual variations that are emphasized in longitudinal studies (Hoppa & FitzGerald, 1999). Studying growth of highly active forager populations in the past, as has been undertaken in the current study, is only possible with the use of cross-sectional data, and sample-specific growth trajectories built from cross-sectional data can provide insights into the average growth patterns across a sample. Issues of comparison with WEIRD samples are also mitigated when analyses of archaeological samples are not mixed with modern reference samples, and between-group differences can be emphasized when cross-sectional data is used on its own. The growth trajectories used in this study, therefore, are based on cross-sectional data and will be discussed in more detail in Chapter 4, Section 4.5.

Most commonly, archaeological studies of growth and development have examined long bone lengths as a means of exploring the health status of past populations (Humphrey, 2000; Mays, 2018). Johnston (1962) presented one of the earliest reports of skeletal growth in his report on the skeletons from Indian Knoll, and several studies have similarly followed suit in the intervening decades. Traditionally, long bone lengths have been compared to dental ages to assess growth rates and velocity (Saunders, 2008). Additional analyses have since been added into the suite of tools used to study growth in the past, including estimations of stature, body mass, and measures of cortical thickness (Mays, 2018).

Archaeological studies of ontogeny often discuss patterns and timing of weaning since its impact on growth and development is notable. Isotopic signatures and dental wear patterns can be used to investigate breastfeeding and weaning (e.g., Clayton *et al.,* 2006; Mays, 2016; Schurr, 2018; Scott & Halcrow, 2017; Tsutaya & Yoneda, 2014), and thus these sorts of analyses have become popular inclusions in archaeological studies involving juvenile human remains. Up until six months of age, infants, regardless of genetic background or geographical location, tend to show similar rates of growth in both length and velocity when breastfed (WHO Multicentre Growth Reference Study Group, 2006). More notable differences in growth typically emerge once weaning foods are introduced and diets become more variable, and once breastmilk alone does not provide sufficient nutrients for the infant (Bogin, 2020). Breastmilk also provides important antibodies and protection against pathogens; once children are weaned, they become more susceptible to sickness and disease since much of their own immunity has not yet been established and they have the potential to ingest contaminated foods (Lönnerdal, 2000; Motarjemi *et al.,* 1993). A child's immune system does not become fully developed until after

five years of age (Newman, 1995), and so this period is one of particular susceptibility to disease.

When studying the past, specifically attributing pathological markers on the skeleton to weaning stress can be challenging, as most of the relevant markers are non-specific (i.e., linear enamel hypoplasia, cribra orbitalia, porotic hyperostosis) and can arise from a variety of stressors (Katzenberg *et al.,* 1996). The introduction of potentially contaminated foods and the increased likelihood of pathogen exposure which can occur around the start of the weaning period seem to have the most impact on infant health (including growth and development) and mortality (Katzenberg *et al.,* 1996). The stress of weaning and the introduction of complementary foods thus have the potential to lead to growth retardation in children (Larsen, 2015a). Other studies have shown that prolonged breastfeeding can help maintain healthy growth of children throughout the introduction of weaning foods, as was the case presented by Mays (2007) where longitudinal growth in a population of medieval children aligned with that of modern standards until after weaning had ceased, at which point growth retardation began to appear. In general, however, it seems that physiological stress is more likely to occur at the start of weaning rather than at the end (Halcrow, King, *et al.,* 2018).

Breastfeeding and weaning practices across the four samples used in the current study can be estimated with varying levels of certainty based on the currently available evidence (to be discussed in greater detail in Chapter 3), but it seems likely that weaning began around 1.5-2 years of age and finished around 4-5 years of age across all groups (Clayton *et al.,* 2006; Guatelli-Steinberg *et al.,* 2014; Schurr, 2018; Sellen, 2001). The period of weaning has been associated with stress due to reduced immune protection and the potential ingestion of contaminated foods and pathogens, and so growth and development during this period is closely

tied to the weaning process. While specifics of the role of weaning in developmental stress cannot be pinpointed in this study without further analyses, weaning nonetheless remains a critical time point in the developmental trajectory and one that should be included when considering factors affecting growth and development in archaeological studies.

2.3 Challenging the Obstetrical Dilemma Hypothesis

Prominent anthropological research of the mid- to late-20th century viewed the form of the female human pelvis as a compromise between a narrow pelvis necessary for efficient bipedalism and a broad pelvis necessary for giving birth to large-brained babies. These contrasting priorities were seen as an evolutionary trade-off between encephalization, bipedal locomotion, and obstetrics and so human pelvic morphology came to be described in terms of an "obstetrical dilemma" (Washburn, 1960). Compared with other mammals, the human childbirth process can be difficult and dangerous, thought to be a result of mechanical constraints necessary for obligate bipedalism (e.g., Wittman & Wall, 2007). Pelvic morphology has thus been viewed as a product of competing selective pressures. The wide female pelvis has further been described as having reduced locomotor efficiency as a result of increased strain on the hip abductors (Ruff, 1995; Zihlman & Brunker, 1979).

Recently, however, researchers have begun to question the obstetrical dilemma hypothesis and to further investigate metabolic costs of gestation, locomotor costs of bipedalism, pelvic floor stability, and biological plasticity of the pelvis (e.g., Betti & Manica, 2018; Dunsworth *et al.,* 2012; Kurki & Decrausaz, 2016; Pavličev *et al.,* 2020; Ricklan *et al.,* 2021; Stansfield *et al.,* 2021; Warrener *et al.,* 2015; Wells *et al.,* 2012). The difficulty of human childbirth (which often involves a tight fit between mother and baby) and the importance of

obstetrics as an evolutionary pressure are not being contested; instead, it is becoming apparent that an explanation of pelvic morphology as purely an evolutionary compromise between encephalization and locomotion is overly simplistic.

Dunsworth and colleagues (2012) have challenged the notion that babies are born at nine months due to size constraints of the pelvis and have shown that timing of birth is tied to metabolic constraints of the mother, while Warrener and colleagues (2015) have demonstrated that a broader female pelvis is no more energetically costly than a narrower male one. Kramer and Sylvester (2023) have further supported these conclusions by presenting a model that shows that modern human males do not walk more efficiently than females and that females do not expend more energy than males maintaining coronal plane stability of the pelvis during bipedal locomotion. Wall-Scheffler (2022) has also shown that people with wider pelves are more efficient load-carriers, particularly when carrying babies over variable terrain.

Kurki (2007) demonstrated that, in a small-bodied population of foragers, selection appears to be acting on the pelvis independent from overall body size and shape. Compared with larger-bodied populations, the small-bodied sample exhibited smaller non-canal pelvic measurements but relatively larger canal dimensions, comparable to those of the larger-bodied samples. The overall shape of the pelvis in the small-bodied sample was therefore quite different from that of the larger-bodied samples, suggesting that selection acts to protect dimensions of obstetric significance from being too small, even when overall body size (and pelvis size) is small. Kurki (2013a) also looked at a larger sample of populations from around the world and concluded that the small-bodied Later Stone Age (LSA) southern Africans are unique in their pelvic canal morphology, even compared with other small-bodied populations, suggesting that pelvic shape variation can be unrelated to body shape and size. Grabowski (2013) supports this

idea by arguing that the human birth canal has a low level of genetic constraint compared with other parts of the pelvis and with those of other apes, suggesting that the human birth canal is highly evolvable. Looking at the individual bones of the pelvis during development, Young and colleagues (2022) concluded that the human ilium shows higher levels of constraint compared to African apes, as well as compared to other elements of the human pelvis (acetabulum, pubis, ischium). They hypothesize that the lower levels of constraint seen in the ischium in comparison to the ilium, therefore, may be related to the ischium's importance for both locomotion and parturition.

Similarly, Betti & Manica (2018) and Kurki (2013a, 2013b) demonstrated that there are high levels of pelvic shape variation around the world, contradicting the concept of a tightly constrained morphology determined by competing processes of evolution. Betti and colleagues (2013) and Betti & Manica (2018) instead argued that neutral evolution and genetic drift have contributed to the patterns of pelvic morphology observed globally, noting evidence for reduced variability in pelvic canal dimensions in populations further from sub-Saharan Africa similar to founder effects observed in worldwide genetic diversity. The low level of constraint in the birth canal highlighted by Grabowski (2013) is further supported by the presence of geographic patterning in pelvic shape, as a highly evolvable pelvis could more easily adapt to climate stresses experienced at high latitudes (Betti, 2017).

Mitteroecker and colleagues (2021), however, have refuted the argument that variation in pelvic form is predominantly driven by neutral evolution (Betti & Manica, 2018). They reanalysed Betti and Manica's data and instead argue that some of the differences observed between populations are likely to be the product of natural selection. Specifically, through a series of statistical tests different to the ones conducted by Betti & Manica (2018), they found

strong correlations between pelvic width and temperature, as well as significant differences between geographically disparate groups, which they argue are stronger than what would be seen were genetic drift and neutral evolution the main driving factors.

It has also been suggested that humans maintain a relatively narrow pelvis to maximize functionality of and support for the muscles of the pelvic floor (Abitbol, 1988; Pavličev *et al.,* 2020; Stansfield *et al.,* 2021). Many of the muscles and fasciae of the pelvic floor attach to the ischial spines of the pelvis, a region which significantly narrows the birth canal. In the case of females in particular, proponents of this hypothesis (e.g., Pavličev *et al.,* 2020, Stansfield *et al.,* 2021, Stansfield *et al.,* 2023) have argued that natural selection acted to maintain a narrow pelvis in order to promote continence as well as properly support the internal organs and a growing fetus. While a broader birth canal might facilitate easier parturition – and Warrener and colleagues (2015) and Kramer & Sylvester (2023) have shown that a wider pelvis does not lead to less efficient bipedalism – a broader pelvis would be less able to support the muscles of the pelvic floor and thereby leave females more susceptible to pregnancy-related injuries.

Finally, the original obstetrical dilemma hypothesis did not consider the possibility of a biologically plastic pelvis. Humans are exposed to a wide variety of ecological stressors, and how our bodies adapt during our lifetimes to such stressors can be defined as biological plasticity (Smith *et al.*, 1985; Waddington, 1942; Wells & Stock, 2007). Incorporating a plasticity framework into the examination of pelvic morphological variation recognizes that while evolution has set some boundaries for human pelvic form (e.g., the sexual dimorphism that is consistently apparent in the human pelvis), a myriad of factors can lead to variation in pelvic morphology by altering the growth trajectories of the skeleton. In lieu of promoting an evolutionary trade-off as the source of dangerous childbirth, Wells and colleagues (2012) have

suggested a number of ecological factors as influencing the persistent tight fit between mother and baby including thermal environment, dietary shifts and energy availability, and infectious disease load. A contributing factor to this "dilemma" is likely the generational offset between the mother and the offspring, creating a lag in formative environments. Wells (2015) argues that "since maternal growth occurs a generation ahead of offspring growth, their co-adaptation to ecological stresses takes on the form of a 'three-legged race,' in which the two traits are linked without the possibility of perfect phenotypic integration" (p.3). An adult phenotype is the result of a suite of developmental stresses and of developmental plasticity, and thus one's environment plays a key role in the generation of pelvic morphology (Wells, 2015). Ultimately, maximum fetal growth appears to be beneficial for a baby, while factors such as diet (particularly undernutrition) and environment can affect the mother's growth and constrain the size of the pelvis (Shirley *et al.,* 2020; Wells, 2015). The obesity epidemic, paired with maternal stunting, poverty, and malnutrition often seen together in low-income countries, likely further exacerbates this issue (Wells, 2017). The difficult human childbirth process that is still experienced today, therefore, seems to not solely be a by-product of evolution, but is likely also driven by ecological circumstances.

The original obstetrical dilemma hypothesis, which foregrounded an evolutionary compromise between bipedalism and obstetrics, now appears overly simplistic in the face of all this new evidence. None of the elements presented here are mutually exclusive (Haeusler *et al.,* 2021), and instead it seems that bipedalism, obstetrics, encephalization, metabolic capacity, thermoregulation (to be discussed further in Section 2.5), pelvic floor stability, biological plasticity, and ecological stressors have all likely contributed to the evolution and morphological

development of the human pelvis. Furthermore, future research will surely continue to contribute and add more layers to the story of human pelvic morphology.

2.4 Biomechanics and Cross-Sectional Geometry

In addition to the aforementioned ecological factors influencing morphology of the skeleton during growth and development, bones also show considerable capacity for functional adaptation to loading. Loading of the long bones during growth in particular has been shown to have notable effects on morphological variation. In order to explore the loading history of a bone, and, by extension, an individual's activity patterns and habitual behaviours, principles of engineering beam theory can be used to quantify the mechanical functionality of bone deposition and loss in response to strain (Huiskes, 1982). Beam theory posits that the magnitude of strain that a cross-sectional portion of a beam can handle is proportional to the distance from the edge to the neutral bending axis or centroid, so cross-sectional measurements taken perpendicular to the long axis are indicative of a beam's ability to resist external pressures (Larsen, 2015b; Mott & Untener, 2017). As a result, material that is located further from the neutral bending axis or centroid will have the ability to resist greater loads and is considered to have greater bending and/or torsional strength and rigidity.

Applying this to long bones means that the distribution of bone around an axis of bending or torsion reflects the functional adaptation to mechanical loading experienced in life by that element. To resist fracture in the face of applied forces, repetitive movements can trigger osteogenic responses leading to increased bone deposition and/or redistribution along diaphyses (Ruff *et al.,* 2006). Cross-sectional geometric (CSG) properties, therefore, can be used to explore and quantify the rigidity and strength of a bone, and, by extension, tell us something

about its loading history. This method of analysis has become widely applied in the field of biological anthropology as a means of exploring habitual behaviours and activity patterns of humans in the past (e.g., Cameron & Pfeiffer, 2014; Kubicka *et al.,* 2022; Macintosh *et al.,* 2014; Marchi *et al.*, 2011; Ruff, 2008; Ruff *et al.,* 2015; Shackelford, 2014a, 2014b; Sládeck *et al.,* 2018; Stock & Pfeiffer, 2004).

Compared with adult long bones, juvenile bones are much more responsive to strain from mechanical loading. When faced with mechanical loading, bones undergo sensory perception, and (if the loading signal is sufficient) cell activation and growth response (Pearson & Lieberman, 2004). Developmental maturation influences how a bone responds to a mechanical load, and bones at different stages of development will respond differently to mechanical loading (Bertram & Swartz, 1991). Growth factors are closely tied to osteoblast function, and so fluctuations in growth hormones (as an example) can impact the extent to which a bone will respond to mechanical strain. Bone formation in long bones is primarily periosteal prior to adolescence, and instances of increased loading during this pre-adolescent period indicate that bone deposition occurs largely on this periosteal surface (Ruff *et al.,* 1994). At adolescence, bone deposition occurs at both the endosteal and periosteal surfaces, influenced by hormonal factors relating to the onset of puberty (Frisancho *et al.,* 1970). Increased mechanical loading in the mid-adolescent to early adulthood period appears to lead to bone deposition on both the endosteal and periosteal surfaces but is often focused on the endosteal surface (Ruff *et al.,* 1994). Inclusion of the endosteal contour in analyses of juvenile CSG properties is, therefore, necessary to accurately capture the distribution of cortical bone (Kurki *et al.,* 2022).

Recent studies have examined the ontogenetic patterns of long bone robusticity from infancy through late adolescence in archaeological samples, using cross-sectional geometry to

examine early life events such as the onset of walking and adaptations to increasing mechanical strain. Harrington (2010), for example, deduced that, in a sample of LSA southern African foragers, relative strength across the bones of the upper limb changes throughout ontogeny, while femoral to tibial strength in the lower limb remains fairly constant. Cowgill (2010) highlighted that developmental differences in acquisition of diaphyseal strength among a number of Holocene populations manifest quite early in life (likely before one year of age) and are maintained throughout ontogeny. These population differences seem to have correlations with certain habitual behaviours but are also likely influenced by other factors including genetics and nutrition (Cowgill, 2010). Osipov and colleagues (2016) also found that population-level differences between four geographically disparate groups manifested very early in life, with these initial variations likely relating to systemic factors and the maintenance of these differences a product of bone functional adaptation to habitual behaviours.

Ontogenetic perspectives on biomechanics particularly highlight the complexity of the form-function relationship in the human skeleton. Many of the aforementioned studies have shown that a relationship exists between mechanical strain and bone morphology but have also highlighted that additional factors contribute to bone morphology throughout ontogeny, making the relationship between mechanical loading and bone shape a complicated one. Genetic constraints can also influence the potential an individual has for robusticity and can thus impact the results of population comparisons (Osipov *et al.*, 2016).

Further, bony elements within the body may respond differently to habitual loading and produce signals reflective of varied loading scenarios. In the lower limb specifically, CSG properties of the femur seem to be more reflective of body size and shape, while those of the tibia, particularly around the midshaft and mid-distal regions, are more reflective of activity-

based loading patterns (Davies, 2012; Davies & Stock, 2014a). Davies (2012) reported that upwards of 80% of the variation seen in cross-sectional properties of the proximal femur in his sample could be explained by measures of body mass, while only 40% of the variation at the midshaft tibia was explained by body mass. Thus, when interpreting results of biomechanical analyses, it is important to not just consider absolute or even size-standardized values, but to also consider from where in the body the results are coming and what might be influencing the biomechanical signatures. Similarly, Pearson (2000) demonstrated that climatic adaptations, in the form of differing body proportions, are highly correlated with long bone diaphyseal robusticity, demonstrating the influence of body shape and size on measures of cross-sectional geometry.

Local terrain can also have an impact on bone morphology, as the skeletal response to an activity undertaken in one terrain can look different than the response to a similar activity undertaken in a different terrain. In a study comparing highly active Late Upper Palaeolithic individuals with more sedentary Iron Age individuals (Sparacello *et al.,* 2014), cross-sectional tibia measurements, expected to show more robusticity in the more active Late Upper Palaeolithic individuals, were actually quite comparable between the two populations. This finding was concluded to be a result of the mountainous terrain inhabited by the Iron Age individuals causing elevated robusticity measures despite lower activity levels (Sparacello *et al.,* 2014). Holt and Whittey (2019) similarly found that terrain had significant impacts on measures of bending and torsional strength in the lower limb bones, particularly among hunter-gatherers and early agriculturalists. Terrain conditions, therefore, are important to consider in biomechanical studies since robusticity measures will not only reflect the type and intensity of activity, but also the environment in which the activity took place.

2.5 Ecogeographic Variation

Variation in human morphology as a result of geography and climate has been well documented, and frequently invokes the "rules" established by Bergmann (1847) and Allen (1877) in the 19th century. Bergmann's rule states that overall body size will increase as temperatures decrease across geographic locales, while Allen's rule correlates surface area and limb length with temperature and thermoregulation. Ruff (1991) further expanded upon these rules by describing a cylindrical model, in which human body shape is represented as a cylinder whereby breadth will vary in relation to temperature regardless of height. Stature, represented by the height of the cylinder in Ruff's model, does not impact the surface area to volume ratio, while diameter does. In colder climates, therefore, wider body breadth (and pelves) can be expected regardless of overall stature (Ruff, 1991, 1994). Accordingly, it has been expected that humans living in colder climates have broader frames (including bi-iliac breadth) and shorter limbs (particularly in the distal elements), while humans living in warmer climates have slimmer frames and longer limbs. Numerous studies have found that these rules generally hold across human populations, as well as many animal and hominin populations (e.g., Ashton, 2002; Foster & Collard, 2013; Katzmarzyk & Leonard, 1998; Roberts, 1978; Ruff, 1994; Tilkens *et al.*, 2007).

In the face of climatic stress, pelvic morphology has often been framed in terms of thermoregulation. Per Bergmann's rule and Ruff's model, a narrower body allows for improved heat dissipation, and so it has been theorized that selection acted to favour a narrower pelvis during human evolution to promote thermoregulation in warm environments as body size was increasing (Ruff, 1991, 1993, 1994). Adaptations to colder climates, including broader pelvic size, have subsequently been found in populations which inhabited higher latitudes (as seen in Neanderthals, for example) (Gruss & Schmitt, 2015; Holliday, 1997; Kurki *et al.,* 2008; Weaver

& Hublin, 2009). While describing Neanderthal morphology solely in terms of climatic adaptation is overly simplistic (Ocobock *et al.*, 2021; Pomeroy, 2023), thermoregulation nonetheless seems to be an important selective pressure acting on pelvic morphological development in both modern humans and their ancestors.

Cowgill and colleagues (2012) focused on the applicability of Bergmann's and Allen's rules to human bodies in development, and found that correlations between climatic variables and stature, weight, body mass index, bi-iliac breadth, and brachial and crural indices are just as strong, if not stronger in some cases, in juveniles as they are in adults. Infants are particularly susceptible to cold stress, and thus thermoregulation in cold climates is particularly important to their survival; Cowgill and colleagues point to this as a possible explanatory factor for the strong correlations they found in their sample. They further highlight the importance of including immature individuals in studies of human evolution, as juveniles may themselves be targets of natural selection in ways different to adults in the same population.

Betti & Manica (2018) reported that pelvic canal shape variation is significantly correlated with geographic location, meaning individuals living closer to one another were more likely to have similar canal shapes. But while overall pelvic breadth and the shape of the os coxae have been shown to correlate with climate (e.g., Betti *et al.,* 2014; Ruff, 1994), Betti & Manica (2018) did not find a significant correlation between climate and canal shape (save for the inlet), despite finding a correlation with overall geographic location. Similarly, Kurki (2013a) demonstrated that populations with body sizes and shapes that fit the ecogeographic expectations do not necessarily reflect similarly in their pelvic shape.

Kurki and colleagues (2008) also showed that populations do not always conform to ecogeographic expectations in terms of proportions and body breadth. Later Stone Age (LSA)

southern Africans are often considered a low-latitude population from a warm environment, but based on the latitude and climate of coastal southern Africa it is actually more logical that the body shape and proportions of these foragers would resemble individuals from mid-latitude, Mediterranean-like environments. Limb proportions of the LSA southern Africans conform to expectations (and are similar to those of a North African sample), but body shape ratios of this population differ from other mid-latitude populations. The LSA southern Africans have narrow body breadths and small overall body sizes and therefore conform more closely to low-latitude ecogeographic expectations. Other small-bodied populations (the Andaman Islanders, the Khoesan, and the African pygmies) similarly do not wholly conform to ecogeographic expectations of body shape and proportions, suggesting that small-bodied populations may adapt to thermoregulatory pressures differently than larger bodied populations. Further, it may be that climate-related selective pressures acting on populations in mid-latitude environments are not as strong as those acting on populations in extreme climatic conditions (Kurki *et al.,* 2008).

Expanding the scope beyond climate to look at global patterns of stature and body proportions as they also relate to population history and ecology, Pomeroy and colleagues (2021) found, in most cases, even stronger correlations between population history, represented by a distance model reflecting dispersal out of Africa, and anthropometric variables (stature, sitting height, and lower limb length) than between temperature/climate and the anthropometric variables. They also found that stature and limb lengths are related to resource availability and pathogen load, further documenting factors beyond climate influence body size and proportions. Nevertheless, their results supported Allen's "rule" as they found a strong correlation between warmer temperatures and longer limbs. Similarly, Yim and colleagues (2023) sought to investigate the multiplicity of evolutionary forces impacting the ontogeny of limb dimensions

and found that population differences (resulting from neutral evolution), allometric variation, and climate-related directional selection all influenced the variation in ontogenetic trajectories noted in their combined archaeological and contemporary sample.

Overall, it appears that human populations generally adhere to Bergmann's and Allen's "rules" and demonstrate geographic patterning of body shapes and proportions consistent with principles of thermoregulation. There does not seem to be one way that the human body adapts to diverse climates, however, and the goals of thermoregulation may be met in different ways by different populations (Wall-Scheffler *et al.,* 2020). Climate is only one of many factors acting in conjunction with diverse ecological and social elements to promote morphological change, although it still appears to be a strong driver of population-level patterns. When considering the growing pelvis and factors influencing ontogenetic trajectories, therefore, climate and ecogeographic patterning are important considerations as they are likely to be evident in growth outcomes. It may be, however, that more extreme temperatures are stronger drivers of adaptation, and that climatic adaptations in milder climates are not as distinct.

CHAPTER 3: MATERIALS

Skeletal samples from four forager populations were included in this study: Later Stone Age (LSA) foragers of southern Africa, semi-sedentary foragers from Indian Knoll, Kentucky, foragers from Point Hope, Alaska, and the Sadlermiut foragers of Nunavut (Figure 3.1). As foragers, all the individuals represented are considered highly active and are thus ideal candidates for biomechanical analyses due to the more obvious markers of activity left on their bones via habitual behaviours (in comparison with sedentary populations). Although all four populations pursued forager lifestyles, their environmental conditions and habitual behaviours, including subsistence strategies, varied widely. Broadly, however, the LSA and Indian Knoll populations pursued terrestrial-based foraging strategies, while the Point Hope and Sadlermiut populations pursued marine-based foraging strategies. Terrestrial foraging strategies do not necessarily preclude the inclusion of marine resources in the diet but imply that foraging was done from land and on foot and typically involves high levels of terrestrial mobility. Marine foraging strategies, conversely, include the use of watercraft as an integral part of food procurement and high levels of engagement of the upper body muscles as a result. This variation, therefore, facilitates comparative analyses of pelvic growth and morphological variation as influenced by lifestyle factors and habitual behaviours.

Ilia and ischia from a total of 169 juveniles and 88 adults were included in the shape analyses of this study, as well as humeri, femora, and tibiae (where present) for biomechanical analyses from all juveniles. Bones were selected based on preservation and completeness, and all juvenile individuals who met these criteria were included in the sample. A selection of adults were included in the sample to represent the end point of growth, and the most complete and best

preserved individuals in each collection were chosen. For a complete list of individuals included in this study see Appendices A (juveniles) and B (adults).

Digital 3D scans were collected for this project using a Konica Minolta Virtuoso structured light scanner (threerivers3D, NJ, USA) and a NextEngine™ laser scanner (NextEngine, Inc., CA, USA). Scans collected using the Konica were fused into digital 3D models in GeoMagic Design X™ (3D Systems, Inc., USA) and scans collected with the NextEngine™ were fused into models in ScanStudio™ (NextEngine, Inc.). See Table 3.1 for a list of collections scanned and names and locations of institutions where they are housed.

Figure 3.1 World map with shapes representing locations of the populations of study: LSA (blue star), Indian Knoll (red circle), Sadlermiut (purple triangle), and Point Hope (green diamond).

Table 3.1 Collections scanned and locations of institutions where they are housed.

Collection	Institution	Location
Later Stone Age southern Africans	Albany Museum	Grahamstown, South Africa
	Iziko South African Museum	Cape Town, South Africa
	McGregor Museum	Kimberley, South Africa
	National Museum Bloemfontein	Bloemfontein, South Africa
	University of Cape Town	Cape Town, South Africa
Sadlermiut	Canadian Museum of History	Gatineau, Québec, Canada
Indian Knoll	University of Kentucky	Lexington, Kentucky, USA
Point Hope	American Museum of Natural History	New York, New York, USA

3.1 Later Stone Age, Southern Africa

The Later Stone Age (LSA) foragers of southern Africa cover the longest time period of the samples included in this study, with individuals dated between approximately 9,000 and 220 BP (Humphreys, 1970; Kurki, 2005 [Sealy pers. comm.]; Pfeiffer & Harrington, 2011; Pfeiffer & Sealy, 2006; Sealy & Pfeiffer, 2000; Sealy, 2006). Eighty-nine LSA individuals were included in this study: 72 juveniles and 17 adults (representing the end point of growth). The 89 individuals are from approximately 40 different sites, representing both archaeologically excavated remains and finds that emerged from eroding dunes. The skeletons are housed at the Albany Museum, the National Museum Bloemfontein, the University of Cape Town, the McGregor Museum, and the Iziko South African Museum. See Appendix C for a specific list of LSA individuals included in this study, including names of the sites at which they were found, the biome from which they came, and the approximate date of the remains (where available).

The geographic region from which the skeletal remains of the LSA foragers were recovered can be divided into four main biomes: forest, fynbos, savanna, and karoo (Figure 3.2). The forest biome is an area with a warm/temperate climate, heavy rainfall, variable terrain, and a continuous canopy; the fynbos biome is an area with a Mediterranean climate, moderate rainfall,

sandy coastline, and a higher proportion of succulents; the savanna biome is an open, grassy bushland (Churchill & Morris, 1998; Pfeiffer & Harrington, 2011; Stock & Pfeiffer, 2004); and the karoo is an area of plains with grassy vegetation, interspersed with occasional mountains (Mitchell, 2002). Individuals living in the fynbos, forest, and savanna biomes would have had access to both terrestrial and marine food resources, while individuals living in the karoo would have relied on terrestrial resources (Barham & Mitchell, 2008; Pfeiffer & Harrington, 2011).

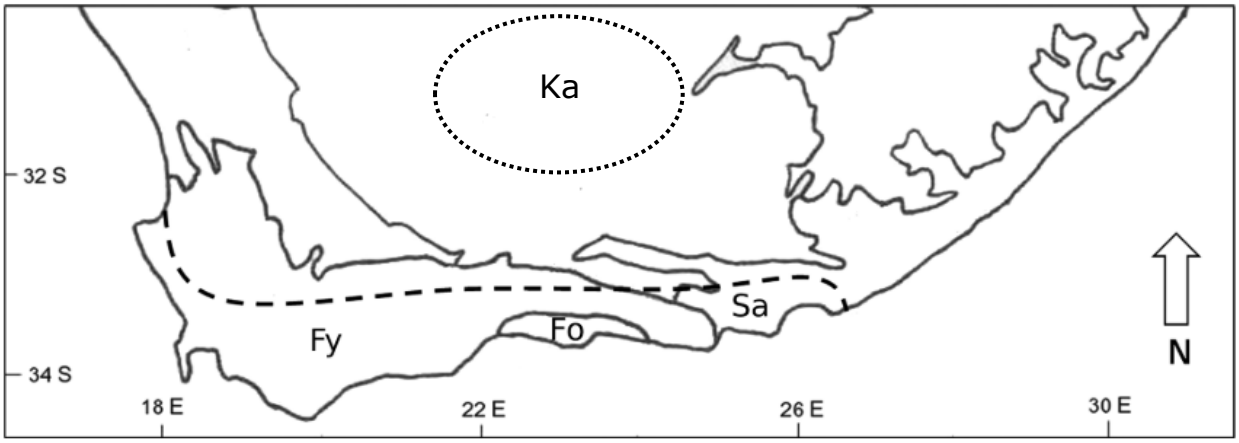

Figure 3.2 Southern Africa. Dashed line bounds the area from which the fynbos, forest, and savanna burials were recovered, dotted line bounds the region from which the karoo burials were recovered. Fy = fynbos, Fo = forest, Sa = savanna, Ka = karoo. Modified from Morris (1992) and Pfeiffer & Harrington (2011).

Subsistence strategies of LSA individuals, particularly those who lived prior to 2000 BP, featured the hunting of small game and terrestrial foraging, as well as extensive exploitation of coastal marine resources by the people living in the fynbos, forest, and savanna biomes (Stock & Pfeiffer, 2001). The types and quantities of marine resources being exploited seem to have varied between groups, but the harvesting of coastal marine resources from land (as opposed to from the water with the use of watercraft) appears to be a constant (Sealy *et al.,* 1992). Based on the territorial availability of resources, Clark (1959) posited that the average group of LSA foragers would cover an area of 2,000-3,000 square miles while hunting and gathering. Sealy

(2006), however, has argued that LSA foragers were more territorial and exploited resources from more limited regions, based on isotopic evidence demonstrating differences in diet between groups residing within relative geographic proximity. Despite potential dietary variation, all the LSA foragers would have been hunting and foraging from land and would have traversed rugged terrain and encountered steep rocky outcrops (Sealy & Pfeiffer, 2000; Stock & Pfeiffer, 2001). Even when compared with other Holocene foraging populations, LSA foragers from the Cape coast and into the karoo region exhibit biomechanical properties associated with high levels of terrestrial mobility (Cameron, 2017). These markers of mobility are visible in the skeleton from an early age, with individuals reaching biomechanical measures comparable to adults by late adolescence (Harrington, 2010). Juvenile skeletal remains of LSA foragers show signs of a locomotor shift by two years of age (including development of the femoral pilaster), which may indicate an earlier onset of walking than is common in modern Western cultures (Harrington, 2010). Independent walking usually begins around 16 months of age in Western cultures, but ethnographic findings report that modern Khoesan caregivers often take a more active role in the motor development of young children than do those in the West (Konner, 1976). Harrington (2010) thus proposes that a similar scenario might explain the biomechanical results of the LSA.

Clayton and colleagues (2006) investigated weaning age in a group of LSA southern African foragers through isotopic analyses and concluded that infants were breastfed for at least the first 1.5 years of life, and that weaning concluded between 2-4 years of age. These findings are consistent with ethnographic reports of the modern-day descendants of the LSA foragers: the hunter-gatherers of the Kalahari (Konner, 2005).

The LSA foragers were a small-bodied people, much like their Khoesan descendants today (Deacon & Deacon, 1999; Schuster *et al.,* 2010). Studies of living foragers in the Kalahari

have documented mean statures around 160 cm for males and 150 cm for females (e.g., Dart, 1937 – males: 155.8±5.51 cm, females: 146.1±5.93 cm; Truswell & Hansen, 1976 – males: 160.9 cm, females: 150.1 cm), and stature estimates from archaeological human remains show similar results (Kurki *et al.,* 2010; Pfeiffer & Sealy, 2006). While small stature is frequently attributed to malnutrition, the LSA foragers maintained their small body size despite apparent access to abundant resources (Pfeiffer & Sealy, 2006). Adaptation to extreme climates also does not appear to be a factor influencing body size of the LSA populations, as the coastal environments where many foragers lived would have had temperate climates (Pfeiffer, 2012). LSA individuals do not appear to differ in growth tempo from modern American children, and instead remain consistently small throughout growth with no evidence suggesting stunting and/or catch-up growth (Pfeiffer & Harrington, 2010; Pfeiffer & Harrington, 2011). Early cessation of growth as a trade-off with sexual maturation and reproduction has been posited as an explanation for small body size in the context of life history theory for populations with high mortality risk amongst young adults (Charnov, 1993, 2001). Evidence for truncated growth and early reproduction is not, however, apparent in LSA skeletal samples (Pfeiffer & Harrington, 2011).

The small size of the LSA foragers, therefore, is more likely a selected trait, favoured throughout the Holocene for a number of reasons which could include hunting efficiency (as described ethnographically in Lee, 1984), culturally determined sexual selection, or periods of dietary insufficiency (Pfeiffer, 2012). That small stature is pervasive across thousands of years amongst the LSA populations suggests the influence of selective pressures, since the likelihood of malnutrition affecting the life course of every individual over thousands of years and simultaneously stunting their growth is quite low. Further, palaeopathological studies have found little evidence of infectious disease amongst the LSA foragers (Gibbon & Davies, 2020;

Pfeiffer, 2007), with degenerative joint disease and trauma being the most commonly observed pathological changes (Pfeiffer, 2016). A selection-based explanation for small body size is, therefore, most likely.

3.2 Indian Knoll, Kentucky

The site of Indian Knoll is a large shell midden on the banks of the Green River in Kentucky, USA (Figure 3.3). Human skeletal remains were excavated from the site during two major excavation projects: the first, in 1915, removed 298 human burials (Moore, 1916) and the second, in 1939, was accompanied by a large-scale excavation of the whole site and recovered 880 human burials (Webb, 1946). Calibrated radiocarbon dates from different samples of midden debris and human remains from Indian Knoll range from 6415 to 4143 BP, equating to the Middle and Late Archaic periods (Herrmann & Konigsberg, 2002; Winters, 1974). Sixty-two individuals from Indian Knoll, whose remains are held at the University of Kentucky, were included in this study: 38 juveniles and 24 adults.

The people of Indian Knoll pursued a terrestrial-based hunter-gatherer mode of subsistence with a large reliance on freshwater mussels foraged from the banks of the Green River (Snow, 1948). Deer meat, plants, and nuts from the local hardwood nut-bearing trees would have constituted the majority of the rest of the diet (Winters, 1974). The landscape surrounding Indian Knoll has both rolling hills and steep bluffs, and is generally forested and fertile (Snow, 1948). Damming of the Green River around the year 1830 CE, as well as continued deforestation in the area, means that the character of the terrain at Indian Knoll during the Middle and Late Archaic periods would have been different than how it appears today. It is likely, however, that the river and its branching streams were somewhat slow-moving and posed

low flood risks, and that the platform of land on which the site resides was a prominent feature of the landscape. While the area is generally hilly, the location of the village at Indian Knoll lies in a 700-acre area that is fairly level, bordered by the river on one side and a creek on the other (Webb, 1974). It is likely that the individuals living here during the Middle and Late Archaic periods would have been semi-sedentary foragers, occupying seasonal sites for long periods of time with fairly dense populations (Cowgill, 2014; Winters, 1974).

Figure 3.3 Location of the Indian Knoll site within the eastern United States. From Herrmann & Konigsberg (2002).

The first major comprehensive study of the Indian Knoll skeletons was published by Snow in 1948. He noticed a general trend of straightening in the lumbar curve of the spine,

accompanied by femoral torsion, flattening of the upper femoral and tibial shafts, defined attachment sites of the gluteal muscles, and defined calcaneal tuberosities, all suggesting high levels of leg muscle engagement. Cowgill (2008) further observed overall high levels of postcranial strength in the juveniles of Indian Knoll. All of these features are indicative of dynamic movement and speak to the high levels of terrestrial mobility undergone by these foragers (Snow, 1948).

Cowgill (2008) also noted high levels of humeral asymmetry within the Indian Knoll population, which she suggested could reflect lifelong atlatl use since a large number of atlatl components were excavated from the site (Webb, 1946). She notes the emergence of this asymmetry in individuals as young as 6-12 years of age, suggesting the implementation (whether practically or recreationally) of unilateral activities from an early age. Further, 36% of the atlatl components recovered from burials at Indian Knoll were recovered from the graves of children, reinforcing the notion that individuals may have begun practicing "adult behaviours" from an early age, and demonstrating the importance of an ontogenetic approach to the study of skeletal morphologies (Cowgill, 2008).

Johnston (1962) studied long bone growth at Indian Knoll in comparison with the results from the Denver Growth Study (Maresh, 1955), and found that overall patterns were similar between the two, but that growth rates diverged with statistical significance (and the Indian Knoll fell below) after two years of age. Johnston largely contributes these results to genetic differences, as his calculated average adult statures for Indian Knoll of 171.42±1.89 cm (using the Stevenson, 1929 formula) and 167.00±3.18 cm (using the Trotter & Gleser, 1958 formula) for males are below the average values for white Americans on whom the Denver Growth Study was based. Isotopic analyses from the Indian Knoll site indicate that weaning began around two

years of age and was complete by five years of age (Schurr & Powell, 2005; Schurr, 2018), which could also explain the slowed growth after two years of age noted by Johnston (1962). Sundick (1978) studied growth at Indian Knoll and found the rates to be comparable to those of a Medieval German population until puberty, when the individuals from Indian Knoll fell behind. Average adult statures in the German samples were approximately 6 cm larger than those from Indian Knoll, which Sundick thus contributes to the differences noted in the pubertal growth spurt. Particularly in comparison to the LSA, however, Indian Knoll is still considered a large-bodied population.

3.3 Sadlermiut, Nunavut

The Sadlermiut were a group of Inuit people who lived on Southampton, Walrus, and Coats Islands in Hudson Bay, Nunavut (Figure 3.4) until the winter of 1902-1903 CE (Ryan & Young, 2013). Individuals excavated from Tunermiut, Southampton Island, the main settlement site of the Sadlermiut, are identified by field catalogue numbers beginning with the prefix "NP," referring to the geographical feature of Native Point located approximately three miles south of Tunermiut (Merbs, 2019). It is thought the Sadlermiut had lived on Southampton Island for at least 500 years (Merbs, 1983), and radiocarbon dates from the site of Tunermiut range as far back as 977 ± 54 BP (Coltrain, *et al.*, 2004). Sixty-four Sadlermiut individuals from Tunermiut, curated by the Inuit Heritage Trust and housed at the Canadian Museum of History in Gatineau, QC were included in this study: 44 juveniles and 20 adults.

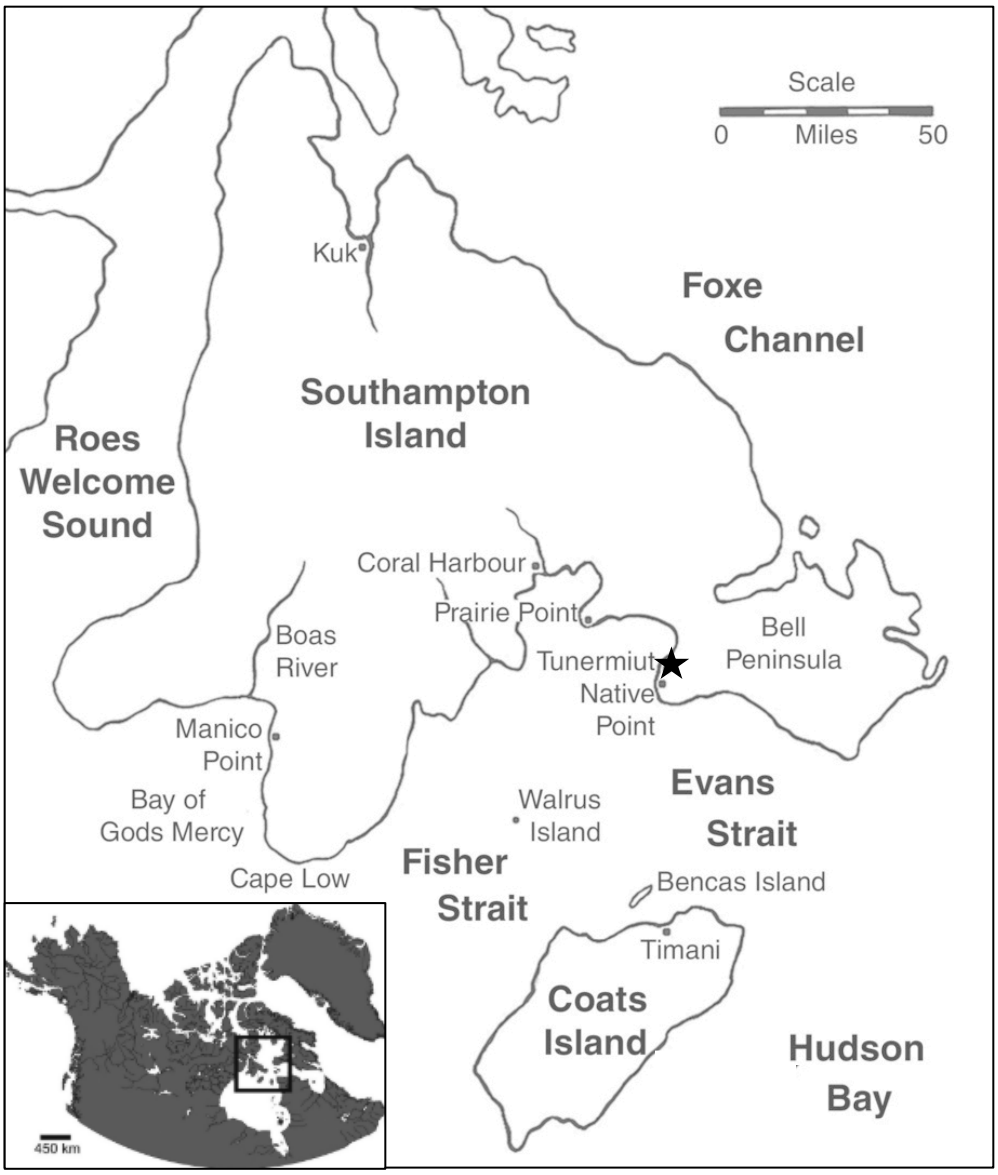

Figure 3.4 Location of Tunermiut on Southampton Island, Nunavut. Modified from Merbs (2019) and Ryan & Young (2013).

The landscape of Southampton Island can be divided roughly in half, with the northern portion made up of Archaean gneiss and the southern portion made up of limestone plains (Manning, 1936). There is also a low mountain range along the northeast coast (Comer, 1910). The land is very flat around Tunermiut, but foothills begin to rise about 25-30 km north of the site. The limestone plateaus of the southern part of the island are relatively bare of vegetation, although patches of marshland separate the limestone outcrops (Manning, 1936).

Compared to many other contemporary Inuit groups, there are very few historical or ethnographic accounts of the Sadlermiut people – they did not frequently visit with neighbouring groups, nor did long term ethnographic research ever take place with them. In the winter of 1902-1903, the last of their population, estimated to be around 60 people, succumbed to a disease brought to their island by a European whaling ship (Mathiassen, 1927; Ryan & Young, 2013). Oral history or descendant knowledge, consequently, has not endured to the present. The information that is known about them, therefore, has been pieced together from accounts of brief encounters with neighbouring Inuit groups and explorers (e.g., Lyon, 1825), secondary oral histories (e.g., Pelly, 1987; Pitseolak & Eber, 1975), second hand information relayed to ethnographers (e.g., Boas, 1907), and archaeologically excavated material (e.g., Merbs, 1983, Ryan & Young, 2013).

Based on isotopic evidence, it appears that the Sadlermiut were heavily reliant on high-trophic level marine foods and did not have large dietary breadth (Coltrain *et al.*, 2004; Coltrain, 2009). Seal, seabirds, and walrus meat were the primary components of the Sadlermiut diet all year round, while caribou and salmon contributed to their diet in the summer months when available (Boas, 1888; Coltrain, 2009). The Sadlermiut also hunted whales and used whale bones and skulls in the construction of houses (Comer, 1910). While there is some debate over the specific contributions and quantities of different types of meat to their diets (see Ryan, 2011 and Coltrain, 2011), it is undisputed that the Sadlermiut ate a largely marine-based diet.

The Sadlermiut developed robust upper limbs through a variety of habitual behaviours including kayaking, harpoon-throwing, sled driving, bow drill use, and hide cutting (Mathiassen, 1927; Merbs, 1983). Sadlermiut adults demonstrate a higher prevalence of osteoarthritic joint changes in their upper limbs compared to their lower limbs; these patterns likely reflect the

intensity and frequency with which they engaged their upper bodies (Merbs, 2019). Sex differences are visible in the way these pathological changes manifest in the humerus in particular, with males showing increased signs of osteoarthritis on the capitulum and females showing increased signs of osteoarthritis on the trochlea. These differences are likely tied to habitual behaviours, with harpoon throwing and kayaking (involving forearm pronation-supination) being key activities for men and hide preparation and scraping skins (involving elbow flexion-extension) important activities for women (Merbs, 1983). It is likely that children began mimicking these adult behaviours from a young age, as Boas (1907) writes:

> The mother will take her infant boy on her knees, and let him throw the fork into the dish from which she is eating. Afterwards she will place him on the bed, and let him go through the movements of paddling and harpooning in the kayak, and of shooting with bow and arrows, in order to make him a successful hunter when he is grown up (p. 484).

While this passage is specifically referring to a mother and child living near Cumberland Sound (Baffin Island), it is likely that Sadlermiut children would have been similarly encouraged to start practicing adult behaviours from a young age. Merbs (1983) also noted a high prevalence of vertebral compression fractures in the adult skeletons, which he likens to "snowmobiler's back," a condition which can result from snowmobiling over rough terrain (Roberts *et al.,* 1971), and which likely manifested in the Sadlermiut as a result of riding on sleds.

Symchych (2016) studied growth patterns of the Sadlermiut juveniles and reported that most individuals who died during childhood appear to have undergone faltering in the tempo of growth when compared with the tempo reported by the Denver Growth Study (Maresh, 1943, 1955, 1970). Overall body size and proportion attainments of adults within the population are consistent with an arctic-adapted population per Bergmann's and Allen's rules, but the juveniles in the sample appear to have experienced a variety of growth retardations prior to death. Other

high latitude populations, like the foragers from Point Hope, do not demonstrate the same faltering of growth tempo, and thus Symchych hypothesizes that some form of persistent nutritional deficiency (perhaps due to their lack of dietary breadth) or infectious disease may have impacted the growth rates of the Sadlermiut children who did not survive.

Isotopic studies of the Sadlermiut have thus far only been undertaken on adults (in the interest of exploring diet – e.g., Coltrain, 2009), so the timing of weaning has to be estimated for this group. Sellen (2001) compiled data from ethnographic and demographic reports collected between 1873 and 1998 of 133 non-industrial societies and reported that the average age for the introduction of weaning foods was 6 months, and the average age for the cessation of weaning was 30 months (2.5 years). There is a large spread reported for the cessation of weaning, however, with ages ranging from 12 to 66 months (1 to 5.5 years). Twelve of the included populations in the study are from the northern portion of North America (between Colorado and the Northwest Territories near Great Bear Lake) and two are from Siberia. The two Siberian samples were reported as ceasing weaning between 2-3 and 3-4 years, and more than half of the 12 northern samples were reported as 2-3 years; the remaining northern groups were mostly reported as 2-4 years, although with some as old as 6-8 years.

Direct mention of the timing of weaning of Sadlermiut children is not obvious in the ethnographic record, nor have previous archaeological studies of bones and teeth focused on this topic, so information has to be inferred from related studies and texts. In reference to the Iglulik peoples who moved onto Southampton Island shortly after the Sadlermiut succumbed to disease, Mathiassen (1928) writes that, “during the first two years the child is normally fed on the breast, and in fact even up to three or four years one occasionally sees them given the breast” (p.214). While this passage is not directly referencing the Sadlermiut, it is not unlikely that they may

have practiced similar behaviours. Mathiassen (1928) also discusses the practice of adoption, which he says was very common amongst the Iglulik peoples at the time (1921-1922). He writes that parents would sometimes give a newborn to another family as an act of friendship or kinship or give the newborn away in exchange for goods or services. He comments that the children seemed to be treated as their own by the adoptive parents, but that:

> For the children themselves this adoption is mostly a bad exchange; as a rule they cannot, of course, get milk and therefore they have to be brought up on soup or chewed meat, which they suck from the mother's mouth, and of course a large number of them die of it…Adoption undoubtedly is very greatly to blame for the terribly high infant mortality. (p.213)

It is once again possible that similar practices may have taken place amongst the Sadlermiut, and that those practices may have had influences on the health outcomes of the children. Ultimately, timing of weaning has to be estimated for the Sadlermiut, but it seems likely that it began around two years of age and ceased around four years of age.

3.4 Point Hope, Alaska

The site of Point Hope lies on the northwestern edge of Alaska, USA (Figure 3.5) and was excavated by Larsen and Rainey between 1939 and 1941 (Rainey, 1947; Larsen and Rainey, 1948). Point Hope lies about 200 km north of the Arctic Circle and has an extreme cold climate; wind speeds in January average 25.2km/h, while the temperature high for the month is typically around -15.7°C (Holliday & Hilton, 2010). Approximately 10,000 artifacts and skeletal remains of 500 individuals were recovered during the Larsen-Rainey expedition which are now housed at the American Museum of Natural History in New York City, USA. For this study, 42 individuals from Point Hope were included: 15 juveniles and 27 adults.

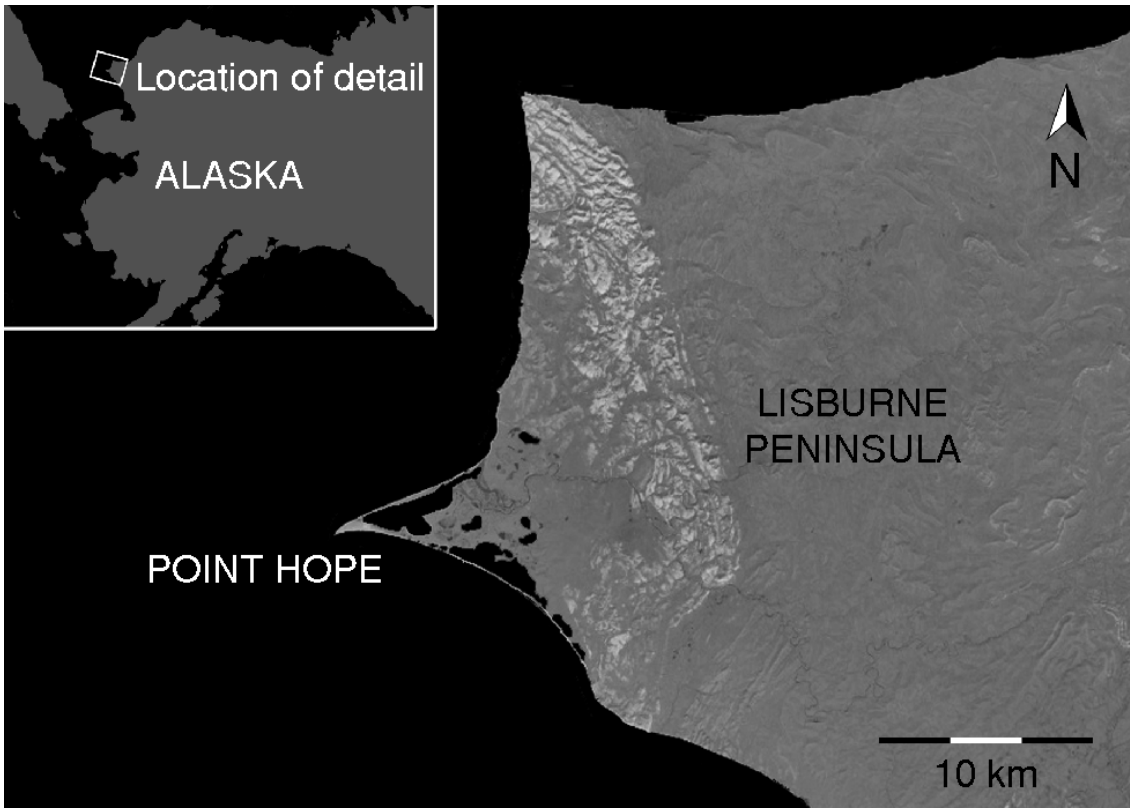

Figure 3.5 Location of Point Hope within Alaska. Image modified from Google Maps, from Hilton *et al.* (2014).

The history of Point Hope can be divided into two distinct cultural periods: the Ipiutak period (c.1600 to 1100 years BP) and the Tigara period (c.800 to 300 years BP) (Larsen and Rainey, 1948). The people of these time periods lived in the same place but had distinct cultures and subsistence strategies. The Ipiutak relied on caribou and followed migrating herds towards inland parts of Alaska on a seasonal basis, while the Tigara relied on marine resources such as whales, walruses, and seals and stayed at Point Hope year-round (Hilton *et al.*, 2014). A study comparing the health status of the Ipiutak and Tigara populations found that, based on the protocol set out in Steckel & Rose (2002), the two populations had equal overall health indices, but that the components of this score varied (Dabbs, 2011). Ipiutak individuals displayed a higher prevalence of chronic stresses (represented by nonspecific infections and degenerative joint disease), while Tigara individuals displayed a higher prevalence of acute stress (represented

by linear enamel hypoplasia and trauma). Dabbs (2011) hypothesized that these differences may be related to subsistence strategies. Specifically, the overland travel necessary for caribou hunting likely contributed to the higher prevalence of degenerative joint diseases seen amongst the Ipiutak, while the risk involved in close-contact whale hunting likely contributed to higher rates of trauma, and shortages of food may have led to periods of stress during growth (exhibited through linear enamel hypoplasia) seen amongst the Tigara. Individuals from both periods are considered high-intensity foragers, however, and thus researchers (e.g., Cowgill, 2014; Shackelford, 2014b) frequently consider both the Ipiutak and Tigara as one sample since significant differences are not detectable in cross-sectional geometric measures. Of the individuals included this study, 10 are from the Ipiutak period, and 35 are from the Tigara period (Cowgill, pers. comm.; Copes, 2012). See Appendix D for a breakdown of which individuals come from which cultural period.

Cowgill (2014) reported that juvenile individuals from Point Hope demonstrate moderate levels of humeral asymmetry and overall high levels of postcranial strength, similar to patterns reported in adults from the site. She did not observe any significant differences between Ipiutak and Tigara individuals in terms of cross-sectional geometric properties, save in the polar second moment of area of humeral asymmetry. Despite the expected differing biomechanical requirements of caribou hunting and whaling, detectable differences in cross-sectional geometry are not apparent. She proposes that these findings may be due to small sample size but could also be the result of compounding factors including nutritional status or genetic background.

The timing of weaning has not been specifically investigated in relation to Point Hope, and dental wear studies of individuals have thus far only been undertaken on adults in the interest of exploring dietary and behavioural patterns (e.g., El Zaatari, 2008; Krueger, 2014). The timing

of weaning, therefore, has to be estimated for this group as well. In a study of linear enamel hypoplasia (LEH) of children from Point Hope, Guatelli-Steinberg and colleagues (2014) estimate a weaning age of four years for this population. As they discuss, however, LEH is not a direct means of determining weaning age and cross-referencing their data with isotopic results (which have yet to be undertaken) would provide a more concrete picture of the weaning patterns of this population. Guatelli-Steinberg and colleagues (2014) reference the 1890 census of Alaska (Porter, 1893) which describes Alaskans living near the site of Point Hope and states that, "children are rarely weaned until they become 4 or 5 years old, and it is no uncommon sight to see a woman pull a child of 8 or 9 years under her shirt to nurse it when the youngster is in any way fractious or angry" (p.137). The individuals included in the current study lived at Point Hope hundreds of years earlier than this census so assumptions cannot be made about the past, however in lieu of direct evidence of weaning from the skeletons of Point Hope these data create starting points to work from.

The individuals from Point Hope represent a cold-adapted population (per Bergmann's and Allen's rules), with foreshortened limbs and wide bi-iliac breadths. They do not, however, have significantly different proportions than European populations also living in cold environments, despite the more extreme environment and climate of northern Alaska (Cowgill, 2014; Holliday & Hilton, 2010). This similarity of body shapes and sizes between individuals from Point Hope and other parts of the world may reflect a selective advantage of cold-adapted body types in any high-latitude environment (Holliday & Hilton, 2010).

CHAPTER 4: METHODS

This study sought to investigate growth and development of the pelvis in forager populations and to assess the roles that adaptive and plastic responses play in driving variation. Morphological variation of the ilium and ischium throughout growth were captured using a geometric morphometrics approach and measures of activity were quantified using cross-sectional geometry. Starting with an overview of geometric morphometrics, this chapter will then outline methods of age estimation, collection of cross-sectional geometric data, statistical analyses used, and the method of maturation analysis.

4.1 Geometric Morphometrics

For this research project, morphology of the pelvis was captured using a geometric morphometrics approach. Morphometrics is a way to characterize and quantify shape and size variation, which can simplify a complex form through abstraction to a series of measurements (Klingenberg, 2012a). This method uses landmarks represented by Cartesian coordinates to look at characteristics of shape by examining relationships between landmarks, curves, and/or surfaces (Bookstein, 1991; Mitteroecker & Gunz, 2009). Within geometric morphometrics, the terms 'size,' 'shape,' and 'form' carry particular and technical meaning: 'size' refers to the scale or magnification of an object; 'shape' refers to all geometric properties of an object excluding size, position, and orientation; and 'form' encompasses both concepts and considers size and shape together (Klingenberg, 2012b). Morphospace is a geometric morphometrics concept in which a point represents an object's form. Within this space, all forms correspond to a point, and so the size and shape of objects can be analyzed based on their locations within morphospace.

The geometry of points can then provide information about morphological relationships (Klingenberg, 2012a). Geometric morphometrics has thus become a widely applied methodology in the field of biological anthropology to answer questions about morphology and variation in the skeletons of humans and other fossil hominin species (e.g., Cofran *et al.,* 2022; Fischer & Mitteroecker, 2017; García-Martínez *et al.,* 2018; Ioannidou *et al.,* 2021; Mopin *et al.,* 2018; Nozaki, *et al.,* 2021; Schuh, *et al.,* 2019). These methods can be performed in 2D or 3D space; 3D geometric morphometrics was pursued for this project as the pelvis is a complex 3D structure whose morphology can more thoroughly and accurately be captured in three dimensions.

Fixed and sliding semi-landmarks were used to capture the shape of the ilium and ischium. Bookstein (1991) classified three types of fixed landmarks: Type I represent the juxtaposition or intersection of tissues (like the cranial landmark bregma), Type II represent points of maxima (like the deepest point in the greater sciatic notch), and Type III represent extremities (like the endpoint of the ischial ramus). Fixed landmarks must be identifiable and homologous across all individuals in a sample. Where features are not as discrete or geometrically homologous, such as across curves, semi-landmarks can be used to investigate shape and morphological relationships. Semi-landmarks are used to map biologically homologous features across a sample, but do not assume that each individual landmark is placed in the exact same position on each specimen (Gunz *et al.,* 2005). Rather, the same number of landmarks is placed on a biologically homologous feature (e.g., 100 semi-landmarks around the iliac crest), and these landmarks can then be allowed to slide along the curve established by the set of landmarks. Sliding the semi-landmarks allows for the minimization of bending energy, meaning that uncertainty in the placement of the landmarks can be reduced by sliding each

landmark along a curve relative to a directional vector projected from the neighbouring landmark (Gunz *et al.,* 2005; Schlager, 2017). For this project, both fixed and sliding semi-landmarks were used to investigate shape throughout growth in the bones of the pelvis. Specific details of landmark selection and placement will be discussed in Sections 4.1.1 and 4.1.2.

4.1.1 Landmark Selection

Landmark coordinates are central to geometric morphometric methods. For this project, digital landmarks were placed on 3D models of ilia and ischia, as well as on fused os coxae. Left pelvic bones were used preferentially, but right bones were mirrored where a left was not available. Unlike the bones of the upper limb, pelvic bones do not display strong patterns of directional asymmetry (Kurki, 2017) and thus this approach was considered acceptable and unlikely to introduce inconsistencies in the data due to asymmetry.

Landmark locations were chosen to capture an overall picture of pelvic shape. Eleven fixed and 100 sliding landmarks were placed on each ilium, and 7 fixed and 114 sliding landmarks were placed on each ischium. A full list of landmarks can be found in Tables 4.1 and 4.2, and Figures 4.1 and 4.2 demonstrate the placement of these landmarks on the bones. Fixed landmarks were placed on easily identifiable homologous points and obvious anatomical landmarks, while sliding semi-landmarks were used to cover rounded edges/surfaces. Preserved cartilage was not present in these samples, so all landmarks were placed directly onto the bony surfaces in 3D space. Specific landmark locations were chosen based on previous studies by Wilson *et al.* (2014) and Estévez Campo *et al.* (2018).

Table 4.1 Landmarks placed on the ilium.

Fixed landmarks (ilium)		
1	Posterior superior iliac spine	Type II
2	Anterior superior iliac spine	Type II
3	Iliac tubercle	Type II
4	Posterior inferior iliac spine	Type II
5	Inferior limit of greater sciatic notch	Type III
6	Inferior limit of auricular surface	Type II
7	Anterior point of auricular surface	Type II
8	Edge of acetabulum at base of arcuate line	Type II
9	Anterior inferior iliac spine	Type II
10	Anterior edge of acetabulum	Type II
11	Anterior tip of greater sciatic notch	Type II
Semi-landmarks (ilium)		
12-51	Iliac crest (medial); between fixed landmarks 1 and 2	
52-58	Iliac crest (lateral to iliac tubercle); between fixed landmarks 2 and 3	
59-95	Rest of iliac crest (lateral); between fixed landmarks 3 and 1	
96-111	Greater sciatic notch; between fixed landmarks 11 and 5	

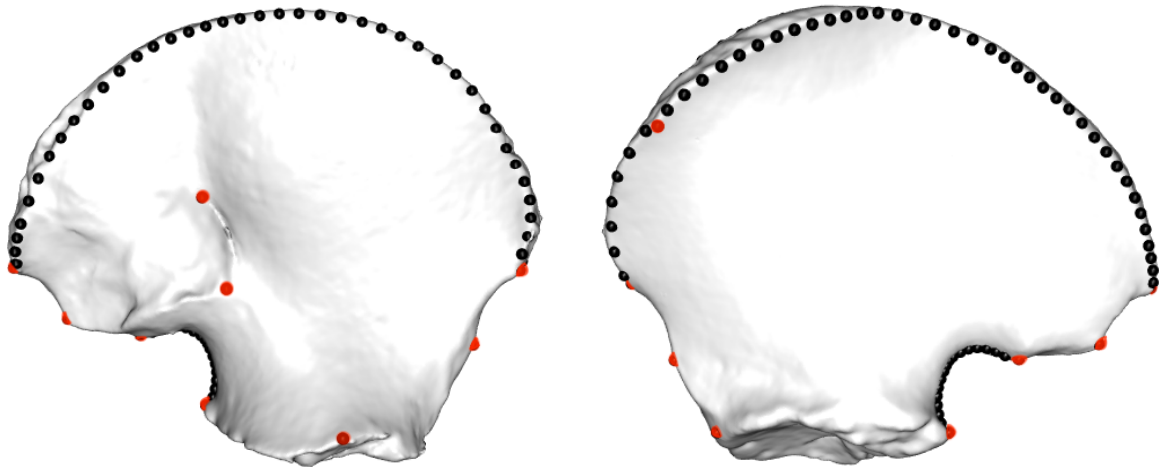

Figure 4.1 Landmark placement across the ilium, highlighting the fixed landmarks (red) and the sliding semi-landmarks (black).

Table 4.2 Landmarks placed on the ischium.

Fixed landmarks (ischium)		
1	Tip of ramus (obturator foramen side)	Type III
2	Base of pubis articulation (obturator foramen side)	Type III
3	Anterior end of acetabular articular surface	Type III
4	Posterior end of acetabular articular surface	Type III
5	Superior extent of ischial tuberosity	Type II
6	Tip of ramus (inferior side)	Type III
7	Ischial spine	Type II
Semi-landmarks (ischium)		
8-38	Along ramus (obturator foramen side); between fixed landmarks 1 and 2	
39-84	Acetabular articular surface; between fixed landmarks 3 and 4	
85-121	Ischial tuberosity; between fixed landmarks 5 and 6	

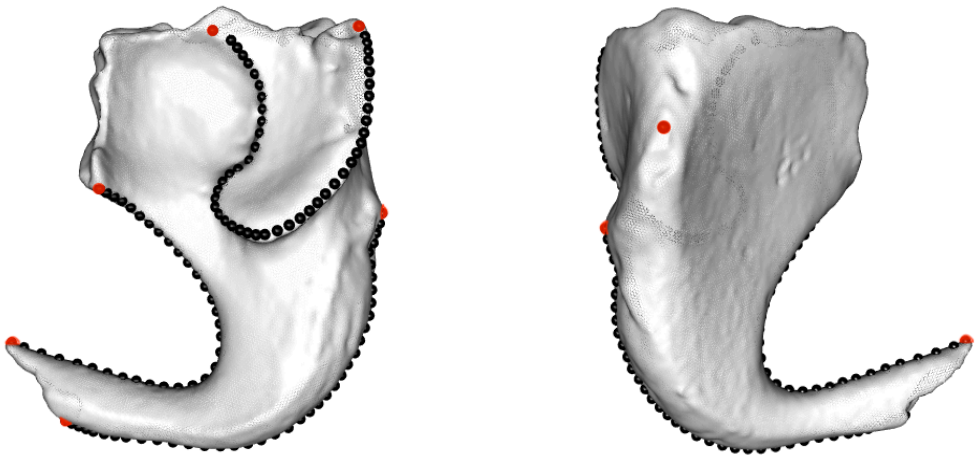

Figure 4.2 Landmark placement across the ischium, highlighting the fixed landmarks (red) and the sliding semi-landmarks (black).

Following Wilson *et al.* (2014), the iliac crest and the greater sciatic notch were semi-landmarked on the ilia. Wilson and colleagues also placed semi-landmarks on the auricular surface but found much lower shape variability between groups at that area, so three fixed landmarks were chosen to represent that region instead. General patterns of landmark placement

established by Estévez Campo *et al.* (2018) were referenced when selecting landmark locations for the ischia, but adjustments had to be made to accommodate the 3D nature of the data in this study since Estévez Campo and colleagues used 2D data in their analyses. Ultimately, landmark locations were selected to capture overall shape for each bone throughout ontogeny.

4.1.2 Landmark Placement

The software package Stratovan Checkpoint (Stratovan Corporation, 2018) was used to lay fixed and semi-landmarks on the 3D models of pelvic bones. In this program, fixed landmarks were placed on each bone (11 for the ilia and 7 for the ischia) and a template of semi-landmarks was created that could be automatically placed on each individual bone based on the fixed landmark locations. The template feature does not always find the edges of features precisely, so the exact placement of the semi-landmarks was manipulated as necessary once the template was lain within the graphical user interface of the Checkpoint software. With the raw landmark data exported into individual spreadsheets (one per bone, per individual) these landmark coordinates were then brought into R v.4.0.3 (R Core Team, 2020) to slide the semi-landmarks using the Morpho package (Schlager, 2017). Using the updated slid coordinates, further analyses could be performed including generalized Procrustes analyses and principal components analyses, which will be discussed in Sections 4.1.3 and 4.4, respectively. See Appendix E for R code.

4.1.3 Generalized Procrustes Analysis

With the landmark data from the pelvis bones, generalized Procrustes analyses (GPA) were performed in R using the Morpho package (Schlager, 2017) to facilitate shape analyses.

GPA extracts size, position, and orientation elements out of the landmark data so that only information about shape remains (Klingenberg, 2012c). To remove size data, each set of landmarks is scaled to a standard size based on its centroid size; the centroid size for each set of landmarks (and therefore for each individual bone) is calculated as the square root of the sum of the squared distances of all the landmarks to a central point (Klingenberg, 2012c). To remove positional data, the centroid of each set of landmarks is shifted to the coordinates of (0, 0, 0). Finally, to remove orientation data, sets of landmarks are rotated so that the squared distances between homologous landmarks across different individuals are minimized as much as possible; a GPA will go through several iterations in order to find the orientation that best fits the data set as a whole (Klingenberg, 2012c). For the ilium landmark data, a GPA was applied to the ontogenetic sample as a whole and then also to each population group individually to facilitate analyses of shape variation both between and within groups. The same analyses were repeated with the ischium landmark data.

4.2 Age Estimation

Estimations of age for all four sample populations were largely provided by Lesley Harrington based on the QMUL Atlas of Dental Eruption (AlQahtani *et al.,* 2010) where dentition and dental x-rays were available. Of the 169 juvenile individuals included in this study, the QMUL method was used to estimate age-at-death for 148 individuals (87.6%).

For individuals from the LSA sample for whom dental data was not available (9 of 72 individuals – 12.5%), age estimations based on long bone lengths, provided by Lesley Harrington, were used. Sample-specific regressions based on nine different long bone lengths were generated and are described in detail in Harrington (2010).

For individuals from the Indian Knoll sample for whom dental x-rays were not taken during the data collection for this project (3 of 38 individuals – 7.9%), estimations based on standards published in Smith (1991) and Liversidge & Molleson (2004) were provided by Libby Cowgill. Details about this data collection are outlined in Cowgill (2008).

For individuals from the Point Hope sample for whom dental data was not available (2 of 15 individuals – 13.3%), age estimations based on long bone lengths, provided by Libby Cowgill, were used. Sample-specific regressions based on femoral, tibial, or humeral length were generated and are described in detail in Cowgill (2008). Distinct formulae were devised for individuals aged two years and younger and those aged three years and older since the relationship between age and long bone length is not linear (Cowgill, 2008).

Finally, for individuals in the Sadlermiut sample for whom dental data was not available (7 of 44 individuals – 15.9%), I devised formulae based on femur length and/or ilium breadth (Cardoso *et al.*, 2014; Cardoso *et al.*, 2017) depending on which elements were present to estimate age at death. Since skeletal growth velocity is quicker in individuals under two years of age than in individuals over two (Humphrey, 2003), different formulae were created for those under and those over two years of age, similar to the approach taken by Cowgill (2008). If both the femur and ilium were present, age estimation results from the two formulae were averaged. See Appendix F for classical calibration plots and equations used to estimate age for the Sadlermiut individuals without dental data. To align the age estimates from the classical calibration formulae to those made with the QMUL atlas, the estimated values were rounded to the nearest 0.5 value and thereby placed into a "bin" per the QMUL method.

Individuals with estimated ages-at-death between 7.5 fetal months and 23.5 years of age were included in the ontogenetic sample of this study; ages-at-death of all individuals, as well as

the method used to estimate age, are listed in Appendix A. While studies of juveniles often use 17 years of age as the end point of the non-adult period (e.g., Lewis, 2007), individuals up to 23.5 years of age were included in this study since the bones of the pelvis continue to grow and fuse during this period. The sample was divided into age cohorts for certain analyses to investigate patterns both within and between age groups. Based on the work of Cowgill (2010), individuals were divided into 6 age groups: less that 1 year of age, 1 to <6 years of age, 6 to <12 years of age, 12 to <18 years of age, 18-24 years of age, and adult (over 24 years of age). These age cohorts were chosen as they are broad enough to ensure sample sizes did not become too small in individual groups but narrow enough to allow for investigation of age-specific patterns.

4.3 Cross-Sectional Geometric Data

4.3.1 CSG Data Collection

Cross-sectional geometric (CSG) measures of the humerus, femur, and tibia were collected for each individual (where available) at the midshaft of each bone. The polar second moment of area (J), a measure of bending and torsional rigidity, was used to quantify loading history of the bone in this study. J is calculated by adding I_{max} (maximum bending rigidity) to I_{min} (minimum bending rigidity) and characterizes a bone's ability to resist bending and torsion, and by extension is considered a good representation of loading history (Ruff, 2019).

Cross-sectional measures were collected by multiple observers: Libby Cowgill provided CSG data for the Indian Knoll and Point Hope samples, Lesley Harrington provided data for the femora and humeri for most of the LSA sample, and research assistant Sydney Holland and I collected the CSG data for the tibiae and remaining humeri and femora of the LSA individuals, and all three bones for the Sadlermiut sample.

Two different methods were used to capture and create cross-sectional images; both methods involve measuring cortical thicknesses on bi-planar radiographs, but the periosteal contour was captured in two different ways. Cowgill and Harrington located the periosteal contour using a method similar to the latex cast method (LCM) (O'Neill & Ruff, 2004; Sakaue, 1997; Stock, 2002; Trinkaus & Ruff, 1989), which involves a silicone mould being placed around a bone to capture the cross-sectional shape of the periosteal contour. The mould is then removed and the contour shape digitized with the use of a flatbed scanner. Using measurements of cortical thickness taken from biplanar radiographs, endosteal contours are drawn onto the digitized periosteal contours following periosteal shape (rather than an ellipse) to create an image that reflects true cross-sectional shape (see Cowgill, 2008, and Harrington, 2010, for more detailed descriptions of these methods). CSG data provided by Cowgill were calculated using a PC-DOS form of SLICE (Nagurka and Hayes, 1980; Eschman, 1992) and data provided by Harrington were calculated using the ImageJ plugin MomentMacroJ (Ruff, n.d.).

For the Sadlermiut and remaining LSA individuals, for whom CSG data had not been provided, cross-sectional periosteal contours were captured in GeoMagic Design X™ by slicing 3D models. Cortical thickness measurements were taken on radiographs using ImageJ2 v.2.3.0. Drawing of endosteal contours onto periosteal contours, based on the radiograph measurements and following the outline of the periosteal contour, was then also done in ImageJ2 (see Figure 4.3 for an example of a completed contour). Finally, CSG properties were calculated using the ImageJ plugin BoneJ v.1.4.2 (Doube *et al.,* 2010). This set of steps will henceforth be referred to as the "3D model method" (or 3DM). To ensure that both the LCM and the 3DM yield comparable results, a validation study was performed which will be discussed in Section 4.3.2.

For the femoral data provided by Cowgill, midshaft was calculated at 45.5% of intermetaphyseal length, while Harrington and I calculated femoral midshaft at 50% (midshaft of the humeri and tibiae were calculated at 50% by all observers). Cowgill used 45.5% due to the unequal contribution of the proximal and distal epiphyses to adult femur length (Ruff, 2003b). Sládek and colleagues (2010), however, report only 4.9% mean error between calculations of CSG properties taken at 45% and 50% of the femur, within an accepted error magnitude of 5.0% (Trinkaus & Ruff, 1989; Stock, 2002), and thus it is unlikely that these differences in section location introduced significant or meaningful error into the data.

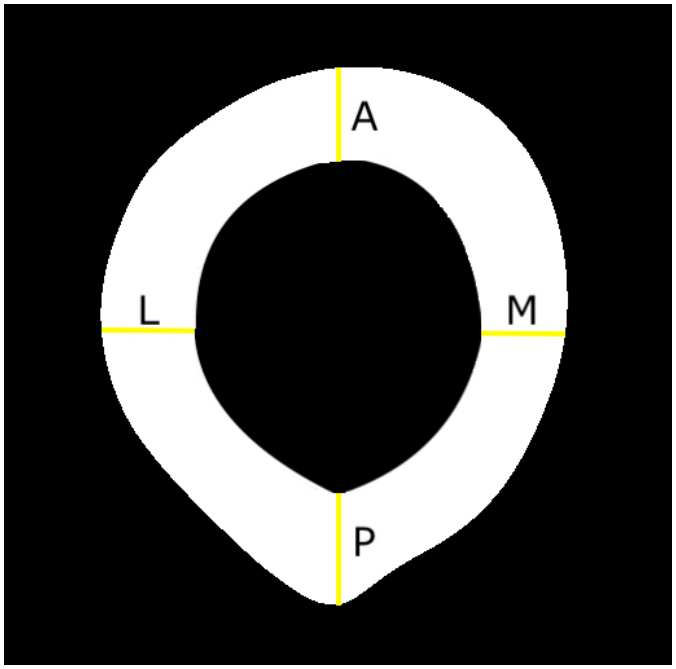

Figure 4.3 Complete cross-sectional image of a femur created using the 3DM with the anterior (A), posterior (P), lateral (L), and medial (M) cortical measurements indicated.

4.3.2 CSG Data Collection Methods Validation

A validation study was conducted to verify that the CSG results obtained using the LCM (collected by Libby Cowgill and Lesley Harrington) and the 3DM (collected by myself and

Sydney Holland) were comparable. Sparacello and Pearson (2010), Stock (2002), and O'Neill and Ruff (2004) all report that CSG data obtained using the LCM are comparable to that of true cross sections (obtained from either direct sectioning or CT scans). While these studies focused on locating the endosteal contour, and this validation test focused on potential differences in the periosteal contour, the positive results from these studies, with their overall aim of comparing results from different methods of cross-sectional data collection, led to the hypothesis that the LCM results would be comparable to those sectioned from 3D models.

For the validation study, femoral CSG data from 30 LSA individuals, captured using the LCM and provided by Lesley Harrington, were selected. I then re-collected the data using the 3DM to compare resulting values with the LCM data. Solid cross-sections were used in order to focus the analysis on differences in the periosteal contour specifically, as the method used to identify the endosteal contour was the same across all observers. Values were natural log transformed to account for non-normal distributions of the raw data, and ordinary least-squares regression was used to calculate how accurately data obtained via the LCM could predict that obtained using the 3DM. Prediction accuracy was assessed through the calculation of percent standard error of the estimate (%SEE) (following Ruff, 2003a) using log-transformed data [equation 1]. Absolute mean percent prediction error (%PE) [equation 2] and directional mean percent prediction error (bias %PE) [equation 3] were calculated using raw 3DM data as the "observed" and back-transformed predicted data as the "estimated."

Equation 1: $\%SEE = \exp(SEE + 4.6052) - 100$

Equation 2: $\%PE = \frac{|observed - estimated|}{estimated} \times 100$

Equation 3: $\text{Bias } \%PE = \frac{observed - estimated}{estimated} \times 100$

Results of the validation test revealed a %SEE of 7.86 (below the accepted magnitude of 8.0, as reported in Macintosh *et al.,* 2013 and citations therein), mean %PE of 5.59 (slightly above the accepted magnitude of 5.0) and a mean bias %PE of 0.27. Although the mean %PE was slightly above the accepted magnitude, the low %SEE and low bias %PE gave confidence that there was no systematic bias in the data, and CSG data obtained from the LCM and the 3D models were deemed comparable.

4.3.3 Size Standardization – Body Mass Estimation

Following Ruff (2019), CSG parameters were size-standardized using estimations of body mass and long bone lengths. Body mass was estimated using the reduced-major axis (RMA) regression equations published in Ruff (2007) (Table 4.3), which were developed using data from the Denver Growth Study (DGS) (Maresh, 1970; McCammon, 1970). In his paper, Ruff (2007) provides two sets of body mass estimation equations generated from the DGS data – ordinary least squares (OLS) regression equations and RMA regression equations, with RMA equations recommended for use with populations outside the expected body size range of the DGS participants (Ruff, 2007).

Table 4.3 Equations used for body mass estimation.

Age (years)	RMA FMB		RMA Log FMB		RMA FHB		RMA Log FHB	
	Slope	**Int**	**Slope**	**Int**	**Slope**	**Int**	**Slope**	**Int**
0.33*	0.357	-3.8	1.649	-3.672				
1	0.304	-1.4	1.157	-1.9				
2	0.343	-3.0	1.235	-2.2				
3	0.445	-7.4	1.503	-3.2				
4	0.518	-9.9	1.595	-3.5				
5	0.543	-10.4	1.600	-3.5				
6	0.581	-11.2	1.581	-3.3				
7	0.606	-11.1	1.544	-3.1	0.695	3.3	0.908	0.1
8					0.918	-2.2	1.123	-0.6
9					1.662	-25.1	1.781	-2.8
10					2.024	-37.9	2.107	-4.0
11					2.502	-54.7	2.397	-5.0
12					2.548	-58.1	2.344	-4.9
13					3.086	-80.2	2.684	-6.1
14								
15								
16								
17							2.186	-4.2
18+**					2.239	-39.9		
18+***					2.268	-36.5		

*Note: equation for the 0.33 is from Harrington (2010) via a personal communication with Ruff. This equation was not published in Ruff (2007) as it did not reach statistical significance.

**Note: equation is from Auerbach & Ruff (2004), derived from McHenry (1992), and was used to estimate body mass of LSA individuals with estimated ages-at-death greater than 17 years.

***Note: equation is from Grine *et al.* (1995) and was used to estimate body mass of Sadlermiut and Indian Knoll individuals with estimated ages-at-death greater than 17 years.

The individuals included in the DGS were middle and upper-middle class individuals of European descent who grew up in the Denver (USA) area in the 20th century and thus would have had low infectious disease burdens, good nutrition, and relatively low levels of physical activity (when compared with hunter-gatherer populations); they are generally considered to

have had optimal conditions for healthy growth (Ruff, 2022). Looking at previous research on growth timing and adult body size attainment that includes the populations in the current study, all four populations seem to differ from each other and from the individuals included in the DGS. Specifically, the LSA are known to have been a small-bodied population (Pfeiffer & Sealy, 2006), with growth curves that are similar in tempo but differ in magnitude to those of the DGS (Harrington & Pfeiffer, 2008; Pfeiffer & Harrington, 2010). Johnston (1962) reported that growth curves of the Indian Knoll population differed from those of the DGS with statistical significance after 2 years of age, and Sundick (1978) reported that individuals from Indian Knoll show similar growth rates to individuals from a 6^{th}-7^{th} century European sample prior to puberty, but that the groups diverge after puberty. For both the Sadlermiut and Point Hope populations, long bones measurements reported by Symchych (2016) demonstrate relatively shorter limbs when compared with the individuals from the DGS. Symchych (2016) also reported that the Sadlermuit juveniles lagged in their growth in comparison to the DGS means, while the Point Hope juveniles showed a diverse range of growth patterns (some were consistent with the growth tempo reported in the DGS, but some lagged and some were accelerated). Due to this variation in growth patterns and body size attainments in comparison to the DGS, RMA regression equations, as reported by Ruff (2007), were chosen to estimate body mass.

Since Ruff (2019) does not provide equations for 14–16-year-olds, body mass estimations for individuals in this age range were calculated by averaging the results of estimations taken with both the 13- and 17-year-old equations. Previous studies (e.g., Harrington, 2010) made population-specific regression equations for the 14–16-year age group using data from the 13- and 17-year age groups, but small sample sizes in those age groups in this study meant this was not a feasible option. Similarly, the equation for the 3-month age category was used for all

individuals aged 6 months and younger. For individuals in the 7-year age class, for whom formulae are available for both the femoral distal metaphysis and the femoral head epiphysis, body mass estimations made using the head epiphysis were used where possible because Ruff (2007) states that femoral head measurements provide better estimations than do distal metaphyseal breadths.

For the LSA individuals over 17 years of age, the body mass estimation equation based on femoral head diameters as reported in McHenry (1992), modified by Auerbach & Ruff (2004), was used since it is well-suited for small-bodied populations (Auerbach & Ruff, 2004; Kurki *et al.,* 2010). The equation from Grine *et al.* (1995) was used to estimate body mass for the individuals over 17 years of age in the Sadlermiut and Indian Knoll populations. This equation has been shown to perform well with larger-bodied populations and was recommended for use with North American archaeological populations (including the Sadlermiut) by Auerbach (2008). There were no individuals between ages 17 to 24 years in the Point Hope sample.

4.4 Statistical Analyses

Principal components analyses (PCA) were performed on each set of Procrustes-fit landmark data to identify major axes of shape variation using the R package Morpho (Schlager, 2017). The resulting principal components (PCs) were plotted against one another to look at relationships of morphological variation, as well as against age and centroid size data to explore age and size-related changes in pelvic morphology. Box plots of residuals from these regressions were created in SPSS v.27 (IBM Corp, 2020) and in R. PCs were also plotted against CSG data to examine relationships between pelvic morphological variation and markers of activity. Both linear and non-linear regressions were used to explore these patterns using the

base package in R v.4.0.3 (R Core Team, 2020) and were visualized using ggplot2 (Wickham, 2016). Residuals from the regressions of PC data on age were plotted onto CSG data (and residuals from regressions of CSG data on age) as a means of controlling for age-related changes when exploring relationships between pelvic shape variation and activity.

To further investigate differences between the samples within the PC data, ANOVAs were conducted in R v.4.0.3 (R Core Team, 2020). Shapiro-Wilk tests and Q-Q plots were used to test for normality, and Levene's tests and scale-location plots were used to test for homogeneity of variance. According to the results of the normality and variance tests, one-way ANOVAs, Welch's ANOVAs, or Kruskal-Wallis tests were applied as relevant. When results indicated that group differences were large, post-hoc Tukey honestly significant difference (HSD) tests, Games-Howell tests, or Dunn's tests were used to compare all populations to each other and see where the differences were significant.

4.4.1 Investigating Allometry

Allometry describes shape variation that is related to size variation and is thus a key concept in studies of ontogenetic morphologies (Klingenberg, 2012d). Static allometry compares organisms of different sizes at the same developmental stage to see how size differences impact shape differences, while ontogenetic allometry considers shape differences that are due to growth, and frequently employs growth trajectories to see how differences in size at different points along the trajectory are related to differences in shape (Klingenberg, 2012d). In order to investigate ontogenetic allometry, regression scores were calculated from a multivariate regression of Procrustes residuals on centroid size (Drake & Klingenberg, 2008; Klingenberg, 2022) using the R package Morpho (Schlager, 2017). Regression scores are a

measure showing the relationship between size and shape, based on a projection of the shape data (Procrustes residuals) onto a vector in the direction of allometric change, calculated from both size and shape data (Rohner, 2020). These regression scores were then plotted onto centroid size data and visualized using ggplot2 (Wickham, 2016) to examine the overall relationship between shape variation and size change (Klingenberg, 2016).

4.5 Maturation Analysis

To explore ontogenetic trajectories within the data, maturation analyses were performed based on the methods described in Wilson *et al.* (2014). Maturity trajectories of both shape and size were calculated to compare trajectories between samples and to explore relationships between size and shape across ontogeny. As per Wilson *et al.* (2014), the term "maturation" is employed here to represent a progression in relation to age between a starting point (i.e., infant shape and size) and an endpoint (i.e., adult shape and size).

The starting point of growth for each sample was established by taking the average mean shape and average centroid size of the five youngest individuals in each sample (all of whom were under 1 year of age). Due to sample size issues, however, the starting point of growth for the Point Hope sample was represented by a single individual. The end point of growth was represented by the mean shape and mean centroid size of a group of approximately 20 adults for each sample; since sex of the juvenile individuals is not known, an even mix (where possible) of male and female adult individuals were chosen to represent an average pelvis shape and size for each population. All the individuals in each sample were then organized in ascending age order, a GPA was performed on each sample group, and Procrustes distances were calculated between each individual within a group.

To calculate size maturation within each sample, the centroid size of each individual was expressed as a percentage of the adult centroid size mean (which represented 100%). To calculate shape maturation within each sample, a cumulative score of the Procrustes distances between individual mean shapes was calculated for each individual by adding together the scores of all the younger individuals (so the score for the third individual in the sample would equal the sum of the Procrustes distances between the mean shape of the starting point and the mean shape of individual 1, between individuals 1 and 2, and between individuals 2 and 3). This method, however, applies longitudinal thinking to cross-sectional data, assuming that an individual at one age has passed through all the shapes associated with the ages before it; a sliding average approach was therefore applied to attempt to mitigate some of this assumption. In groups of five with an overlap of three individuals per group, the average Procrustes distance values were calculated to represent that group (so group 1 was represented by the average of the Procrustes distances between the mean shapes of individuals 1-5, group 2 was individuals 3-7, etc.). These sliding group averages were then expressed as percentages of the adult mean, with the adult means representing 100% of growth completed. This maturation analysis was conducted in R v.4.0.3 (R Core Team, 2020) using the geomorph (Adams & Otárola-Castillo, 2013) and shapes (Dryden, 2021) packages, and the maturity trajectories were represented graphically using ggplot2 (Wickham, 2016). See Appendix G for R code.

CHAPTER 5: ILIUM SHAPE RESULTS

In this chapter, results of the ilium shape analyses are presented. With Procrustes-fit ilium landmark data, principal components analyses (PCA) were used to look at variation both within and among samples. As such, PCAs were run on the combined-sample ilium landmark data, and then on each individual sample (Indian Knoll, LSA, Point Hope, and Sadlermiut). With these results, variation across the whole sample (and among groups), as well as variation within groups, were explored using regression and ANOVA. Age and centroid size data were analysed in conjunction with PCA scores as a means of investigating ontogenetic patterns and were combined with Procrustes distances to explore maturity trajectories of shape and size. Further, regression scores were calculated from Procrustes residuals and centroid size data to explore allometric relationships within the data. General patterns of long bone robusticity between samples were explored through measures of J standardized by body mass and ratios of measures of J. Graphs of ilium PCA data plotted onto measures of J are then presented to explore relationships between ilium shape and activity.

To look at overall patterns of size change, ilium centroid size data were plotted on age (Figure 5.1). The youngest individuals in all samples are quite closely clustered, but by five years of age the trajectory of the LSA sample has diverged from the others and remains smaller throughout the growth trajectory; due to the overall small body size of the LSA population, this is an expected result. In contrast, the Point Hope sample consistently plots slightly larger in centroid size for a given age compared to the other samples. In all samples, the data are best fit with a quadratic curve, showing that the relationship between size and age is not linear. PCA

results were, therefore, regressed onto both age and centroid size as a means of exploring ontogenetic patterns.

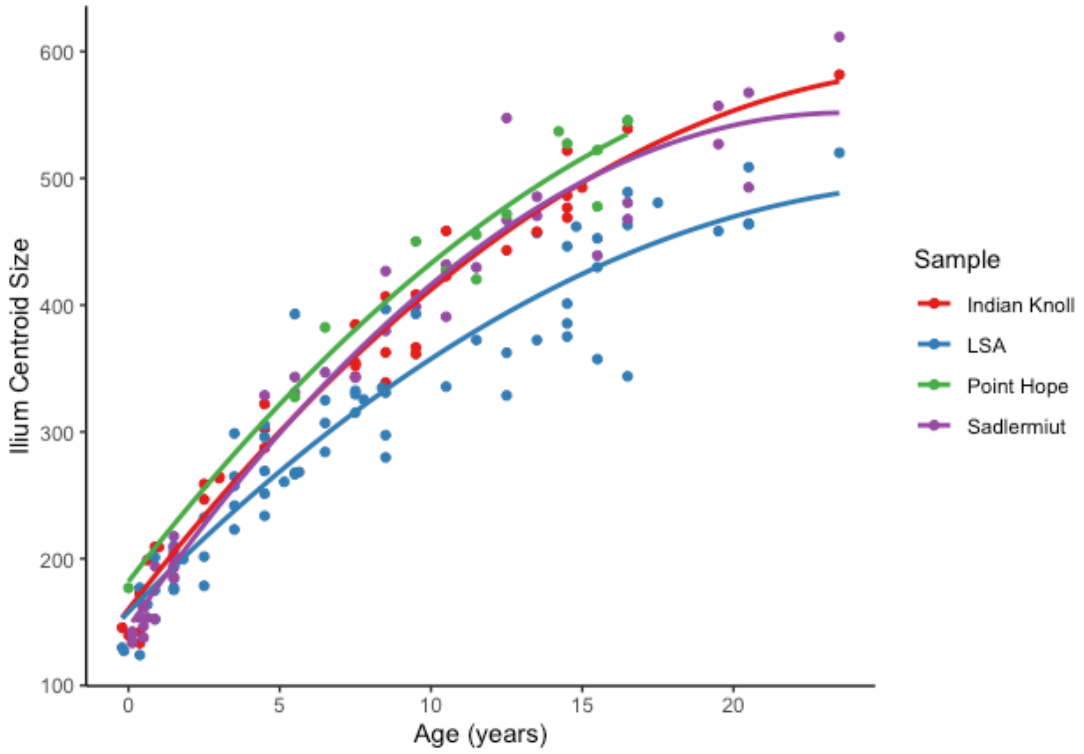

Figure 5.1 Ilium centroid size plotted on age, fitted with quadratic lines of best fit.

5.1 Principal Components Analysis – Introduction

In the combined-sample principal components analysis (PCA), principal component (PC) 1 and PC2 together represent more than half of the total variation in the ilium sample (53.38%) (Table 5.1). In the within-sample PCAs, PC1 of the LSA captures the lowest percent of the overall variation compared to the other groups (25.54%), meaning that the variation in this sample is spread out across more axes, while PC1 of the Sadlermiut captures the highest percentage of the overall variation in comparison with the other groups (40.04%). The percentage of variance captured by PCs 1-9 are reported for the combined sample as well as for each individual sample in Table 5.1; PC9 was chosen as a cut-off since more than 80% of the

variance is represented across the PCs by this point in all samples. As a summary, the cumulative total of variance captured is provided at PC10.

Table 5.1 Percentage of shape variance in the ilia captured by PCs 1-9, with the cumulative total provided at PC10, for the combined sample and each sample separately.

Principal Component	Combined Ilium Sample (n=161)	LSA (n=66)	Indian Knoll (n=38)	Sadlermiut (n=43)	Point Hope (n=14)
PC1	30.50	25.54	32.06	40.04	32.44
PC2	22.88	20.71	16.05	16.18	25.53
PC3	7.65	9.56	8.69	8.75	11.86
PC4	5.56	6.79	7.58	6.57	9.14
PC5	4.32	4.79	6.26	4.26	5.82
PC6	3.71	4.53	4.27	3.79	3.84
PC7	3.01	3.79	3.84	2.89	3.25
PC8	2.69	2.91	3.31	2.25	2.56
PC9	2.14	2.38	2.25	1.80	1.98
PC10 (cumulative)	84.19	83.23	86.13	88.19	97.80

5.2 Principal Components Analysis – Combined Sample

5.2.1 Overview

As the percentage of the total variance that is captured by the PCs drops off fairly substantially after PC3 (values for PC4 and higher are below 10% across all samples), the first three PCs were selected for further examination. These are displayed using lollipop graphs to visually inspect the axes of variation; 3D lollipop graphs plot landmark points at one extreme of the variation represented by a PC and a line extends out to the other extreme, representing the magnitude and direction of the variation captured at that landmark. In the lollipop graph of the combined-sample ilium data (Figure 5.2), PC1 (representing 30.50% of the total variance in the sample) appears to capture variation in three main regions of the ilium: the inferior

limit/acetabular area, the greater sciatic notch, and the iliac crest. Along this PC1 axis, landmarks placed at the base of the arcuate line, on the anterior edge of the acetabulum, and on the anterior inferior iliac spine capture variation in the superior-inferior direction at the inferior limit of the bone, representing variation in the overall length of the ilium. This PC also captures variation in the depth of the greater sciatic notch, which ranges from a flattened curve to a deep notch. Finally, PC1 captures variation along the iliac crest, mainly in the superior-inferior direction, capturing variation in both the height and asymmetry of the curve. See Figure 5.3 for examples of variation seen across this PC.

PC2 of the combined-sample ilium landmark data (representing 22.88% of the total variance) captures variation in the overall curvature of the bone. This can be seen in the medio-lateral variation captured by PC2 along the iliac crest and at the greater sciatic notch, as well as the medio-lateral movement of the landmarks around the auricular surface. PC2 also captures variation in the landmarks on the anterior edge of the acetabulum and the anterior inferior iliac spine in a diagonal direction (a combination of medio-lateral and superior-inferior movement), representing variation in the protrusion of the inferior portion of the ilium compared with the superior portion (Figure 5.4). PC3 (representing 7.65% of the total variance) appears to mainly capture variation in breadth towards the anterior end of the bone, as well as curvature in the iliac crest.

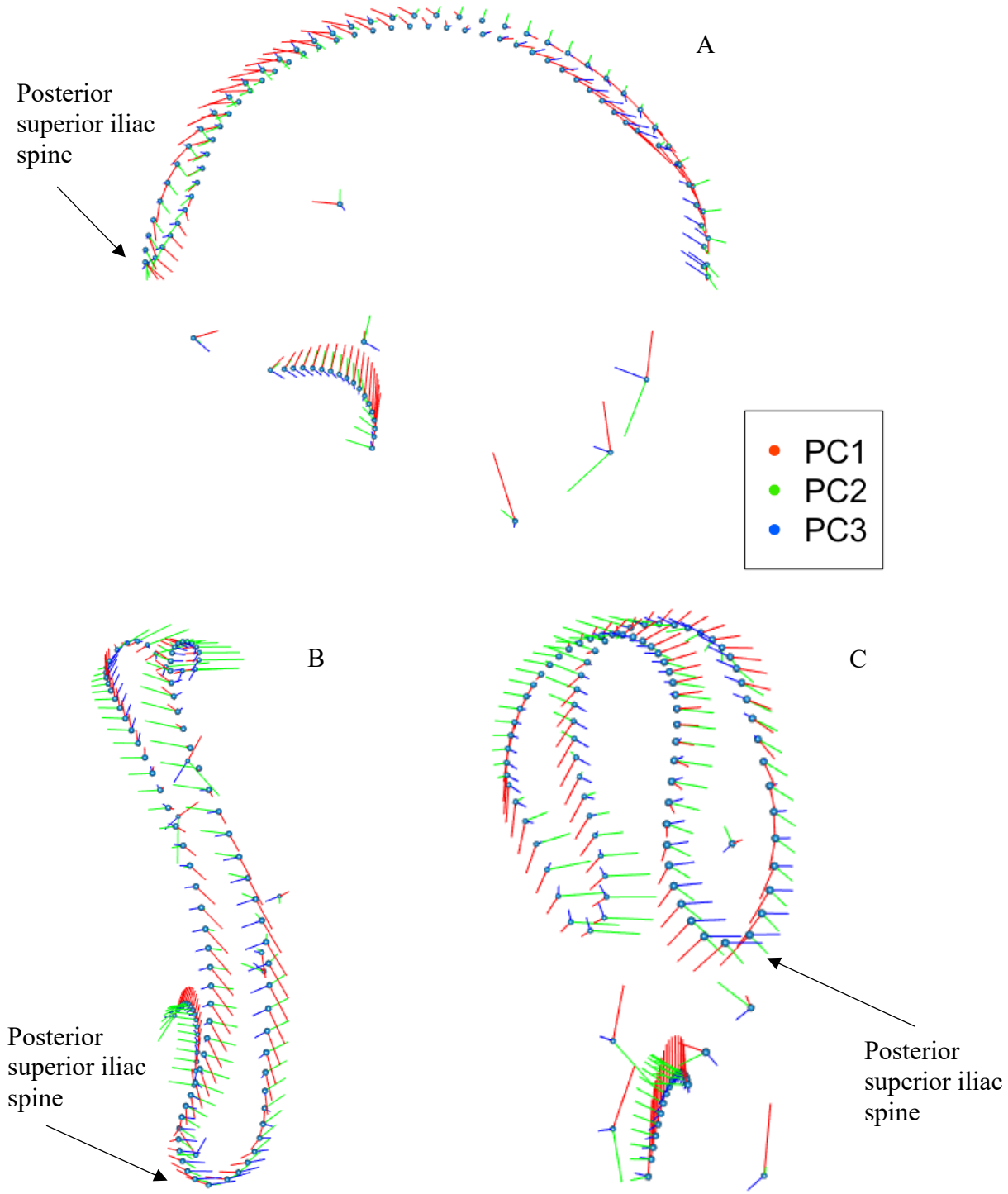

Figure 5.2 PCs 1-3 of the ilium for the combined sample, with lines representing the extent of variation represented by each PC at each landmark location. A) pelvic view (medial); B) superior view; C) posterior view.

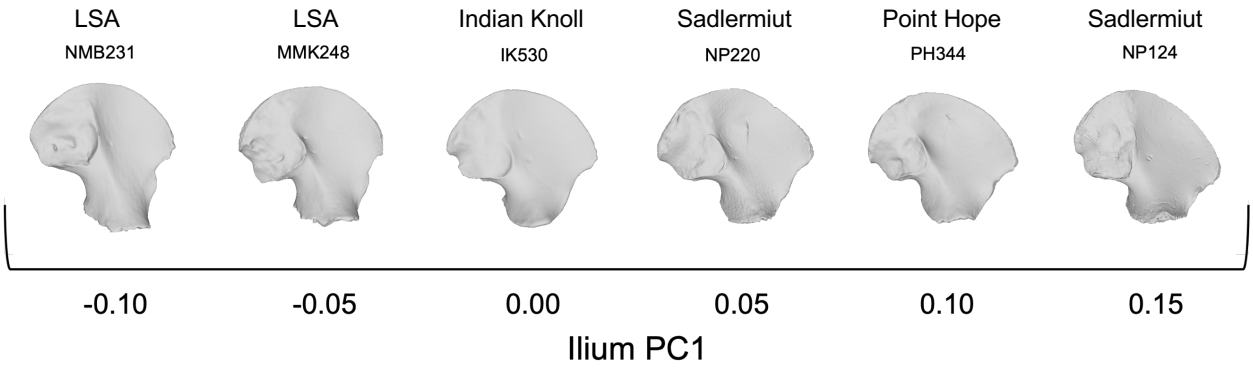

Figure 5.3 Examples of variation as represented along PC1 in the combined sample.

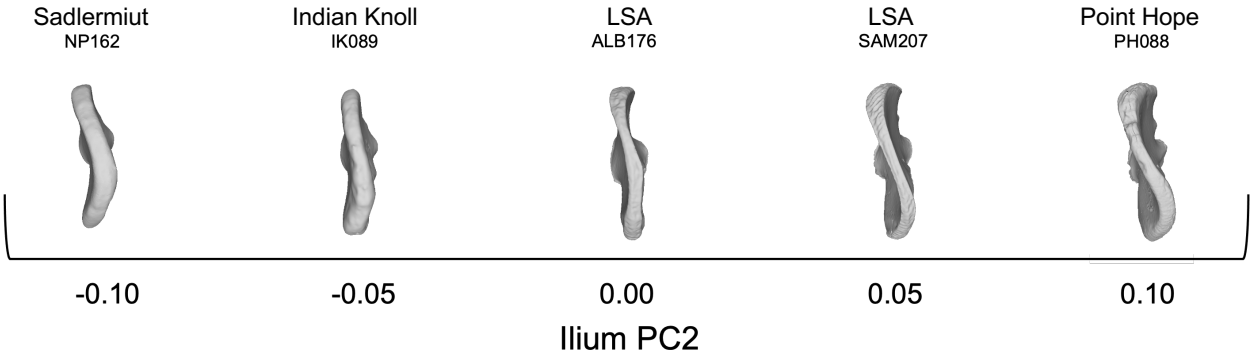

Figure 5.4 Examples of variation as represented along PC2 in the combined sample.

When plotted against one another, PC1 and PC2 of the combined-sample ilium data do not show a consistent pattern (Figure 5.5), meaning that the variation in ilium curvature captured by PC2 does not vary consistently with the length and breadth variation captured by PC1. A degree of separation is visible between the samples along the PC1 axis, with the Point Hope and Sadlermiut plotting towards one end of the x-axis, and the Indian Knoll and LSA plotting towards the other; sample separation is not seen along the PC2 axis, however. When age categories are identified, a rough gradient is visible along the y-axis, showing some patterning of age categories along the PC2 axis. To further illustrate the distinction of the age categories along the PC2 axis, Figure 5.6 plots the confidence ellipses distinguishing age categories instead of the sample groups. While overlap between the age groups is certainly evident, a gradient is visible

across the y-axis, with the youngest age categories plotting at one end and the oldest at the other.

See Appendix H for comparative plots of further PCs.

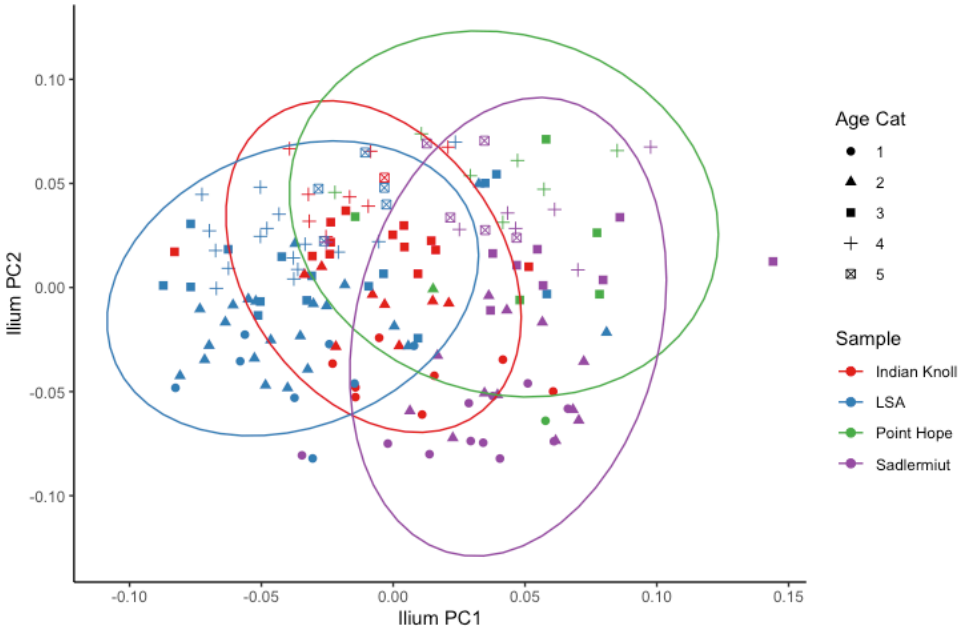

Figure 5.5 PC1 vs. PC2 of the combined-sample ilium data, shown with 95% confidence ellipses around sample groups. Age categories: 1 (less that 1 year of age), 2 (1-<6 years), 3 (6-<12 years), 4 (12-<18 years), and 5 (18-24 years).

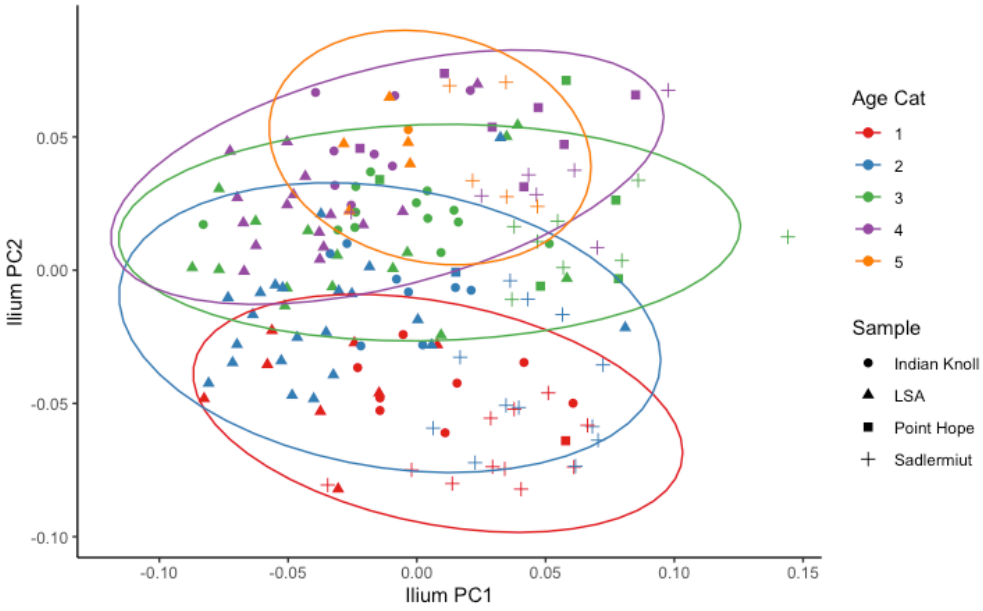

Figure 5.6 PC1 vs. PC2 of the combined-sample ilium data, shown with 95% confidence ellipses around age categories. Age categories: 1 (less that 1 year of age), 2 (1-<6 years), 3 (6-<12 years), 4 (12-<18 years), and 5 (18-24 years).

5.2.2 PC1 vs. Age

As seen in Figure 5.5, PC1 of the combined-sample ilium landmark data demonstrates a degree of separation between the terrestrial foraging groups (Indian Knoll and LSA) and the Arctic/marine foraging groups (Sadlermiut and Point Hope). When PC1 is plotted onto age data (Figure 5.7), the pattern remains consistent across age, with the extreme on the negative end of the principal component (made up largely of the LSA) representing an ilium shape that is long through the arcuate line and relatively narrow between the iliac spines, and the extreme on the other end (where the Sadlermiut and Point Hope fall) representing an ilium shape that is shorter through the arcuate line, broader between the spines, and slopes somewhat asymmetrically across the iliac crest. In the plot of PC1 on age, the lines of best fit are largely horizontal (Figure 5.7, B); it is notable that the variation in ilium morphology represented by PC1, that of the most significant axis of variation, does not show a relationship with age in any of the forager samples (see Table 5.2 for regression results) but does seem to highlight group separation. A plot of the standardized residuals calculated from a common regression line of the combined sample (Figure 5.8) also shows the medians of the Indian Knoll and LSA plotting lower than those of the Point Hope and Sadlermiut and shows that the spread of data points is broadest in the LSA. ANOVA results and group separation will further be discussed in Section 5.2.4.

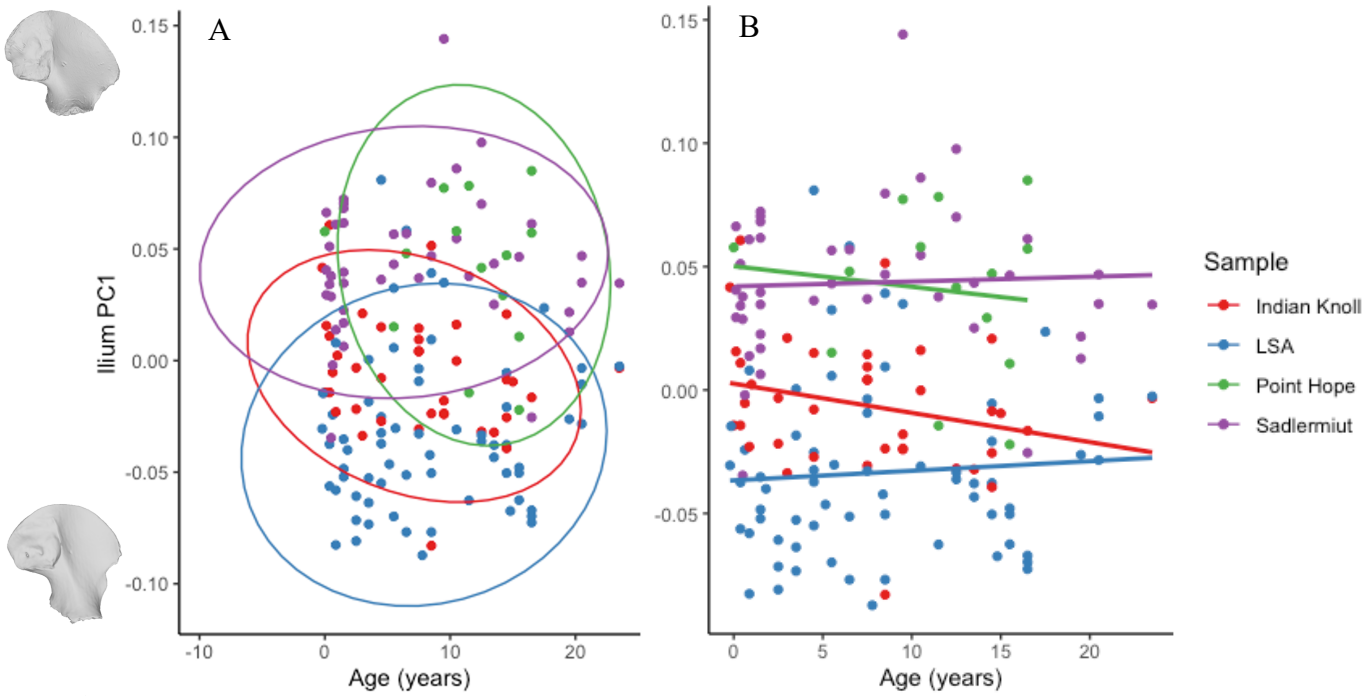

Figure 5.7 Age vs. ilium PC1 shown with A) ellipses representing 95% confidence intervals, and B) linear regression lines. Marine-based foragers plot towards the top, while terrestrial foragers plot towards the bottom. No clear relationship with age is evident.

Table 5.2 Results of the linear regression of the combined-sample ilium PC1 data on age, separated by sample.

Sample	**R^2**	**SEE**	**p-value**
Indian Knoll	0.066	0.026	0.119
Later Stone Age	0.005	0.035	0.577
Point Hope	0.014	0.034	0.682
Sadlermiut	0.002	0.031	0.772

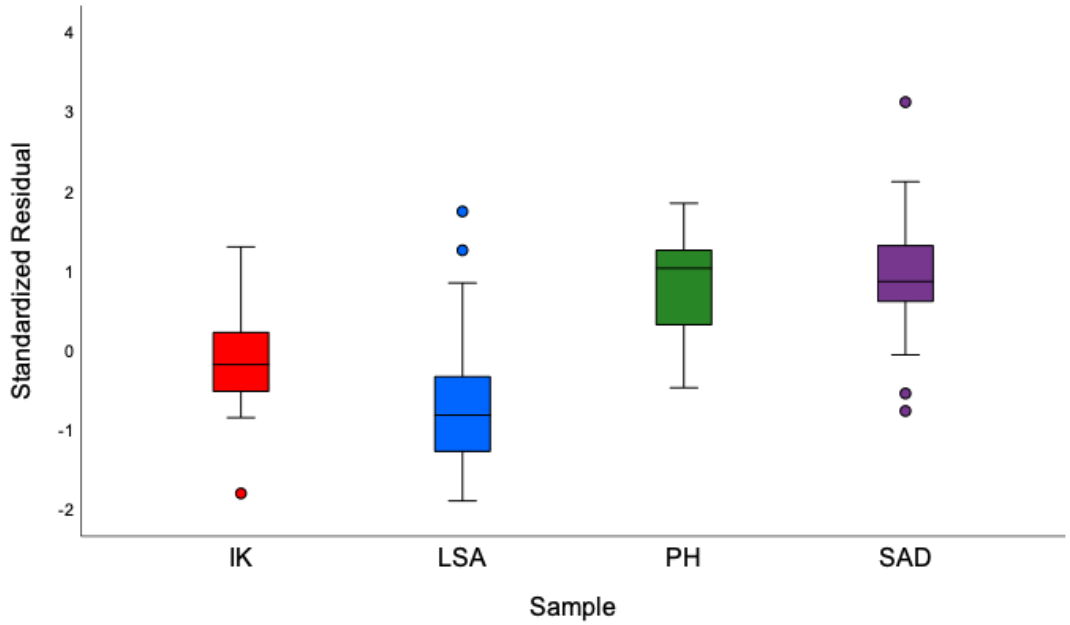

Figure 5.8 Standardized residuals from the linear regression of the combined-sample ilium PC1 on age, separated by sample. Marine-based foragers plot further up while terrestrial foragers plot further down. Boxes represent the middle 50% of the data, between quartiles 1 and 3, the line through the box represents the median of the data, and whiskers extend to the minimum and maximum values in each sample, up to 1.5x the interquartile range; the dots represent values that are greater or lesser than the 1.5x range.

5.2.3 PC2 vs. Age

Where the first principal component does not show a relationship with age, the second PC from the combined-sample PCA of the ilium landmark data demonstrates a positive relationship with age, and no separation between the samples (Figure 5.9). The lines-of-best-fit for the LSA and Sadlermiut fall below those of the Indian Knoll and Point Hope, but the LSA sample in particular has quite a large spread of points about the curve (see Table 5.3 for regression results, and Section 5.2.4 for ANOVA results). This variation in the LSA ilium data is highlighted by the relatively low R^2 value of the quadratic regression (0.651) compared to the other groups, and in the spread of the standardized residuals from a common regression line (Figure 5.10).

This PC mainly highlights variation in the curvature of the iliac crest, as well as complexity of shape in the iliac blade, which progresses in a somewhat consistent manner in all samples across age. In the youngest individuals, the crest is mainly a simple C-shaped curve, and the shape of the iliac blade as a whole follows this curve, but during the course of ontogeny the curvature of the crest becomes S-shaped, and the blade takes on a more complex form which does not mirror the crest as directly.

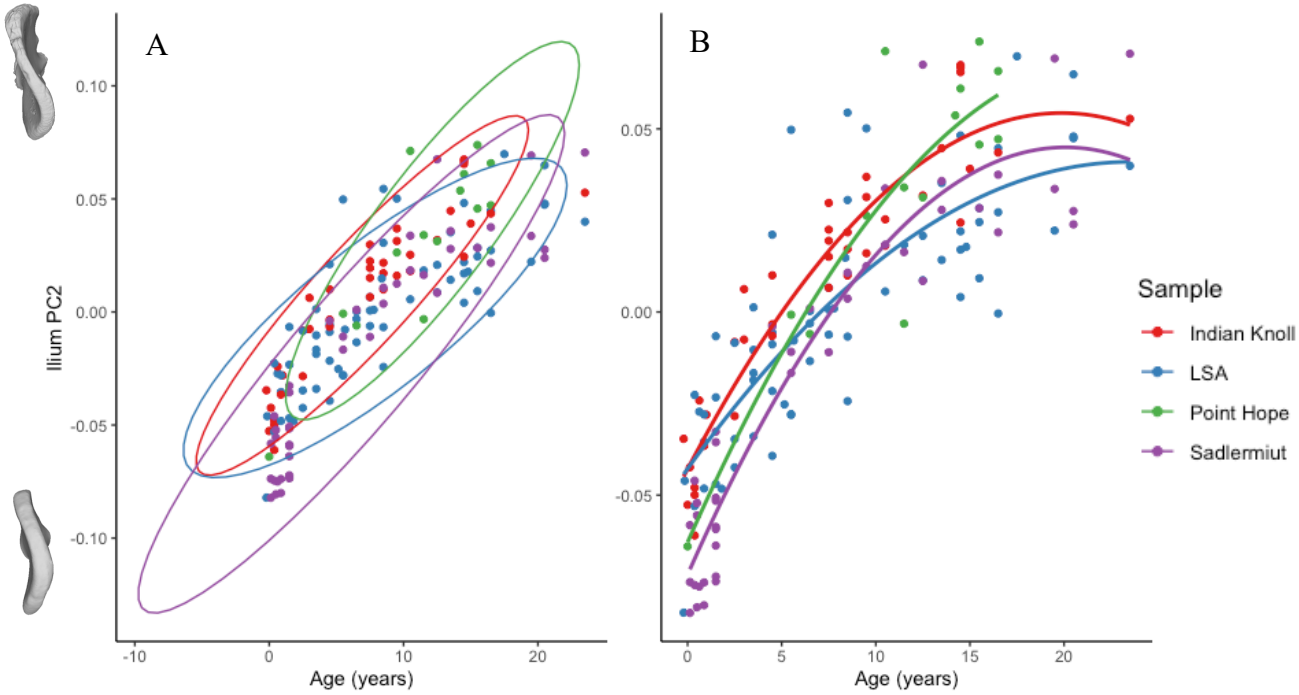

Figure 5.9 Age vs. ilium PC2 shown with A) ellipses representing 95% confidence intervals, and B) quadratic regression lines. All samples show a similar age-related pattern, and no group distinctions are obvious.

Table 5.3 Results of the quadratic regression of the combined-sample ilium PC2 data on age, separated by sample.

Sample	**R^2**	**SEE**	**p-value**
Indian Knoll	0.886	0.012	<0.001*
Later Stone Age	0.651	0.019	<0.001*
Point Hope	0.743	0.020	<0.001*
Sadlermiut	0.895	0.015	<0.001*

*significant result at alpha of $p<0.05$

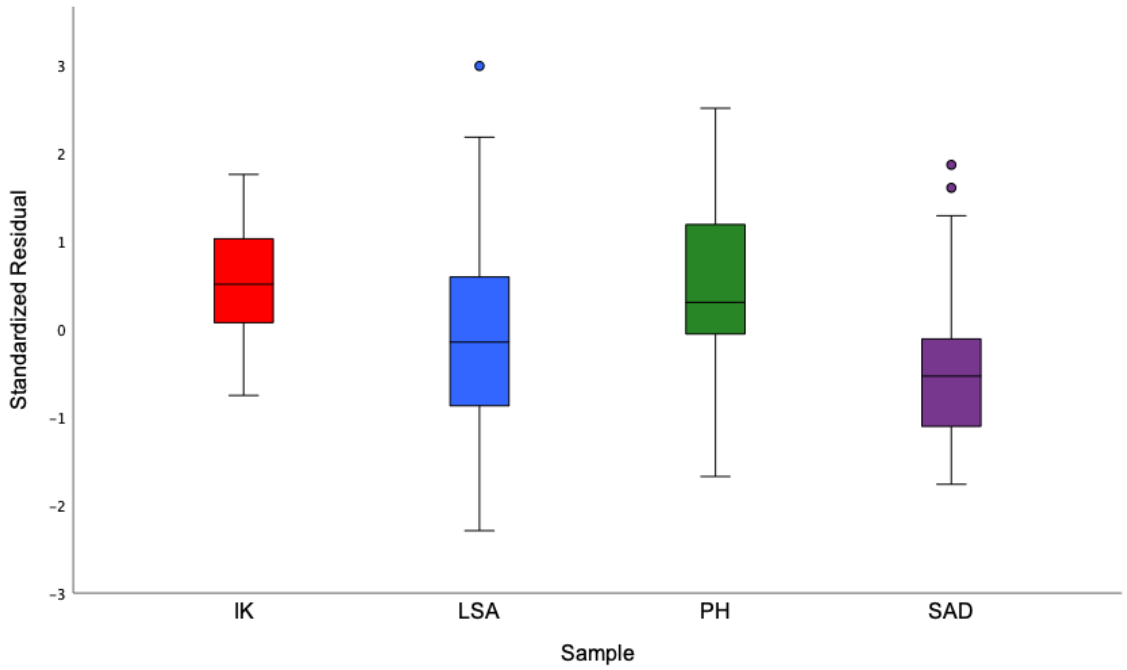

Figure 5.10 Standardized residuals from the quadratic regression of the combined-sample ilium PC2 on age, separated by sample. Boxes represent the middle 50% of the data, between quartiles 1 and 3, the line through the box represents the median of the data, and whiskers extend to the minimum and maximum values in each sample, up to 1.5x the interquartile range; the dots represent values that are greater than the 1.5x range.

5.2.4 Sample Differences

As a means of exploring differences among the samples, an ANOVA was conducted on the PC scores from PC1 of the combined-sample ilium data. Results of Shapiro-Wilk normality tests for each sample within the data (IK: W = 0.959, p-value = 0.177; LSA: W = 0.937, p-value = 0.002; PH: W = 0.935, p-value = 0.357; SAD: W = 0.957, p-value = 0.109) indicate that the data follow a normal distribution for all samples save the LSA. A scale-location plot (Appendix I, Figure I.1) and the results of a Levene's test (F = 0.753, p-value = 0.522) demonstrate that homogeneity of variances can be assumed. Even though the LSA data does not have a normal distribution, ANOVAs are robust to minor divergences from normality; since the other assumptions were met and the other samples had normal distributions of data, one-way ANOVA

was deemed an appropriate test to explore differences among the samples on the PC1 axis of the ilium data. Results suggest that the main effect of the sample on PC1 is statistically significant and large ($F (3, 157) = 58.39$, $p < 0.001$; $Eta^2 = 0.53$, 95% CI [0.44, 1.00]). Eta^2 indicates that more than half (53%) of the variation represented is occurring between the groups, rather than within. Results of a post-hoc Tukey HSD test reveal statistically significant differences between all groups save between the Sadlermiut and Point Hope (Table 5.4, and see Appendix I, Figure I.2 for graphical representation of the results).

Table 5.4 Results of the combined-sample ilium PC1 Tukey HSD test.

Samples Compared	**Adjusted p-value**
LSA-Indian Knoll	<0.001*
Point Hope-Indian Knoll	<0.001*
Sadlermiut-Indian Knoll	<0.001*
Point Hope-LSA	<0.001*
Sadlermiut-LSA	<0.001*
Sadlermiut-Point Hope	0.992

*significant result at alpha of $p<0.05$

Along the PC2 axis, results of Shapiro-Wilk normality tests for each sample within the data (IK: $W = 0.961$, p-value = 0.202; LSA: $W = 0.988$, p-value = 0.793; PH: $W = 0.895$, p-value = 0.094; SAD: $W = 0.918$, p-value = 0.005) indicate that the data follow a normal distribution for all samples save the Sadlermiut. A scale-location plot (Appendix I, Figure I.3) and the results of a Levene's test ($F = 5.331$, p-value = 0.002) demonstrate that homogeneity of variances cannot be assumed. Due to the heteroscedasticity of the data, Welch's ANOVA was used to explore differences between the samples on the PC2 axis of the ilium data. Results indicate that the main effect of the sample on PC2 is statistically significant and moderate ($F (3, 49) = 5.34$, $p = 0.003$; $Eta^2 = 0.24$, 95% CI [0.04, 0.41]). Eta^2 indicates that 24% of the variation

represented is happening between the groups. Results of a post-hoc Games-Howell test reveal statistically significant differences between the Sadlermiut and Indian Knoll samples and the Sadlermiut and Point Hope samples in the PC2 data (Table 5.5).

Table 5.5 Results of the combined-sample ilium PC2 Games-Howell test.

Samples Compared	**Adjusted p-value**
LSA-Indian Knoll	0.712
Point Hope-Indian Knoll	0.218
Sadlermiut-Indian Knoll	0.039*
Point Hope-LSA	0.053
Sadlermiut-LSA	0.152
Sadlermiut-Point Hope	0.003*

*significant result at alpha of $p<0.05$

5.2.5 PCs vs. Centroid Size

To explore the relationship between shape and size, PCA results were regressed onto centroid size data. Particularly since, as noted above, the relationship between age and centroid size is not linear, and the patterns and rate of change of centroid size across age differ between groups, it was deemed important to compare the PCA results to size. Results of both PC1 and PC2 regressed onto centroid size are similar to those seen with age, with no linear relationship observed with PC1, and a positive linear relationship seen with PC2 (Figure 5.11). This indicates that the second largest axis of shape variation in the ilium data can primarily be explained by size variation, while the primary axis cannot (see Tables 5.6 and 5.7 for regression results). When compared with the results of PC2 regressed on to age (Table 5.3), the relationship with centroid size is even stronger than that with age along this axis of variation in all samples save Indian Knoll, although the difference between the R^2 values of the two regressions is negligible. PC2, therefore, is strongly correlated with both age and size, with size

being a slightly stronger predictor of the variation in shape captured by PC2. These results may be a reflection of the potential for error that is introduced into age estimation, as well as the variation that is present between individuals in how size changes with age. Ultimately, size appears to be a more relevant variable than age in the relationship with shape along this axis of variation.

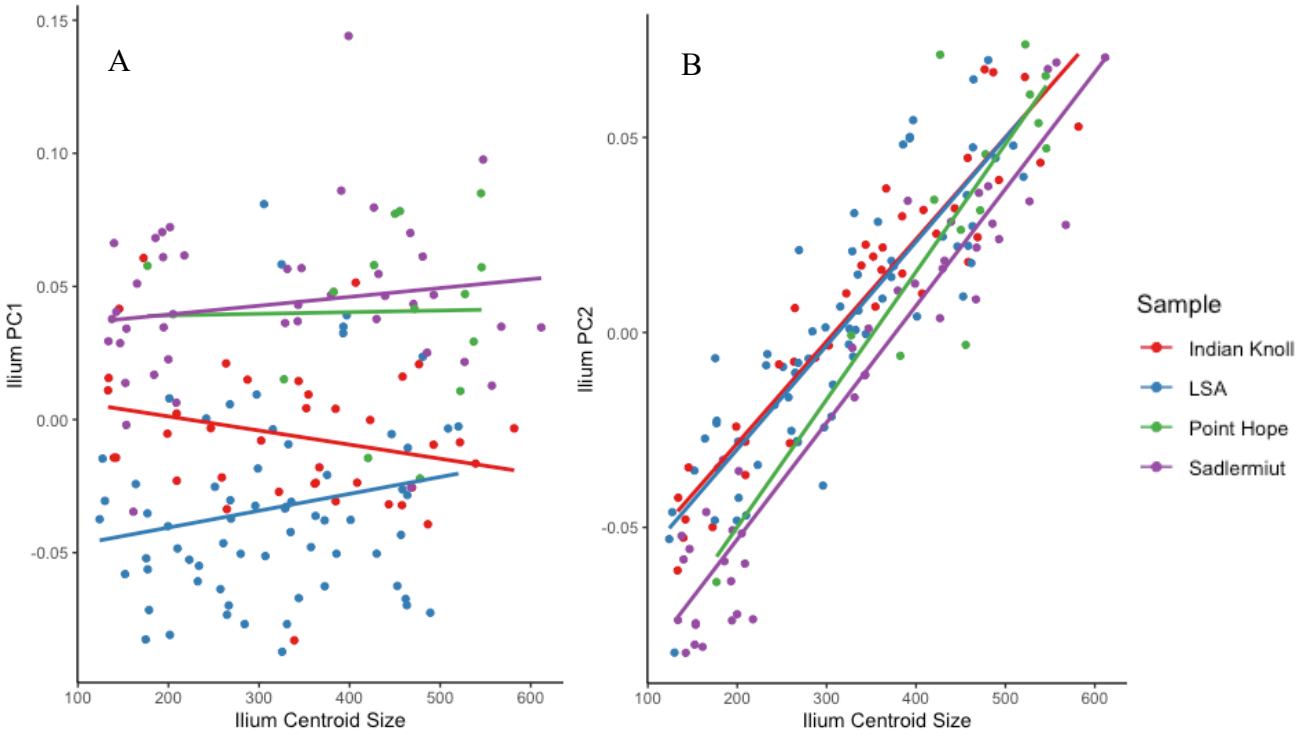

Figure 5.11 Ilium centroid size vs A) PC1, where marine-based foragers plot towards the top, terrestrial foragers plot towards the bottom, and no clear relationship with age is evident; and B) PC2, where all samples show a similar age-related pattern and no group distinctions are obvious, fitted with linear lines of best fit.

Table 5.6 Regression results of the combined-sample ilium PC1 data plotted on ilium centroid size, separated by sample.

Sample	**R^2**	**SEE**	**p-value**
Indian Knoll	0.062	0.026	0.132
Later Stone Age	0.036	0.035	0.126
Point Hope	0.000	0.035	0.949
Sadlermiut	0.026	0.031	0.299

Table 5.7 Regression results of the combined-sample ilium PC2 data plotted on ilium centroid size, separated by sample.

Sample	R^2	SEE	p-value
Indian Knoll	0.884	0.012	<0.001*
Later Stone Age	0.748	0.016	<0.001*
Point Hope	0.749	0.020	<0.001*
Sadlermiut	0.917	0.014	<0.001*

*significant result at alpha of $p<0.05$

5.3 Principal Components Analysis – Individual Samples

5.3.1 Overview

Three-dimensional lollipop graphs were generated to inspect the three main axes of variation from the sample-specific PCAs, and to compare the results to those of the combined sample. In the LSA (Figure 5.12), PC1 (representing 25.54% of the total variance in this sample) mainly captures variation in the depth of the greater sciatic notch, in the curvature and breadth of the iliac crest, and in the length of the bone as a whole, as captured through the landmark at the base of the arcuate line (Figure 5.13). PC2 (representing 20.71% of the total variance) captures variation in the breadth and length of the bone as represented by movement in the landmark at the anterior inferior iliac spine, in the width of the bone as captured by the landmarks at the anterior superior iliac spine, and in the curvature of the iliac crest in general. PC3 (representing 9.56% of the total variance) captures variation in the breadth of the iliac crest, as well as the placement and angulation of the auricular surface. Much of the variation seen along these three PCs is similar in direction to what was seen in the combined sample, with the magnitude of the variation (as represented by length of the individual lines, or "lollipops") somewhat less than what was seen in the combined sample. A noteable difference from the combined sample along PC1 can be seen at the landmarks on the anterior inferior iliac spine and at the anterior edge of

the acetabulum; in the combined sample, these landmarks showed substantial movement in the superior-inferior direction, where in the LSA sample much less movement is captured and what is present is in a more medio-lateral direction. Similarly, the variation in the width of the bone captured along PC3 in the combined sample by the landmarks at the anterior end of the iliac crest is not as obvious in the LSA sample.

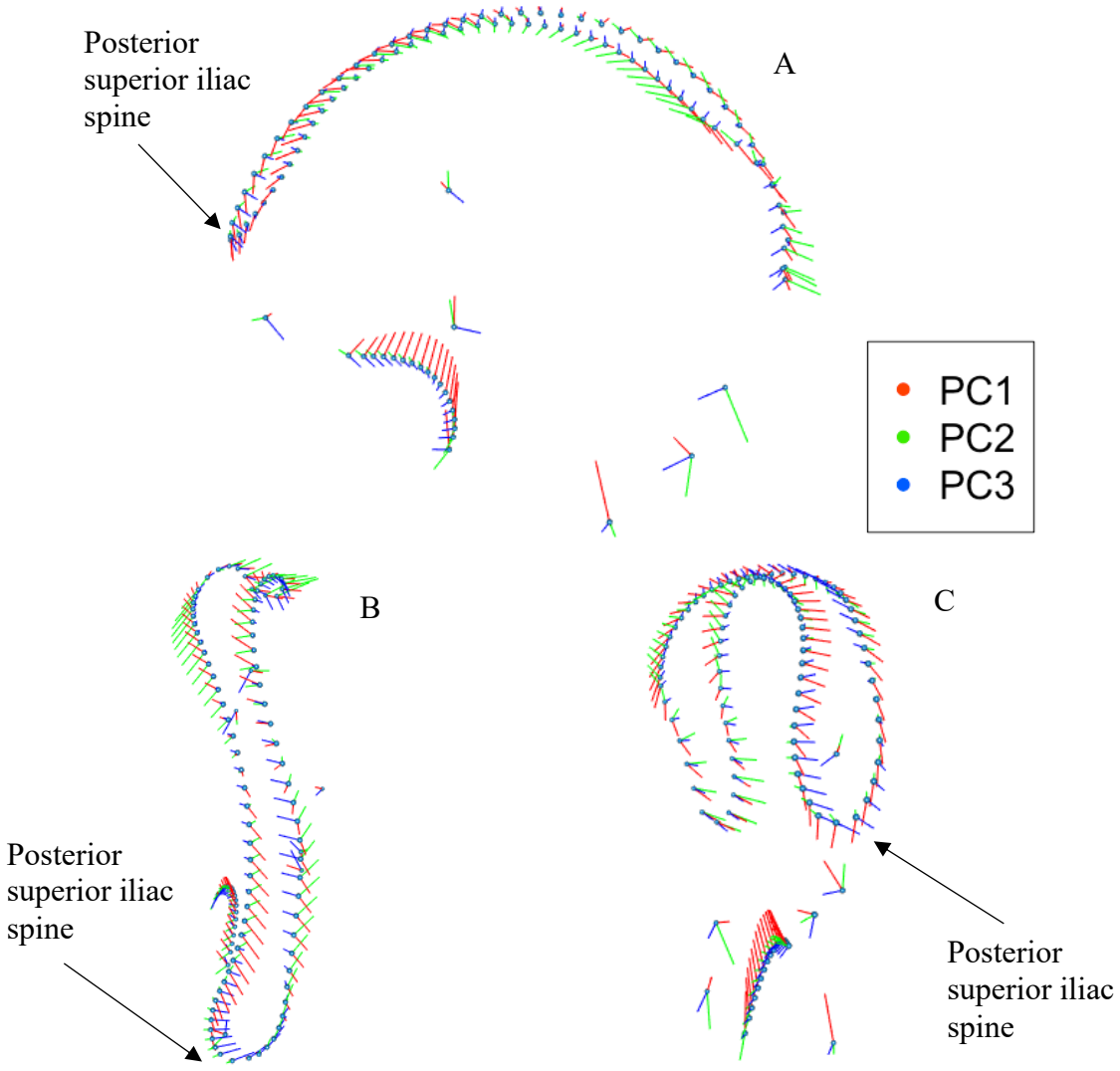

Figure 5.12 PCs 1-3 of the ilium for the LSA sample, with lines representing the extent of variation represented by each PC at each landmark location. A) pelvic view (medial); B) superior view; C) posterior view.

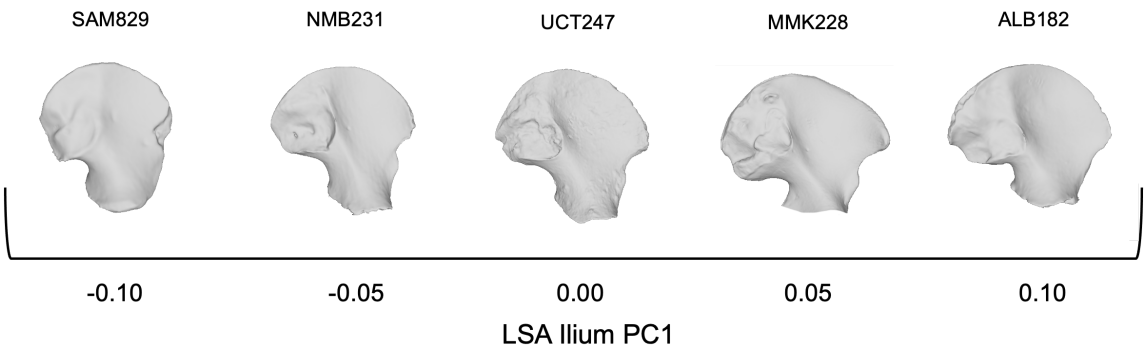

Figure 5.13 Examples of variation seen along the PC1 axis of the LSA sample.

In the Indian Knoll sample (Figure 5.14), PC1 (representing 32.06% of the total variance in the sample) captures variation in the curvature of the iliac crest, particularly at the anterior end, in the depth of the greater sciatic notch, particularly the inferior portion, and in the length and width of the bone as a whole, as highlighted by the movement of the landmarks at the anterior inferior iliac spine and at the inferior end of the bone in general (Figure 5.15). PC2 (representing 16.05% of the total variance) captures medio-lateral movement in the landmarks on the inferior portion of the bone, as well as some variation in the height and breadth of the iliac crest. PC3 (representing 8.69% of the total variance) mainly captures variation in the length of the greater sciatic notch, as well as around the placement of the iliac tubercle. Compared with the variation captured by the first three PCs in the combined sample, variation in the curvature of the iliac crest, captured particularly by PC2 of the combined sample, is evident here along PC1 in the Indian Knoll sample instead. The extent of the variation captured by PCs 2 and 3 in this sample appears much reduced in comparison to the combined sample.

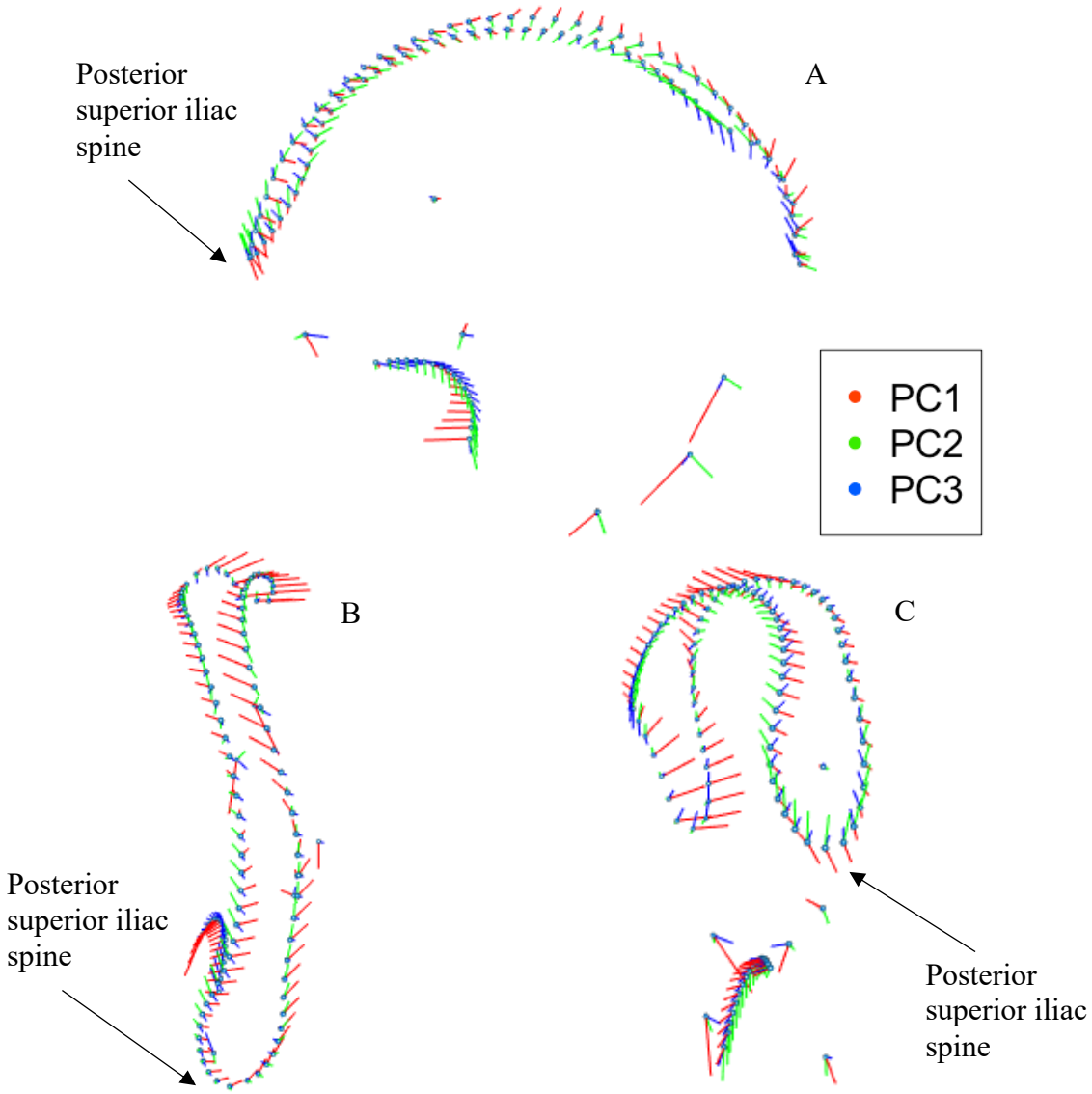

Figure 5.14 PCs 1-3 of the ilium for the Indian Knoll sample, with lines representing the extent of variation represented by each PC at each landmark location. A) pelvic view (medial); B) superior view; C) posterior view.

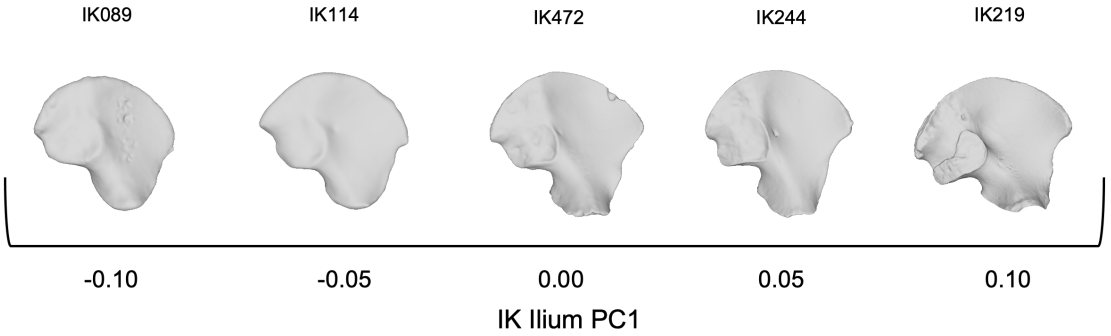

Figure 5.15 Examples of variation seen along the PC1 axis of the Indian Knoll sample.

For the Point Hope sample (Figure 5.16), PC1 (representing 32.44% of the overall variance in the sample) demonstrates variation in the breadth and curvature of the bone as a whole, as captured by the landmarks along the iliac crest and the greater sciatic notch, and in the width of the bone, as captured by the landmarks at the anterior inferior iliac spine and the anterior edge of the acetabulum (Figure 5.17). PC2 (representing 25.53% of the variance) mainly captures variation in the depth of the greater sciatic notch, and in the width of the iliac crest. PC3 (representing 11.86% of the variance) captures variation in the length of the iliac crest overall, as seen in the movement of the landmarks at the anterior end of the crest, in the width of the inferior end of the bone, captured by the medio-lateral movement of the landmarks around the acetabulum, and in the depth of superior portion of the greater sciatic notch. Compared to the first three PCs of the combined sample, PC1 of the Point Hope sample, like that of the Indian Knoll sample, highlights variation in the curvature of the iliac crest, where similar variation is captured along PC2 in the combined sample. PC1 of the Point Hope sample also highlights variation in the breadth and alignment of the greater sciatic notch, where PC1 of the combined sample highlights variation in the depth of the notch; variation in the depth of the greater sciatic notch is highlighted in PC2 of the Point Hope sample.

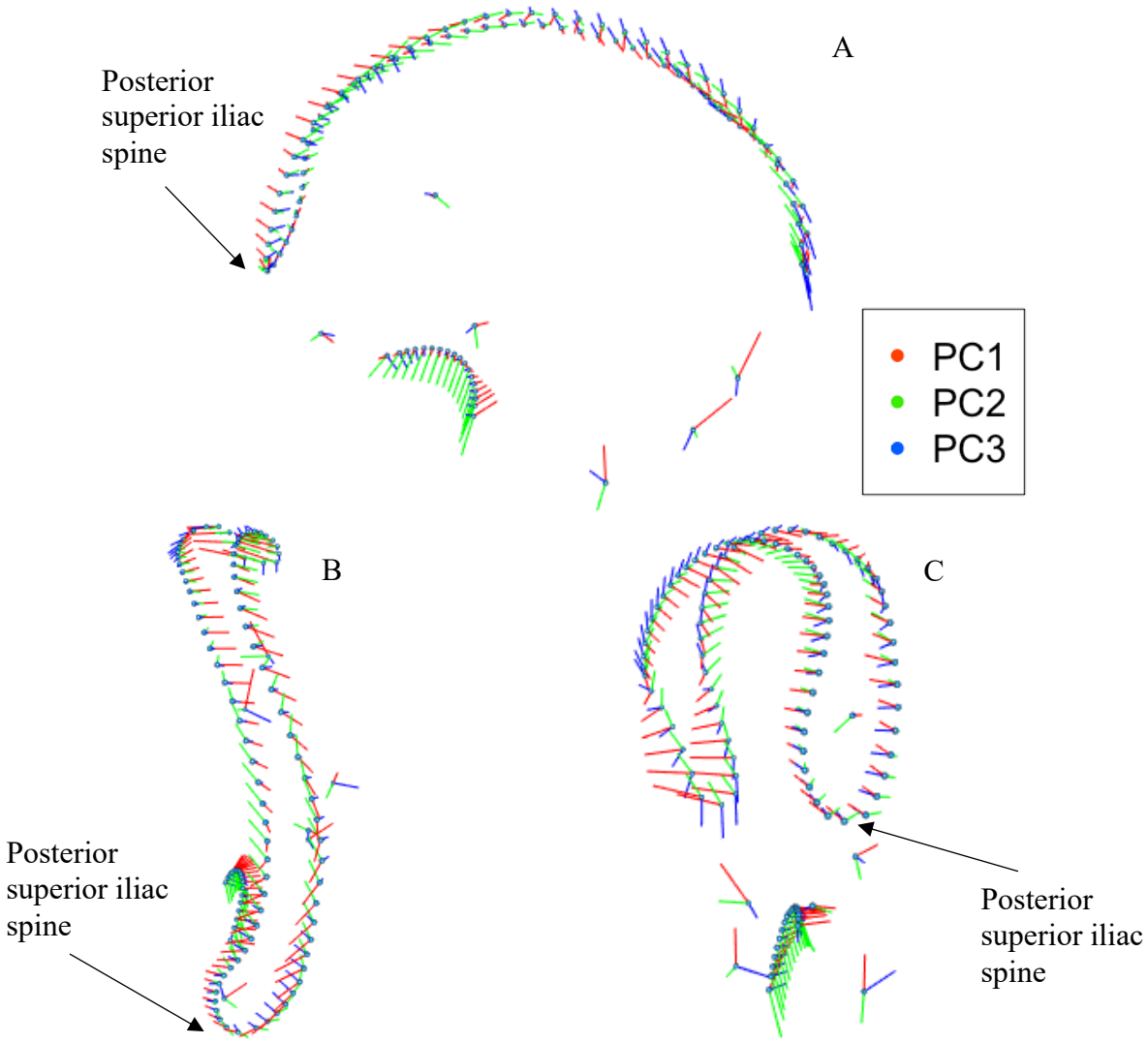

Figure 5.16 PCs 1-3 of the ilium for the Point Hope sample, with lines representing the extent of variation represented by each PC at each landmark location. A) pelvic view (medial); B) superior view; C) posterior view.

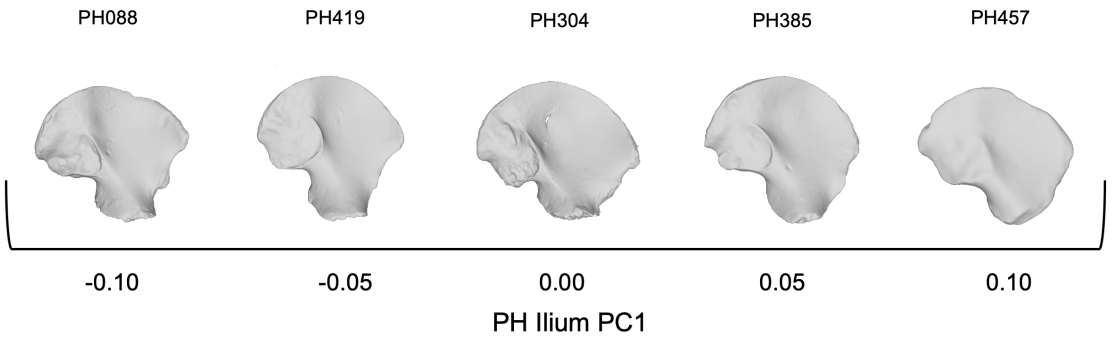

Figure 5.17 Examples of variation seen along the PC1 axis of the Point Hope sample.

Finally, in the PCA results for the Sadlermiut sample (Figure 5.18), PC1 (representing 40.04% of the total variance in the sample) captures variation in the curvature and height of the iliac crest, in the breadth and alignment of the greater sciatic notch, in the protrusion of the auricular surface and the arcuate line, and in the breadth of the bone as a whole, as reflected in the movement of the landmarks on the inferior portion of the bone (Figure 5.19). PC2 (representing 16.18% of the total variance) captures variation in the length of the bone, as seen in the inferior landmarks, and in the depth of the greater sciatic notch. PC3 (representing 8.75% of the total variance) mainly captures variation in length and angle of the iliac crest, highlighted by the movement of the landmarks at the posterior end of the crest. Compared with the PCA results of the combined sample, variation in the curvature and breadth of the iliac crest, and the bone as a whole, as highlighted through the movement of the landmarks around the iliac crest and at the greater sciatic notch, is evident here along PC1, where it was more prominent in PC2 of the combined sample. Length of the bone was also highlighted on PC1 of the combined sample, where breadth seems to be more prominent along PC1 of the Sadlermiut sample.

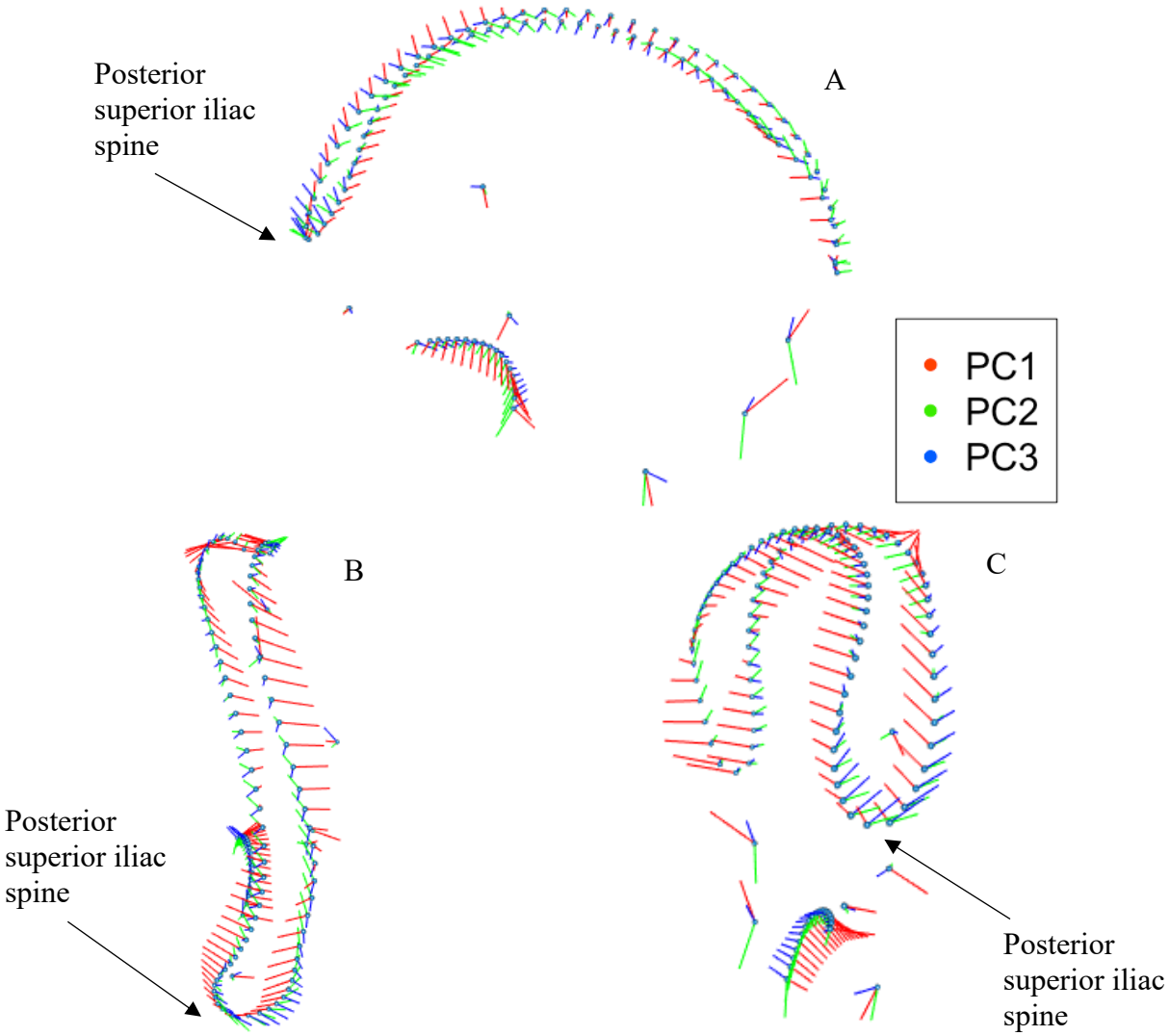

Figure 5.18 PCs 1-3 of the ilium for the Sadlermiut sample, with lines representing the extent of variation represented by each PC at each landmark location. A) pelvic view (medial); B) superior view; C) posterior view.

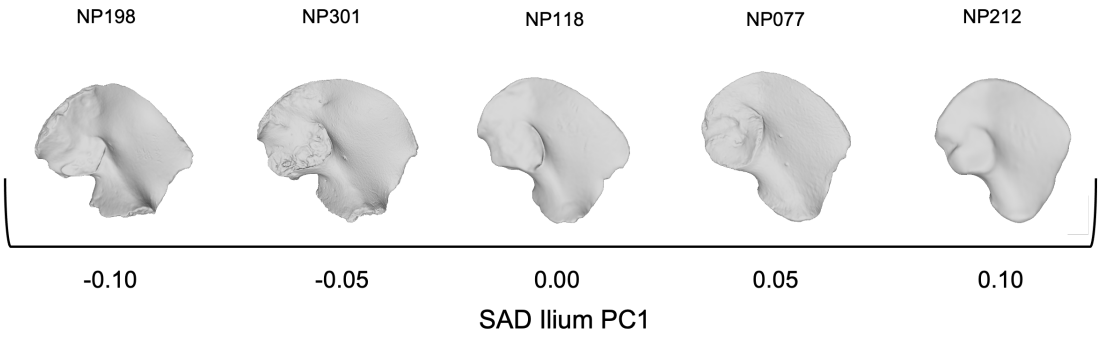

Figure 5.19 Examples of variation seen along the PC1 axis of the Sadlermiut sample.

5.3.2 PC1 vs. Age

When PCA results for the individual samples are plotted on age, age-related changes are more strongly represented along PC1 in a way that they were not when all samples were pooled. Across these four graphs (Figure 5.20), the LSA has the largest spread of data and the weakest relationship with age (see Table 5.8 for regression results), where the other three samples show a somewhat tighter relationship between age and shape change along this axis of variation. Plots are shown with lines of best fit that suit the data, which for the Indian Knoll and Sadlermiut (Figure 5.20, A & C) are quadratic curves, and for the LSA and Point Hope (Figure 5.20, B & D) are linear regression lines; regression results (Table 5.8) reflect the type of fit shown in the plots. It should be noted that, while all samples show some degree of relationship between PC1 and age, the nature of that relationship is not consistent across the samples.

The LSA sample also has a notable group of six outliers towards the top of the PC1 axis. These individuals are not from one single sub-group within the LSA sample (they are spread across three), they are not from one particular time period, they are not in one specific age cohort, the bones do not have any notable damage, and the landmarks do not appear misplaced. Rather, it is likely that the extent of variation represented by the LSA is broad, and that the gap between these six individuals and the rest of the sample would be filled in were more individuals to be included in the study.

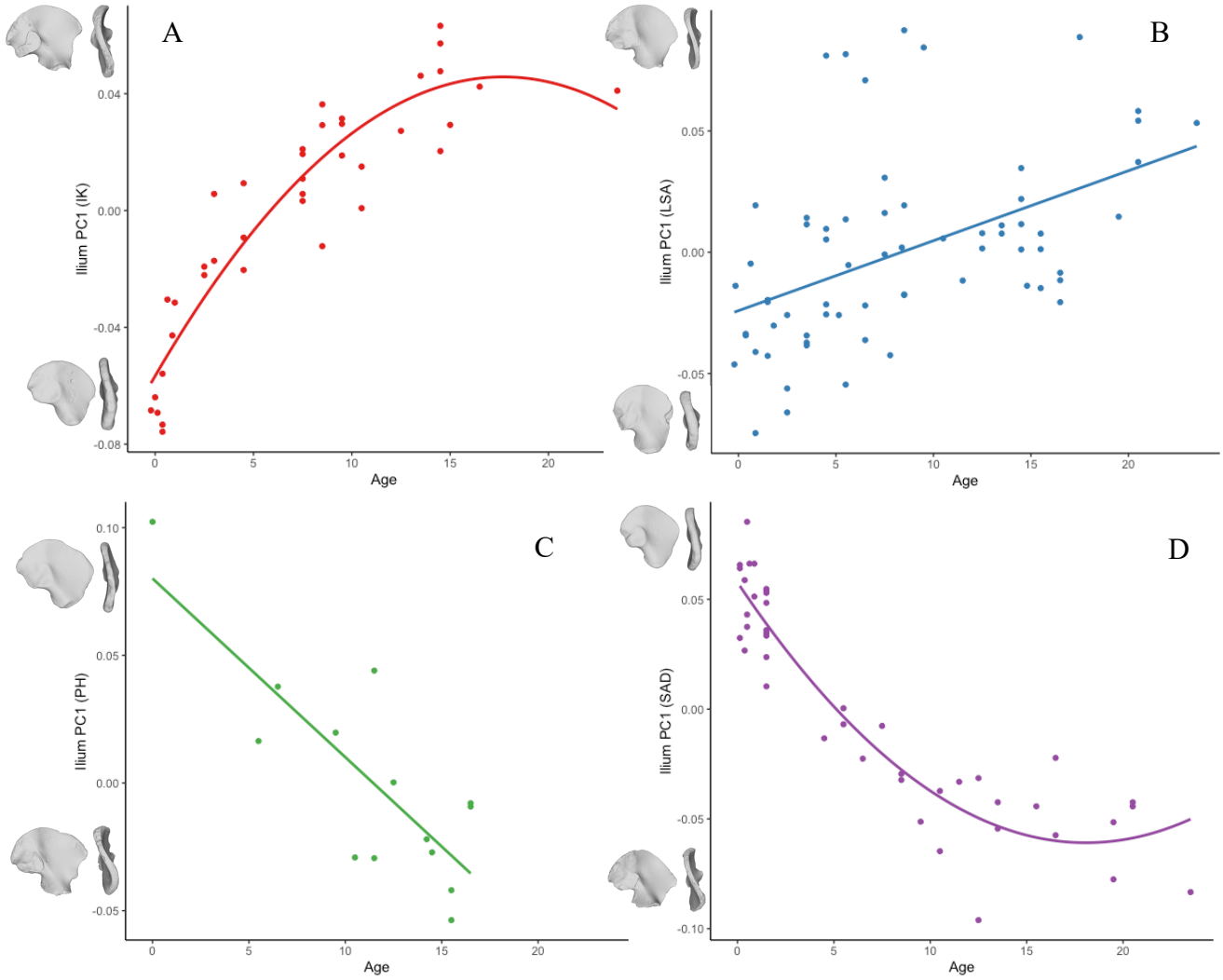

Figure 5.20 Age vs. ilium PC1 for the A) Indian Knoll sample (where PC1 represents 32.06% of the overall variation), B) LSA sample (25.54% of the overall variation), C) Point Hope sample (32.44% of the overall variation), and D) Sadlermiut sample (40.04% of the overall variation). All samples demonstrate some degree of age-related patterning.

Table 5.8 Regression results of the individual samples' ilium PC1 data plotted on age.

Sample	**R^2**	**SEE**	**p-value**
Indian Knoll	0.853	0.015	<0.001*
Later Stone Age	0.225	0.034	<0.001*
Point Hope	0.657	0.025	<0.001*
Sadlermiut	0.864	0.018	<0.001*

*significant result at alpha of p<0.05

5.3.3 PC2 vs. Age

When PC2 for each individual sample is plotted on age (Figure 5.21), the relationships between the variables demonstrate differing patterns between the groups. The data for all samples save the Sadlermiut are best fit with a linear regression, although the relationships are not strong, while the Sadlermiut data are best fit with a quadratic curve (see Table 5.9 for regression results). Of the four samples, the LSA has the strongest relationship with age (with an R^2 of 0.482). The LSA demonstrates a different pattern than the other samples between PCs 1 and 2; the relationship between PC2 and age is stronger than that between PC1 and age for this sample, while all the other samples have the opposite pattern. Thus, for the LSA, PC2 better captures age-related changes, while for the Indian Knoll, Point Hope, and Sadlermiut, PC1 better captures age-related changes.

Notable patterns did not emerge when PCs 3 and 4 were plotted on age, so those graphs can be found in Appendix H (Figures H.3 and H.4).

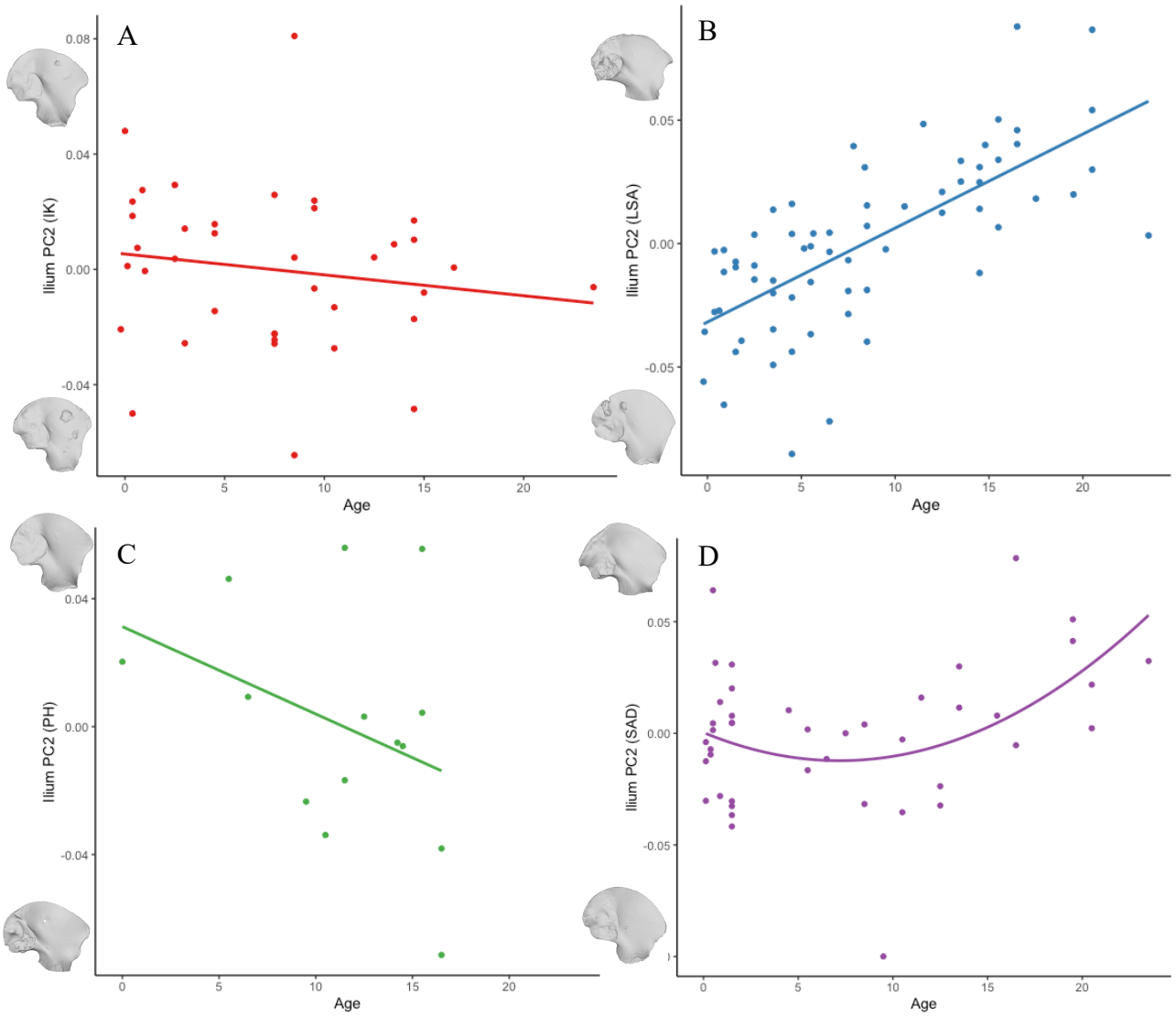

Figure 5.21 Age vs. ilium PC2 for the A) Indian Knoll sample (where PC2 represents 16.05% of the overall variation), B) LSA sample (20.71% of the overall variation), C) Point Hope sample (25.53% of the overall variation), and D) Sadlermiut sample (16.18% of the overall variation), fitted with lines of best fit. Some age-related patterning is present in all samples, albeit with varying degrees of strength.

Table 5.9 Regression results of the individual samples' ilium PC2 data plotted on age.

Sample	**R^2**	**SEE**	**p-value**
Indian Knoll	0.023	0.028	0.360
Later Stone Age	0.482	0.025	<0.001*
Point Hope	0.127	0.036	0.211
Sadlermiut	0.145	0.029	0.016

*significant result at alpha of p<0.05

5.3.4 PCs vs. Centroid Size

Much like the results seen in the combined sample data, the results of the individual samples' PC1 data plotted onto centroid size (Figure 5.22) are generally similar to the results seen with age, although they differ in a few small ways. The regression results (Table 5.10) for the Indian Knoll and Sadlermiut are quite similar to those of the PC1 data plotted on age (Table 5.9), although the Sadlermiut data is best fit here with a linear regression, where a quadratic curve yielded a higher R^2 value when PC1 was plotted on age. The LSA shows a slightly stronger relationship with size over age (R^2 values of 0.353 and 0.225, respectively), while the Point Hope shows the opposite (R^2 values of 0.657 and 0.577 for age and size, respectively). This indicates that for the LSA, size is a slightly better predictor of the variation in shape captured along PC1, while for the Point Hope the opposite is true. Results of the individual samples' PC2 data plotted on centroid size are also quite comparable to the results seen with age. For this reason, they are not included here, but can been found in Appendix J.

The six LSA outliers noted in Figure 5.20 are once again present in this plot, although they are shifted up along the x-axis. This suggests that these six individuals are large for their estimated ages and continue to exhibit unique morphologies in comparison to the rest of the sample; this larger size may thus be contributing, at least in part, to the uniqueness of their morphologies.

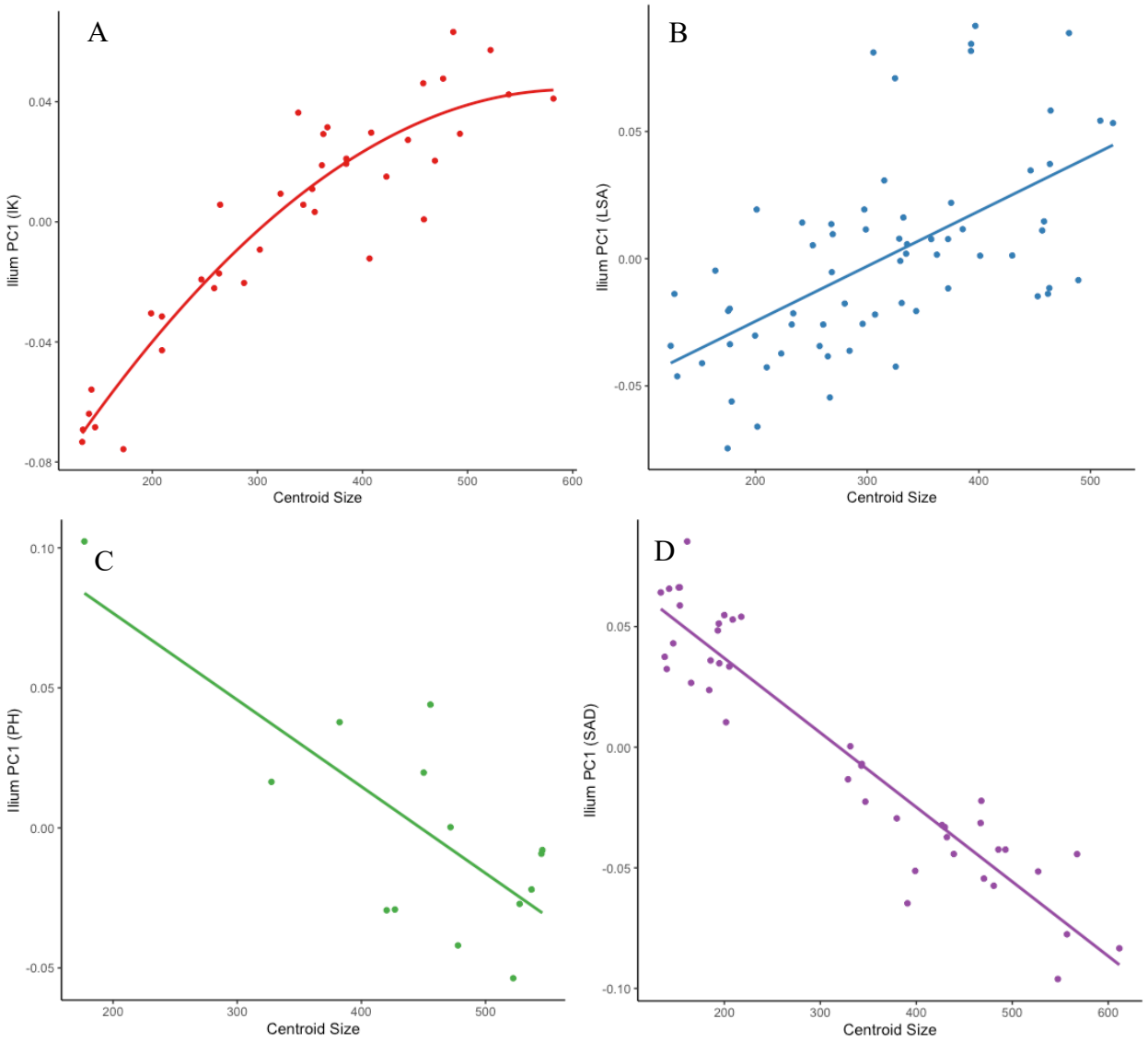

Figure 5.22 Ilium centroid size vs PC1 from the individual sample PCAs for the A) Indian Knoll, B) LSA, C) Point Hope, and D) Sadlermiut samples, fitted with lines of best fit. All samples demonstrate some degree of age-related patterning.

Table 5.10 Regression results of the individual samples' ilium PC1 data plotted on centroid size.

Sample	**R^2**	**SEE**	**p-value**
Indian Knoll	0.866	0.014	<0.001*
Later Stone Age	0.353	0.031	<0.001*
Point Hope	0.577	0.028	0.002*
Sadlermiut	0.884	0.017	<0.001*

*significant result at alpha of p<0.05

5.4 Allometry

To investigate allometry, or changes in shape that are related to changes in size, regression scores were calculated through a multivariate regression of Procrustes residuals on log-transformed centroid size. Regression scores were then plotted back onto log-transformed centroid size to visualize and quantify the amount of shape change for a given unit of size change across the sample (Figure 5.23). The ilium data show a positive linear relationship between the variables, with an R^2 value for the regression of 0.839, indicating the presence of allometric effects on shape variation. Given that this is an ontogenetic data set, the overall presence of allometric effects in the sample was expected. Although PC1 of the combined-sample ilium data did not show a relationship between shape change and size, when shape change as a whole is considered (instead of individual axes of variation) allometric effects become apparent. Group separation between the samples is not apparent in the plot of regression scores on centroid size, and the age categories plot logically, with the youngest individuals having the smallest centroid sizes and regression scores, and the oldest individuals having the largest across all samples. Separation between the age categories is not discrete, however, with overlap between the categories. Overlap is especially notable in age categories 3 through 5, indicating that the relationship between shape and size varies somewhat between individuals, particularly after six years of age.

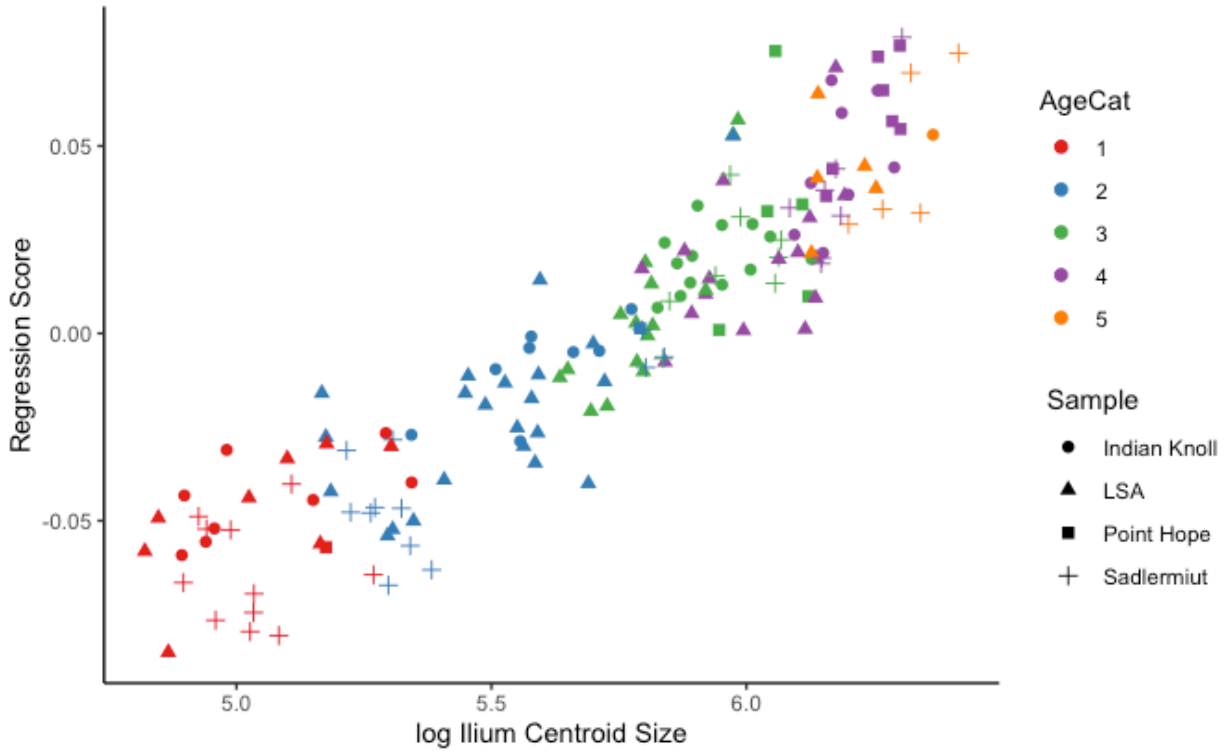

Figure 5.23 Regression scores plotted on log-transformed centroid sizes, organized by age category and sample for the ilium data. Age categories: 1 (less that 1 year of age), 2 (1-<6 years), 3 (6-<12 years), 4 (12-<18 years), and 5 (18-24 years).

5.5 Maturity Trajectories

Figure 5.24 shows the maturity trajectories of both ilium shape and size across all four populations. Results indicate that for the Indian Knoll, LSA, and Sadlermiut, percentages of shape maturity are reached prior to those of size maturity (e.g., 50% shape maturity is achieved by an earlier age than 50% size maturity), while the opposite seems to be true for the Point Hope sample. For a breakdown of the approximate ages at which 25%, 50%, and 75% maturity are reached in shape and size across all four populations, see Table 5.11.

For the Indian Knoll, shape appears to have a quicker trajectory than size, meaning adult shape is reached while growth in size is still occurring. The shape trajectory is quite consistent in pace until about age 15 when it slows down, and the size trajectory appears somewhat quicker

before the age of five when it then slows and progresses consistently across growth. For the LSA, the shape trajectory is fairly gradual and consistent, although has a slightly faster pace prior to about age seven, and the size trajectory has an initial quicker pace and slows down around 10 years of age. The biggest disparity between size and shape appears to be around 10 years of age, where rate of change in size slows down and that of shape picks up. For the Point Hope, the shape trajectory has a different pattern to the other populations, with a quickening of the pace after age 10, and a plateau around age 17; this differing pattern could be a product of a small sample size, as there is only one individual under the age of 5.5 years, and no individuals over the age of 16.5 years. The size trajectory is fairly consistent across growth with a slight slowing of pace after age five. Finally, for the Sadlermiut, there is quite a quick rate of change in the shape trajectory from birth, which then levels off just before age five and has a slight dip in pace around age 10. The size trajectory is fairly consistent across growth, with a somewhat quicker pace prior to age five. There is a gap between the two trajectories for the entirety of growth, showing that shape is closer to the adult form from birth than is size.

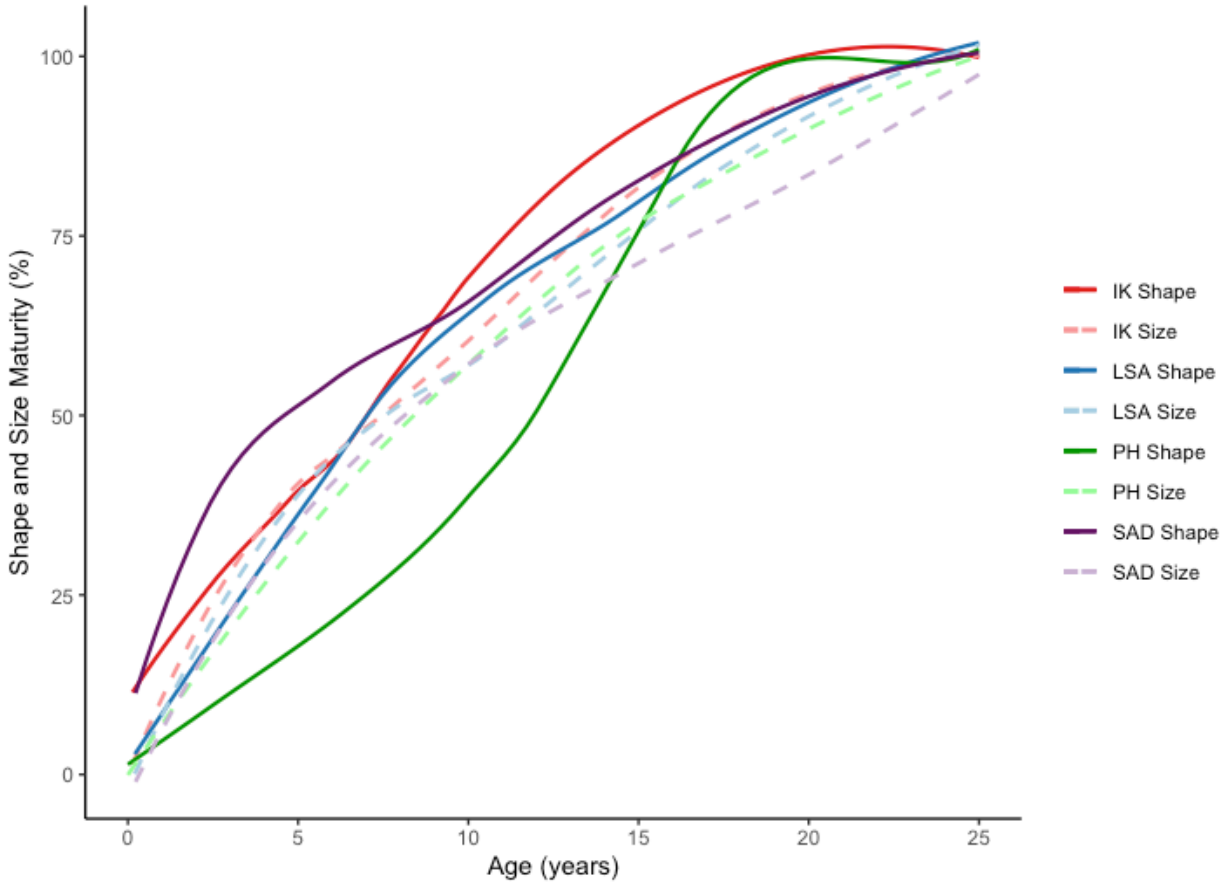

Figure 5.24 Ilium size (solid lines) and shape (dashed lines) maturity trajectories.

Table 5.11 Approximate ages at which percentages of shape and size maturity of the ilium are reached across all four populations.

Sample	Age at 25%		Age at 50%		Age at 75%	
	Shape	**Size**	**Shape**	**Size**	**Shape**	**Size**
Indian Knoll	2 yrs	3.5 yrs	7.5 yrs	8.5 yrs	10.5 yrs	13.5 yrs
LSA	3.5 yrs	4.5 yrs	7 yrs	9 yrs	14.5 yrs	15 yrs
Point Hope	7 yrs	4 yrs	12 yrs	9 yrs	15 yrs	14 yrs
Sadlermiut	1 yr	4 yrs	5.5 yrs	10 yrs	12.5 yrs	18.5 yrs

5.6 Ilium Shape and Cross-Sectional Geometry

5.6.1 Overview of Cross-Sectional Geometry

Cross-sectional geometric (CSG) values from midshaft of the humerus, femur, and tibia, that have been size-standardized using measures of body mass, were plotted on age (Figure 5.25). Results show the greatest variation in CSG values in the youngest individuals in the sample across all three bones, particular within the Sadlermiut, which then decreases with age. Since the bones of these youngest individuals would not have yet been loaded, markers of activity and habitual behaviours cannot yet be detected; the variation in the data, therefore, likely reflects variation in birth weight and size. Around the age of 5, the spread of data points becomes smaller as individuals are more consistently loading their bones and CSG values begin to reflect patterns of activity.

The arctic samples (Sadlermiut and Point Hope) plot slightly higher than the terrestrial samples (LSA and Indian Knoll) in values of size standardized humeral and femoral J, although the trend lines for all samples remain close throughout. Values of size standardized tibial J show the Sadlermiut plotting highest on the graph in the youngest individuals but decreasing the most throughout ontogeny, meaning that the tibiae of the Sadlermiut individuals have high J values for their body masses in the youngest individuals. The LSA individuals, on the other hand, plot alongside the Indian Knoll and Point Hope in the youngest age group, but then plot highest on the graph by the end of ontogeny, meaning that by the end of growth their tibiae have high J values for their body masses. It is possible that Point Hope individuals from the oldest age category (18-24 years of age) might have plotted high on this graph of standardized tibial J values as well, since the Point Hope individuals in the 12-<18-year age category plot highest on the graph, but no individuals in that age group are included in the sample. Given that femoral

CSG values often reflect body size and tibial CSG values often more closely reflect habitual behaviours (Davies, 2012), the result that the arctic populations, in particular the Point Hope, plot highest on the graph of standardized femoral J and that the LSA plot highest on the graph of standardized tibial J by the end of growth, was expected.

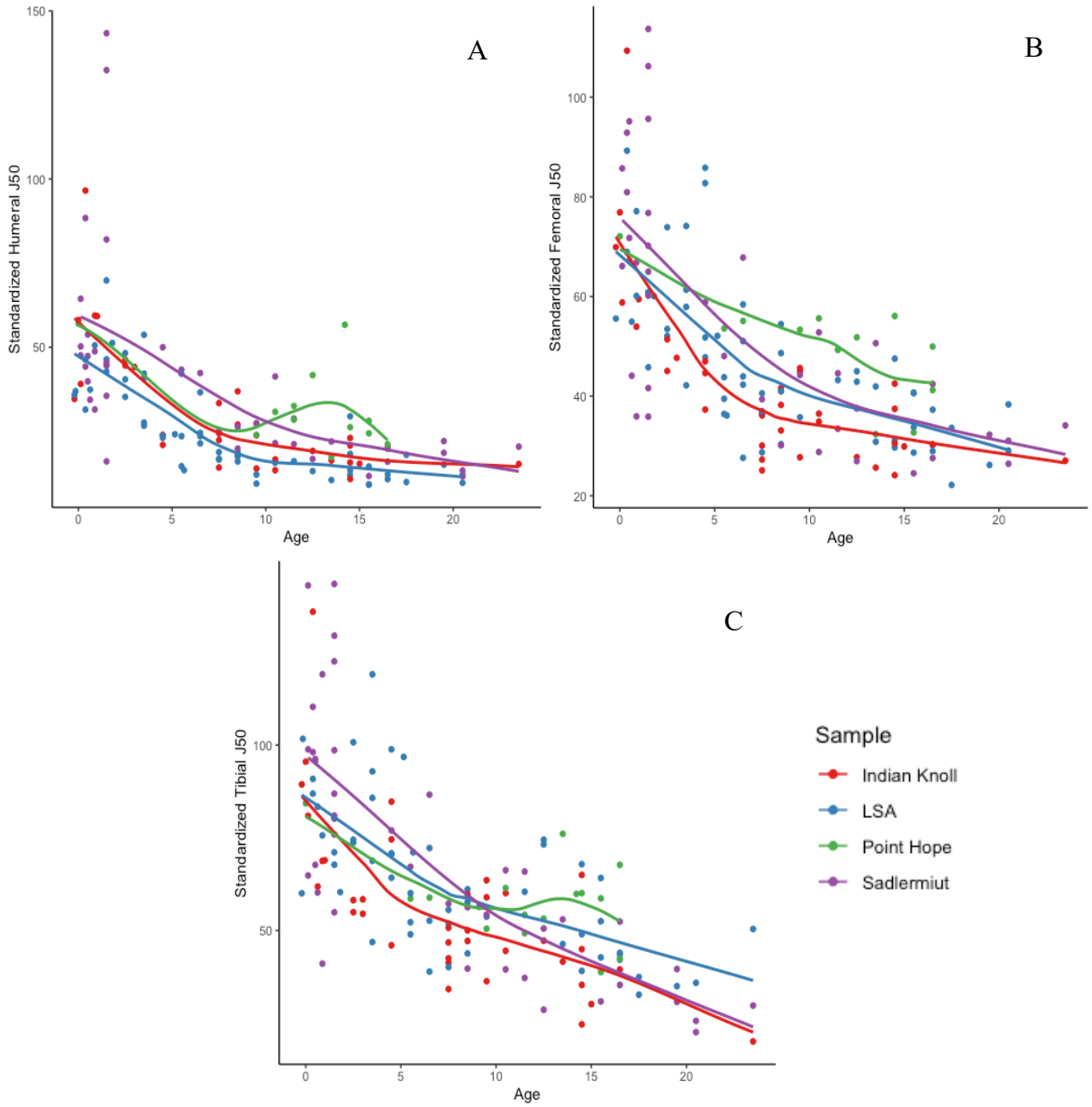

Figure 5.25 Cross-sectional geometric values size standardized using body mass estimations, plotted on age. A) humeral J, B) femoral J, and C) tibial J, all fitted with LOESS curves.

As another means of size standardization, ratios of unstandardized J values were plotted on age (Figure 5.26). By using a ratio of the J value of the femur or tibia divided by the humeral J, the effect of individual body size is somewhat removed. The trend lines on these plots, therefore, represent the strength of an individual's femur or tibia in comparison to their humerus; a trend line that plots higher on the graph, consequently, represents a stronger lower limb bone for a given humerus. As can be seen in these plots, the strength of the lower limbs of the LSA in comparison to their humeri far exceed that of the individuals in the other samples. Looking at the graph of the tibia/humerus ratio in particular (Figure 5.26, B), the arctic samples plot the lowest on the graph, the Indian Knoll in the middle, and the LSA the highest. Based on activity data that is known about the adults from these populations, it is expected that the arctic samples would present with stronger humeri for a given femur or tibia due to their reliance on watercraft and general use of the upper body during daily activities, and it is expected that the LSA would present with stronger lower limbs for a given humerus due to the uneven terrain in coastal southern Africa and the high level of terrestrial mobility amongst this group. It is evident that even in the youngest individuals in the sample, some traces of these population-wide patterns in CSG exist.

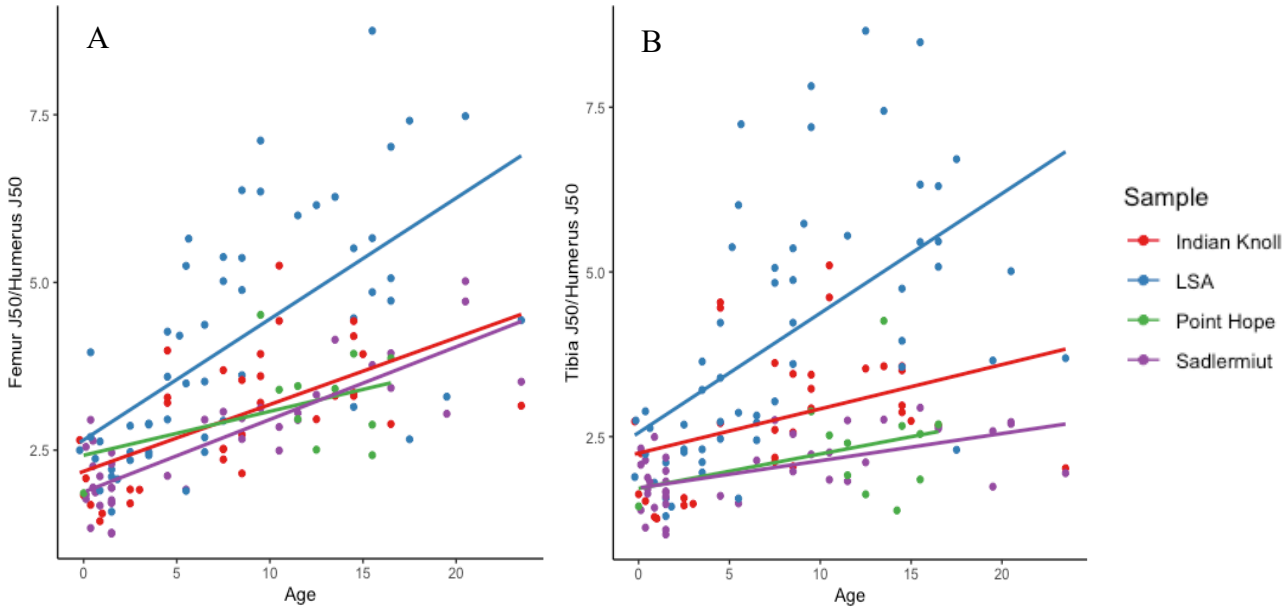

Figure 5.26 Ratios of lower limb to upper limb J values plotted on age, shown with linear lines of best fit. A) ratio of femoral J to humeral J, and B) ratio of tibial J to humeral J. Separation of the LSA sample from the rest is particularly notable.

Since the LSA individuals from the karoo biome (labelled as "MMK") lived in an environment that was drier and less mountainous than the other LSA groups, they were separated out in a plot of ratios of J on age to see how their activity data compares to that of the rest of the LSA sample (Figure 5.27). Although the MMK sample is small (n=11), results show that ratios of femoral and tibial J on humeral J of the MMK plot more in line with the other three samples, and with the Indian Knoll specifically in the graph of tibial J/humeral J, than with the other LSA individuals. Due to the environment in which they lived, it is unsurprising that the activity data of the MMK are more similar to the Indian Knoll individuals, who also lived in fairly flat terrain. The divergence of the LSA from the other groups in the plots of ratio J data becomes even more pronounced when the MMK group is removed. When considering pelvic shape variation, the MMK sample falls within the range of the other LSA individuals (see Appendix H, Figure H.6

for plots), but when looking at CSG data, it is apparent that the MMK group is more similar to the other three groups than to the rest of the LSA sample.

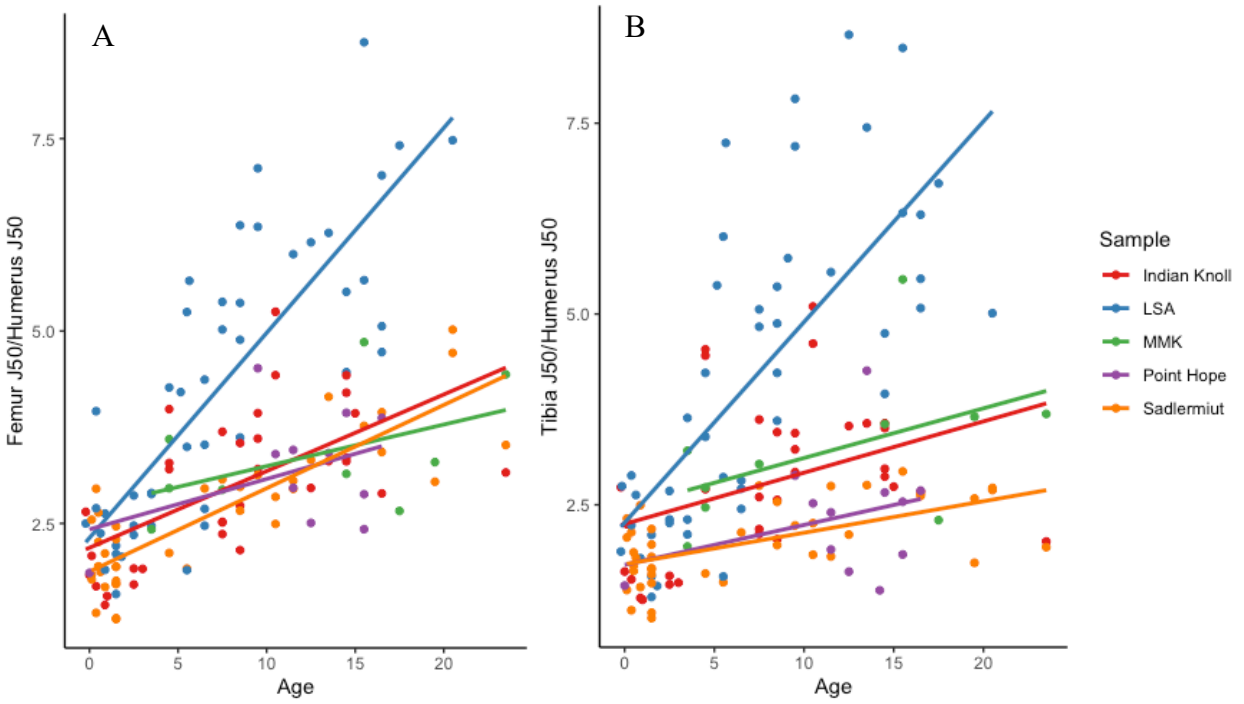

Figure 5.27 Ratios of lower limb to upper limb J values plotted on age, with the MMK group separated from the rest of the LSA sample (green points and line). A) ratio of femoral J to humeral J, and B) ratio of tibial J to humeral J.

5.6.2 PCA Data and Standardized J Values

In order to explore relationships between ilium shape variation and activity data, PC scores were plotted onto measures of cross-sectional geometry. The first and second PCs of the combined-sample ilium data were plotted onto each of the standardized measures of J (Figures 5.28 and 5.29, respectively). No relationships are visible between variables in the PC1 plots (Figure 5.28), indicating that the shape change captured by PC1 does not vary in a consistent way with the measures of activity calculated via size-standardized J values. The Sadlermiut appear to have the most variation in CSG values for all bones, and the separation between samples that has been observed in the PC1 data is maintained in these plots.

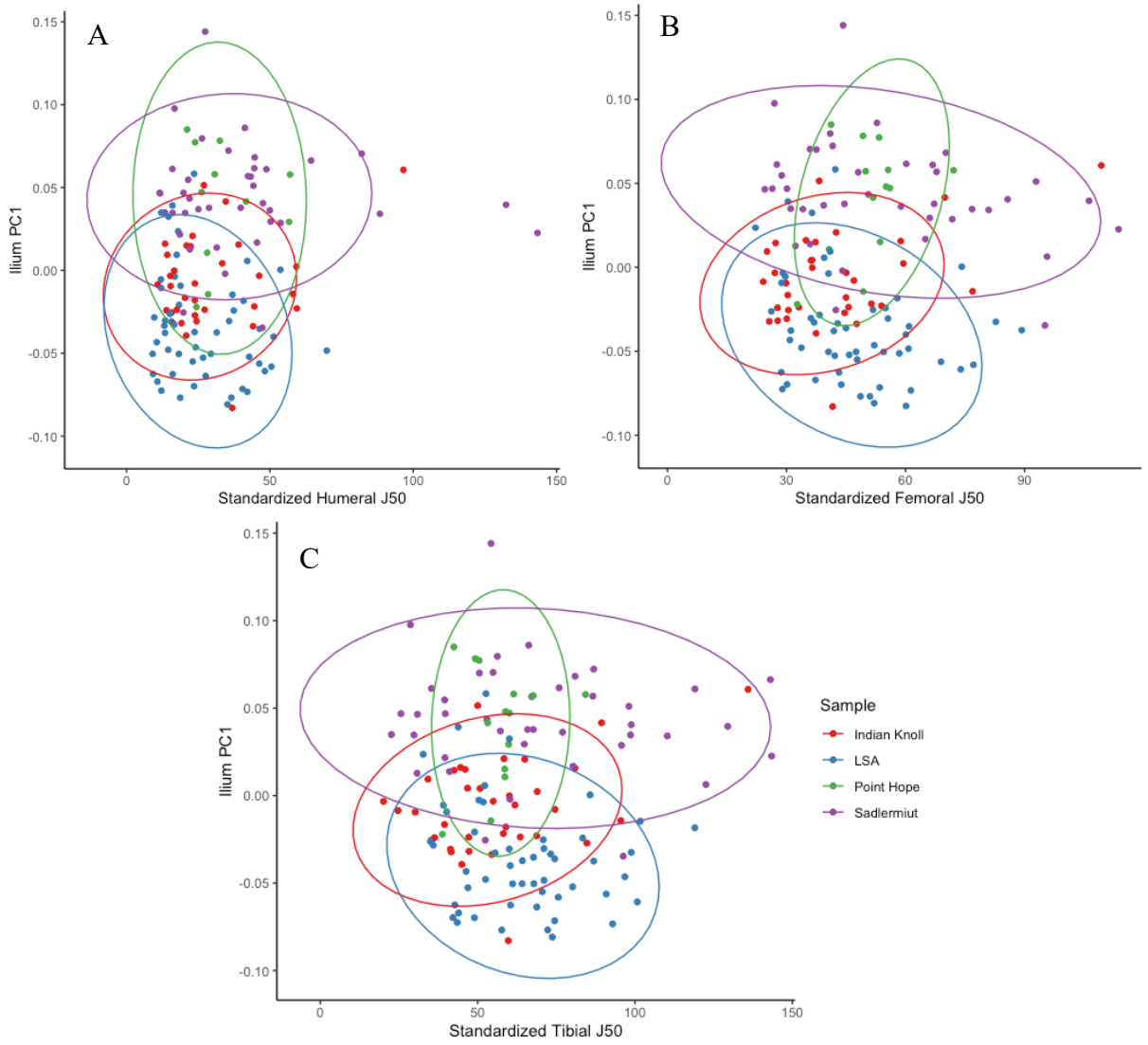

Figure 5.28 PC1 of the combined sample ilium data plotted on A) standardized humeral J, B) standardized femoral J, and C) standardized tibial J, all shown with 95% confidence ellipses.

In plots of the ilium PC2 data on standardized J values (Figure 5.29), a linear relationship is more apparent between the variables, indicating that the shape change captured by PC2 does vary somewhat consistently with changes in J. This relationship can likely be explained, at least in part, by a relationship with age, since both variables showed correlations when plotted on age (Figures 5.9 and 5.25). Residuals from quadratic regressions of both variables on age were, therefore, plotted against one another to examine a relationship for which age effects have been

controlled; quadratic regressions were chosen over linear regressions as they better fit the data in both cases. Results of the ilium PC2 residuals plotted on the standardized femoral J residuals are presented here (Figure 5.30) since the relationship between the ilium PC2 data, particularly in the Point Hope sample, appears strongest with the standardized femoral J data (Figure 5.29, B). All three bones, however, produced similar results, and the plots of the humerus and tibia residuals can be found in Appendix K. Once the effect of age is removed, the linear pattern disappears. What remains evident is that the Sadlermiut data has the largest spread of variation represented across the standardized J values.

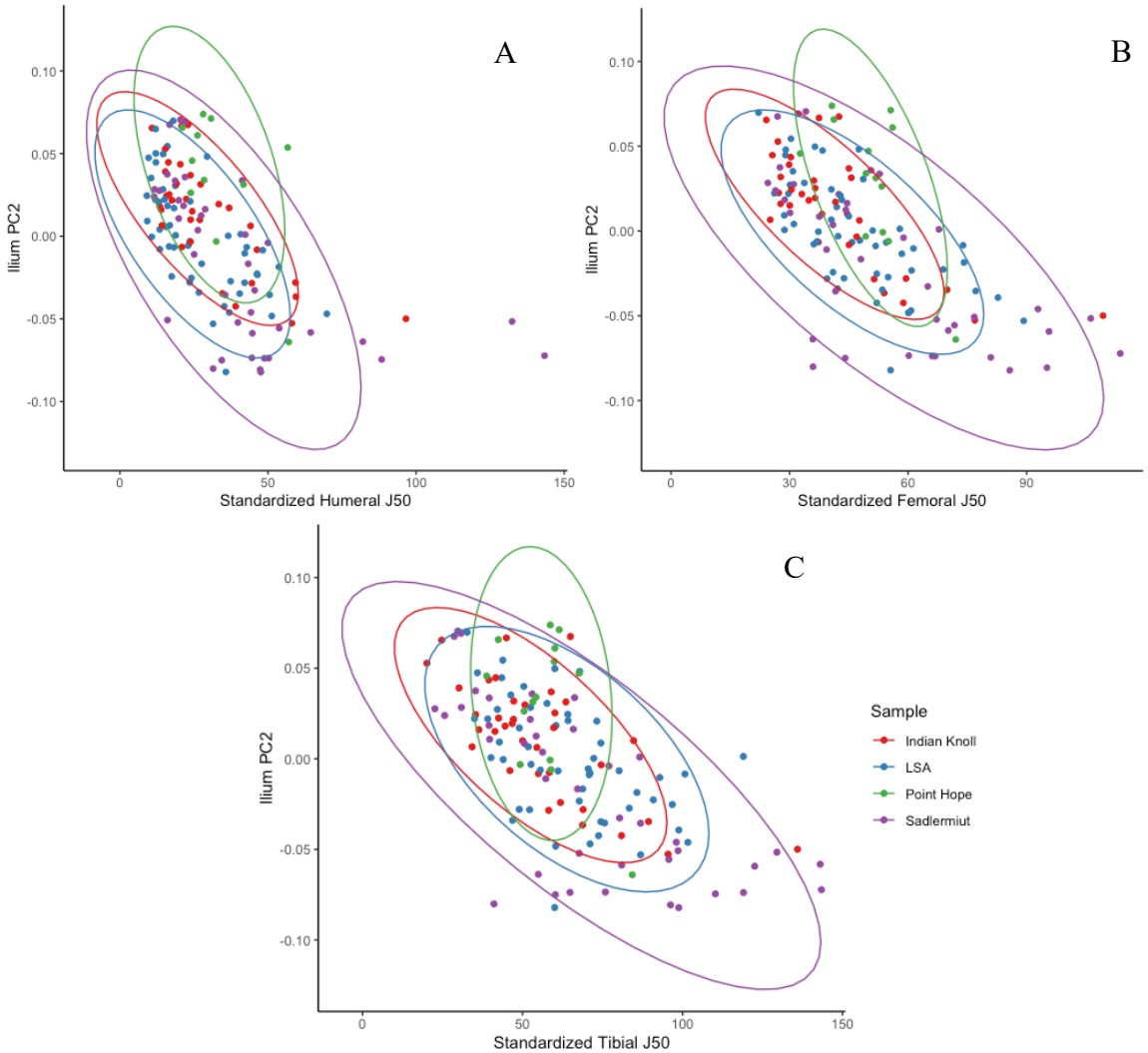

Figure 5.29 PC2 of the combined sample ilium data plotted on A) standardized humeral J, B) standardized femoral J, and C) standardized tibial J, all shown with 95% confidence ellipses.

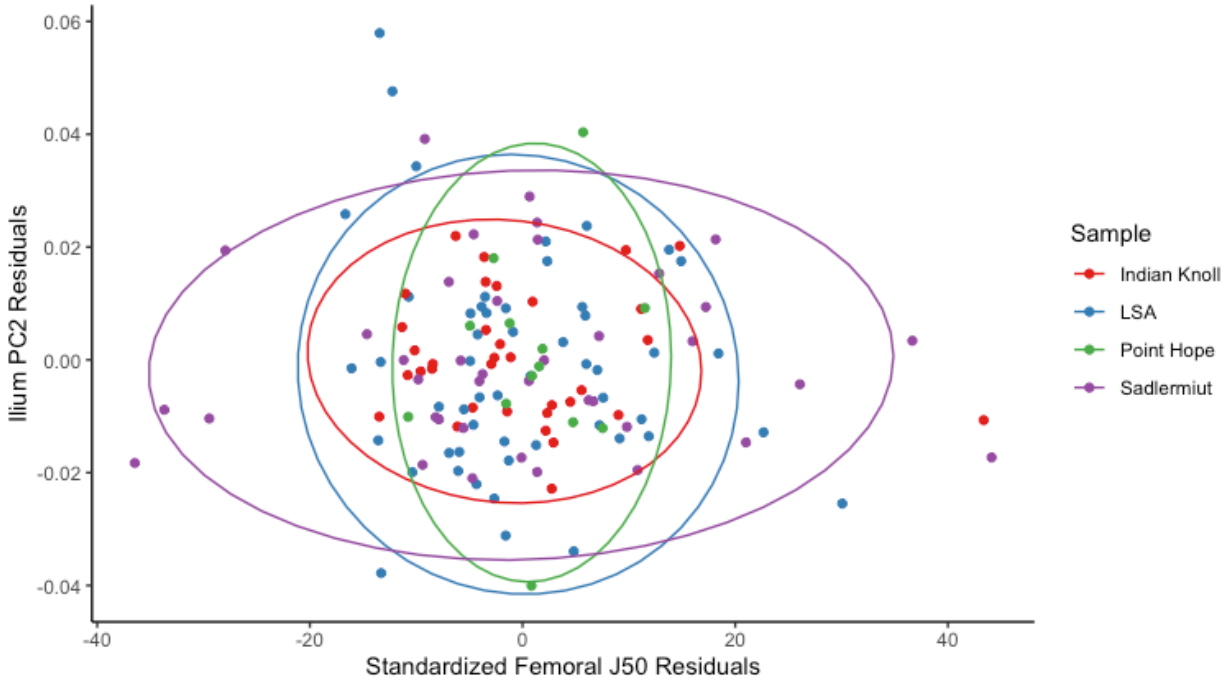

Figure 5.30 Residuals from the regression of standardized femoral J on age vs. the residuals from the regression of ilium PC2 on age, shown with 95% confidence ellipses. No relationships between the variables are notable.

5.6.3 PCA Data and Ratio J Values

Since a degree of separation between the samples was more evident in the ratio of tibia to humerus J values than in the ratio of femur to humerus J values (Figure 5.26), PC1 and PC2 data were plotted onto the ratio of tibia J/humerus J to see if patterns emerge (Figure 5.31). No strong relationships between the variables are obvious, although a linear relationship between the ilium PC2 data and the tibia/humerus ratio does appear in the LSA data. To once again consider the effect that age-related changes might have on the relationship, the residuals from the regression of the ilium PC2 data on age were plotted onto the tibia/humerus ratio data (Figure 5.32). In this plot, the positive linear relationship disappears, and what remains evident is that, in the ratio of tibia J to humerus J, the LSA sample has the most variation.

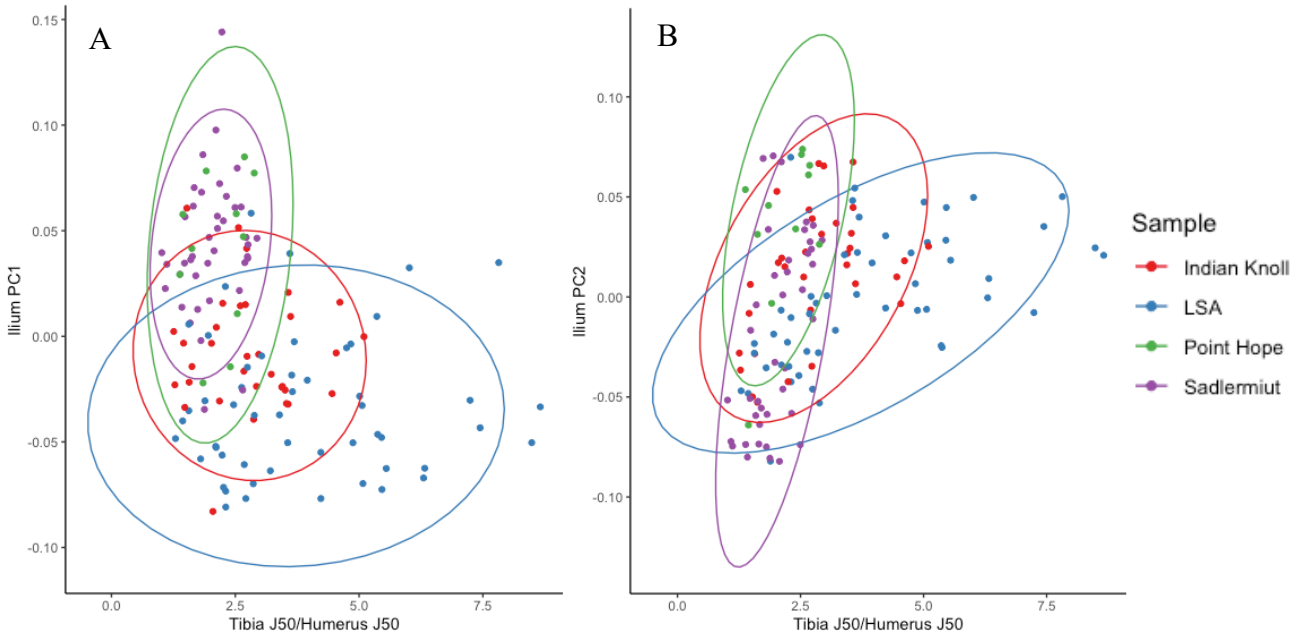

Figure 5.31 Ratios of lower limb to upper limb J values vs. A) ilium PC1, and B) ilium PC2.

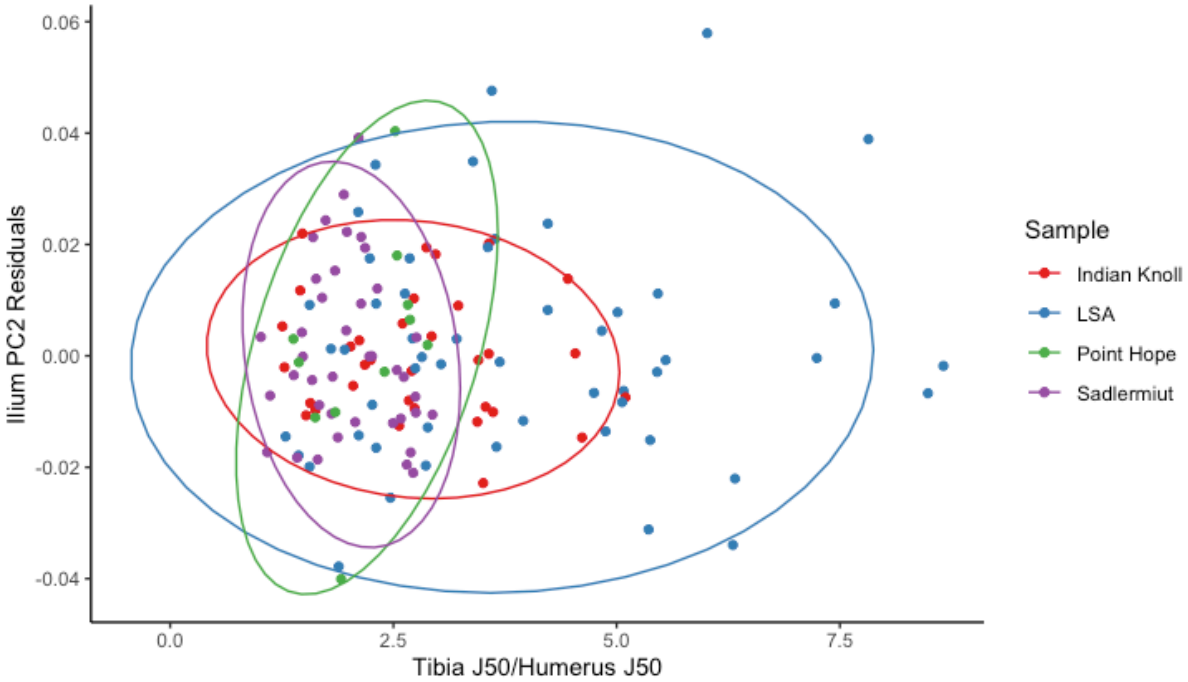

Figure 5.32 Ratio of tibial J to humeral J vs. residuals of ilium PC2 on age. No relationships between the variables are notable.

Linear regressions of PCs 1-20 of the combined sample ilium data on the tibia/humerus J ratio data were also calculated to look for potential relationships with subsequent PCs. Results show no large R^2 values in both the regressions of the combined sample data as a whole, as well as of each sample individually within the combined sample data (full regression results, including R^2, p, and SEE values for the combined sample for each PC, and the R^2 values for the individual samples within each regression, are reported in Appendix K, Table K.1). The highest R^2 value for a whole sample regression was that of PC2 ($R^2 = 0.138$, $p = <0.001$), and the highest R^2 values for the individual samples within the combined-sample data were in the PC2 regression (IK $R^2 = 0.206$, $p = 0.008$; LSA $R^2 = 0.301$, $p = <0.001$; PH $R^2 = 0.276$, $p = 0.097$; SAD $R^2 = 0.305$, $p = <0.001$), the PC5 regression (PH $R^2 = 0.254$, $p = 0.114$), and the PC12 regression (PH $R^2 = 0.213$, $p = 0.153$). While some of these regressions reached statistical significance, the low R^2 values throughout indicate that there is not a strong relationship between ilium shape variation, as represented by the PCA results, and activity data, as represented by the ratio of tibial J to humeral J.

CHAPTER 6: ISCHIUM SHAPE RESULTS

In this chapter, results of the ischium shape analyses are presented. Methods of analysis are consistent with those presented for the ilium data: principal components analyses were run on combined-sample and individual-sample Procrustes-fit landmark data, and the resulting principal components were analysed using regression and ANOVA. Age data, centroid size data, and regression scores were also analysed as a means of exploring ontogenetic patterns, maturity trajectories, and allometry. Relationships between ischium PCs and J are examined graphically to explore relationships between ischium shape and activity.

As with the ilium data, ischium centroid size was plotted on age to look at overall patterns of size change with age (Figure 6.1). The data across all four populations are best fit with quadratic curves, demonstrating that the relationship between size and age is not linear (as was the case with the ilium data). The Point Hope sample consistently plots slightly larger in centroid size across the whole age spectrum compared to the other samples, although the fit lines (particularly between the Indian Knoll, Point Hope, and Sadlermiut) are all very close and the differences are not likely to be statistically significant. The LSA sample diverges from the other samples around five years of age and remains consistently smaller throughout the rest of growth.

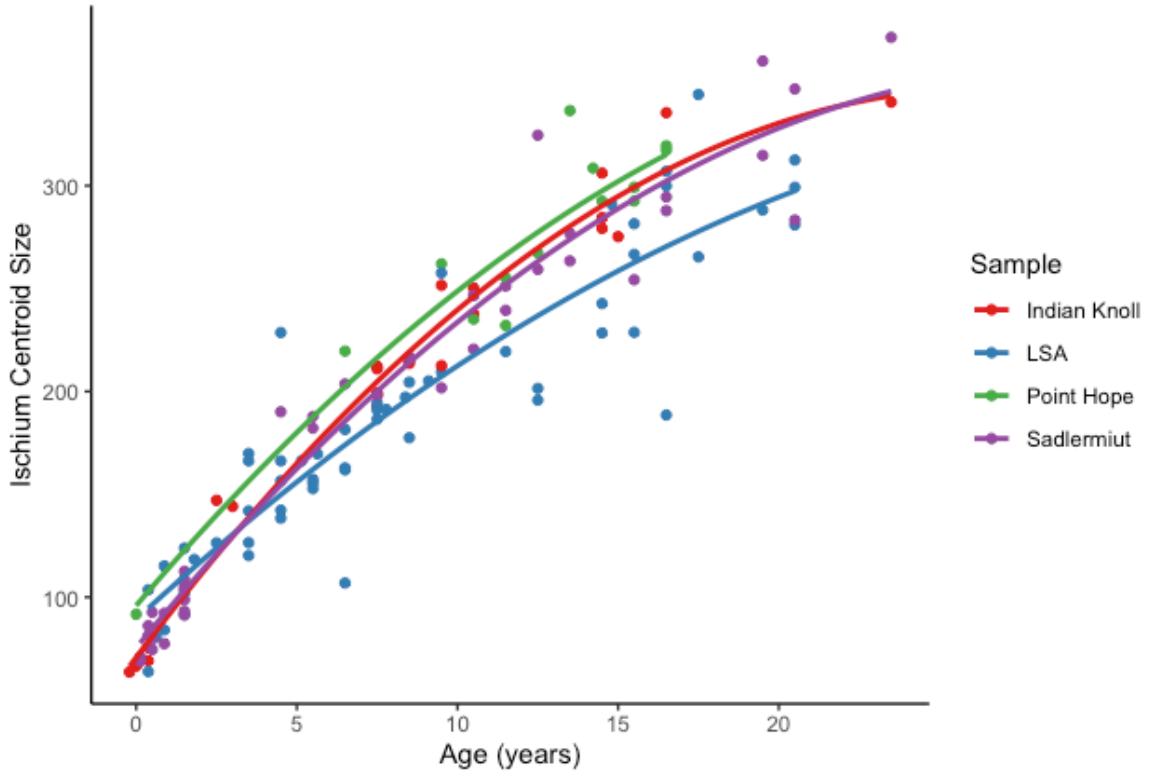

Figure 6.1 Ischium centroid size plotted on age, fitted with quadratic lines of best fit.

6.1 Principal Components Analysis – Introduction

Results of the combined-sample principal components analysis (PCA) are presented in Table 6.1. The percentage of variance captured by PCs 1-9 are reported for the combined sample, as well as for each individual sample, to be consistent with the results presented for the ilium data (where PC9 was chosen as a cut-off since more than 80% of the variance was represented by that point in all samples). As a summary, the cumulative total of variance captured is provided at PC10.

Principal component (PC) 1 represents more of the total variance in the combined ischium sample (60.3%) than all the other PCs combined. In the within-sample PCAs, PC1 for the LSA captures the lowest percent of the overall variation compared to the other samples (53.88%), meaning that more of the variation in this sample is spread out across more axes and

one direction of shape change does not capture as much of the overall variation as in the other samples. PC1 of the Sadlermiut captures the highest percentage of the overall variation in comparison with the other samples (74.92%), indicating that almost three-quarters of the total variation in the sample is captured by this one axis of shape change. The LSA, therefore, appear to have a less dominant axis of shape variation than the other samples, particularly in comparison with the Sadlermiut.

Table 6.1 Percentage of shape variance in the ischia captured by PCs 1-9, with the cumulative total provided at PC10, for the combined sample and each sample separately.

Principal Component	**Combined Ischium Sample (n=135)**	**LSA (n=58)**	**Indian Knoll (n=23)**	**Sadlermiut (n=40)**	**Point Hope (n=14)**
PC1	60.34	53.88	66.04	74.92	54.61
PC2	8.37	12.77	11.36	5.63	14.61
PC3	5.46	6.87	4.76	3.80	9.36
PC4	3.85	4.67	3.18	2.46	5.07
PC5	3.42	4.01	2.88	2.28	4.94
PC6	2.82	2.85	2.53	1.89	2.62
PC7	2.23	2.10	2.10	1.33	2.42
PC8	1.75	1.87	1.26	1.04	2.10
PC9	1.26	1.55	1.15	0.91	1.78
PC10 (cumulative)	90.86	91.74	96.33	95.08	98.49

6.2 Principal Components Analysis – Combined Sample

6.2.1 Overview

Three-dimensional lollipop graphs were generated to visually examine the variation in shape captured by the first three PCs (Figure 6.2). In the combined-sample ischium data, PC1, representing 60.34% of the overall variance, captures curvature of the bone as a whole and the length of the ischial ramus. This PC also highlights variation in the depth and curvature of the

acetabular surface. PC2, representing 8.37% of the overall variance, captures variation in the depth of the lateral portion of the acetabular surface, variation in breadth across the ischial ramus, and superior-inferior variation in the position of the ischial spine. Finally, PC3, representing 5.46% of the overall variance, predominantly captures variation in the angulation and length of the inferior portion of the pubis articulation site, as represented by the landmarks at the superior portion of the obturator foramen curve and in the depth of the lunate surface. See Figure 6.3 for examples of variation captured along PCs 1-3.

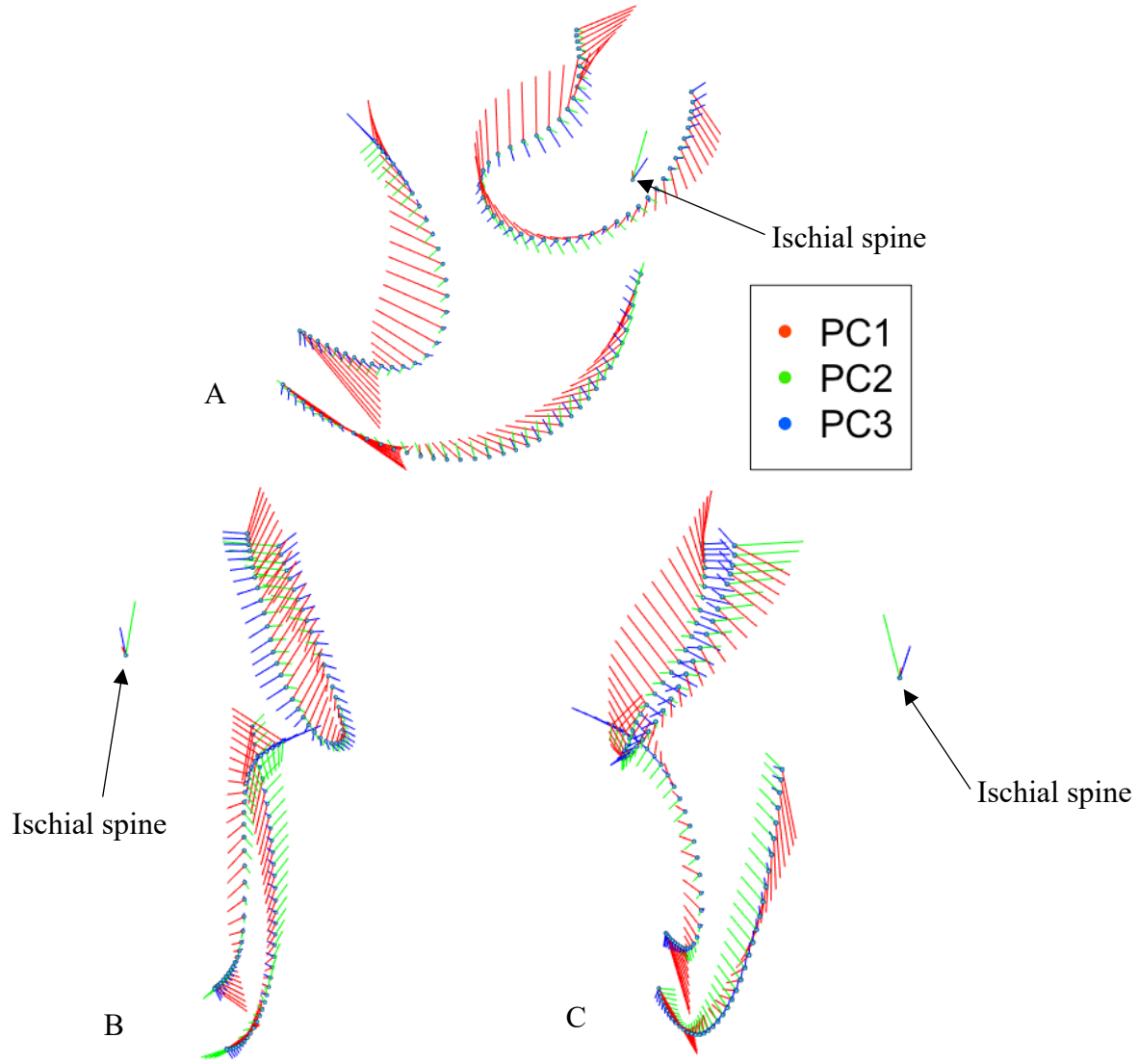

Figure 6.2 PCs 1-3 of the ischium for the combined sample, with lines representing the extent of variation represented by each PC at each landmark location. A) lateral view; B) anterior view; C) posterior view.

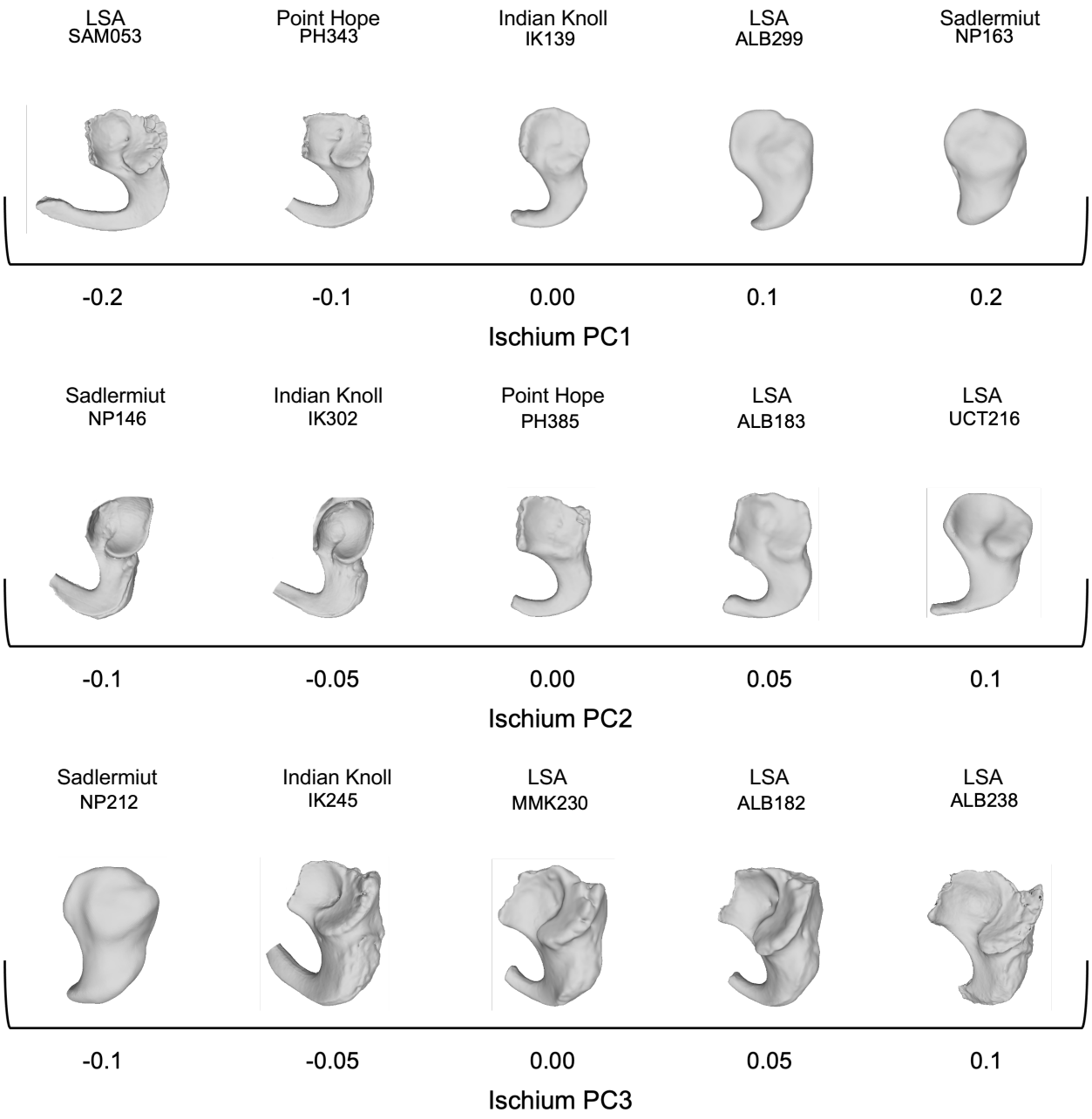

Figure 6.3 Examples of variation represented along PCs1-3 in the combined sample.

When PC2 of the combined-sample ischium data is regressed onto PC1, no relationships between the data are evident (Figure 6.4). The variation in length and curvature of the ischial ramus that is captured by PC1, therefore, does not seem to vary in a consistent way with the variation in ramus breadth and lunate surface depth captured by PC2. When age categories are

distinguished, some clustering of groups does show up, particularly amongst the oldest individuals in the sample, as they cluster towards the negative end on both axes. To further highlight the age category distinctions, a second plot of PC2 on PC1, in which confidence ellipses encircle the age categories, is shown in Figure 6.5. In this plot, age categories 1 (individuals less than 1 year of age), 3 (6 to <12 years of age), and 5 (18-24 years of age) are all distinct from one another. Age categories 2 (1 to <6 years of age) and 4 (12 to <18 years of age), however, have much larger distributions of data points. This suggests that morphology of the ischium for individuals in age categories 1, 3, and 5 is less variable between individuals, while there is greater variation present among the individuals in age categories 2 and 4. As age categories 2 and 4 include the onset of walking (1 to <6 years of age) and the pubertal growth spurt (12 to <18 years of age) it is not surprising that there is much more variation present in these groups than in the surrounding age categories. Further, these patterns appear to remain consistent across samples, as separation between the four samples is not apparent (Figure 6.4). See Appendix H for comparative plots of subsequent PCs.

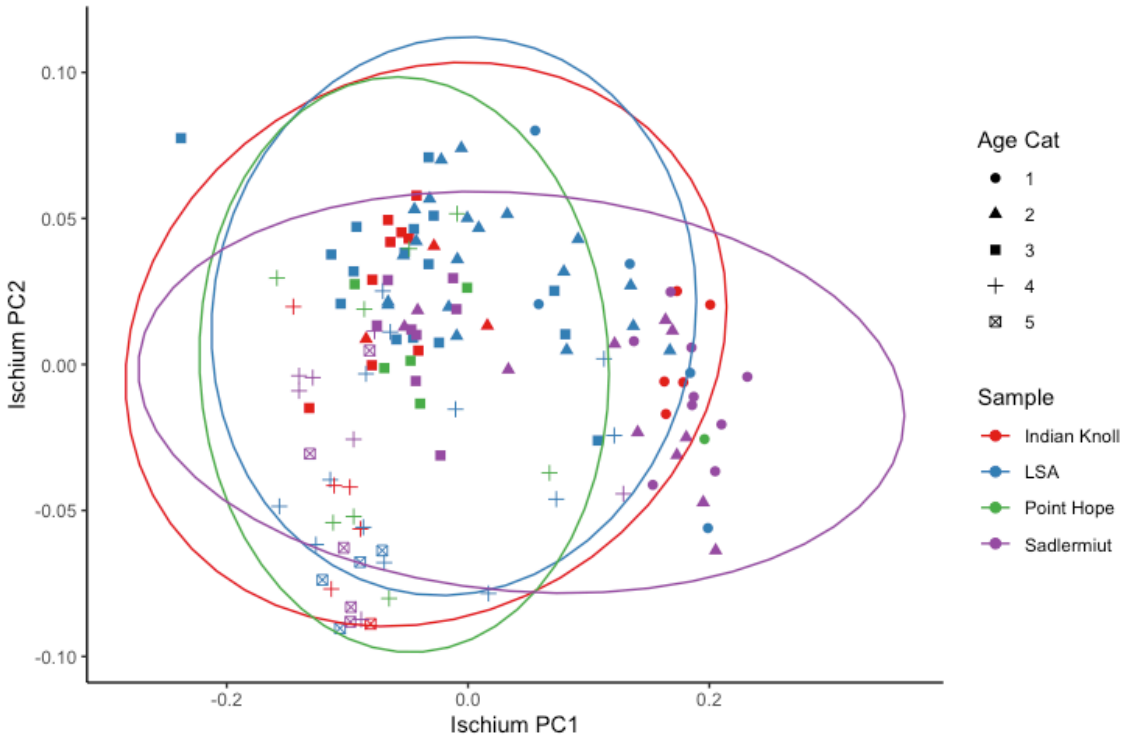

Figure 6.4 Combined-sample ischium data PC1 vs. PC2, shown with 95% confidence ellipses around the sample groups. Age categories: 1 (less that 1 year of age), 2 (1-<6years), 3 (6-<12 years), 4 (12-<18 years), and 5 (18-24 years).

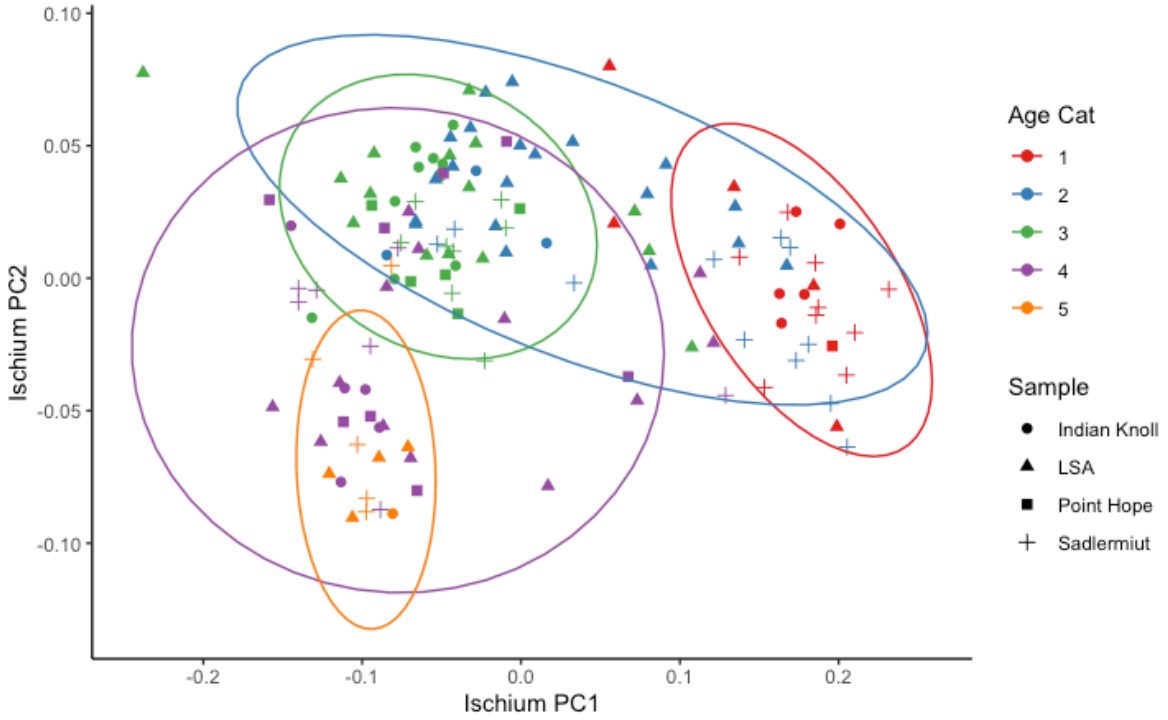

Figure 6.5 Combined-sample ischium data PC1 vs. PC2, shown with 95% confidence ellipses around the age categories. Age categories: 1 (less that 1 year of age), 2 (1-<6years), 3 (6-<12 years), 4 (12-<18 years), and 5 (18-24 years).

6.2.2 PC1 vs. Age

Where age related changes were not highlighted by the primary axis of variation in the ilium data, the opposite is true in the ischium data. PC1 of the combined-sample ischium data has a positive relationship with age that is best fit with a quadratic curve (Figure 6.6). The strength of the relationship, however, is not equal across all four samples. The Indian Knoll and Sadlermiut have high R^2 values for the fit of the quadratic regression line, while those of the LSA and the Point Hope are much lower (Table 6.2). In a plot of the standardized residuals from the quadratic regression (Figure 6.7), it is particularly apparent that the spread of the LSA data is greater than that of the other populations. Overall, in all the samples and with age, the ischium progresses from a comma-shaped bone, with a bulbous superior portion and a small tail pointing infero-medially, to a C-shaped bone with a squared-off medial edge on the superior portion, a pronounced curve around the acetabular surface, and a long, curved ramus extending medially. Unlike the primary axis of variation in the ilium data, separation between the samples is not evident along PC1 of the ischium data; slight differences in group medians are visible in the box plot of standardized residuals (Figure 6.7), but the differences are not as distinct as was seen in PC1 of the ilium data (Figure 5.8). See Section 6.2.4 for ANOVA results and further discussion of group separation.

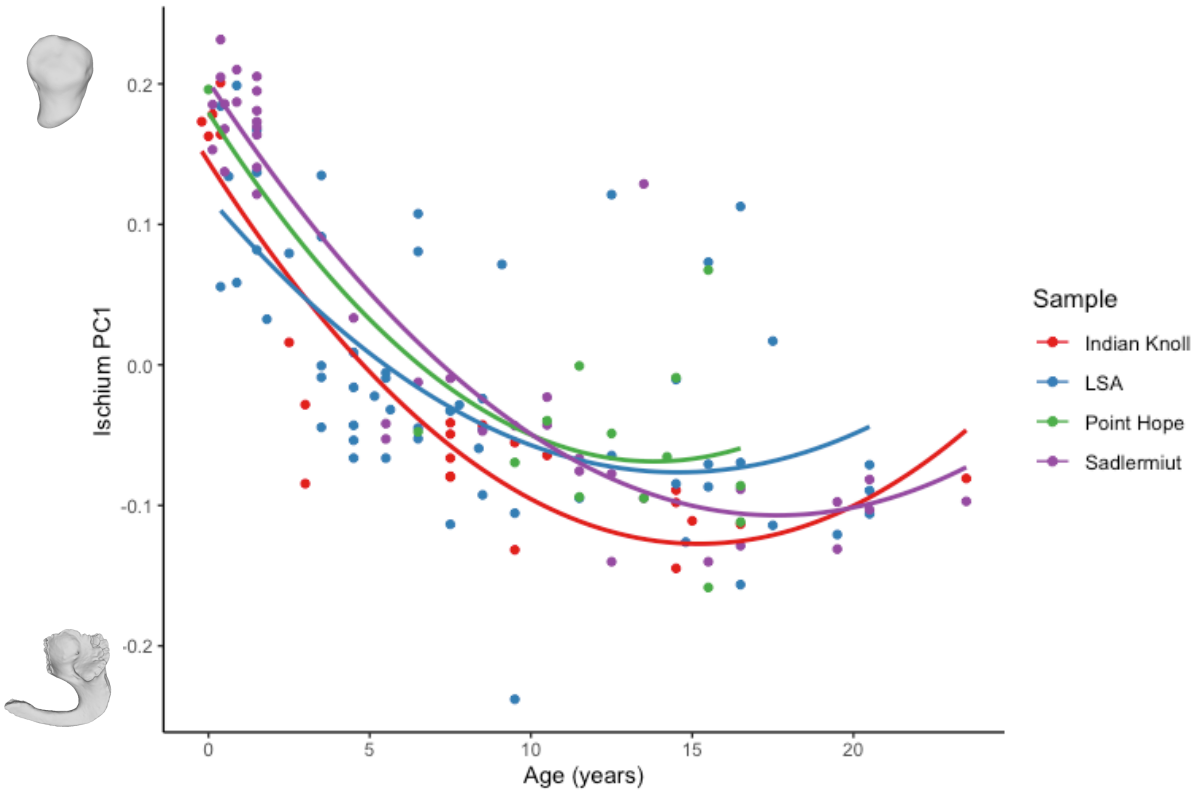

Figure 6.6 Age vs. ischium PC1, shown with quadratic lines of best fit. All samples show a similar age-related pattern, and no group distinctions are obvious.

Table 6.2 Results of the quadratic regression of the whole-group ischium PC1 data on age, separated by sample.

Sample	**R^2**	**SEE**	**p-value**
Indian Knoll	0.820	0.047	<0.001*
Later Stone Age	0.367	0.074	<0.001*
Point Hope	0.491	0.062	0.010*
Sadlermiut	0.855	0.049	<0.001*

*significant result at alpha of $p<0.05$

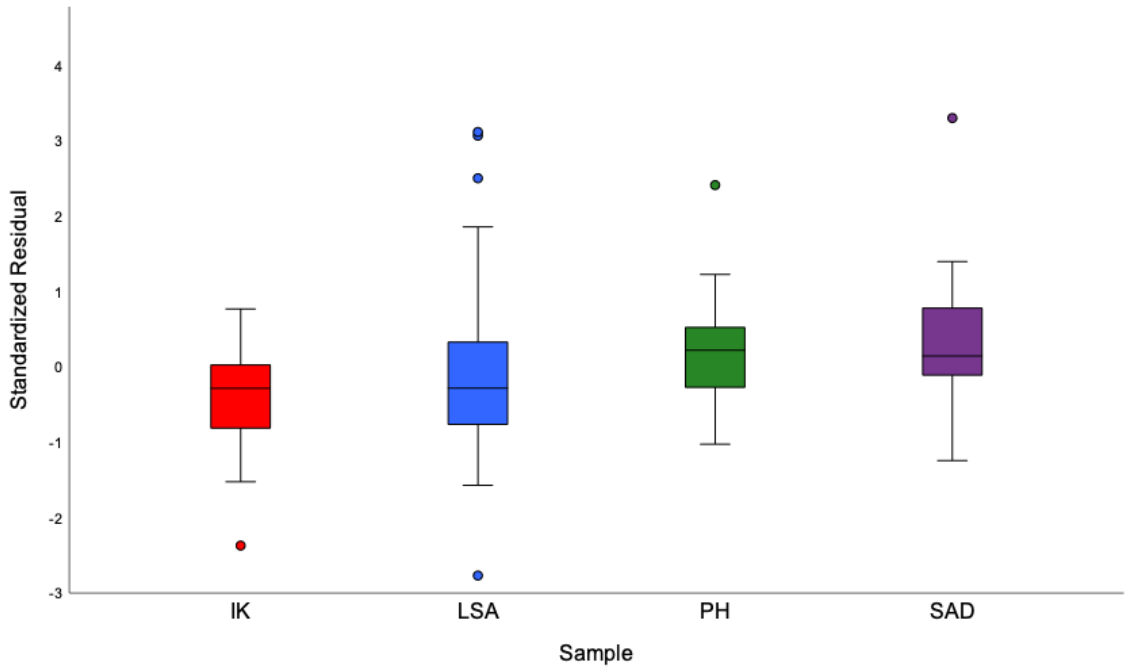

Figure 6.7 Standardized residuals from the quadratic regression of ischium PC1 on age, separated by sample. Boxes represent the middle 50% of the data, between quartiles 1 and 3, the line through the box represents the median of the data, and whiskers extend to the minimum and maximum values in each sample, up to 1.5x the interquartile range; the dots represent values that are greater or lesser than the 1.5x range.

6.2.3 PC2 vs. Age

The second PC of the whole-sample ischium data also shows a relationship with age that is best fit with a quadratic curve (Figure 6.8). This relationship, however, is much weaker than that of PC1 on age for all populations save the LSA, as can be seen in the R^2 values from the quadratic regressions (Table 6.3). A box plot of the standardized residuals from the quadratic regression of PC2 on age further shows the large spread of data points in each sample; the Point Hope median is lower than those of the other groups, demonstrating a small degree of separation between it and the terrestrial-foraging groups (Figure 6.9). The primary source of variation that appears to be captured along this axis is the thickness, angle, and depth of the curve of the ischial ramus, as well as the depth of the lunate surface of the acetabulum.

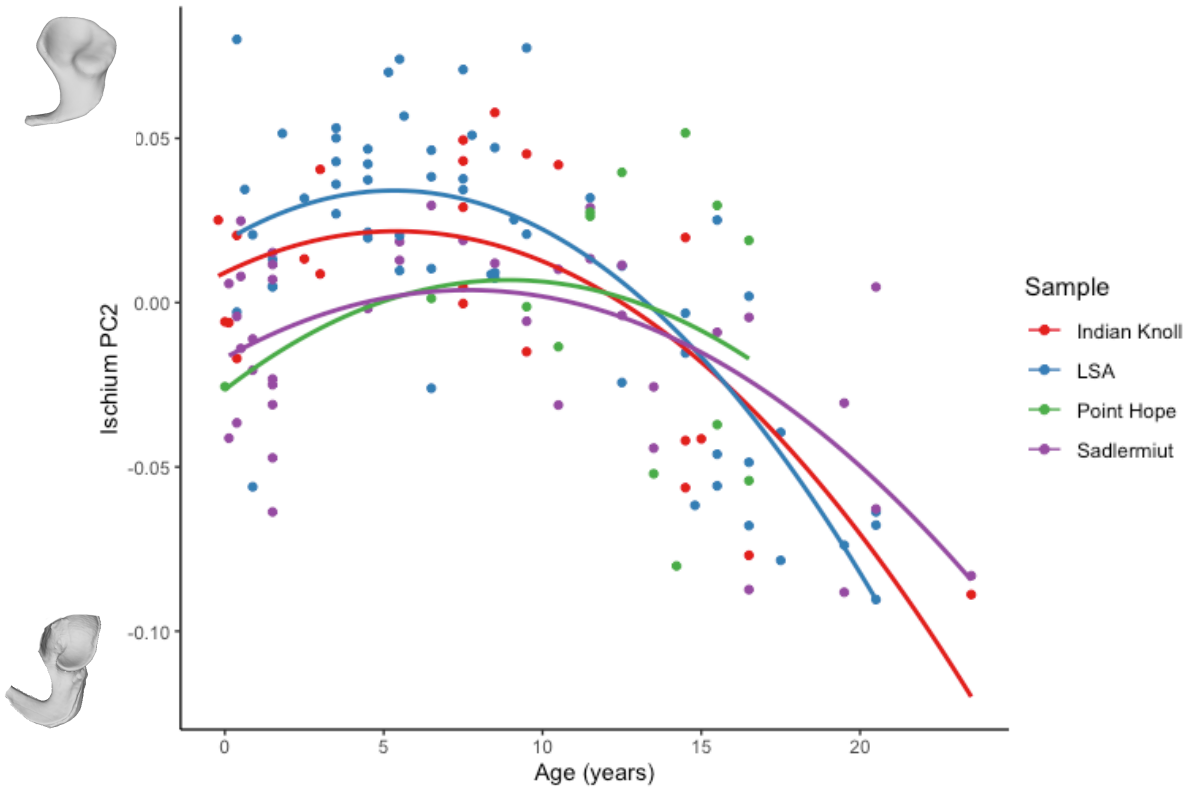

Figure 6.8 Age vs. ischium PC2, shown with quadratic lines of best fit.

Table 6.3 Results of the quadratic regression of the whole-group ischium PC2 data on age, separated by sample.

Sample	**R^2**	**SEE**	**p-value**
Indian Knoll	0.520	0.028	<0.001*
Later Stone Age	0.618	0.027	<0.001*
Point Hope	-0.103	0.042	0.684
Sadlermiut	0.306	0.027	<0.001*

*significant result at alpha of p<0.05

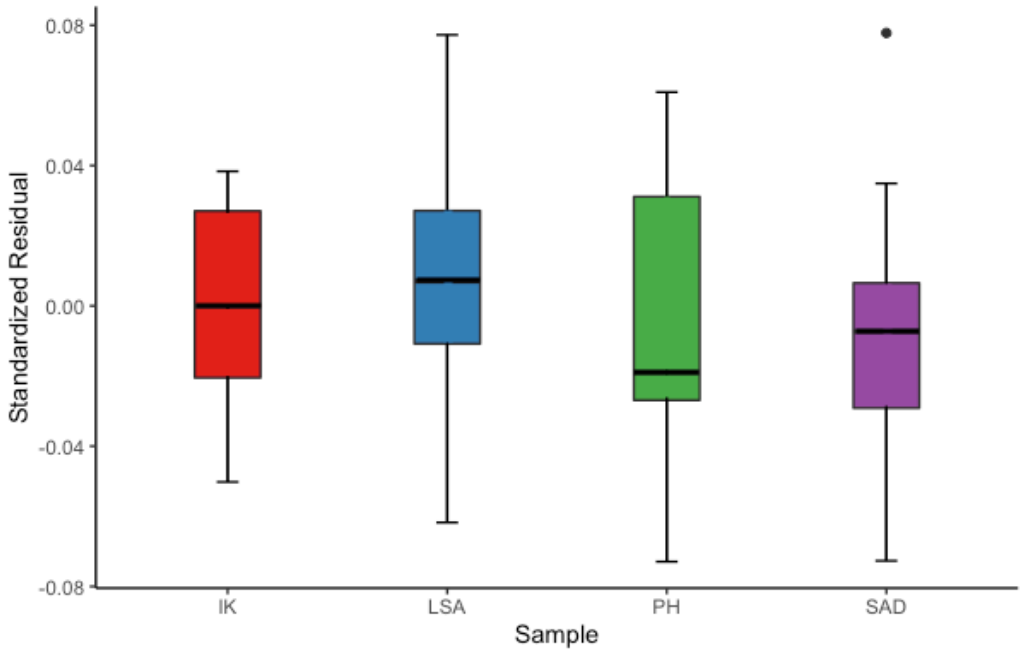

Figure 6.9 Standardized residuals from the quadratic regression of ischium PC2 on age, separated by sample. Boxes represent the middle 50% of the data, between quartiles 1 and 3, the line through the box represents the median of the data, and whiskers extend to the minimum and maximum values in each sample, up to 1.5x the interquartile range; the dot represents a value that is greater than the 1.5x range.

6.2.4 Sample Differences

To begin exploring sample differences within the ischium PC1 data, normality and variance tests were run. Results of Shapiro-Wilk normality tests for each sample indicate that only the LSA data have a normal distribution (IK: W = 0.788, p-value = 0.000; LSA: W = 0.965, p-value = 0.088; PH: W = 0.863, p-value = 0.034; SAD: W = 0.859, p-value = 0.000). A scale-location plot (Appendix I, Figure I.4) and the results of a Levene's test (F = 4.598, p-value = 0.004) demonstrate that homogeneity of variances cannot be assumed. Therefore, a Kruskal-Wallis test was used to explore sample differences in the data. Results indicate that the main effect of the sample on PC1 is not statistically significant and small (chi-squared = 5.550, p = 0.136; Eta^2 = 0.016, 95% CI [-0.01, 0.11]). Eta^2 indicates that only 1.6% of the variation that is being represented is happening between the groups.

Within the PC2 data, results of Shapiro-Wilk normality tests for each sample (IK: W = 0.935, p-value = 0.139; LSA: W = 0.932, p-value = 0.003; PH: W = 0.951, p-value = 0.583; SAD: W = 0.921, p-value = 0.008) indicate that the Indian Knoll and Point Hope follow a normal distribution, but that the LSA and Sadlermiut do not. A scale-location plot (Appendix I, Figure I.5) and the results of a Levene's test (F = 1.030, p-value = 0.382) demonstrate that homogeneity of variances can be assumed. Despite the non-normality of some of the data, one-way ANOVA was chosen to explore sample differences in the ischium PC2 data. Results suggest that the main effect of the sample on PC2 is statistically significant and moderate (F (3, 131) = 2.98, p = 0.034; Eta^2 = 0.06, 95% CI [0.003, 1.00]), with Eta^2 indicating that 6% of the variation captured is happening between the groups. Results of a post-hoc Tukey HSD test show that the only significant difference is between the Sadlermiut and LSA (Table 6.4, and see Appendix I, Figure I.6 for graphical representation of the results).

Table 6.4 Results of the ischium PC2 Tukey HSD test.

Samples Compared	**Adjusted p-value**
LSA-Indian Knoll	0.853
Point Hope-Indian Knoll	0.953
Sadlermiut-Indian Knoll	0.408
Point Hope-LSA	0.590
Sadlermiut-LSA	0.020*
Sadlermiut-Point Hope	0.882

*significant result at alpha of $p<0.05$

While group differences do not seem to explain significant amounts of the variation captured in the first two PCs of the ischium data, they do become more significant in PCs 3 and 4 (see Appendix H for these PCs plotted on age). This stands in contrast to the ilium data in which group differences did explain significant amounts of variation along the primary axis of

variation, but less so in subsequent PCs. PCs 3 and 4 capture 5.46% and 3.85% of the overall variation, respectively. While these are not substantial portions, it is still notable that group differences become apparent at this point.

Results of Shapiro-Wilk normality tests for each sample in the PC3 data (IK: W = 0.965, p-value = 0.567; LSA: W = 0.973, p-value = 0.226; PH: W = 0.940, p-value = 0.421; SAD: W = 0.966, p-value = 0.265) indicate that the data follow normal distributions, and a scale-location plot (Appendix I, Figure I.7) and the results of a Levene's test (F = 1.841, p-value = 0.143) demonstrate that homogeneity of variances can be assumed. Results of a one-way ANOVA suggest that the main effect of the sample on the variation captured by PC3 is statistically significant and large (F (3, 131) = 26.69, p <0.001; Eta^2 = 0.38, 95% CI [0.27, 1.00]) with 38% of the variation along this PC coming from between-group differences. Results of a post-hoc Tukey's HSD test show significant differences between the LSA and Indian Knoll, Point Hope and the LSA, and Sadlermiut and the LSA (Table 6.5, and see Appendix I, Figure I.8 for graphical representation of the results), highlighting the particular separation of the LSA from the other samples.

Table 6.5 Results of the ischium PC3 Tukey HSD test.

Samples Compared	**Adjusted p-value**
LSA-Indian Knoll	<0.001*
Point Hope-Indian Knoll	0.463
Sadlermiut-Indian Knoll	0.100
Point Hope-LSA	0.002*
Sadlermiut-LSA	<0.001*
Sadlermiut-Point Hope	0.366

*significant result at alpha of p<0.05

As seen in the 3D lollipop graphs (Figure 6.2), PC3 mainly captures variation in the angulation of the pubis articulation site relative to the ischial ramus, as represented by the landmarks at the superior portion of the obturator foramen curve. This PC also captures variation in the placement of the ischial spine, and some variation in the depth of the acetabular surface. The variation being captured along this axis, therefore, separates the LSA population out from the rest, with the positive end of the PC3 axis (where the LSA individuals fall) representing an ischial shape that is elongated towards the superior end of the curve of the obturator foramen.

Results of Shapiro-Wilk normality tests for each sample in the PC4 data (IK: $W = 0.963$, p-value = 0.531; LSA: $W = 0.979$, p-value = 0.426; PH: $W = 0.937$, p-value = 0.379; SAD: $W = 0.973$, p-value = 0.453) indicate that the data follow normal distributions, and a scale-location plot (Appendix I, Figure I.9) and the results of a Levene's test ($F = 1.324$, p-value = 0.270) demonstrate that homogeneity of variances can be assumed. Results of a one-way ANOVA suggest that the main effect of the sample on the variation captured by PC4 is statistically significant and moderate ($F (3, 131) = 6.49$, $p < 0.001$; $Eta^2 = 0.13$, 95% CI [0.04, 1.00]) with 13% of the variation coming from group differences. A post-hoc Tukey's HSD test shows significant differences between Point Hope and Indian Knoll, Point Hope and the LSA, and Sadlermiut and the LSA (Table 6.6). Thus, with the exception of the Sadlermiut and Indian Knoll samples, it seems that PC4 provides a degree of separation between the terrestrial- and marine-foraging groups.

Table 6.6 Results of the ischium PC4 Tukey HSD test.

Samples Compared	Adjusted p-value
LSA-Indian Knoll	1.000
Point Hope-Indian Knoll	0.009*
Sadlermiut-Indian Knoll	0.100
Point Hope-LSA	0.002*
Sadlermiut-LSA	0.021*
Sadlermiut-Point Hope	0.419

*significant result at alpha of $p<0.05$

6.2.5 PCs vs. Centroid Size

To explore the relationship between ischium shape and size, PC data were regressed onto centroid size (Figure 6.10). As expected, patterns of the results are similar to those of the PC data plotted on age, although the strength of the relationships, as assessed through the R^2 values (Tables 6.7 and 6.8), vary somewhat. Overall, size is a slightly stronger predictor of shape along the PC1 axis than is age, as was seen in the ilium data. This mostly holds true for PC2 as well, apart from the LSA for whom age is a slightly better predictor of shape than size.

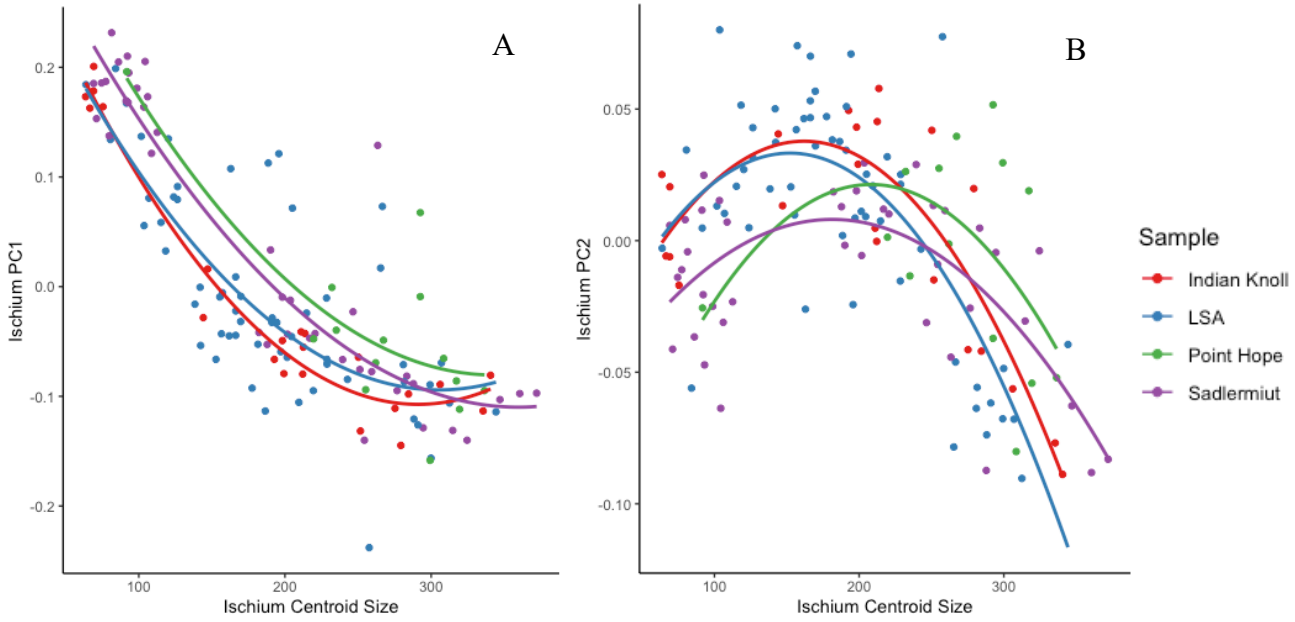

Figure 6.10 Ischium centroid size vs. A) ischium PC1, and B) ischium PC2, fitted with quadratic lines of best fit. All samples show similar age-related patterns, and no group distinctions are obvious.

Table 6.7 Regression results of the combined-sample ischium PC1 data plotted on ischium centroid size, separated by sample.

Sample	R^2	SEE	p-value
Indian Knoll	0.956	0.024	<0.001*
Later Stone Age	0.561	0.061	<0.001*
Point Hope	0.571	0.057	0.004*
Sadlermiut	0.871	0.047	<0.001*

*significant result at alpha of $p<0.05$

Table 6.8 Regression results of the combined-sample ischium PC2 data plotted on ischium centroid size, separated by sample.

Sample	R^2	SEE	p-value
Indian Knoll	0.709	0.023	<0.001*
Later Stone Age	0.540	0.030	<0.001*
Point Hope	0.125	0.038	0.191
Sadlermiut	0.384	0.025	<0.001*

*significant result at alpha of $p<0.05$

6.3 Principal Components Analysis – Individual Samples

6.3.1 Overview

As with the ilium data, lollipop graphs of PCs 1-3 were generated from each individual sample's PCA data to look at ischium variation within groups, as well as to compare the variation within the individual samples to that of the combined sample. For the LSA (Figure 6.11), the variation captured by PCs 1-3 closely resembles that of the combined sample, albeit with a few differences. The primary axis (representing 53.88% of the total variance in this sample) mainly captures variation in the length and curvature of the ramus, as well as in the depth of the acetabular surface. The second PC (representing 12.77% of the total variance) captures movement in the placement of the ischial spine, in the depth of the acetabular surface, particularly in the superior portion, and in the breadth of the ischial ramus. PC3 (representing

6.87% of the total variance) captures variation in the width of the acetabular surface amd in the breadth of the end of ischial ramus, as well as in the length and angulation of the superior portion of the obturator foramen, as captured by the landmarks at the superior end of the curve. The main differences between the variation captured by the PCA of the LSA sample and that of the combined sample can be found in the depth of the acetabular surface as captured by PC1 (particularly notable from the posterior view seen in Figure 6.11, C), and in the breadth of the end of the ischial ramus, as captured by PC3.

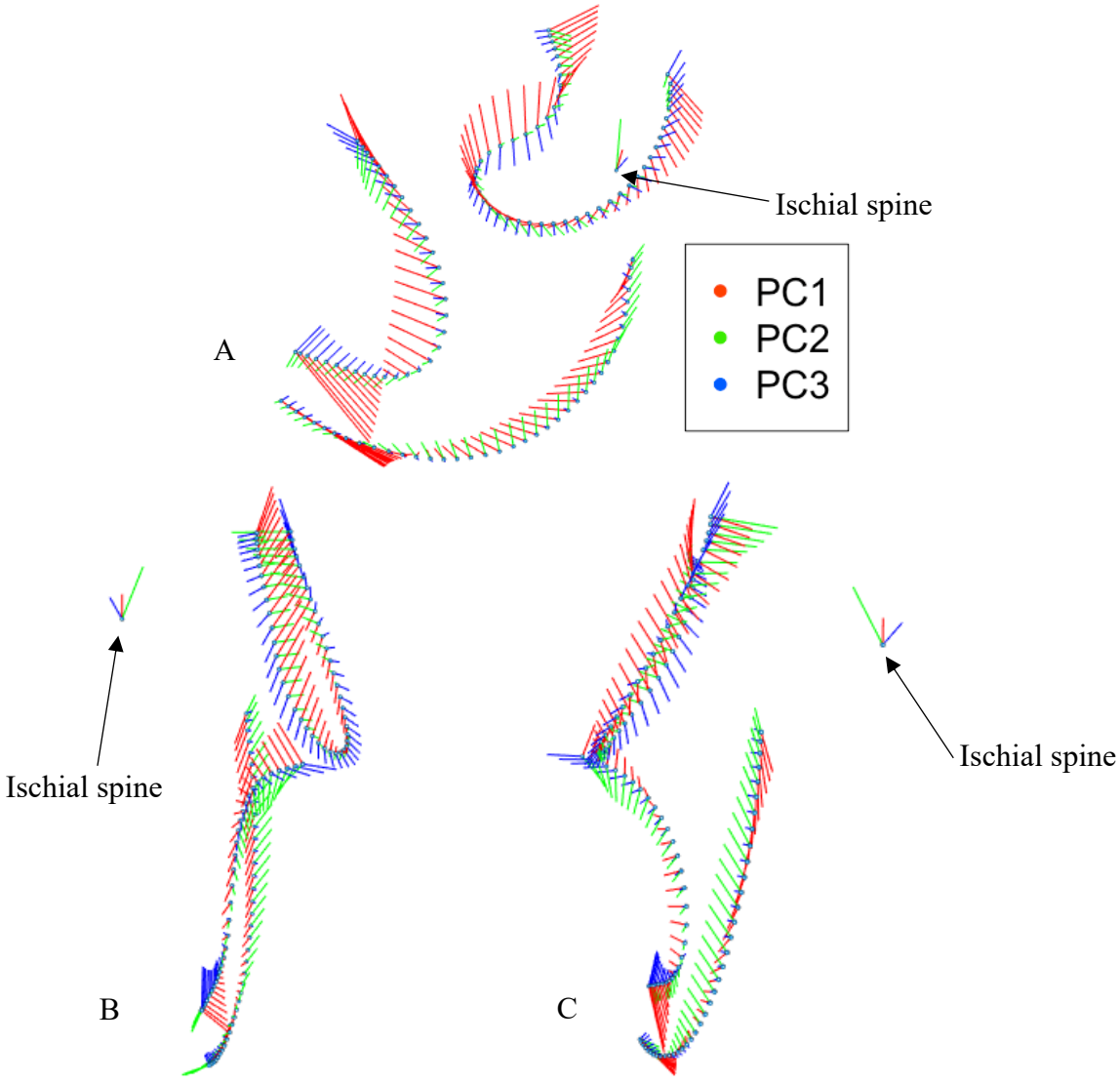

Figure 6.11 PCs 1-3 of the ischium for the LSA sample, with lines representing the extent of variation represented by each PC at each landmark location. A) lateral view; B) anterior view; C) posterior view.

In the Indian Knoll sample (Figure 6.12), PC1 (representing 66.04% of the total variance in this sample) captures variation in the length and curvature of the ischial ramus, as well as in the depth of the acetabular surface. PC2 (representing 11.36% of the total variance) captures variation in the placement of the ischial spine and in the depth of the posterior portion of the acetabular surface. PC3 (representing 4.76% of the total variance) mainly represents variation in the width of the obturator foramen as captured by the landmarks at the superior end of the curve. While the general locations of shape change captured by each PC are similar to those of the combined sample, the directionality and magnitude differs somewhat in the Indian Knoll sample. The length of the ischial ramus, as the most obvious example, captures a greater magnitude of variation in PC1 of this sample than what was captured along PC1 of the combined sample. Similarly, the extent of variation captured around the acetabular surface by PC1 has a greater magnitude than in the combined sample, as displayed by the length of the lollipops (particularly notable from the posterior view, seen in Figure 6.12, C).

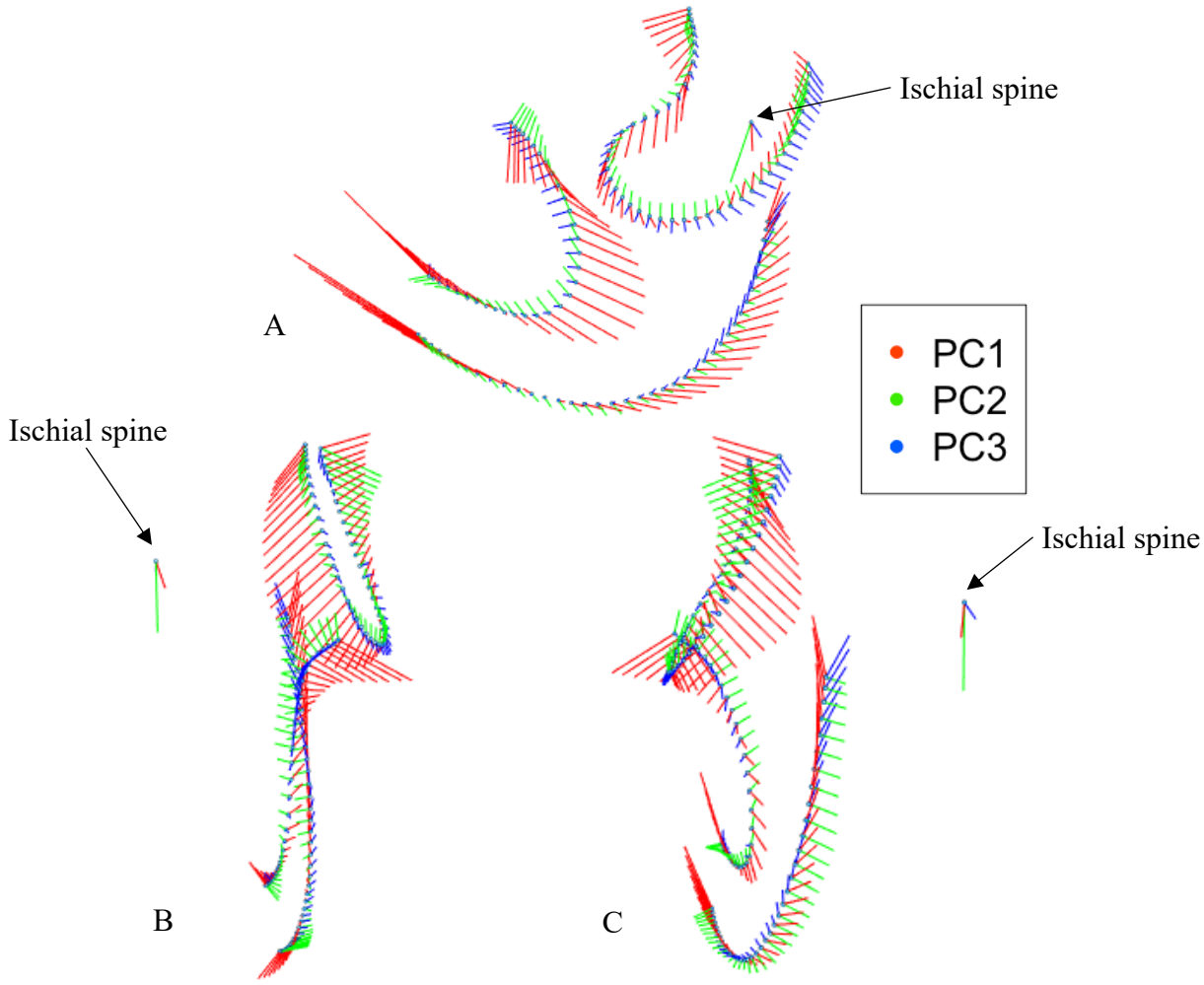

Figure 6.12 PCs 1-3 of the ischium for the Indian Knoll sample, with lines representing the extent of variation represented by each PC at each landmark location. A) lateral view; B) anterior view; C) posterior view.

In the Point Hope sample (Figure 6.13), the directions of variation captured by PCs 1-3 are similar to those from the Indian Knoll PCA, with some notable differences in magnitude (as represented by the length of the lollipops). Specifically, the magnitude of shape change captured along PC1 (which represents 54.61% of the total variance in this sample) appears smaller than that of the Indian Knoll, while the magnitude of shape change captured by PC2 (representing 14.61% of the total variance) appears somewhat greater, particularly in the depth of the acetabular surface. The shape change captured by PC3 (representing 9.36% of the total

variance) varies from that of the Indian Knoll in the direction of variation along the posterior border of the ischial ramus. Overall, the ways in which the variation captured by the Point Hope PCA differs from that of the combined sample is comparable to what was described previously concerning the Indian Knoll, with longer rami being a notable feature captured by PC1. For Point Hope in particular, the long rami can likely be explained by the lack of very young individuals in the sample (only two individuals are present across age categories 1 and 2, representing individuals less than 6 years of age).

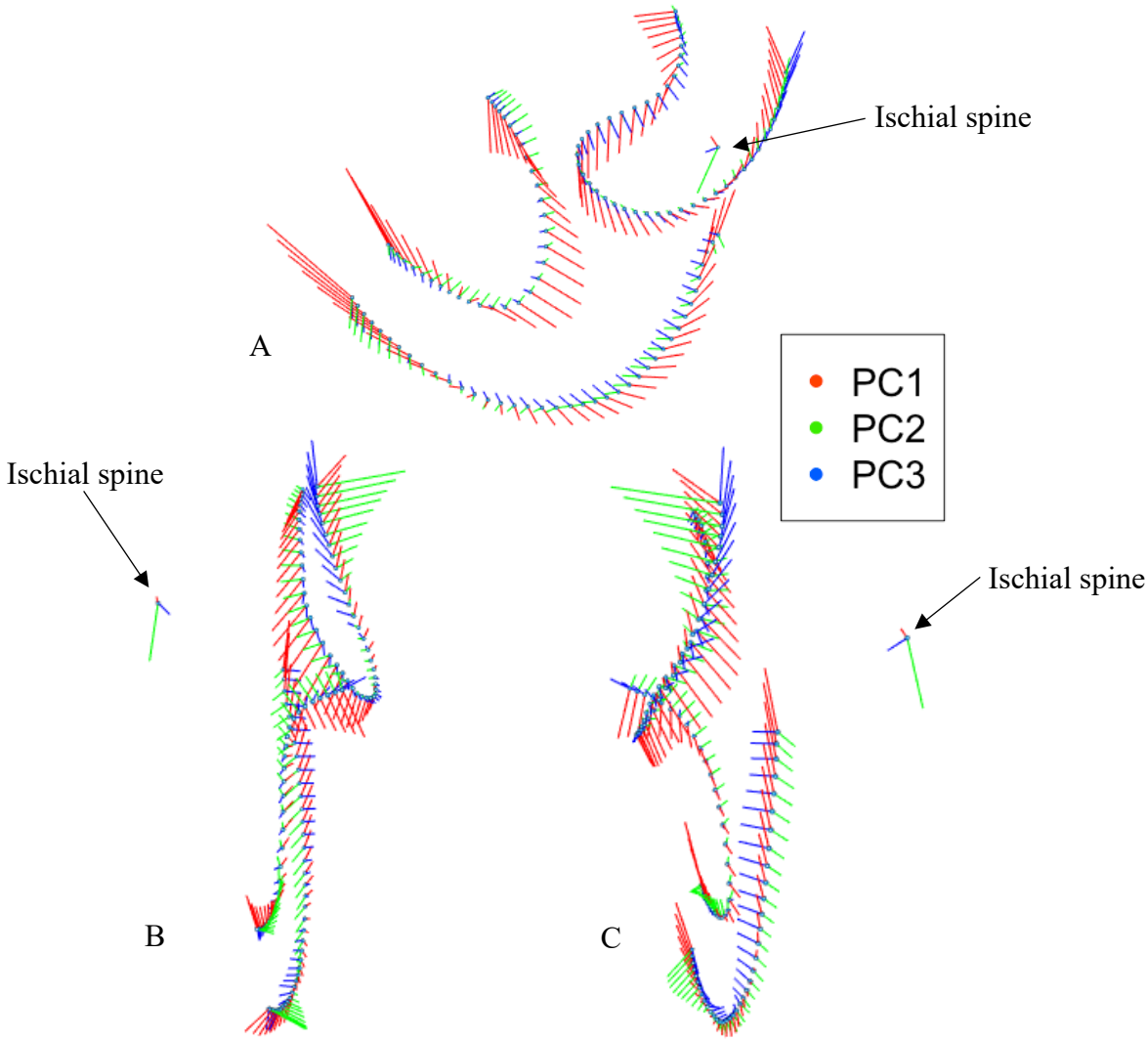

Figure 6.13 PCs 1-3 of the ischium for the Point Hope sample, with lines representing the extent of variation represented by each PC at each landmark location. A) lateral view; B) anterior view; C) posterior view.

Finally, in the Sadlermiut sample (Figure 6.14), the magnitude of variation captured by PC1 (which represents 74.92% of the total variance in the sample), represented by the length of the lollipops, is much greater than either PC2 or PC3. PC1 captures variation in the length and curvature of the ischial ramus, as well as the depth of the acetabular surface, while PC2 (representing 5.63% of the total variance) predominantly highlights variation at the posterior portion of the acetabular surface, and PC3 (representing 3.80% of the total variance) captures some movement in the length of the acetabular surface and the length of curve along the obturator foramen. The variation captured by this PCA differs from that of the combined sample in that PC1 captures a much greater magnitude of variation, while PCs 2 and 3 represent much smaller changes in shape. The direction of shape change captured by PC1, therefore, captures the majority of the variation in the Sadlermiut sample.

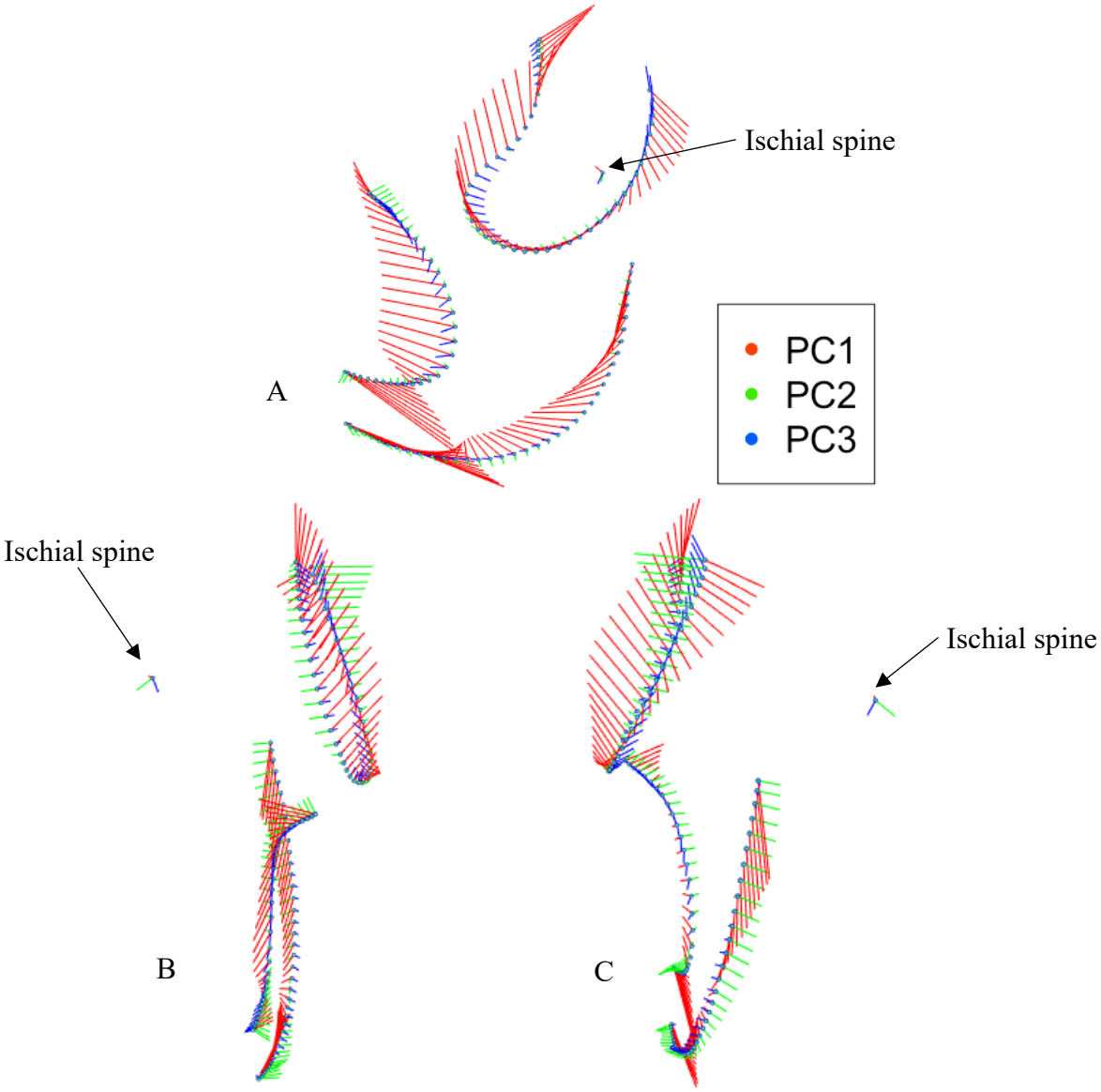

Figure 6.14 PCs 1-3 of the ischium for the Sadlermiut sample, with lines representing the extent of variation represented by each PC at each landmark location. A) lateral view; B) anterior view; C) posterior view.

6.3.2 PC1 vs. Age

In contrast to the PCA results from the ilium data, the combined sample and the individual sample PCA results for the ischium data show similar patterns when plotted on age. When the samples were pooled, as seen above in Section 6.2.2, an age-related trend was apparent

along PC1, with the LSA sample having the weakest relationship between shape variation captured by PC1 and age; these patterns hold when individual-sample PCs are plotted on age (Figure 6.15). R^2 values for the quadratic regressions of individual sample PC1s on age (Table 6.9) are similar to those from the combined sample (Table 6.2), with the Indian Knoll and Sadlermiut showing the strongest relationship and the LSA showing the weakest.

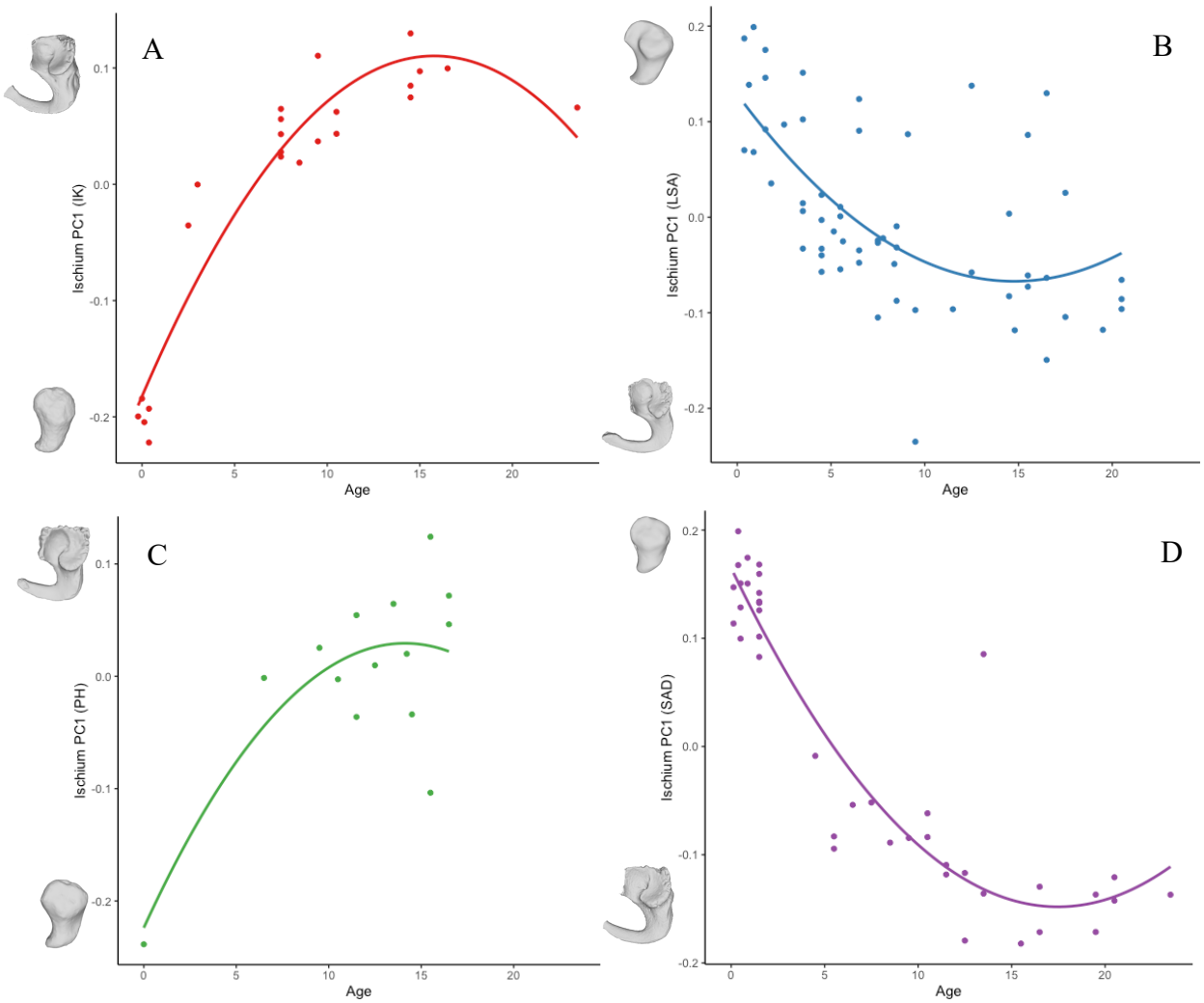

Figure 6.15 Age vs. ilium PC1 for the A) Indian Knoll sample (where PC1 represents 66.04% of the overall variation), B) LSA sample (53.88% of the overall variation), C) Point Hope sample (54.61% of the overall variation), and D) Sadlermiut sample (74.92% of the overall variation), all fitted with quadratic curves. Patterns are similar to what was seen in the combined sample.

Table 6.9 Results of the quadratic regressions of the individual samples' ischium PC1 data on age.

Sample	R^2	SEE	p-value
Indian Knoll	0.904	0.035	<0.001*
Later Stone Age	0.357	0.075	<0.001*
Point Hope	0.505	0.062	0.008*
Sadlermiut	0.857	0.050	<0.001*

*significant result at alpha of $p<0.05$

While the regression results for the Point Hope sample are fairly strong, the small sample size and single young individual in the sample make the patterns less reliable and more difficult to interpret; a larger sample size would be necessary to make more concrete conclusions about the strength of this relationship.

6.3.3 PC2 vs. Age

When PC2 from each individual sample's PCA is plotted onto age (Figure 6.16), the results are once again similar to what was seen in the combined-sample data. All the relationships are best fit with quadratic curves, and the LSA demonstrates the strongest relationship between the variables (Table 6.10). No strong relationship is evident in the Point Hope data between PC2 and age, likely a product of the small sample size once again.

Like in the combined sample, the Indian Knoll, Point Hope, and Sadlermiut samples show stronger relationships between PC1 and age than between PC2 and age, while the opposite is true for the LSA. This is similar to the pattern seen in the individual-sample results of the ilium, where all samples save the LSA showed stronger relationships between PC1 and age, and the opposite was true for the LSA. While the ilium and ischium data show different patterns from one another when all samples are combined, individual sample results of ilium and ischium

data plotted on age become much more alike. However, only some of the individual-sample ilium data were best fit with quadratic curves when plotted on age (PC1 for the Indian Knoll and Sadlermiut, and PC2 for the Sadlermiut), whereas the data for all samples are best fit with quadratic curves for PC1 and PC2 of the ischium.

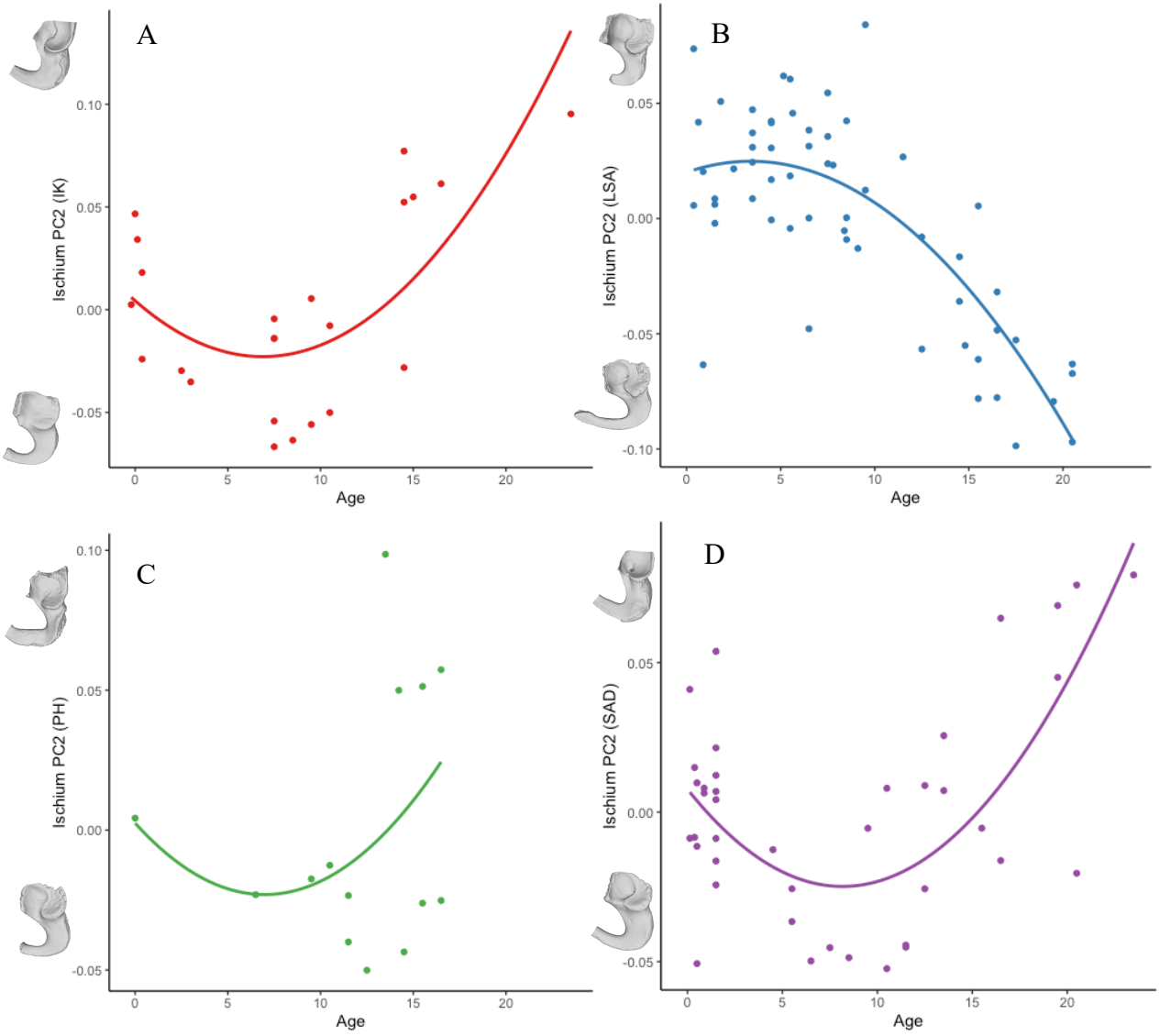

Figure 6.16 Age vs. ilium PC2 for the A) Indian Knoll sample (where PC2 represents 11.36% of the overall variation), B) LSA sample (12.77% of the overall variation), C) Point Hope sample (14.61% of the overall variation), and D) Sadlermiut sample (5.63% of the overall variation), all fitted with quadratic curves.

Table 6.10 Results of the quadratic regressions of the individual samples' ischium PC2 data on age.

Sample	**R^2**	**SEE**	**p-value**
Indian Knoll	0.448	0.035	0.001*
Later Stone Age	0.586	0.029	<0.001*
Point Hope	-0.040	0.047	0.495
Sadlermiut	0.412	0.028	<0.001*

*significant result at alpha of $p<0.05$

6.3.4 PCs vs. Centroid Size

As with the combined-sample data, individual-sample PCs were plotted onto centroid size data to explore relationships between size and shape. Results of PC1 plotted on centroid size (Figure 6.17) are similar to the results seen when PC1 was plotted on age (Figure 6.15), although the relationships, as described through R^2 values (Table 6.11), are stronger here indicating that size is a slightly better predictor of shape than is age in all samples. Results of the individual samples' PC2 data plotted on centroid size are also quite comparable to the results seen with age, with the only notable difference being the strength of the relationship in the Point Hope data (the R^2 value for the regression of PC2 on centroid size is 0.365 while that for PC2 on age was -0.040). For this reason, the graphs and regression results of PC2 and centroid size are not included here, but can been found in Appendix J.

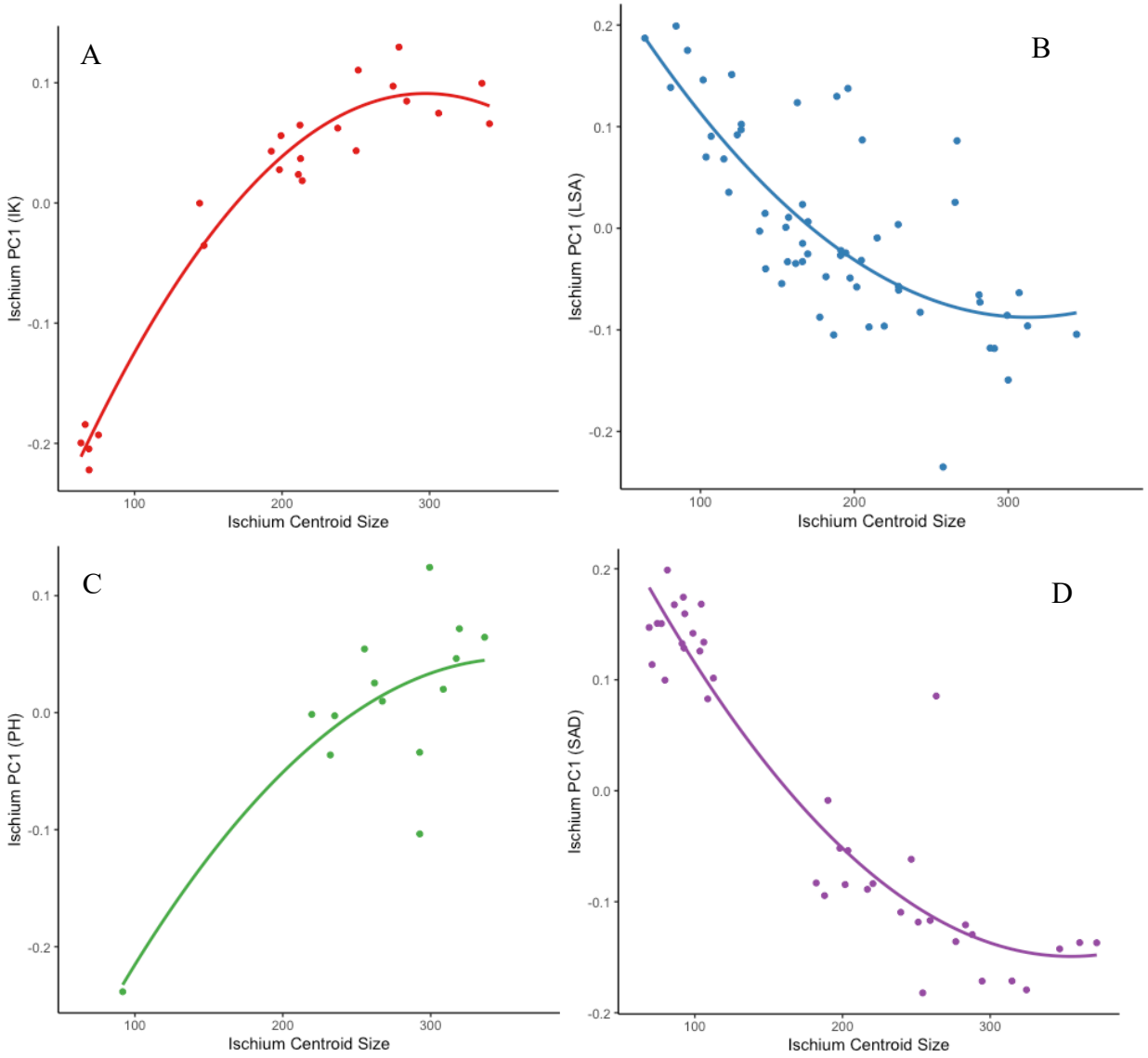

Figure 6.17 Ischium centroid size vs PC1 from the individual sample PCAs for the A) Indian Knoll, B) LSA, C) Point Hope, and D) Sadlermiut samples, fitted with quadratic curves. All samples show a degree of age-related patterning.

Table 6.11 Regression results of the individual samples' ischium PC1 data plotted on centroid size.

Sample	**R^2**	**SEE**	**p-value**
Indian Knoll	0.960	0.023	<0.001*
Later Stone Age	0.547	0.063	<0.001*
Point Hope	0.581	0.057	0.003*
Sadlermiut	0.873	0.047	<0.001*

*significant result at alpha of $p<0.05$

6.4 Allometry

To investigate allometry, regression scores were plotted onto log-transformed centroid size to visualize and quantify the amount of shape change for a given unit of size change across the sample (Figure 6.18). Results from the ischium data show a positive linear relationship between the variables, indicating the presence of allometric effects on shape variation, with an R^2 value for the regression of 0.780.

When age categories are separated out, individuals in age category 4 (12-<18 years of age) have the largest spread of points across the regression score axis (y). This indicates that individuals between the ages of 12 and <18 years of age (in all samples save the Indian Knoll) have more variation in ischium shape for a given centroid size than do individuals in other age categories, and therefore the relationship between shape and size is not as predictable in this age group as it is in others. This corresponds to the patterns seen when PC2 was plotted on PC1 (Figure 6.5), where the spread of data points in age category 4 was much larger than that of the other groups. Age category 2 also had a large spread of points in that plot, and while that has not translated to a larger spread of data points across a single axis alone in this plot, individuals in age category 2 do have a larger spread of points along both axes than do the other age categories here. This, once again, demonstrates a larger scope of variation in the relationship between shape and size in individuals aged between 1 and <6 years of age, although in the case of this age category that relationship has remained more predictable.

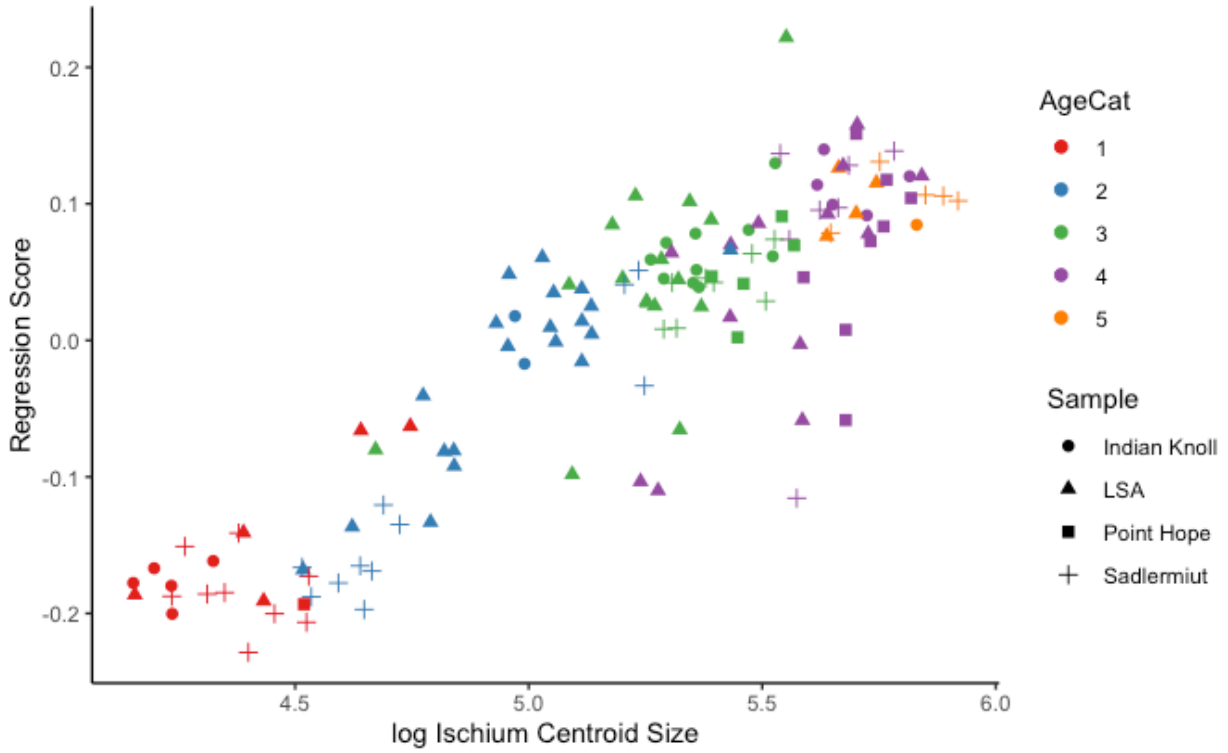

Figure 6.18 Regression scores plotted on log-transformed centroid sizes, organized by age category and sample for the ischium data. Age categories: 1 (less that 1 year of age), 2 (1-<6 years), 3 (6-<12 years), 4 (12-<18 years), and 5 (18-24 years).

6.5 Maturity Trajectories

While some of the overall trends in maturity trajectories of the ischium appear similar to those of the ilium, there are some key differences. Where, apart from the Point Hope sample, the shape maturity trajectories sat consistently higher than the size maturity trajectories in the ilium data, such is not the case in the ischium data as the trajectories appear intertwined (Figure 6.19). For a breakdown of the approximate ages at which 25%, 50%, and 75% maturity are reached in shape and size across all four populations, see Table 6.12.

For Indian Knoll, size and shape trajectories are closely intertwined, although the rate of change for size increases slightly around age five where that of shape decreases. The trajectories meet up again around 10 years of age, and then the shape trajectory slows somewhat after 15

years of age; full size maturity is reached for this sample before shape maturity. For the LSA, the size and shape trajectories are virtually identical; there is a slight dip in the size trajectory compared to the shape trajectory between 10 and 15 years of age, but otherwise the two trajectories are indistinguishable. For Point Hope, much like in the ilium data, the shape trajectory seems to have a different pattern to the other populations, with a slower pace in the early years, a quickening of the pace after age 10, and a plateau around age 17; this pattern could, however, once again be a product of a small sample size and a single individual representing the starting point of growth. The size trajectory is similar to that of the other populations, but there is an increase in the rate of change between 11 and 15 years of age. Finally, for the Sadlermiut, the shape trajectory shows a similar pattern to that of the ilium data, with a steep trajectory prior to the age of five, which then levels off and proceeds at a fairly consistent rate after age 10. The size trajectory falls consistently below the shape trajectory but proceeds at a steady pace across growth, indicating that shape maturity is reached before size maturity.

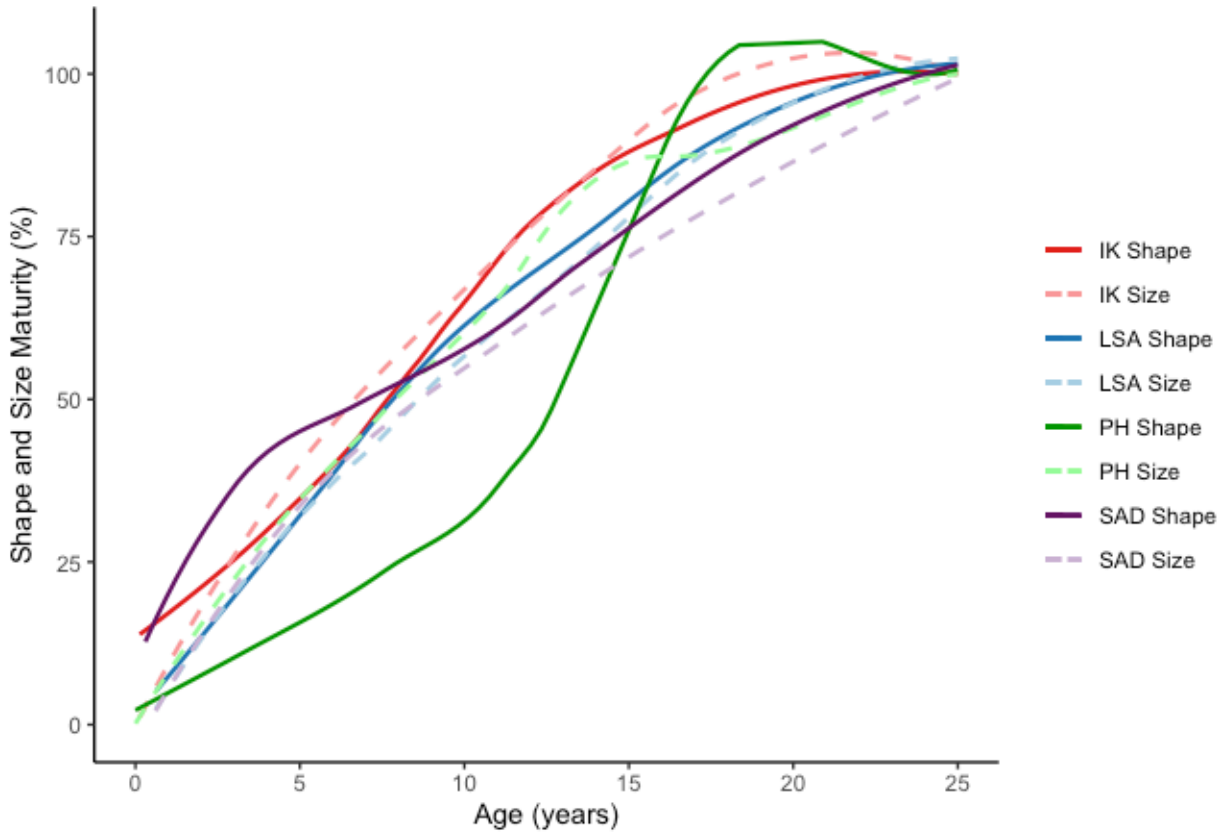

Figure 6.19 Ischium size (solid lines) and shape (dashed lines) maturity trajectories.

Table 6.12 Approximate ages at which percentages of shape and size maturity of the ischium are reached across all four populations.

Sample	Age at 25%		Age at 50%		Age at 75%	
	Shape	**Size**	**Shape**	**Size**	**Shape**	**Size**
Indian Knoll	2.5 yrs	2.5 yrs	8 yrs	6.5 yrs	12 yrs	12 yrs
LSA	4 yrs	4 yrs	8 yrs	8 yrs	14.5 yrs	14.5 yrs
Point Hope	8 yrs	3.5 yrs	13 yrs	8 yrs	15 yrs	12 yrs
Sadlermiut	1.5 yrs	3.5 yrs	8 yrs	9 yrs	14 yrs	17 yrs

6.6 Ischium Shape and Cross-Sectional Geometry

6.6.1 PCA Data and Standardized J Values

When the ischium PC1 data is plotted onto size-standardized J values (Figure 6.20), a positive linear relationship between the PC data and each of the CSG parameters is apparent. As was seen when the ilium PC2 data was plotted onto CSG parameters, the Sadlermiut sample has the largest spread of data across both axes, although no separation between the four samples is evident.

To control for potential age-related changes captured in the plots of PC1 on the standardized J values, residuals from the regression of PC1 on age were plotted onto the residuals of the regressions of the CSG parameters on age. As with the ilium data, results of standardized femoral J are shown here (Figure 6.21), while humerus and tibia results can be found in Appendix K. The linear pattern that existed in the plots of PC1 on the J values disappears once age is controlled for. Notably, a slight negative relationship emerges in the Point Hope data, while the LSA becomes the most variable sample along the y-axis and the Sadlermiut retains the most variation along the x-axis. This is a change from the results seen in Figure 6.20, where the Sadlermiut sample had the largest spread of data points overall.

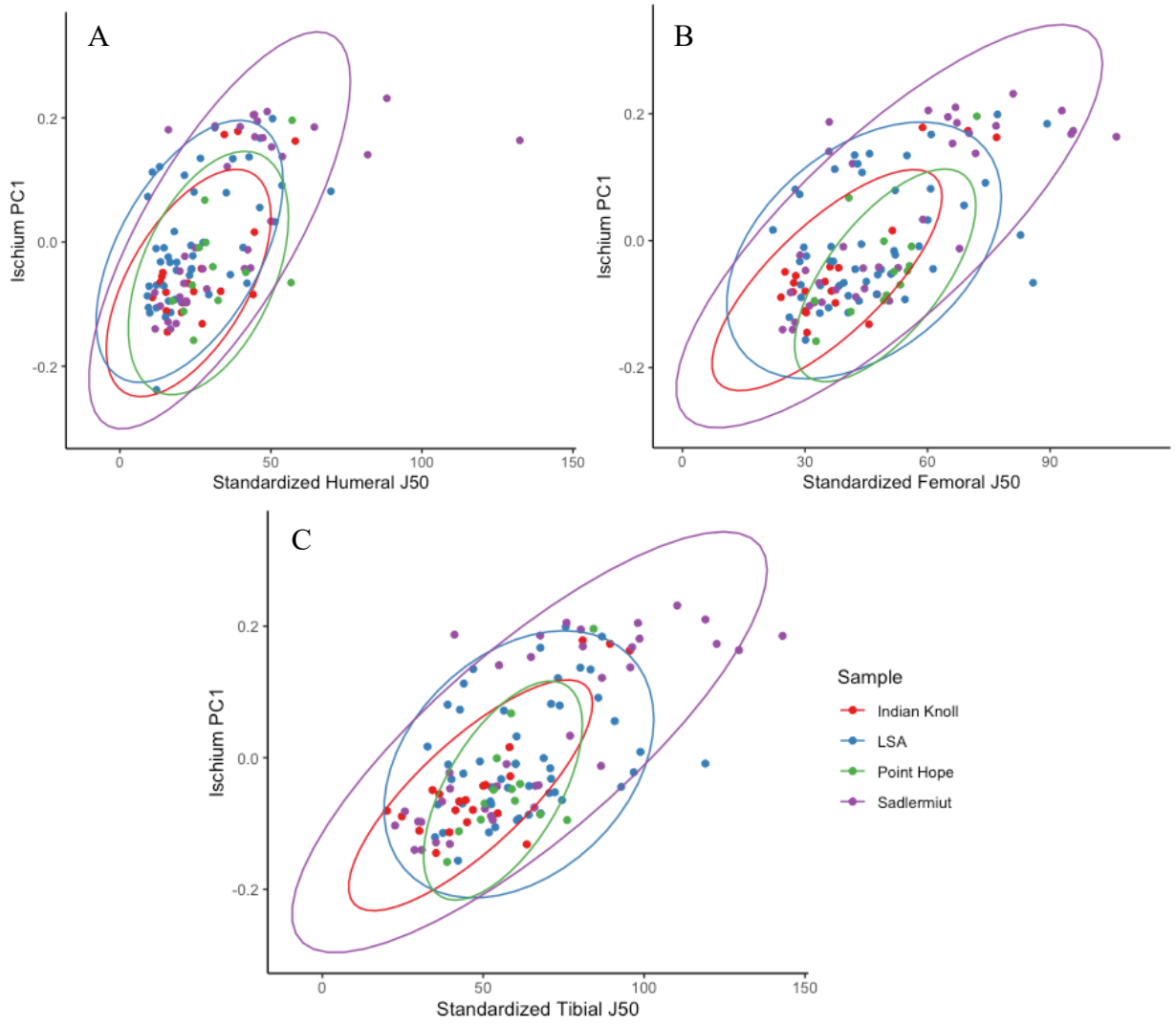

Figure 6.20 PC1 of the combined sample ischium data plotted on A) standardized humeral J, B) standardized femoral J, and C) standardized tibial J, all shown with 95% confidence ellipses.

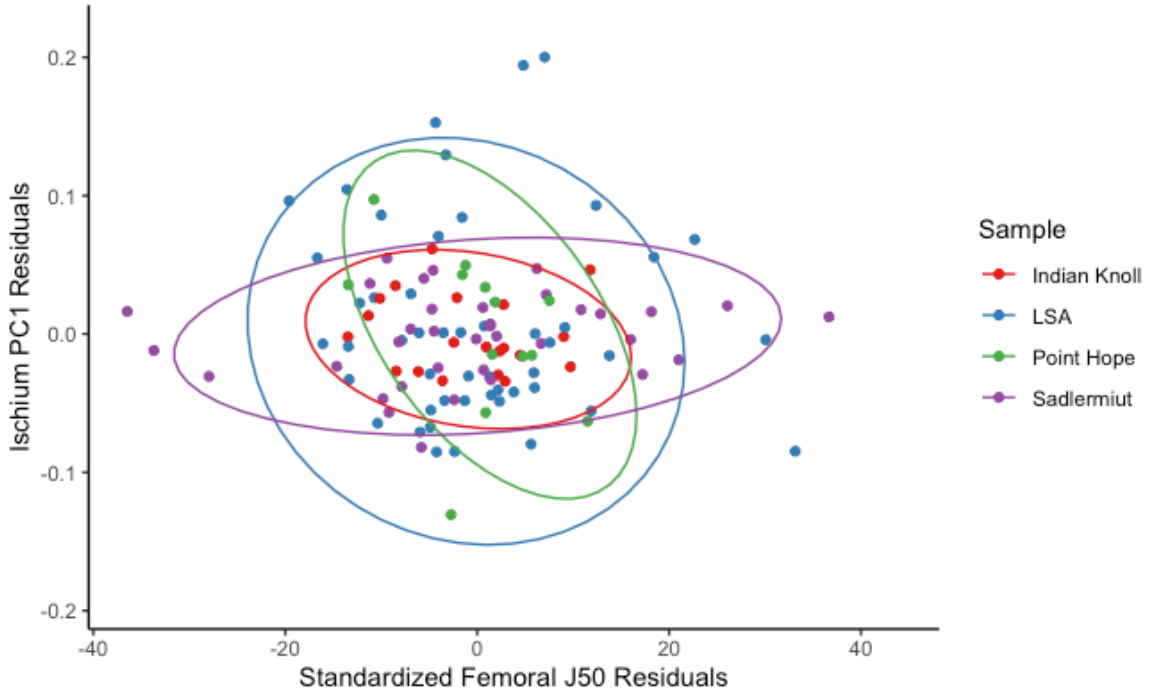

Figure 6.21 Residuals from the regression of standardized femoral J on age vs. the residuals from the regression of ischium PC1 on age, shown with 95% confidence ellipses. No relationships are evident between the variables.

In plots of the ischium PC2 data on the standardized measures of J, no relationships between the variables are obvious (Figure 6.22). This indicates that the shape change captured by PC2, mainly the thickness, angle, and depth of the curve of the ischial ramus, as well as the depth of the lunate surface of the acetabulum, does not vary consistently with measures of activity in any of the three bones examined.

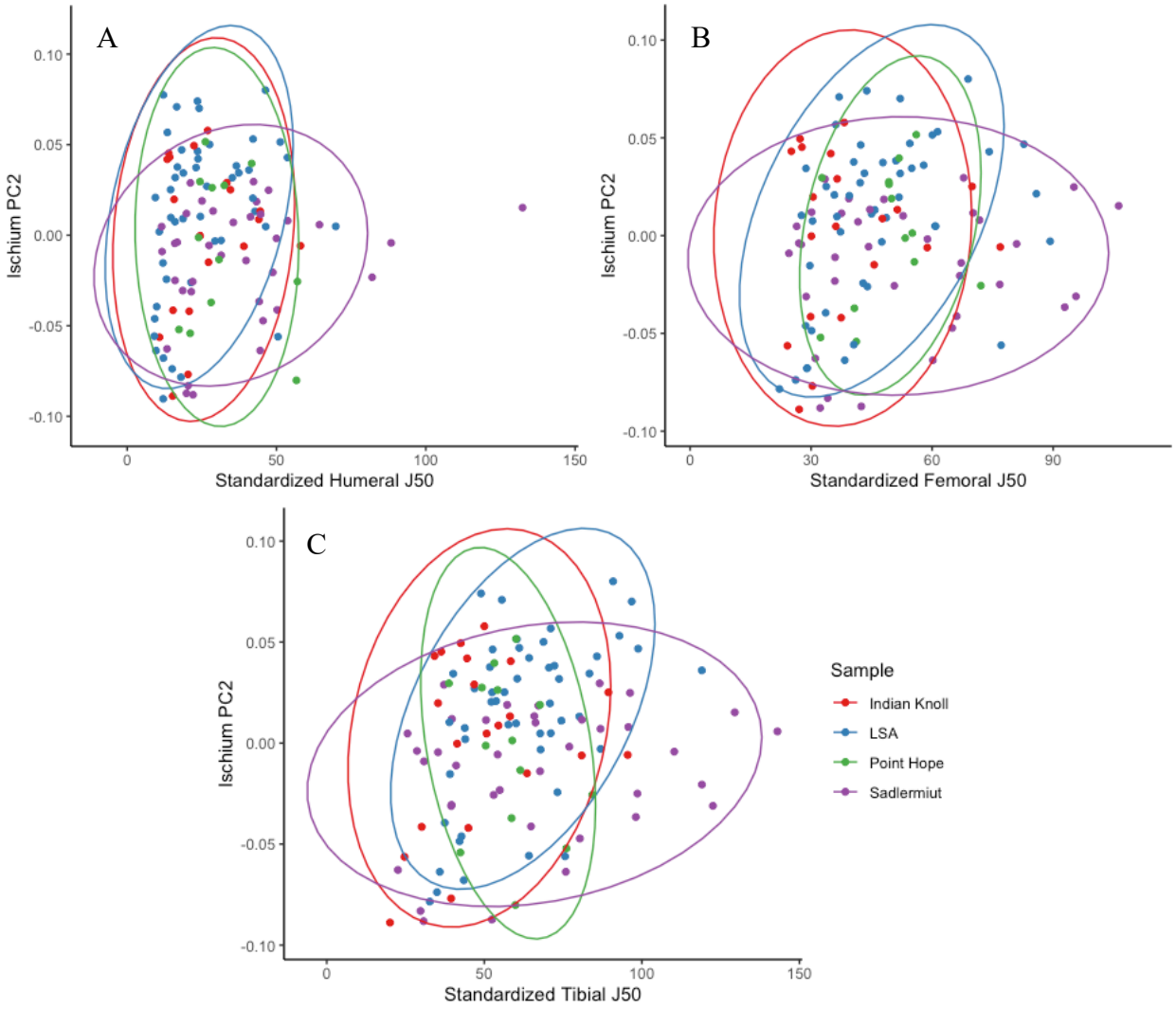

Figure 6.22 PC2 of the combined sample ischium data plotted on A) standardized humeral J, B) standardized femoral J, and C) standardized tibial J, all shown with 95% confidence ellipses.

6.6.2 PCA Data and Ratio J Values

When the first two PCs of the combined-sample ischium data are plotted onto the ratio data of tibial J/humeral J (Figure 6.23), no strong relationships between the CSG data and the ischium PC data are evident. It is also once again apparent that the LSA sample has the largest spread of data points compared to the other samples. A negative linear relationship is somewhat apparent in the PC1 data, particularly in the LSA sample, but again, both data sets have a

relationship with age and size, and it is therefore that relationship that is likely being captured here as well. When the residuals of the regression of the ischium PC1 data on age are plotted on the J ratio data (Figure 6.24), the negative linear relationship mostly disappears, and the large spread of the LSA data again becomes the most notable feature of the plot. Separation between the marine and terrestrial foraging groups is not evident in these graphs, but differences in patterns between the LSA and the other samples are.

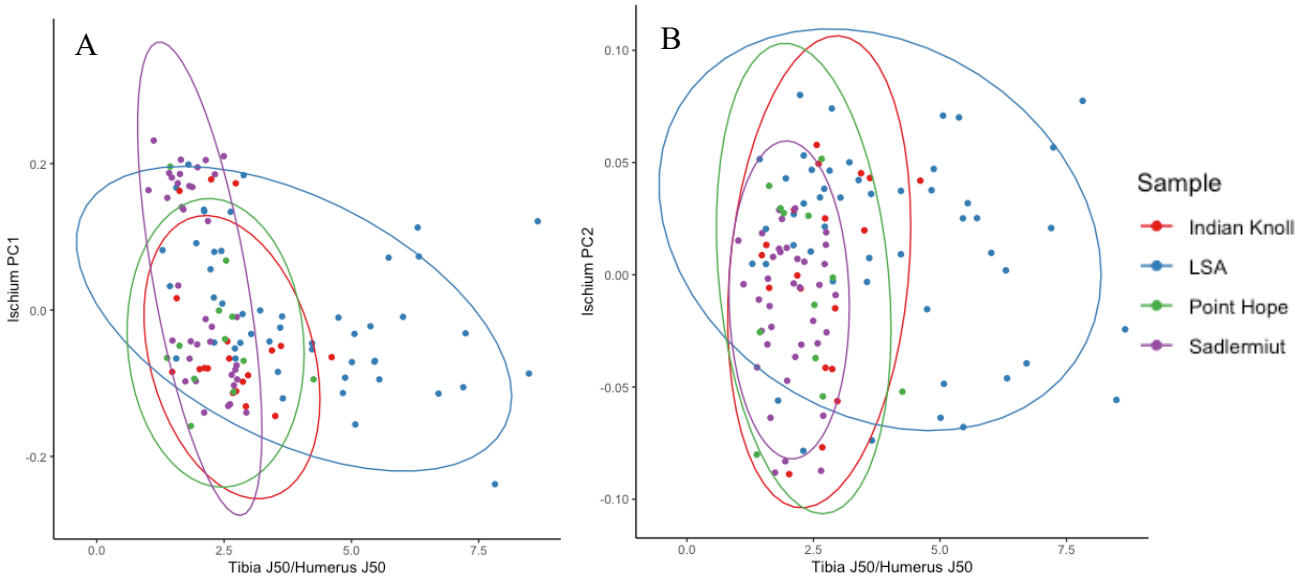

Figure 6.23 Ratios of lower limb to upper limb J values vs. A) ischium PC1, and B) ischium PC2, shown with 95% confidence ellipses.

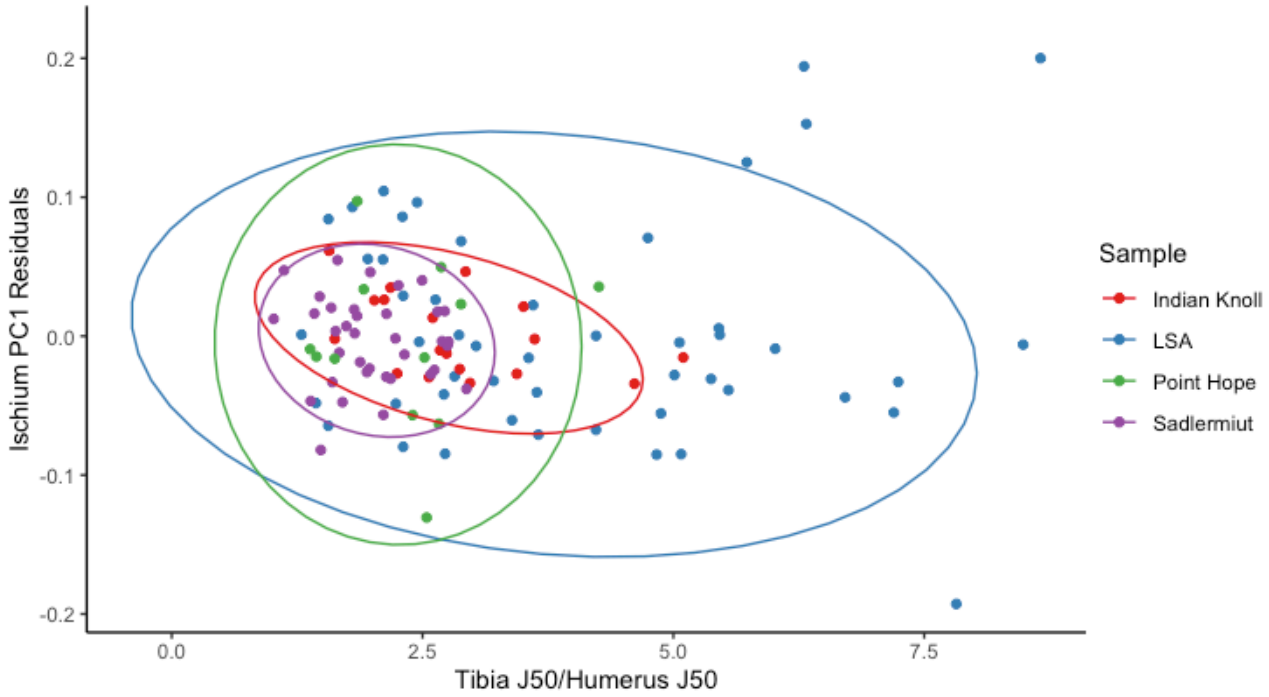

Figure 6.24 Ratio of tibial J to humeral J vs. residuals of ischium PC1 on age. No relationships between the variables are evident and the LSA sample shows the most variation, particularly along the x-axis.

Results of the linear regressions of ischium PCs 1-20 on J ratio data (tibia/humerus) show no large R^2 values in both the regressions of the combined-sample PCA data as well as the individual samples within each regression (full regression results, including R^2, p, and SEE values for the combined sample for each PC, and the R^2 values for the individual samples within each regression, are reported in Appendix K, Table K.2). The highest R^2 value for a whole sample regression was that of PC3 ($R^2 = 0.216$, $p = <0.001$), and the highest R^2 values for the individual samples within the combined-sample data were all found in the Point Hope sample (PC3 $R^2 = 0.507$, $p = 0.009$; PC5 $R^2 = 0.369$, $p = 0.036$; PC12 $R^2 = 0.541$, $p = 0.006$; PC16 $R^2 = 0.309$, $p = 0.061$; and PC20 $R^2 = 0.352$, $p = 0.042$). As with the ilium data, no results indicate a strong relationship between ischium shape variation, as represented by the PCA results, and activity data, as represented by the ratio of tibial J to humeral J.

CHAPTER 7: DISCUSSION AND CONCLUSIONS

This study sought to explore three questions: 1) *What patterns of inter- and intra-population variation in pelvic growth are apparent in archaeological skeletal remains of forager populations?* (2) *When during development do these patterns appear?* and (3) *What are the ecological and cultural factors that contribute to this variation?* Through a geometric morphometrics analysis of ilium and ischium shape in an ontogenetic skeletal sample of four forager populations, patterns of morphological change throughout growth and development have been presented and will be discussed in greater detail in this chapter. Cross-sectional geometric data have been examined as a means of exploring loading patterns and habitual behaviours and will here be presented in concert with results of the pelvic shape analyses to explore the potential impact of activity on ontogenetic trajectories of human pelvic morphology.

Important to any study that includes archaeological human skeletal remains, and particularly those that include juvenile remains, is recognition of the osteological paradox (Wood *et al.,* 1992). All the juvenile skeletons included in this project belong to individuals who did not survive to adulthood, and therefore they may not be representative of the norms of healthy growth and development in their populations. No individuals with obvious pathological changes to the skeleton were included in this study, but it is always a possibility that the included individuals may have suffered from conditions or diseases that did not leave markers on the skeleton but nevertheless affected growth. Consideration of heterogeneous frailty and selective mortality – the notion that not all individuals in a birth cohort have the same risk of death, and that individuals who end up in the archaeological record are not likely representative of the health status of those who survived – are particularly important in studies of palaeopathology,

and in studies that look at stress and disease markers as indicators of overall population health (DeWitte & Stojanoski, 2015; Wood *et al.,* 1992). Since the aims of this study are not strictly related to population health and instead focus on morphology and patterns of shape change between and among groups, the osteological paradox is somewhat less likely to be a factor that greatly skews the results. The concept of the paradox nonetheless remains an important consideration, and the lens of understanding that the individuals included in the study are non-survivors will remain present throughout this discussion. For the Sadlermiut in particular, the concept of selective mortality is a more significant consideration since previous studies (e.g., Symchych, 2016) have proposed that the juveniles in the sample may have suffered from growth perturbations as a result of poor health prior to death. The osteological paradox, therefore, provides an interpretive framework with which to approach aspects of this discussion.

This chapter is organized by major findings, with Section 7.1 summarizing key patterns of morphological variation identified from the results, Section 7.2 discussing potential drivers of variation (activity/functional adaptation, ecogeographic patterning, and neutral variation), Section 7.3 examining sample-specific patterns of variation, and Section 7.4 considering ontogenetic allometry. Overall themes are then synthesized in a final concluding section.

7.1 Key Patterns of Morphological Variation

7.1.1 Ilium

The main axis of variation in the combined-sample ilium data highlighted group structuring and mainly captured variation in the breadth, length, and angulation of the bone as a whole. Age- and size-related changes were not apparent along this axis, but a degree of separation between the four individual samples was, with the Point Hope and Sadlermiut samples

clustering towards one end of the PC1 axis, and the LSA and Indian Knoll samples falling closer to the other end. ANOVA results indicated that group affiliation was a significant source of variation, and that more than half of the variance was between the groups rather than within. Differences between all groups (except between the Sadlermiut and Point Hope) were also statistically significant. Age-related changes did become apparent along the second axis of variation in the combined-sample ilium data; the group structuring that was evident along the primary axis disappeared and a strong relationship with age and size emerged.

7.1.2 Ischium

The primary axis of variation in the combined-sample ischium data highlighted age- and size-related changes. This variation was notable along the ischial ramus in particular, as the bone progressed from a small, comma-shape in the youngest individuals to an elongated c-shape in the oldest individuals. More than half of the total variation seen across the sample lay in this direction. An age- and size-related pattern remained present along PC2, although the relationship was not as strong as was seen with PC1.

In the combined-sample PCA results, a high degree of shape variation was noted in age categories 2 (1-<6 years of age) and 4 (12-<18 years of age) relative to the other age groups. Age categories 2 and 4 align with the onset of walking and the pubertal growth spurt, respectively, events that likely lead to loading changes on the bones as well as an increased rate of growth and therefore greater shape change. These processes can also be highly variable among individuals, thereby increasing the shape variation in these age categories.

7.1.3 Comparative Results

The main axis of variation in the ischium data captured a much larger percentage of the overall variance compared with the ilium data (60.34% vs. 30.5%), indicating that the ischia vary in a more consistent direction overall. Ilium shape is more variable, with portions of morphological change happening in several directions. The ilium is a complex bone, with shape change happening, for example, at the iliac portion of the acetabulum, around the spines, and at the iliac crest. The shape of the ischium appears less complex overall, and a significant portion of the changes seen across this ontogenetic sample occurred along the ramus as it lengthened with age. More PCs across the ilium data were needed to capture a similar amount of variation as the ischium data; 80% of the overall variation was captured by the first five PCs in the ischium data, where it took until PC9 to get over 80% in the ilium data. The data also indicated that different factors are driving morphological variation between the two bones of the pelvis when the samples are combined, as the primary axis of variation in the ischium identified age-related changes, and the primary axis of variation in the ilium highlighted sample differences.

7.1.4 Population Differences

Even in the youngest individuals in the sample, a degree of separation was evident between groups along the PC1 axis of the combined-sample ilium data, suggesting that, from birth, population-level differences are detectable. It is particularly notable that the higher-latitude samples (Sadlermiut and Point Hope) clumped towards one end of the axis of variation, while the lower-latitude samples (LSA and Indian Knoll) clustered closer to the other end. The groupings were not discrete, but ANOVA results indicated that differences between groups (except for between the two high-latitude groups) were significant. These patterns were not,

however, seen in the ischium data, where group separation appeared minimal along the primary axes of variation. Between-group variation as a result of ecogeographic patterning and neutral variation will be discussed in Sections 7.2.2 and 7.2.3, respectively.

7.2 Drivers of Morphological Variation

7.2.1 Activity/Functional Adaptation

This study sought to examine the relationship between pelvic shape and activity, and to consider habitual behaviours as a driver of morphological development. As such, cross-sectional geometric data, which provide information about the loading history of a long bone, were examined in conjunction with the results of the pelvic shape analyses. Recent research has indicated that pelvic morphological development is not solely a by-product of competing evolutionary forces (bipedalism vs. encephalization and obstetrics), but that ecological factors and biological plasticity also influence morphological variation. Wells (2015) argues that:

> …beyond any genetic determinants, there is now substantial evidence that body size and proportions are also characterized by *plasticity* prior to adulthood and are strongly shaped by experience early in the life-course. Through developmental plasticity, growth patterns are subject to reaction norms, and adult phenotype bears the cumulative influence of multiple developmental stresses (p.3-4).

When considering morphology, therefore, it is prudent to not just consider the adult form, but to consider the developmental processes that shaped that form. Pelvic morphology cannot solely be explained by evolutionary forces but is also likely the result of plastic responses to environmental stimuli.

Cross-sectional geometry and markers of habitual behaviours have been found to show distinctions between different populations, specifically between groups with different foraging and subsistence strategies (Davies & Stock, 2014b; Holt *et al.,* 2018; Ruff, 2000; Stock &

Pfeiffer, 2001). Population differences in cross-sectional properties have been shown to manifest very early in development, often even before one year of age, indicating that there could also be a genetic component influencing the early development of long bone shape (Cowgill, 2010). It was hypothesized in the current study, therefore, that habitual loading may be impacting development of the pelvis via biological plasticity, as it affects the development of limb bone strength. Both properties – pelvic morphology and measures of limb bone strength – show population-level patterning, and many muscles that are important for locomotion (and therefore some habitual behaviours, particularly those relating to subsistence) originate on the pelvis.

Results of this study, however, do not show evidence of strong relationships between cross-sectional geometric properties of long bones, which reflect habitual loading patterns, and measures of pelvic shape variation. Sample differences were detected in both the CSG data and the pelvic shape data, particularly in ratios of J and in PC1 of the combined-sample ilium data; however, no relationships were detected between CSG parameters and axes of pelvic bone shape (PCs). The presence of age-related patterns in both ischium shape and CSG measures made it initially appear that shape change in the ischium may be related to activity, but when residuals from the regressions of the two variables on age were plotted against one another the positive relationship between the variables disappeared, indicating that age was a confounding variable.

It may be that activity influences morphology of the bony pelvis as a whole and that the spatial relationships of the individual pelvic bones are impacted by activity-induced loading. Due to the nature of the data used in this study, however, it is not possible to address this question since the ilium and ischium were landmarked and analysed individually. It is possible that a relationship between habitual loading and pelvic morphology could be detected in a whole-pelvis analysis and could produce results different than those of the individual bones, but it is

impossible to speculate on the outcomes of such an analysis here; it would be interesting for future work to tackle this question.

Based on the shape data captured through landmarks in this study and the activity data captured through cross-sectional geometric properties, it does not seem that habitual behaviours and subsistence strategies are influencing growth and development of the bones of the pelvis. It seems, therefore, that pelvic morphology does not show a plastic response to loading in the same way that long bones do. Muscle action and weight transfer through the pelvis do not appear to be affecting bone shape throughout growth in the same way they affect limb bone shape. Epiphyseal and joint surface morphology have been argued to be more canalized in shape than diaphyses throughout ontogeny due to the functional significance of these regions (Lieberman *et al.,* 2001; Buck *et al.* 2010); it may be, therefore, that a similar explanation can be applied to pelvic morphology. Canalization refers to the buffering of developmental processes in the face of environmental perturbations (Hallgrímsson *et al.,* 2002), and so it may be that morphology of the pelvis is buffered against plastic changes resulting from differential loading. The pelvis is a site of key functional significance in the skeleton, and thus one possible explanation for the lack of relationship found in the current study between measures of activity and pelvic shape is that pelvic form is more canalized and less plastic than the cross-sectional parameters of long bones when faced with variability in loading regimes.

Compared with great apes, the human pelvis has been found to be less constrained by inter-trait correlations, meaning that the individual elements of the pelvis show lower levels of integration compared with those of great apes (Grabowski *et al.*, 2011). This lower level of constraint is tied to the human ability to adapt to diverse selection pressures and changing environments. Due to the nature of the data collected in this study, morphological integration of

the elements of the pelvis cannot explicitly be tested. Based on the results of the principal components analysis, however, it does seem likely that different selective pressures are driving variation in the ilium versus the ischium. It does not seem that the growing pelvis is adapting differently between groups to pressures induced by mechanical loading, as neither the ilium nor the ischium shape data showed a relationship with the CSG data. It is more likely that a shared human commitment to obligate bipedalism has fueled morphological changes that separate humans from the other great apes, and pressures like thermoregulation and neutral variation are instead contributing to group differences noted in ilium morphology (to be discussed further in Sections 7.2.2 and 7.2.3). Thermoregulatory pressures do not seem to be as important in the development of ischium morphology, and instead widespread adaptation to obligate bipedalism, common amongst all human groups regardless of activity levels and differing behaviours, is likely driving the morphological development of the ischium leading to more consistent morphologies between groups. Differences in habitual behaviours and activity, therefore, do not seem to be significant enough to distinguish pelvic morphologies of groups with different activity patterns from one another, as obligate bipedalism is a stronger driver of morphological development overall. Ultimately, it appears that the pelvis, due to its functional significance, has a form that is more canalized and less plastic than the cross-sectional parameters of long bones, but that morphologies of elements within the pelvis are being shaped by different drivers of variation throughout growth and development.

7.2.2 Ecogeographic Patterning

Compared with the breadth of literature examining ecogeographic patterning of adult human (and fossil hominin) morphology, relatively few studies have focused on juvenile and

ontogenetic patterns. It is, however, becoming an increasingly popular area of study, and research that has looked at juveniles has found that morphological patterns conforming with ecogeographic expectations are present in the skeleton at least from mid-childhood (with some studies showing even earlier), and remain consistent throughout ontogeny (e.g., Cowgill *et al.,* 2012; Osipov *et al.,* 2016; Ruff *et al.,* 2002; Temple *et al.,* 2011; Yim *et al.,* 2023). Cowgill and colleagues (2012), for example, note strong correlations between temperature/climate and certain anthropometric measures (namely bi-iliac breadth and intralimb indices) in a sample of juvenile individuals from a wide spread of geographic locations. The results from the current study are consistent with these findings. While temperature and climate were not specifically modelled as variables in this study, two populations (Point Hope and Sadlermiut) lived in arctic climates while the other two (Indian Knoll and LSA) lived in warmer, mid-latitude environments in the central (what is now) United States and in southern Africa. A degree of separation is evident between the cold and warm climate samples across all age groups in the combined-sample ilium data, indicating that differences in ilium morphology align with differences in climate and are present early in life.

Past studies have largely focused on measures of pelvic width (bi-iliac breadth, specifically) in relation to thermoregulation and ecogeographic patterning (e.g., Kurki *et al.,* 2008; Ruff, 1991), rather than on specific aspects of pelvic shape. Results consistently demonstrate wider bi-iliac breadths in higher latitude population and narrower bi-iliac breadths in lower latitude groups. Betti and colleagues (2013, 2014) have explored global patterning of pelvic morphology in adults from a shape perspective using geometric morphometrics, although they do not discuss what these shape differences look like in detail. Betti and colleagues (2013) focus mainly on inter-landmark distances and discuss "shape" as a whole, rather than discussing

specific aspects of morphological variation that correlate with the geographic patterning they note. Betti and colleagues (2014) provide a bit more detail on actual shape variation in their sample through the use of wireframe graphs, although they describe the shape changes noted as "too subtle and diffused to be readily described and interpreted" (p.72). Ontogenetic studies that do include detailed descriptions of morphological change based on the results of geometric morphometrics analyses have instead tended to focus on sexual dimorphism rather than population-level differences (e.g., Huseynov *et al.,* 2016). Data with which to directly compare the specific patterns of shape change noted in the current study, therefore, are sparse, as this study did not include pelvic breadth measurements (as are commonly used in ecogeographic studies), and previous work has not prioritized specific descriptions of morphological change in relation to ecogeographic patterning.

It can be hypothesized, however, that the ilium shape identified at one end of the main axis of variation in the current study aligns with an overall pelvic shape that is broader, and those at the other end are narrower. Specifically, movement of the ilium landmarks capturing length of the bone overall suggests that the Sadlermiut and Point Hope samples have relatively shorter ilia in comparison to the LSA and Indian Knoll. Further, the relationship between ilium length and width (as captured between the iliac spines) appears to shift across the main axis of shape variation, with the Sadlermiut and Point Hope showing greater distance between the spines in comparison to the overall length, and the LSA and Indian Knoll showing greater length compared to width. It may be, therefore, that this ratio ultimately contributes to bi-iliac breadth, resulting in overall broader pelves in the Sadlermiut and Point Hope compared to the LSA and Indian Knoll.

In thinking about climate-related population differences seen amongst juveniles, Cowgill and colleagues (2012) present a compelling argument that thermoregulation is not just as important in juveniles as it is in adults, but potentially even more so. In high-latitude populations in particular, infants are acutely susceptible to cold stress and thus thermoregulation can prove key to the survival of the youngest members of a population. Cowgill and colleagues cite a number of clinical and medical science studies which implicate hypothermia as a leading cause of death amongst infants in non-industrialized nations (Asakura, 2004; Baumgart, 2008; Bruck, 1961; Mance, 2008; Thomas, 1994), and thus argue that adaptation to cold environments is key to infant survival. Similarly, infants do not have the same capacity as older individuals to deal with heat stress (infant sweat glands are smaller, for example), and thus morphological adaptations may be important for thermoregulation in hot climates as well (Cowgill *et al.,* 2012). It might be, therefore, that the infant form is a target of thermoregulatory selection, even more so than the adult form, to ensure survival in harsh environments.

This argument distinguishes thermoregulatory adaptations that are selected for (as early as) in utero from plastic responses to climatic stress that develop during growth. The developmental hypothesis (e.g., Frisancho, 1993) proposes that differences in adult body shape and proportions observed across diverse climates are acquired during growth, and that population-level differences are therefore less detectable in infants. The alternative hypothesis (i.e., that put forth by Cowgill, 2012, as well as by Wells, 2002) is that the infant form itself is a target of natural selection, and that climatic adaptations are present from birth to avoid climatic stress in the very young (Hadley & Hruschka, 2014). The results of the current study support the latter argument, as group differences were detectable in the youngest members of the sample and major changes in group structure were not notable throughout the course of ontogeny.

7.2.3 Neutral Variation

Temperature and climate are not expected to be the only factors influencing body shape and size, however, as population genetics and neutral evolution also likely influenced the morphological patterning seen in this study. Betti and colleagues (2014) point out that there is a theoretical problem in attributing population-based patterns solely to thermoregulation and climatic adaptation without also accounting for phylogenetic relationships. They argue that "the underlying neutral pattern of variation due to population history should represent the null hypothesis against which to test the effect of additional, non-neutral processes" (p.66). Their results did show a relationship between adult pelvic shape/size and temperature/precipitation even once geographic distances (representing population history) were accounted for, although the relationship they found between pelvic shape and signatures of neutral variation (represented by phenotypic and geographic distances) was even stronger. Migration, gene flow, and genetic drift, as aspects of population history, therefore, likely play important roles in the formation of pelvic morphology.

Hruschka and colleagues (2015) explored the relative contributions of environmental stimuli and inherited traits to patterns of body shape and size observed globally. Their aim was to discern plastic responses to climate within an individual's lifetime from genetically inherited characteristics. They examined the genetic affinity of a large contemporary sample of children and adults spanning Asia, sub-Saharan Africa, and the Americas; genetic affinity was ascribed using the results from a study by Tishkoff and colleagues (2009) who identified 14 ancestral population clusters across Africa. Genetic affinity accounted for upwards of 50% of the variation in body mass index noted in their sample, whereas, once genetic affinity was controlled for, contemporary temperature differences only accounted for about 4% of the observed

variation. They concluded that, in these contemporary populations at least, genetic affinity, rather than plastic responses to temperature/climate, is influencing surface to volume ratios in the human body. Past populations, therefore, likely adapted to certain climatic conditions via directional selection, and these adaptations then continue to be expressed in descendant populations via genetic inheritance. From the results presented by Hruschka and colleagues it does not appear that plastic responses to climatic conditions manifest during an individual's lifetime, but instead that ecogeographic adaptations are largely inherited.

Thinking about the pelvis specifically, the MMK individuals from the LSA sample provide support for the argument that population history and genetic inheritance are strong drivers of ilium morphology. In plots of CSG measures (e.g., tibial J/humeral J), MMK individuals plot closer to the Indian Knoll sample than to the rest of the LSA. Individuals from the MMK sample, like those from Indian Knoll, lived in a relatively flat environment and pursued terrestrial-based subsistence strategies; the rest of the LSA foragers, in contrast, lived in coastal regions with more varied and mountainous terrain, and were thus moving around and loading their limbs in different ways to the MMK group. In a plot of ilium shape (PC1) on age, however, the MMK group fell in line with the rest of the LSA sample, demonstrating a group affinity in ilium morphology that is not reflected in limb robusticity. Population differences, therefore, seem to contribute to the structuring of the data seem across PC1 and are likely a strong driver in the development of ilium morphology.

Ultimately, neutral variation and ecogeographic patterning are inextricably linked, as natural selection has acted on the human form to allow it to adapt to thermal stress, and neutral variation has maintained these patterns at the population level through genetic inheritance. Plastic responses to temperature within an individual's lifetime seem to play less of a role in the

development of body shape and proportions, and it seems more likely that ecogeographic patterning and neutral variation have contributed to the group separation noted in the ilium shape data of the current study.

7.3 Sample-Specific Patterns of Variation

Within the sample-specific PCAs, variation in the LSA sample was consistently spread across more axes than the other groups, while variation in the Sadlermiut sample was consistently spread across less in both the ilium and the ischium. These patterns indicate a greater degree of morphological variation as a whole within the LSA sample, since one axis of shape change (PC) was not able to capture as much of the overall variance, as well as a higher degree of homogeneity in shape within the Sadlermiut sample, since one axis of shape change captured a greater degree of the overall variance. Because of this, the patterns of variation within the LSA and Sadlermiut samples specifically will be discussed in more detail later in this section.

While age and size did not show a relationship with the primary axis of shape change in the combined-sample ilium data, age- and size-related changes became a significant driver of variation in both the ilium and ischium once sample-specific PCA results were analysed. All four samples showed a positive relationship when PC1 was plotted on age in both the ilium and the ischium, although the strength of the relationships was not consistent among samples. The LSA showed the weakest relationship between PC1 and age, while the Sadlermiut and Indian Knoll samples showed the strongest. Individuals from the LSA sample, therefore, have more variation between one another across age than do individuals in other populations. Evidently, when all samples are pooled, population differences are a significant predictor of ilium

morphology, but once samples are separated age-related changes become a primary driver of variation.

7.3.1 LSA

In comparison with the other samples, the LSA consistently demonstrated greater variability, both in terms of pelvic shape and ratios of bone strength. PC1 from the LSA sample for both the ilium and ischium captured a smaller percentage of the overall variation compared with the other samples, signifying that variation is happening in a greater number of directions in morphospace. Further, when combined-sample data was examined, the LSA individuals showed a larger range of variation, as represented through the spread of data points along the PC1 axis, indicating greater variation in the morphology represented by that axis of shape change. The LSA sample also had a much bigger spread of data points in the CSG ratios data, notable in the plots of ratios of J on age. It is well known that populations with African ancestry have greater genetic diversity than populations from outside of Africa due to the evolution of our species on the African continent (e.g., Campbell & Tishkoff, 2008; Choudhury *et al.,* 2018; Gurdasani *et al.,* 2015; Mallick *et al.,* 2016; Tishkoff & Verrelli, 2003; The 1000 Genomes Project Consortium, 2012), and thus the variation seen within the LSA sample lends support to the idea of genetic inheritance as a driver of variation within the samples of this study. It is not well known, however, the extent to which genetics directly influence pelvic bone shape and size (Cox, 2021), and thus it cannot conclusively be determined that genetic diversity contributes to morphological diversity. The LSA sample is a much less cohesive sample compared with the other samples, as it spans both greater temporal and geographic locales. This variation in temporality and location likely has a major impact on the degree of variation noted in both pelvic

morphology and CSG data of the LSA sample and helps explain the spread of data points seen in the plots.

7.3.2 Sadlermiut

In contrast to the LSA, the Sadlermiut demonstrated lower levels of variation in a number of measures in comparison to the other samples. The primary axis of variation of the Sadlermiut sample in both the ilium and ischium sample-specific PCAs captured a higher percentage of the total variation than those of the other samples. The total morphological variation captured by the PCA was spread across fewer axes in morphospace and the overall variability across the sample, therefore, appears reduced in comparison to the other groups.

In the case of the Sadlermiut sample, it is worth revisiting the notion of the osteological paradox, particularly in context of the results presented by Symchych (2016). Symchych studied growth and body proportion development of the Sadlermiut children and noted that "the Sadlermiut who died as juveniles were generally faltering in growth as compared to a modern North American sample [the Denver Growth Study], even taking into account their short adult stature" (p.131). Symchych reports that the Point Hope individuals who died as children, in contrast, exhibited a variety of growth outcomes, including some faltering, some alignment with, and some acceleration in comparison to the Denver Growth Study. A range of factors may have contributed to the growth faltering seen amongst the Sadlermiut, including a narrow resource base and exposure to infection disease. Body proportionality, however, followed expected patterns of development in Symchych's results, supporting the idea that linear growth is more susceptible to immediate environmental stressors than are body proportions.

While it cannot be said whether or not this growth faltering had any effect on the development of pelvic morphology, it is worth noting that the individuals included in this study were non-survivors and thus may not be representative of the morphological development of individuals of the same age who survived. It may be that growth faltering has restricted variation, contributing to the patterns that have been noted. Nevertheless, it is notable that axes of variation identified through a PCA of the Sadlermiut data in the current study displayed decreased directions of variance in comparison to the other samples, as fewer PCs were able to capture greater percentages of overall variation.

The Sadlermiut also lived in an extreme environment which may have contributed to greater constraints in pelvic morphological variation. It has been argued that cold-mediated natural selection is responsible for morphological differences between arctic populations and the rest of the world (Roseman, 2004), and that evidence of climate signatures in the cranium may be confined to arctic populations (Harvati & Weaver, 2006). It could be that climate stress acts in a similar way on pelvic morphology, leading to a reduction in variation within arctic populations. This idea would be supported by the theory that climate-related selective pressures are stronger in extreme environments. Future work involving a larger Point Hope sample, or additional high-latitude groups, could help confirm if this pattern holds true across multiple arctic populations.

7.4 Ontogenetic Allometry

Allometric variation characterizes shape change in the ilium and the ischium as it relates to change in size. In the current study, allometry was examined using regression scores plotted on centroid size. While both bones evidently have a strong relationship between shape change and size, that of the ilium appeared slightly stronger than that of the ischium (R^2 values were

0.839 and 0.780, respectively). Allometric results differed from those of the principal components analysis in that specific aspects and percentages of shape variation were observed independently across axes of variation in the PCA, while shape is considered as a whole in the allometric analysis. The predominant axis of shape change in the ilium PCA did not show a relationship with centroid size, but the allometric results indicated that, when overall shape change is considered instead of specific axes of variation, size is a strong driver of morphological change in both the ilium and the ischium. PC1 of the ilium data captured 30.5% of the overall variation, leaving almost 70% of the variation still to be described. Based on the allometric results, it is possible that ontogenetic allometry could be explaining some of the remaining 70% that is not described by group differences. Consequently, ontogenetic allometry appears to be a potentially meaningful driver of both ilium and ischium morphological variation.

7.4.1 Maturity Trajectories of Shape and Size

The maturity trajectories presented in Sections 5.5 and 6.5 help visualize the relationship between changes in shape and changes in size in both the ilium and the ischium. Consistently in the ilium, percentages of shape maturity were reached before size maturity, while in the ischium the two trajectories were closely intertwined. Based on the PCA results, it seems that ilium shape overall is more complex than ischium shape, as more PCs were needed to capture similar amounts of shape variation in the ilium than in the ischium (i.e., it took nine PCs to reach 80% of the variation in the ilium, where it only took five to reach a comparable level in the ischium). It appears, based on percentages of maturity, that these complex ilium shapes are being attained earlier in development than the ilium sizes and ischium shapes. Ischium shape and size, conversely, mature at quite similar rates throughout development.

In both the ilium and the ischium, shape trajectories of the Sadlermiut sample have a rate of change faster than the other groups prior to the age of five. It also appears that the pelvic bones of the Sadlermiut individuals vary in more consistent directions compared with those of the other samples, as evidenced by the amount of variation captured by their PC1, and the maturity trajectories indicate that these shapes are being attained earlier in development as well. The reduced morphological variation noted in the Sadlermiut may explain this pattern of shape attainment, as the group as a whole may be reaching percentages of shape maturity before the other groups because there is less variation among individuals.

Timing and duration of weaning may also have influenced the trajectories of growth noted in the current study. The introduction of weaning foods and the potential exposure to pathogens that accompanies the start of weaning may lead to a slowing of growth (Katzenberg *et al.,* 1996), as is notable around 5 years of age in the ilium sample of the current study. It is more common, however, for growth disturbances related to weaning to occur at the start of the weaning period than at the end (Halcrow, King, *et al.,* 2018), which, in the samples included in this study, would likely have occurred around 1.5-2 years of age. Yet particularly in the case of the Sadlermiut, it may be that breastfeeding helped maintain a steady pace of growth throughout the entirety of the weaning period, as was proposed by Mays (2007) to have occurred with the medieval children from Wharram Percy, and that growth perturbations occurred once weaning stopped completely. It has been suggested that the Sadlermiut experienced a lack of dietary breadth and relied mainly on a few key resources (Coltrain *et al.,* 2004; Coltrain, 2009) which may have led to periods of food insecurity. Breastfeeding may thus have helped maintain the nutrient intake of children during periods of food insecurity, leading to the dips noted in the growth trajectories around five years of age once weaning had stopped. Availability of

transitional foods to be weaned onto likely also impacted growth during the weaning period. A heavily meat-based diet, such as that of the Sadlermiut, is not ideal for weaning and may explain the potentially elongated nursing period and slowing of growth after five years of age. The maturity trajectories of size in this study further correspond with patterns of linear growth and growth tempos reported in previous studies for both the LSA (Pfeiffer & Harrington, 2010) and Indian Knoll (Sundick, 1978), showing a faster rate of growth compared to a North American reference sample prior to the age of five, and a slowing of tempo after the age of five.

A notable exception to these patterns is the Point Hope sample, whose shape maturity trajectories in both bones lag behind those of size maturity for the majority of development; these patterns, however, are likely a product of the small sample size. Nevertheless, the Point Hope sample is the only group to show a slower rate of change between birth and 10 years of age, and an increase in the rates of change between 10 and 15 years of age. This quickened rate corresponds to the timing of the pubertal growth spurt, and the slowed pace in early life could be representative of a more stable diet in this population (and thus less stress in the post-weaning period) as it known that they exploited a wider range of dietary resources, particularly in comparison to the Sadlermiut (El Zaatari, 2014; Symchych, 2016). Ischium shape of the Indian Knoll sample is an exception as well, as it shows a somewhat increased rate of change after five years of age and slows again after the age of 15. It would be interesting to explore these maturity trajectories further with a larger Point Hope sample size, to see how the patterns do or do not hold in comparison to the other groups when more individuals are included.

Ultimately, maturity trajectories of shape and size in the pelvis seem to mirror developmental patterns of stature reported in previous studies (i.e., Pfeiffer & Harrington, 2010), with a quicker pace of growth prior to age five and a slower pace of growth thereafter.

Trajectories of shape maturity, however, progress less consistently overall and exhibit more variation in rates of change throughout the course of ontogeny. Size and shape maturity, therefore, are likely being influenced by different developmental factors and stressors and thus present different patterns of change. Since the pelvis is a complex 3D structure, timing of the fusion of epiphyses may have an impact on shape and size differently. Shape of the ilium in particular is very complex and so the timing of the closure of the epiphyses may be more tightly controlled than growth of the primary centre. This complexity of shape, and the functional significance of the shape, may explain why the trajectories of shape maturation of the ilium consistently plotted above those of size maturity. Once an epiphysis has closed, growth in that region can no longer continue and thus shape maturation may go through periods of fluctuation and latency of change, while growth in size of the primary centre may continue more consistently. Ischium shape is less complex than ilium shape, which may explain why its size and shape trajectories are more closely intertwined throughout growth.

7.5 Conclusions

This study sought to investigate pelvic morphological variation in forager populations using an ontogenetic approach. Results showed that: 1) population-based patterning is apparent along the primary axis of variation in the ilium, but a similar pattern is not apparent in the ischium where age-related changes are the most prominent. When samples are analysed independently from one another, age-related changes become a prominent driver of variation in both bones, with the ilium increasing in complexity of shape with age, and the ischium elongating and curving with age. 2) In consideration of when during development the noted patterns appear, it seems that a degree of group separation is apparent in ilium morphology from

birth. Population-based patterning is apparent even in the youngest individuals in the combined sample ilium data, and the separation remains consistent across growth. 3) Signatures of climatic adaptation and neutral variation appear to be significant in the ilium, and ontogenetic allometry appears to be a prominent driver of shape change in both the ilium and ischium. Activity, however, does not seem to be a meaningful driver of morphological variation in the bones of the pelvis.

A principal components analysis of the landmark data showed that the primary axis of shape change in the combined-sample ilium data identified statistically significant differences between groups, demonstrating that group differences are a meaningful driver of variation in the ilium and are present early in life. Clustering of the arctic populations towards one end of the axis of variation and the lower-latitude populations towards the other suggests that a combination of neutral evolutionary forces and climatic adaptation are likely at play. Key aspects of ilium shape change included variation in the length of the bone as a whole, variation in the curve and asymmetry of the iliac crest, and variation in breadth between the iliac spines. The combined-sample ischium data, however, did not demonstrate any meaningful degrees of group separation along the primary axis of variation, and instead captured age-related changes. Key aspects of ischium shape change included variation in the curvature of the bone as a whole, length of the ischial ramus, and variation in depth and curvature of the acetabular surface. More axes of variation were needed in the principal components analysis to capture shape variation in the ilium than in the ischium, indicating that shape overall is more complex in the ilium. Sample-specific principal components analyses captured age-related changes along the primary axes of variation in both bones and mainly highlighted the increasing complexity of the ilium and the increasing length of the ischial ramus throughout ontogeny.

Measures of allometry indicated that changes in shape that are related to changes in size are strong drivers of variation in both bones. While the primary axis of variation from the ilium PCA did not show a relationship with age, results of allometric analyses demonstrated that size is an important driver of shape change in the pelvis when morphological variation is considered as a whole.

It was hypothesized that activity would be a driver of morphological variation in the bones of the pelvis, but data from this study failed to capture meaningful relationships between measures of activity, represented by cross-sectional geometric properties of long bones, and pelvic shape, represented by results of a geometric morphometrics analysis, suggesting that activity and habitual behaviours may not be significant drivers of morphological variation in the pelvis. While group differences were detectable in ilium morphology between the marine (Point Hope, Sadlermiut) and the terrestrial (Indian Knoll, LSA) foragers, it does not seem that differences in habitual behaviours are driving these distinctions. Instead, it seems that group differences, which may be driven by climate-related directional selection or neutral evolutionary processes (or, most likely, a combination thereof), as well as ontogenetic allometry, are the strongest drivers of morphological variation in the ilium and the ischium.

Moving beyond this study to consider future directions of research, inclusion of the pubis would add a further layer to this analysis and deepen our understanding of the myriad factors driving morphological variation in the pelvis as a whole. Modelling of specific climate, temperature, and latitude variables would further enhance our understanding of the role these factors contribute to morphological variation, as would the inclusion of additional samples from diverse geographic locations. Further samples from populations who undertook different subsistence strategies would also contribute more nuance to our understanding of this topic. The

pelvis is a complex structure that is integral to the human experience, and no doubt future research will continue to contribute to our understanding of its growth, development, form, and function.

BIBLIOGRAPHY

Abitbol, M.M. (1988). Evolution of the ischial spine and of the pelvic floor in the hominoidea. *American Journal of Physical Anthropology, 75*(1), 53-67. https://doi.org/10.1002/ajpa.1330750107

Adair, F.L. (1918). The ossification centers of the fetal pelvis. *Transactions of the American Gynecological Society for the Year, 43*, 89.

Adams, D.C. & Otárola-Castillo, E. (2013). geomorph: an R package for the collection and analysis of geometric morphometric shape data. *Methods in Ecology and Evolution, 4*(4), 393-399. https://doi.org/10.1111/2041-210X.12035

Allen, J.A. (1877). The influence of physical conditions in the genesis of species. *Radical Review, 1*, 108–140.

AlQahtani, S.J., Hector, M.P., & Liversidge, H.M. (2010). Brief communication: The London atlas of human tooth development and eruption. *American Journal of Physical Anthropology, 142*(3), 481-490. https://doi.org/10.1002/ajpa.21258

Asakura, H. (2004). Fetal and neonatal thermoregulation. *Journal of Nippon Medical School, 71*(6), 360-370. https://doi.org/10.1272/jnms.71.360

Ashton, K.G. (2002). Patterns of within-species body size variation of birds: strong evidence for Bergmann's rule. *Global Ecology and Biogeography*, *11*(6), 505-523. https://doi.org/10.1046/j.1466-822X.2002.00313.x

Auerbach, B.M. & Ruff, C.B. (2004). Human body mass estimation: a comparison of "morphometric" and "mechanical" methods. *American Journal of Physical Anthropology*, *125*(4), 331-342. https://doi.org/10.1002/ajpa.20032

Auerbach, B.M. (2008). *Human skeletal variation in the New World during the Holocene: Effects of climate and subsistence across geography and time – Part I*. PhD Thesis, The Johns Hopkins University.

Aykroyd, R.G., Lucy, D., Pollard, A.M., & Solheim, T. (1997). Technical note: Regression analysis in adult age estimation. *American Journal of Physical Anthropology, 104*(2), 259–265. https://doi.org/10.1002/(SICI)1096-8644(199710)104:2<259::AID-AJPA11>3.0.CO;2-Z

Barham, L. & Mitchell, P. (2008). *The First Africans: African Archaeology from the Earliest Toolmakers to Most Recent Foragers.* New York, NY: Cambridge University Press.

Bass, W. (1995). *Human Osteology: A Laboratory and Field Method*. Springfield, IL: Charles C. Thomas.

Baumgart, S. (2008). Iatrogenic hyperthermia and hypothermia in the neonate. *Clinics in Perinatology, 35*(1), 183-197. https://doi.org/10.1016/j.clp.2007.11.002

Beaumont, L.A., Dillon, M., & Harrington, N. (2020). *Children in Antiquity: Perspectives and Experiences of Childhood in the Ancient Mediterranean.* London: Routledge. https://doi.org/10.4324/9781315542812

Becker, M.J. (2006). The archaeology of infancy and childhood: Integrating and expanding research into the past. *American Journal of Archaeology, 110*(4), 655-658. https://www.jstor.org/stable/40025063

Bergmann, K.G.L.C. (1847). Über die Verhältnisse der wärmeokönomie der Thiere zu ihrer Grösse. *Göttinger Studien*, *3*, 595–708.

Bertram, J.E.A. & Swartz, S.M. (1991). The "law of bone transformation": A case of crying Wolff? *Biological Reviews*, *66*(3), 245–273. https://doi.org/10.1111/j.1469-185X.1991.tb01142.x

Betti, L. (2017). Human variation in pelvic shape and the effects of climate and past population history. *The Anatomical Record, 300*(4)*,* 687-697. https://doi.org/10.1002/ar.23542

Betti, L. & Manica, A. (2018). Human variation in the shape of the birth canal is significant and geographically structured. *Proceedings of the Royal Society B, 285*(1889), 20181807. https://doi.org/10.1098/rspb.2018.1807

Betti, L., von Cramon-Taubadel, N., Manica, A., & Lycett, S.J. (2013). Global geometric morphometric analyses of the human pelvis reveal substantial neutral population history effects, even across sexes. *PLoS ONE, 8*(2), e55909. https://doi.org/10.1371/journal.pone.0055909

Betti, L., von Cramon-Taubadel, N., Manica, A., & Lycett, S.J. (2014). The interaction of neutral evolutionary processes with climatically-driven adaptive changes in the 3D shape of the human os coxae. *Journal of Human Evolution, 73*, 64–74. https://doi.org/10.1016/j.jhevol.2014.02.021

Boas, F. (1888). *The Central Eskimo*. Washington, DC: Smithsonian Institute.

Boas, F. (1907). Second report on the Eskimo of Baffin Land and Hudson Bay. From notes collected by Captain George Comer; Captain James S. Mutch, and Rev. E.J. Peck. *Bulletin of the American Museum of Natural History, 15*(2), 371–570.

Bogin, B. (2020). *Patterns of Human Growth. Third Edition.* Cambridge: Cambridge University Press. https://doi-org.ezproxy.library.uvic.ca/10.1017/9781108379977

Bookstein, F.L. (1991). *Morphometric Tools for Landmark Data: Geometry and Biology*. New York: Cambridge University Press.

Brooks, S. & Suchey, J.M. (1990). Skeletal age determination based on the os pubis: a comparison of the Acsádi-Nemeskéri and Suchey-Brooks methods. *Human Evolution*, *5*(3), 227-238.

Bruck, K. (1961). Temperature regulation in the newborn infant. *Biologia Neonatorum, 3*(2-3), 65-119. https://doi.org/10.1159/000239810

Buck, L.T., Stock, J.T., & Foley, R.A. (2010). Levels of intraspecific variation within the catarrhine skeleton. *International Journal of Primatology, 31,* 779-795. https://doi.org/10.1007/s10764-010-9428-0

Cameron, M.E. (2017). *Behaviour, Biology, and Ecology: Investigating the Impact of Ecological Constraints on Prehistoric Southern African Skeletal Phenotypes.* PhD Thesis, University of Cambridge.

Cameron, M.E. & Pfeiffer, S. (2014). Long bone cross-sectional geometric properties of Later Stone Age foragers and herder-foragers. *South African Journal of Science*, *110*(9-10), 01-11. http://dx.doi.org/10.1590/sajs.2014/20130369

Campbell, M.C. & Tishkoff, S.A. (2008). African genetic diversity: Implications for human demographic history, modern human origins, and complex disease mapping. *Annual Review of Genomics and Human Genetics, 9,* 403-433. https://doi.org/10.1146/annurev.genom.9.081307.164258

Cardoso, H.F.V., Abrantes, J., & Humphrey, L.T. (2014). Age estimation of immature human skeletal remains from the diaphyseal length of the long bones in the postnatal period. *International Academy of Legal Medicine, 127*, 997–1004. https://doi.org/10.1007/s00414-013-0925-5

Cardoso, H.F. & Saunders, S.R. (2008). Two arch criteria of the ilium for sex determination of immature skeletal remains: a test of their accuracy and an assessment of intra-and inter-observer error. *Forensic Science International*, *178*(1), 24-29. https://doi.org/10.1016/j.forsciint.2008.01.012

Cardoso, H.F.V., Spake, L., & Humphrey, L.T. (2017). Age estimation of immature human skeletal remains from the dimensions of the girdle bones in the postnatal period. *American Journal of Physical Anthropology, 163*(4)*,* 772-783. https://doi.org/10.1002/ajpa.23248

Charnov, E.L. (1993). *Life History Invariants: Some Explorations of Symmetry in Evolutionary Ecology.* Oxford: Oxford University Press.

Charnov, E.L. (2001). Evolution of mammal life histories. *Evolutionary Ecology Research, 3*, 521–535.

Choudhury, A., Aron, S., Sengupta, D., Hazelhurst, S., & Ramsay, M. (2018). African genetic diversity provides novel insights into evolutionary history and local adaptations. *Human Molecular Genetics, 27*(R2), R209-R218. https://doi.org/10.1093/hmg/ddy161

Churchill, S.E. & Morris, A.G. (1998). Muscle marking morphology and labour intensity in prehistoric Khoisan foragers. *International Journal of Osteoarchaeology, 8*(5), 390–411. https://doi.org/10.1002/(SICI)1099-1212(1998090)8:5<390::AID-OA435>3.0.CO;2-N

Clark, J.D. (1959). *The Prehistory of Southern Africa*. Harmondsworth: Penguin Books.

Clayton, F., Sealy, J., & Pfeiffer, S. (2006). Weaning age among foragers at Matjes River Rock Shelter, South Africa, from stable nitrogen and carbon isotope analyses. *American Journal of Physical Anthropology, 129*(2)*,* 311-317. https://doi.org/10.1002/ajpa.20248

Cofran, Z., VanSickle, C., Valenzuela, R., García-Martínez, D., Walker, C.S., Hawks, J., Zipfel, B., Williams, S.A., & Berger, L.R. (2022). The immature *Homo naledi* ilium from the Lesedi Chamber, Rising Star Cave, South Africa. *American Journal of Biological Anthropology,* 179(1), 3-17. https://doi.org/10.1002/ajpa.24522

Coltrain, J.B. (2009). Sealing, whaling and caribou revisited: additional insights from the skeletal isotope chemistry of eastern Arctic foragers. *Journal of Archaeological Science, 36*(3), 764-775. https://doi.org/10.1016/j.jas.2008.10.022

Coltrain, J.B. (2011). Invited response to K. Ryan's comments on Coltrain et al. (2004) and Coltrain (2009): is Native Point "Burial 21" Dorset in age; were historic-era burials European in origin and how important were caribou in Sadlermiut diets? *Journal of Archaeological Science, 38*(10), 2866-2871. https://doi.org/10.1016/j.jas.2011.02.012

Coltrain, J.B., Hayes, M.G., & O'Rourke, D.H. (2004). Sealing, whaling and caribou: the skeletal isotope chemistry of Eastern Arctic foragers. *Journal of Archaeological Science, 31*(1), 39–57. https://doi.org/10.1016/j.jas.2003.06.003

Comer, G. (1910). A geographical description of Southampton Island and notes upon the Eskimo. *Bulletin of the American Geographical Society, 42*(2), 84–90.

Copes, L. (2012). Appendix B. In *Comparative and Experimental Investigations of Cranial Robusticity in Mid-Pleistocene Hominins.* PhD Thesis, Arizona State University.

Corron, L.K., Santos, F., Adalian, P., Chaumoitre, K., Guyomarc'h, P., Marcha, F., & Brůžek, J. (2021). How low can we go? A skeletal maturity threshold for probabilistic visual sex estimation from immature human os coxae. *Forensic Science International, 325,* 110854. https://doi.org/10.1016/j.forsciint.2021.110854

Cowgill, L.W. (2008). *The Ontogeny of Recent and Late Pleistocene Human Postcranial Robusticity*. PhD Thesis, Washington University.

Cowgill, L.W. (2010). The ontogeny of Holocene and Late Pleistocene human postcranial strength. *American Journal of Physical Anthropology, 141*(1), 16-37. https://doi.org/10.1002/ajpa.21107

Cowgill, L.W. (2014). Postcranial growth and development of immature skeletons from Point Hope, Alaska. In C.E. Hilton, B.M. Auerbach, & L.W. Cowgill (Eds.), *The Foragers of Point Hope: The Biology and Archaeology of Humans on the Edge of the Alaskan Arctic* (pp. 212–232). Cambridge: Cambridge University Press.

Cowgill, L.W., Eleazer, C.D., Auerbach, B.M., Temple, D.H., & Okazaki, K. (2012). Developmental variation in ecogeographic body proportions. *American Journal of Physical Anthropology, 148*(4), 557-570. https://doi.org/10.1002/ajpa.22072

Cox, S.L. (2021). A geometric morphometric assessment of shape variation in adult pelvic morphology. *American Journal of Physical Anthropology, 176*(4), 652-671. https://doi.org/10.1002/ajpa.24399

Dabbs, G.R. (2011). Health status among prehistoric Eskimos from Point Hope, Alaska. *American Journal of Physical Anthropology, 146*(1), 94-103. https://doi.org/10.1002/ajpa.21556

Dart, R.A. (1937). The physical characters of the /?auni-≠khomani Bushmen: Appendices A-W. *Bantu Studies, 11*(1), 175-246. https://doi.org/10.1080/02561751.1937.9676051

Davies, T.G. (2012). *Cross-Sectional Variation in the Human Femur and Tibia: The influence of physique and habitual mobility on diaphyseal morphology.* PhD Dissertation, University of Cambridge.

Davies, T.G., Shaw, C.N., & Stock, J.T. (2012). A test of a new method and software for the rapid estimation of cross-sectional geometric properties of long bone diaphyses from 3D laser surface scans. *Archaeological and Anthropological Sciences*, *4*(4), 277-290. https://doi.org/10.1007/s12520-012-0101-8

Davies, T.G. & Stock, J.T. (2014a). The influence of relative body breadth on the diaphyseal morphology of the human lower limb. *American Journal of Human Biology, 26*(6), 822-835. https://doi.org/10.1002/ajhb.22606

Davies, T.G. & Stock, J.T. (2014b). Human variation in the periosteal geometry of the lower limb: Signatures of behaviour among human Holocene populations. In K. Carlson & D. Marchi (Eds.), *Mobility: Interpreting Behavior from Skeletal Adaptations and Environmental Interactions,* (pp. 67-90)*,* New York: Springer.

Deacon, H.J. & Deacon, J. (1999). *Human Beginnings in South Africa: Uncovering the Secrets of the Stone Age*. Walnut Creek, CA: Rowman Altamira.

DeWitte, S.H. & Stojanowsk, C.M. (2015). The osteological paradox 20 years later: Past perspectives, future directions. *Journal of Archaeological Research, 23,* 397-450. https://doi.org/10.1007/s10814-015-9084-1

Doube, M., Kłosowski, M.M., Arganda-Carreras, I., Cordeliéres, F., Dougherty, R.P., Jackson, J., Schmid, B., Hutchinson, J.R., & Shefelbine, S.J. (2010). BoneJ: free and extensible bone image analysis in ImageJ. *Bone*, *47*, 1076-9. https://doi.org/10.1016/j.bone.2010.08.023

Drake, A.B. & Klingenberg, C.P. (2008). The pace of morphological change: historical transformation of skull shape in St Bernard dogs. *Proceedings of the Royal Society B: Biological Sciences, 275*(1630), 71-76. https://doi.org/10.1098/rspb.2007.1169

Dryden, I.L. (2021). *shapes package*. R Foundation for Statistical Computing, Vienna, Austria. Contributed package. Version 1.2.6 URL http://www.R-project.org

Dunsworth, H.M., Warrener, A.G., Deacon, T., Ellison, P.T., & Pontzer, H. (2012). Metabolic hypothesis for human altriciality. *PNAS, 109*(38), 15212–15216. https://doi.org/10.1073/pnas.1205282109

El Zaatari, S. (2008). Occlusal molar microwear and the diets of the Ipiutak and Tigara populations (Point Hope) with comparisons to the Aleut and Arikara. *Journal of Archaeological Science, 35*(9), 2517-2522. https://doi.org/10.1016/j.jas.2008.04.002

El Zaatari, S. (2014). The diets of the Ipiutak and Tigara (Point Hope, Alaska): Evidence from occlusal molar microwear texture analysis. In C.E. Hilton, B.M. Auerbach, & L.W. Cowgill (Eds.), *The Foragers of Point Hope: The Biology and Archaeology of Humans on the Edge of the Alaskan Arctic* (pp. 120-137). Cambridge: Cambridge University Press.

Eschman, P.N. (1992). *SLCOMM Version 1.6.* Eschman Archaeological Services, Albuquerque, NM.

Estévez, E.J., López-Lázaro, S., López-Morago, C., Alemán, I., & Botella, M.C. (2017). Sex estimation of infants through geometric morphometric analysis of the ilium. *International Journal of Legal Medicine*, *131*(6), 1747-1756. https://doi.org/10.1007/s00414-017-1659-6

Estévez Campo, E.J., López-Lázaro, S., López-Morago Rodríguez, C., Aguilera, I.A., & Botella López, M.C. (2018). Specific-age group sex estimation of infants through geometric morphometrics analysis of pubis and ischium. *Forensic Science International, 286*, 185–192. https://doi.org/10.1016/j.forsciint.2018.03.012

Fischer, B. & Mitteroecker, P. (2017). Allometry and sexual dimorphism in the human pelvis. *The Anatomical Record, 300*(4), 698-705. https://doi.org/10.1002/ar.23549

Foster, F. & Collard, M. (2013). A reassessment of Bergmann's rule in modern humans. *PLoS ONE, 8*(8), e72269. https://doi.org/10.1371/journal.pone.0072269

Frisancho, A.R. (1993). *Human Adaptation and Accommodation*. Ann Arbor: University of Michigan.

Frisancho, A.R., Garn, S.M., & Ascoli, W. (1970). Subperiosteal and endosteal bone apposition during adolescence. *Human Biology*, *42*(4), 639–664. https://www.jstor.org/stable/41462255

Frisancho, A.R., Guire, K., Babler, W., Borkan, G., & Way, A. (1980). Nutritional influence on childhood development and genetic control of adolescent growth of Quechuas and Mestizos from the Peruvian lowlands. *American Journal of Physical Anthropology, 52*(3), 367–375. https://doi.org/10.1002/ajpa.1330520308

Garn, S.M. & Shamir, Z. (1958). *Methods for Research in Human Growth*. Springfield, IL: Charles C. Thomas.

Gibbon, V.E. & Davies, B. (2020). Holocene Khoesan health: A biocultural analysis of cranial pathology and trauma. *International Journal of Osteoarchaeology, 30*(3), 287-296. https://doi.org/10.1002/oa.2854

Gooderham, E., Matias, A., Liberato, M., Santos, H., Walshaw, S., Albanese, J., & Cardoso, H.F.V. (2019). Linear and appositional growth in children as indicator of social and economic change during the Medieval Islamic to Christian transition in Santarém, Portugal. *International Journal of Osteoarchaeology, 29*(5), 736-746. https://doi.org/10.1002/oa.2784

Grabowski, M.W., Polk, J.D., & Roseman, C.C. (2011). Divergent patterns of integration and reduced constraint in the human hip and the origins of bipedalism. *Evolution, 65*(5), 1336-1356. https://doi.org/10.1111/j.1558-5646.2011.01226.x

Grabowski, M.W. (2013). Hominin obstetrics and the evolution of constraints. *Evolutionary Biology, 40*, 57-75. https://doi.org/10.1007/s11692-012-9174-7

Gray, H. (1918). *Anatomy of the Human Body*. Philadelphia, Pennsylvania: Lea & Febiger.

Grine, F.E., Jungers, W.L., Tobias, P.V., & Pearson, O.M. (1995). Fossil *Homo* femur from Berg Aukas, northern Namibia. *American Journal of Physical Anthropology*, *97*(2), 151-185. https://doi.org/10.1002/ajpa.1330970207

Gruss, L.T. & Schmitt, D. (2015). The evolution of the human pelvis: changing adaptations to bipedalism, obstetrics and thermoregulation. *Philosophical Transactions of the Royal Society B, 370,* 20140063. http://dx.doi.org/10.1098/rstb.2014.0063

Guatelli-Steinberg, D., Stinespring-Harris, A., Reid, D.J., Larsen, C.S., Hutchinson, D.L., & Smith, T.M. (2014). Chronology of linear enamel hypoplasia formation in the Krapina Neanderthals. *PaleoAnthropology, 2014,* 431-445. https://doi.org/10.4207/PA.2014.ART84

Gunz, P., Mitteroecker, P., & Bookstein, F. (2005). Semilandmarks in three dimensions. In D. Slice (Ed.), *Modern Morphometrics in Physical Anthropology,* (pp. 73-98), Springer: Boston.

Gurdasani, D., Carstensen, T., Tekol-Ayele, F., Pagani, L., Tachmazidou, I…. Sandhu, M.S. (2015). The African Genome Variation Project shapes medical genetics in Africa. *Nature, 517,* 327-332. https://doi.org/10.1038/nature13997

Guy, H., Masset, C., & Baud, C.-A. (1997). Infant taphonomy. *International Journal of Osteoarchaeology, 7*(22), 221-229. https://doi.org/10.1002/(SICI)1099-1212(199705)7:3<221::AID-OA338>3.0.CO;2-Z

Hadley, C. & Hruschka, D.J. (2014). Population level differences in adult body mass emerge in infancy and early childhood: Evidence from a global sample of low and lower-income countries. *American Journal of Physical Anthropology, 154*(2), 232-238. https://doi.org/10.1002/ajpa.22496

Haeusler, M., Grunstra, N.D.S., Martin, R.D., Krenn, V.A., Fornai, C., & Webb, N.M. (2021). The obstetrical dilemma hypothesis: there's life in the old dog yet. *Biological Reviews, 96*(5), 2031-2057. https://doi.org/10.1111/brv.12744

Halcrow, S.E., King, C.L., Millard, A.R., Snoddy, A.M.E., Scott, R.M., Elliot, G.E., Gröcke, D.R., Buckley, H.R., Standen, V.G., & Arriaza, B.T. (2018). Out of the mouths of babes and sucklings: Breastfeeding and weaning in the past. In C. Tomori, A.E.L. Palmquist, & E.A. Quinn (Eds.) *Breastfeeding: New Anthropological Approaches* (pp. 155-169). London: Routledge. https://doi-org.ezproxy.library.uvic.ca/10.4324/9781315145129

Hallgrímsson, B., Willmore, K., & Hall, B.K. (2002). Canalization, developmental stability, and morphological integration in primate limbs. *Yearbook of Physical Anthropology, 119*(S35), 131-158. https://doi.org/10.1002/ajpa.10182

Harrington, L. (2010). *Ontogeny of Postcranial Robusticity Among Holocene Hunter-Gatherers of Southernmost Africa.* PhD Thesis, University of Toronto. https://doi.org/10.1080/0067270X.2012.707483

Harrington, L. & Pfeiffer, S. (2008). Juvenile mortality in southern African archaeological contexts. *South African Archaeological Bulletin, 63*(188), 95–101.

Harvati, K. & Weaver, T.D. (2006). Human cranial anatomy and the differential preservation of population history and climate signatures. *The Anatomical Record, 288A*(12), 1225-1233. https://doi.org/10.1002/ar.a.20395

Herrmann, N.P. & Konigsberg, L.W. (2002). A re-examination of the age-at-death distribution of Indian Knoll. In R.D. Hoppa & J.W. Vaupel (Eds.), *Paleodemography: Age Distribution from Skeletal Samples* (pp. 243–257). Cambridge: Cambridge University Press.

Hillson, S. (2009). The world's largest infant cemetery and its potential for studying growth and development. *Hesperia Supplements, 43,* 137-154. https://www.jstor.org/stable/27759962

Hilton, C.E., Auerbach, B.M., & Cowgill, L.W. (2014). Introduction: Humans on the edge of the Alaskan Arctic. In C.E. Hilton, B.M. Auerbach, & L.W. Cowgill (Eds.), *The Foragers of Point Hope: The Biology and Archaeology of Humans on the Edge of the Alaskan Arctic* (pp. 1-8). Cambridge: Cambridge University Press.

Holliday, T.W. (1997). Postcranial evidence of cold adaptation in European Neanderthals. *American Journal of Physical Anthropology, 104*(2), 155-265. https://doi.org/10.1002/(SICI)1096-8644(199710)104:2<245::AID-AJPA10>3.0.CO;2-#

Holliday, T.W. & Hilton, C.E. (2010). Body proportions of circumpolar peoples as evidenced from skeletal data: Ipiutak and Tigara (Point Hope) versus Kodiak Island Inuit. *American Journal of Physical Anthropology, 142*(2), 287–302. https://doi.org/10.1002/ajpa.21226

Holt, B., Whittey, E., Niskanen, M., Sládek, V., Berner, M., & Ruff, C.B. (2018). Temporal and geographic variation in robusticity. In C.B. Ruff (Ed.), *Skeletal Variation and Adaptation in Europeans: Upper Paleolithic to the Twentieth Century*, (pp. 91-132), Hoboken, NJ: John Wiley & Sons, Inc.

Holt, B. & Whittey, E. (2019). The impact of terrain on lower limb bone structure. *American Journal of Physical Anthropology, 168*(4), 729-743. https://doi.org/10.1002/ajpa.23790

Hoppa, R.D. & FitzGerald, C. M. (1999). From head to toe: integrating studies from bones and teeth in biological anthropology. In Hoppa, R. D., & FitzGerald, C. M. (Eds.), *Human Growth in the Past: Studies from Bones and Teeth.* Cambridge Studies in Biological and Evolutionary Anthropology, Vol. 25. Cambridge, UK: Cambridge University Press.

Hruschka, D.J. (2021). One size does not fit all. How universal standards for normal height can hide deprivation and create false paradoxes. *American Journal of Human Biology, 33*(5), e23552. https://doi.org/10.1002/ajhb.23552

Hruschka, D.J., Hadley, C., Brewis, A.A., & Stojanowski, C.M. (2015). Genetic population structure accounts for contemporary ecogeographic patterns in tropic and subtropic-dwelling humans. *PLoS ONE, 10*(3), e0122301. https://doi.org/10.1371/journal.pone.0122301

Huiskes, R. (1982). On the modelling of long bones in structural analyses. *Journal of Biomechanics, 15*(1), 65-69. https://doi.org/10.1016/0021-9290(82)90036-7

Humphrey, L.T. (1998). Growth patterns in the modern human skeleton. *American Journal of Physical Anthropology, 105*(1), 57–72. https://doi.org/10.1002/(SICI)1096-8644(199801)105:1<57::AID-AJPA6>3.0.CO;2-A

Humphrey, L.T. (2000). Growth studies of past populations: An overview and an example. In M. Cox & S. Mays (Eds.), *Human Osteology in Archaeology and Forensic Science* (pp. 23-38). Cambridge: Cambridge University Press.

Humphrey, L.T. (2003). Linear growth variation in the archaeological record. In: J.L. Thompson, G.E. Krovitz, & A.J. Nelson (Eds.), *Patterns of Growth Variation in the genus* Homo (pp. 144-169). Cambridge: Cambridge University Press.

Humphreys, A.J.B. (1970). The remains from Koffiefontein burials excavated by W. Fowler and Preserved in the McGregor Museum, Kimberley. *The South African Archaeological Bulletin, 25*(99/100), 104-115. https://doi.org/10.2307/3888134

Huseynov, A., Zollikofer, C.P.E., Coudyzer, W., Gascho, G., Kellenberger, C., Hinzpeter, R., & Ponce de León, M.S. (2016). Developmental evidence for obstetric adaptation of the human female pelvis. *PNAS, 113*(19), 5227-5232. https://doi.org/10.1073/pnas.1517085113

IBM Corp. (2020). *IBM SPSS Statistics for Windows, Version 27.0*. Armonk, NY: IBM Corp.

Ioannidou, M., Koufos, G.D., de Bonis, L., & Harvati, K. (2021). 3D geometric morphometrics analysis of mandibular fragments of *Ouranopithecus macedoniensis* from the late Miocene deposits of Central Macedonia, Greece. *American Journal of Biological Anthropology, 177*(1), 48-62. https://doi.org/10.1002/ajpa.24420

Johnston, F.E. (1962). Growth of the long bones of infants and young children at Indian Knoll. *American Journal of Physical Anthropology, 20*(3), 249-254. https://doi.org/10.1002/ajpa.1330200309

Katzenberg, M.A., Herring, D.A., & Saunders, S.R. (1996). Weaning and infant mortality: Evaluating the skeletal evidence. *Yearbook of Physical Anthropology, 101*(S23), 177-199. https://doi.org/10.1002/(SICI)1096-8644(1996)23+<177::AID-AJPA7>3.0.CO;2-2

Katzmarzyk, P.T. & Leonard, W.R. (1998). Climatic influences on human body size and proportions: ecological adaptations and secular trends. *American Journal of Physical Anthropology, 106*(4), 483-503. https://doi.org/10.1002/(SICI)1096-8644(199808)106:4<483::AID-AJPA4>3.0.CO;2-K

Kelly, R.L. (2013). *The Lifeways of Hunter-Gatherers: The Foraging Spectrum*. New York, NY: Cambridge University Press.

Klales, A.R. & Burns, T.L. (2017). Adapting and applying the Phenice (1969) adult morphological sex estimation technique to subadults. *Journal of Forensic Sciences, 62*(3), 747-752. https://doi.org/10.1111/1556-4029.13332

Klingenberg, C.P. (2012a). Introduction: What is Morphometrics? *Lecture notes, Analysis of Organismal Form* (University of Manchester).

Klingenberg, C.P. (2012b). Size and Shape. *Lecture notes, Analysis of Organismal Form* (University of Manchester).

Klingenberg, C.P. (2012c). Shape of Landmark Configurations: Procrustes Superimposition. *Lecture notes, Analysis of Organismal Form* (University of Manchester).

Klingenberg, C.P. (2012d). Allometry. *Lecture notes, Analysis of Organismal Form* (University of Manchester).

Klingenberg, C.P. (2016). Size, shape, and form: concepts of allometry in geometric morphometrics. *Development Genes and Evolution, 226,* 113-137. https://doi.org/10.1007/s00427-016-0539-2

Klingenberg, C.P. (2022). Methods for studying allometry in geometric morphometrics: a comparison of performance. *Evolutionary Ecology, 36*(4), 439-470. https://doi.org/10.1007/s10682-022-10170-z

Kubicka, A.M., Balzeau, A., Kosicki, J., Nowaczewska, W., Haduch, E., Spinek, A., & Piontek, J. (2022). Variation in cross-sectional indicator of femoral robusticity in *Homo sapiens* and Neandertals. *Scientific Reports*, *12*(1), 1-13. https://doi.org/10.1038/s41598-022-08405-8

Kurki, H.K. (2005). *Adaptive Allometric Modeling of the Pelvis in Small-Bodied Later Stone Age (Holocene) Foragers from Southern Africa*. PhD Thesis, University of Toronto.

Kurki, H.K. (2007). Protection of obstetric dimensions in a small-bodied human sample. *American Journal of Physical Anthropology, 133*(4), 1152-1165. https://doi.org/10.1002/ajpa.20636

Kurki, H.K. (2013a). Bony pelvic canal size and shape in relation to body proportionality in humans. *American Journal of Physical Anthropology, 151*(1), 88-101. https://doi.org/10.1002/ajpa.22243

Kurki, H.K. (2013b). Skeletal variability in the pelvis and limb skeleton of humans: Does stabilizing selection limit female pelvic variation? *Journal of Human Biology, 25*(6), 795-802. https://doi.org/10.1002/ajhb.22455

Kurki, H.K. (2017). Bilateral asymmetry in the human pelvis. *The Anatomical Record, 300*(4), 653-665. https://doi.org/10.1002/ar.23546

Kurki, H.K. & Decrausaz, S.-L. (2016). Shape variation in the human pelvis and limb skeleton: Implications for obstetric adaptation. *American Journal of Physical Anthropology, 159*(4), 630-638. https://doi.org/10.1002/ajpa.22922

Kurki, H.K., Ginter, J.K., Stock, J.T., & Pfeiffer, S. (2008). Adult proportionality in small-bodied foragers: A test of ecogeographic expectations. *American Journal of Physical Anthropology, 136*(1), 28–38. https://doi.org/10.1002/ajpa.20774

Kurki, H.K., Ginter, J.K., Stock, J.T., & Pfeiffer, S. (2010). Body size estimation of small-bodied humans: Applicability of current methods. *American Journal of Physical Anthropology*, *141*(2), 169-180. https://doi.org/10.1002/ajpa.21127

Kurki, H.K., Holland, S., MacKinnon, M., Cowgill, L., Osipov, B., & Harrington, L. (2022). Appositional long bone growth: Implications for cross-sectional geometry. *American Journal of Biological Anthropology, 179*(2), 291-306. https://doi.org/10.1002/ajpa.24602

Konner, M. (1976). Maternal care, infant behavior and development among the !Kung. In R.B. Lee & I. Devore (Eds.), *Kalahari Hunter-Gatherers: Studies of the !Kung San and Their Neighbors* (pp. 218-245). Cambridge, Massachusetts: Harvard University Press.

Konner, M. (2005). Hunter-gather infancy and childhood: The !Kung and others. In M.E. Hewlett & B.S. Lamb (Eds.), *Hunter-Gatherer Childhoods: Evolutionary, Developmental and Cultural Perspectives* (pp. 19-64). New Brunswick, NJ: Aldine Transaction.

Kramer, P.A. & Sylvester, A.D. (2023). Hip width and metabolic energy expenditure of abductor muscles. *PLoS ONE, 18*(4), e0284450. https://doi.org/10.1371/journal.pone.0284450

Krueger, K.L. (2014). Contrasting the Ipiutak and Tigara: Evidence from incisor microwear texture analysis. In C.E. Hilton, B.M. Auerbach, & L.W. Cowgill (Eds.), *The Foragers of Point Hope: The Biology and Archaeology of Humans on the Edge of the Alaskan Arctic* (pp. 99-119). Cambridge: Cambridge University Press.

Larsen, C.S. (2015a). Stress and deprivation during growth and development and adulthood. In *Bioarchaeology: Interpreting Behavior from the Human Skeleton*, *Second Edition* (pp. 7-65). Cambridge Studies in Biological and Evolutionary Anthropology. Cambridge, UK: Cambridge University Press.

Larsen, C.S. (2015b). Activity Patterns: 2. Structural adaptation. In *Bioarchaeology: Interpreting Behavior from the Human Skeleton*, *Second Edition* (pp. 214-255). Cambridge Studies in Biological and Evolutionary Anthropology. Cambridge, UK: Cambridge University Press.

Larsen, H.E. & Rainey, F.G. (1948). Ipiutak and the Arctic whale hunting culture. *Anthropological Papers of the American Museum of Natural History, 42*. New York, NY: American Museum of Natural History.

Laurenson R.D. (1964). The primary ossification of the human ilium. *The Anatomical Record, 148*, 209-217.

Lee, R.B. (1984). *The Dobe !Kung*. New York, NY: CBS College Publishing.

Lewis, M.E. (2007). *The Bioarchaeology of Children: Perspectives from Biological and Forensic Anthropology* (Vol. 50). Cambridge, UK: Cambridge University Press.

Lieberman, D.E., Devlin, M.J., & Pearson, O.M. (2001). Articular area responses to mechanical loading: effects of exercise, age, and skeletal location. *American Journal of Physical Anthropology, 116*(4), 257-357. https://doi.org/10.1002/ajpa.1123

Liversidge, H.M. & Molleson, T. (2004). Variation in crown and root formation and eruption of human deciduous teeth. *American Journal of Physical Anthropology, 123*(2), 172-180. https://doi.org/10.1002/ajpa.10318

Lönnerdal, B. (2000). Breast milk: a truly functional food. *Nutrition, 16*(7-8), 509-511. https://doi.org/10.1016/S0899-9007(00)00363-4

Lyon, G.F. (1825). *A Brief Narrative of An Unsuccessful Attempt to Reach Repulse Bay, Through Sir Thomas Rowe's "Welcome"; in His Majesty's Ship Griper, in the Year MDCCCXXIV*. London: John Murray.

Macintosh, A.A., Davies, T.G., Ryan, T.M., Shaw, C.N., & Stock, J.T. (2013). Periosteal versus true cross-sectional geometry: A comparison along humeral, femoral, and tibial diaphyses. *American Journal of Physical Anthropology, 150*(3), 442-452. https://doi.org/10.1002/ajpa.22218

Macintosh, A.A., Pinhasi, R., & Stock, J.T. (2014). Divergence in male and female manipulative behaviors with the intensification of metallurgy in Central Europe. *PLoS One*, *9*(11), e112116. https://doi.org/10.1371/journal.pone.0112116

Mallick, S., Li, H., Lipson, M., Mathieson, I., Gymrek, M…. Reich, D. (2016). The Simons Genome Diversity Project: 300 genomes from 142 diverse populations. *Nature, 538,* 201-206. https://doi.org/10.1038/nature18964

Mance, M.J. (2008). Keeping infants warm: Challenges of hypothermia. *Advances in Neonatal Care, 8*(1), 6-12. https://doi.org/10.1097/01.ANC.0000311011.33461.a5

Manning, T.H. (1936). Some notes on Southampton Island. *The Geographical Journal, 88*(3), 232-242. https://doi.org/10.2307/1786097

Marchi, D., Sparacello, V., & Shaw, C. (2011). Mobility and lower limb robusticity of a pastoralist Neolithic population from north-western Italy. In R. Pinhasi & J.T. Stock (Eds.), *Human Bioarchaeology of the Transition to Agriculture*, (p 317–346), New York: Wiley-Blackwell.

Maresh, M.M. (1943). Growth of major long bones in healthy children: A preliminary report on successive roentgenograms of the extremities from early infancy to twelve years of age. *American Journal of Diseases of Children, 66*(3), 227-257. https://doi.org/10.1001/archpedi.1943.02010210003001

Maresh, M.M. (1955). Linear growth of long bones of extremities from infancy through adolescence; continuing studies. *American Journal of Diseases of Children, 89*(6), 725-742. https://doi.org/10.1001/archpedi.1955.02050110865010

Maresh, M.M. (1970). Measurements from roentgenograms, heart size, long bone lengths, bone, muscles and fat widths, skeletal maturation. In R.W. McCammon (Ed.), *Human Growth and Development,* (p 155-200), Springfield: Charles C. Thomas.

Mathiassen, T. (1927). *Archaeology of the Central Eskimos*. Copenhagen: Gyldendalske Boghandel, Nordisk Forlag.

Mathiassen, T. (1928). Material culture of the Iglulik Eskimos. *Report of the Fifth Thule Expedition 1921-24, The Danish Expedition to Arctic North America in Charge of Knud Rasmussen, PhD, VI*(1). Copenhagen: Gyldendalske Boghandel, Nordisk Forlag.

Mays, S. (2007). The Human Remains. In S. Mays, C. Harding, & C. Heighway (Eds.), *Wharram: A Study of Settlement on the Yorkshire Wolds, XI The Churchyard* (pp. 77-192, 337-397). York University Archaeological Publications, 13. York: University of York.

Mays, S. (2016). A study of the potential of deciduous incisor wear as an indicator of weaning using a human skeletal population. *International Journal of Osteoarchaeology, 26*(4), 725-731. https://doi.org/10.1002/oa.2464

Mays, S. (2018). The study of growth in skeletal populations. In S. Crawford, D.M. Hadley, & G. Shepherd (Eds.), *The Oxford Handbook of the Archaeology of Childhood* (pp. 71-89). Oxford, UK: Oxford University Press. https://doi-org.ezproxy.library.uvic.ca/10.1093/oxfordhb/9780199670697.013.4

Mays, S., Gowland, R., Halcrow, S., & Murphy, E. (2017). Child bioarchaeology: Perspectives on the past 10 years. *Childhood in the Past, 10*(1), 38-56. https://doi.org/10.1080/17585716.2017.1301066

McCammon, R.W. (1970). *Human Growth and Development*. Springfield, Illinois: Charles C. Thomas.

McHenry, H.M. (1992). Body size and proportions in early hominids. *American Journal of Physical Anthropology*, *87*(4), 407-431. https://doi.org/10.1002/ajpa.1330870404

Merbs, C.F. (1983). Patterns of activity-induced pathology in a Canadian Inuit population. *National Museum of Man Mercury Series, Archaeological Survey of Canada*, Paper No. 119, Ottawa.

Merbs, C.F. (2019). The discovery and rapid demise of the Sadlermiut. In D.H. Temple & C.M. Stojanowski (Eds.). *Hunter-Gatherer Adaptation and Resilience: A Bioarchaeological Perspective* (pp. 302-327). Cambridge: Cambridge University Press.

Mitchell, P. (2002). *The Archaeology of Southern Africa*. Cambridge: Cambridge University Press.

Mitteroecker, P., Grunstra, N.D.S., Stansfield, E., Waltenberger, L., & Fischer, F. (2021). Did population differences in human pelvic form evolve by drift or selection? *Bulletins et mémoires de la Société d'Anthropologie de Paris, 33*(1), 10-25. https://doi.org/10.4000/bmsap.7460

Mitteroecker, P., Gunz, P., Bernhard, M., Schaefer, K., & Bookstein, F.L. (2004). Comparison of cranial ontogenetic trajectories among great apes and humans. *Journal of Human Evolution, 46*(6), 679-698. https://doi.org/10.1016/j.jhevol.2004.03.006

Mitteroecker, P. & Gunz, P. (2009). Advances in geometric morphometrics. *Evolutionary Biology*, *36*(2), 235-247. https://doi.org/10.1007/s11692-009-9055-x

Moore, C.B. (1916). Some aboriginal sites on the Green River, Kentucky. *Journal of the Academy of Natural Sciences, Philadelphia, 16*, 431-487.

Mopin, C., Chaumoître, K., Signoli, M., & Adalian, P. (2018). Developmental stability and environmental stress: A geometric morphometrics analysis of asymmetry in the human femur. *American Journal of Physical Anthropology, 167*(1), 144-160. https://doi.org/10.1002/ajpa.23613

Morris, A.G. (1992). *A Master Catalogue: Holocene Human Skeletons from South Africa*. Johannesburg: Witwatersrand University Press.

Motarjemi, Y., Kaferstein, F., Moy, G., & Quevedo, F. (1993). Contaminated weaning foods – a major risk factor for diarrhoea and associated malnutrition. *Bull World Health Organization, 71*(1), 79-92.

Mott, R.L. & Untener, J.A. (2017). *Applied Strength of Materials, 6th edition, SI Units Version*. Boca Raton, FL: CRC Press.

Nagurka, M.L. & Hayes, W.C. (1980). An interactive graphics package for calculating cross sectional properties of complex shapes. *Journal of Biomechanics*, *13*(1), 59-64. https://doi.org/10.1016/0021-9290(80)90008-1

Newman, J. (1995). How breast milk protects newborns. *Scientific American*, *273*(6), 76-79. https://www.jstor.org/stable/24985584

Nowell, A. (2021). *Growing Up in the Ice Age: Fossil and Archaeological Evidence of the Lived Lives of Plio-Pleistocene Children.* Oxford, UK: Oxbow Books.

Nozaki, S., Watanabe, K., Kamiya, T., Katayose, M., & Ogihara, N. (2021). Morphological variations of the human talus investigated using three-dimensional geometric morphometrics. *Clinical Anatomy, 34*(4), 536-543. https://doi.org/10.1002/ca.23588

Ocobock, C., Lacy, S., & Niclou, A. (2021). Between a rock and a cold place: Neanderthal biocultural cold adaptations. *Evolutionary Anthropology, 30*(4)*,* 262-279. https://doi.org/10.1002/evan.21894

O'Neill, M.C. & Ruff, C.B. (2004). Estimating human long bone cross-sectional geometric properties: a comparison of noninvasive methods. *Journal of Human Evolution*, *47*(4), 221-235. https://doi.org/10.1016/j.jhevol.2004.07.002

O'Rahilly, R. & Gardner, E. (1975). The timing and sequence of events in the development of the limbs in the human embryo. *Anatomy and Embryology, 148,* 1-23. https://doi.org/10.1007/BF00315559

Osipov, B., Temple, D., Cowgill, L., Harrington, L., Bazaliiskii, V.I., & Weber, A.W. (2016). Evidence for genetic and behavioral adaptations in the ontogeny of prehistoric hunter-gatherer limb robusticity. *Quaternary International, 405*(Part B), 134-146. https://doi.org/10.1016/j.quaint.2015.09.093

Pavličev, M., Romero, R., & Mitteroecker, P. (2020). Evolution of the human pelvis and obstructed labor: new explanations of an old obstetrical dilemma. *American Journal of Obstetrics and Gynecology, 222*(1), 3-16. https://doi.org/10.1016/j.ajog.2019.06.043

Pearson, O.M. (2000). Activity, climate, and postcranial robusticity: Implications for modern human origins and scenarios of adaptive change. *Current Anthropology, 41*(4), 569-607. https://doi.org/10.1086/317382

Pearson, O.M. & Lieberman, D.E. (2004). The aging of Wolff's "law": Ontogeny and responses to mechanical loading in cortical bone. *Yearbook of Physical Anthropology*, *125*(S39), 63-99. https://doi.org/10.1002/ajpa.20155

Pelly, D.F. (1987). Sadlermiut mystery: Isolated group of Inuit perished in one winter, and we still don't know why or how. *Canadian Geographic, 107*(5), 28-32.

Pfeiffer, S. (2007). The health of foragers: people of the Later Stone Age, Southern Africa. In M. Cohen, & G. Crane-Kramer (Eds.), *Ancient Health: Skeletal Indicators of Agricultural and Economic Intensification* (pp. 223-236). Gainsville: University Press of Florida.

Pfeiffer, S. (2012). Conditions for evolution of small adult body size in southern Africa. *Current Anthropology, 53*(S6), S383-S394. https://doi.org/10.1086/667521

Pfeiffer, S. (2016). An exploration of interpersonal violence among Holocene foragers of Southern Africa. *International Journal of Paleopathology, 13*, 27-38. https://doi.org/10.1016/j.ijpp.2016.01.001

Pfeiffer, S. & Harrington, L. (2010). Child growth among south African foragers in the past. In T. Moffat & T. Prowse (Eds.), *Human Diet and Nutrition in Biocultural Perspective* (pp. 35-56). New York: Berghahn Books.

Pfeiffer, S. & Harrington, L. (2011). Bioarchaeological evidence for the basis of small adult stature in southern Africa. *Current Anthropology, 52*(3), 449–461. https://doi.org/10.1086/659452

Pfeiffer, S. & Sealy, J. (2006). Body size among Holocene foragers of the Cape ecozone, southern Africa. *American Journal of Physical Anthropology, 129*(1), 1–11. https://doi.org/10.1002/ajpa.20231

Phenice, T.W. (1969). A newly developed visual method of sexing the os pubis. *American Journal of Physical Anthropology*, *30*(2), 297-301. https://doi.org/10.1002/ajpa.1330300214

Pitseolak, P. & Eber, D.H. (1975). *People from Our Side*. Edmonton: Hurtig.

Pomeroy, E. (2023). Review: The different adaptive trajectories in Neanderthals and *Homo sapiens* and their implications for contemporary human physiological variation. *Comparative Biochemistry and Physiology Part A: Molecular & Integrative Physiology, 280,* 111420. https://doi.org/10.1016/j.cbpa.2023.111420

Pomeroy, E., Stock, J.T., & Wells, J.C.K. (2021). Population history and ecology, in addition to climate, influence human stature and body proportions. *Nature Scientific Reports, 11,* 274. https://doi.org/10.1038/s41598-020-79501-w

Porter, R.P. (1893). *Report on Population and Resources of Alaska at the Eleventh Census: 1890*. Government Printing Office, Washington D.C.

R Core Team (2020). *R: A language and environment for statistical computing*. [software] R Foundation for Statistical Computing, Vienna, Austria. URL: https://www.R-project.org/

Rainey, F.G. (1947). The whale hunters of Tigara. *Anthropological Papers of the American Museum of Natural History, 41*(2), 227-284.

Ricklan, S.J., Decrausaz, S.-L., Wells, J.C.K., & Stock, J.T. (2021). Obstetric dimensions of the female pelvis are less integrated than locomotor dimensions and show protective scaling patterns: Implications for the obstetrical dilemma. *American Journal of Human Biology,* 33(1), e23451. https://doi.org/10.1002/ajhb.23451

Roberts, D.F. (1978). *Climate and Human Variability*. San Fransisco, CA: Benjamin-Cummings Publishing Company.

Roberts, V.L., Noyes, F.R., Hubbard, R.P., & McCabe, J. (1971). Biomechanics of snowmobile spine injuries. *Journal of Biomechanics, 4*(6), 569-577. https://doi.org/10.1016/0021-9290(71)90046-7

Rohner, P.T. (2020). Evolution of multivariate wing allometry in schizophoran flies (Diptera: Schhizophora). *Journal of Evolutionary Biology, 33*(6), 831-841. https://doi.org/10.1111/jeb.13613

Roseman, C.C. (2004). Detecting interregionally diversifying natural selection on modern human cranial form by using matched molecular and morphometric data. *PNAS, 101*(35), 12824-12829. https://doi.org/10.1073/pnas.0402637101

Ruff, C.B. (1991). Climate and body shape in hominid evolution. *Journal of Human Evolution, 21*(2), 81-105. https://doi.org/10.1016/0047-2484(91)90001-C

Ruff, C.B. (1993). Climatic adaptation and hominid evolution: The thermoregulatory imperative. *Evolutionary Anthropology, 2*(2), 53-60. https://doi.org/10.1002/evan.1360020207

Ruff, C.B. (1994). Morphological adaptation to climate in modern and fossil hominids. *American Journal of Physical Anthropology, 37*(S19), 65-107. https://doi.org/10.1002/ajpa.1330370605

Ruff, C.B. (1995). Biomechanics of the hip and birth in early Homo. *American Journal of Physical Anthropology, 98*(4), 527-574. https://doi.org/10.1002/ajpa.1330980412

Ruff, C.B. (2000). Body size, body shape, and long bone strength in modern humans. *Journal of Human Evolution, 38*(2), 269-290. https://doi.org/10.1006/jhev.1999.0322

Ruff, C.B. (2003a). Long bone articular and diaphyseal structures in Old World monkeys and apes. II: Estimation of body mass. *American Journal of Physical Anthropology, 120*(1), 16-37. https://doi.org/10.1002/ajpa.10118

Ruff, C.B. (2003b). Growth in bone strength, body size, and muscle size in a juvenile longitudinal sample. *Bone, 33*(3), 317-329. https://doi.org/10.1016/S8756-3282(03)00161-3

Ruff, C.B. (2007). Body size prediction from juvenile skeletal remains. *American Journal of Physical Anthropology, 133*(1), 698-716. https://doi.org/10.1002/ajpa.20568

Ruff, C.B. (2008). Femoral/humeral strength in early African *Homo erectus*. *Journal of Human Evolution, 54*(3), 383-390. https://doi.org/10.1016/j.jhevol.2007.09.001

Ruff, C.B. (2019). Biomechanical analyses of archaeological human skeletons. In M. Katzenberg & A. Grauer (Eds.), *Biological Anthropology of the Human Skeleton, Third Edition* (pp.189-224), John Wiley & Sons Inc.

Ruff, C.B. (2022). Bone structural data for the Denver longitudinal growth study. *American Journal of Biological Anthropology, 178*(3), 544-547. https://doi.org/10.1002/ajpa.24518

Ruff, C.B. (n.d.). *MomentMacroJ.* Retrieved from http://www.hopkinsmedicine.org/FAE/mmacro.htm/

Ruff, C.B., Garofalo, E., & Holmes, M.A. (2013). Interpreting skeletal growth in the past from a functional and physiological perspective. *American Journal of Physical Anthropology, 150*(1), 29-37. https://doi.org/10.1002/ajpa.22120

Ruff, C.B., Holt, B., & Trinkaus, E. (2006). Who's afraid of the big bad Wolff?: "Wolff's Law" and bone functional adaptation. *American Journal of Physical Anthropology*, *129*(4), 484-498. https://doi.org/10.1002/ajpa.20371

Ruff, C.B., Holt, B., Niskanen, M., Sládek, V., Berner, M., Garofalo, E., Garvin, H.M., Hora, M., Junno, J-A., Schuplerova, E., Vilkama, R., & Whittey, E. (2015). Gradual decline in mobility with the adoption of food production in Europe. *Proceedings of the National Academy of Sciences*, *112*(23), 7147-7152. https://doi.org/10.1073/pnas.1502932112

Ruff, C.B., Trinkaus, E., Holliday, T.W. (2002). Body proportions and size. In J. Zilhão J. & E. Trinkaus (Eds.). *Portrait of the Artist as a Child: The Gravettian Human Skeleton from the Abrigo do Lagar Velho and its Archaeological Contex*t (pp. 365-391). Lisbon: Instituto Português de Arqueologia.

Ruff, C.B., Walker, A., & Trinkaus, E. (1994). Postcranial robusticity in *Homo*. III: Ontogeny. *American Journal of Physical Anthropology, 93*(1), 35–54. https://doi.org/10.1002/ajpa.1330930103

Ryan, K. (2011). Comments on Coltrain et al., Journal of Archaeological Science 31, 2004 "Sealing, whaling and caribou: the skeletal isotope chemistry of eastern Arctic foragers", and Coltrain, Journal of Archaeological Science 36, 2009 "Sealing, whaling and caribou revisited: additional insights from the skeletal isotope chemistry of eastern Arctic foragers." *Journal of Archaeological Science, 38*(10), 2858-2865. https://doi.org/10.1016/j.jas.2010.11.028

Ryan, K. & Young, J. (2013). Identification of a probable Aarnguaq in a Sadlermiut grave from Native Point. *Arctic Anthropology, 50*(1), 20-48. https://doi.org/10.3368/aa.50.1.20

Sakaue, K. (1997). Bilateral asymmetry of the humerus in Jomon people and modern Japanese. *Anthropological Science, 105*(4), 231-246. https://doi.org/10.1537/ase.105.231

Saunders, S.R. (2008). Juvenile skeletons and growth-related studies. In M.A. Katzenberg & S.R. Saunders (Eds.), *Biological Anthropology of the Human Skeleton* (pp. 117-147). John Wiley & Sons, Inc.

Scheuer, L. & Black, S. (2000). *Developmental Juvenile Osteology.* San Diego, CA: Elsevier Academic Press.

Schlager, S. (2017). Morpho and Rvcg—Shape Analysis in R. In G. Zheng, S. Li, & G. Szekely, (Eds.). *Statistical Shape and Deformation Analysis* (pp. 217-256), Academic Press.

Schuh, A., Kupczik, K., Gunz, P., Hublin, J-J., & Freidline, S.E. (2019). Ontogeny of the human maxilla: a study of intra-population variability combining surface bone histology and geometric morphometrics. *Journal of Anatomy, 235*(2), 233-245. https://doi.org/10.1111/joa.13002

Schurr, M.R. (2018). Exploring ideas about isotopic variation in breastfeeding and weaning within and between populations: Case studies from the American midcontinent. *International Journal of Osteoarchaeology, 28*(5), 479-491. https://doi.org/10.1002/oa.2698

Schurr, M.R. & Powell, M.L. (2005). The role of changing childhood diets in the prehistoric evolution of food production: An isotopic assessment. *American Journal of Physical Anthropology, 126*(3), 278-294. https://doi.org/10.1002/ajpa.20034

Schuster, S.C., Miller, W., Ratan, A., Tomsho, L.P., Giardine, B., Kasson, L.R., Harris, R.S…Hayes, V.M. (2010). Complete Khoisan and Bantu genomes from southern Africa. *Nature, 463*, 943-947. https://doi.org/10.1038/nature08795

Scott, E. (1999). The archaeology of infancy and infant death. *BAR International Series 819*. Oxford, UK: Archaeopress.

Scott, R.M. & Halcrow, S.E. (2017). Investigating weaning using dental microwear analysis: A review. *Journal of Archaeological Science: Reports, 11*, 1-11. https://doi.org/10.1016/j.jasrep.2016.11.026

Sealy, J. (2006). Diet, mobility, and settlement pattern among Holocene hunter-gatherers in southernmost Africa. *Current Anthropology, 47*(4), 569-595. https://doi.org/10.1086/504163

Sealy, J., Patrick, M.K., Morris, A.G., & Alder, D. (1992). Diet and dental caries among Later Stone Age inhabitants of the Cape Province, South Africa. *American Journal of Physical Anthropology, 88*(2), 123-134. https://doi.org/10.1002/ajpa.1330880202

Sealy, J. & Pfeiffer, S. (2000). Diet, body size, and landscape use among Holocene people in the Southern Cape, South Africa. *Current Anthropology, 41*(4), 642-655. https://doi.org/10.1086/317392

Sellen, D.W. (2001). Comparison of infant feeding patterns reported for nonindustrial populations with current recommendations. *The Journal of Nutrition, 131*(10), 2707-2715. https://doi.org/10.1093/jn/131.10.2707

Shackelford, L.L. (2014a). Variation in mobility and anatomical responses in the Late Pleistocene. In K. Carlson & D. Marchi (Eds.), *Mobility: Interpreting Behavior from Skeletal Adaptations and Environmental Interactions,* (pp. 153-171)*,* New York: Springer.

Shackelford, L.L. (2014b). Bone strength and subsistence activities at Point Hope. In C.E. Hilton, B.M. Auerbach, & L.W. Cowgill (Eds.), *The Foragers of Point Hope: The Biology and Archaeology of Humans on the Edge of the Alaskan Arctic* (pp. 181-211). Cambridge, UK: Cambridge University Press.

Shirley, M.K., Cole, T.J., Arthurs, O.J., Clark, C.A., & Wells, J.C.K. (2020). Developmental origins of variability in pelvic dimensions: Evidence from nulliparous South Asian women in the United Kingdom. *American Journal of Human Biology, 32*(2), e23340. https://doi.org/10.1002/ajhb.23340

Sládek, V., Berner, M., Holt, B., Niskanen, M., & Ruff, C.B. (2018). Past human manipulative behavior in the European Holocene as assessed through upper limb asymmetry. In C.B. Ruff (Ed.), *Skeletal Variation and Adaptation in Europeans: Upper Paleolithic to the Twentieth Century*, (pp. 163-208), Hoboken, NJ: John Wiley & Sons, Inc.

Smith, B.H. (1991). Standards of human tooth formation and dental age assessment. In M.A. Kelley & C.S. Larsen (Eds.), *Advances in Dental Anthropology* (pp.143-168). New York: Wiley-Liss.

Smith, J.M., Burian, R., Kauffman, S., Alberch, P., Campbell, J., Goodwin, B., Lande, R., Raup, D., & Wolpert, L. (1985). Developmental constraints and evolution: A perspective from the Mountain Lake conference on development and evolution. *The Quarterly Review of Biology, 60*(3), 265-287. https://doi.org/10.1086/414425

Snow, C.E. (1948). Indian Knoll skeletons of site Oh 2, Ohio County, Kentucky. *The University of Kentucky Reports in Anthropology and Archaeology, 4*(3), Part II, 371-555. Lexington: Department of Anthropology.

Sparacello, V.S., Marchi, D., & Shaw, C.N. (2014). The importance of considering fibular robusticity when inferring the mobility patterns of past populations. In Carlson, K.J., & Marchi, D. (Eds.). *Reconstructing Mobility: Environmental, Behavioral, and Morphological Determinants* (pp. 91-110). New York: Springer.

Sparacello, V.S. & Pearson, O.M. (2010). The importance of accounting for the area of the medullary cavity in cross-sectional geometry: A test based on the femoral midshaft. *American Journal of Physical Anthropology*, *143*(4), 612-624. https://doi.org/10.1002/ajpa.21361

Stansfield, E., Mitteroecker, P., Umek, W., & Fischer, B. (2023). The variation in shape and thickness of the pelvic floor musculature in males and females: a geometric-morphometric analysis. *International Urogynecology Journal, 34,* 453-461. https://doi.org/10.1007/s00192-022-05311-5

Stansfield, E., Kumar, K., Mitteroecker, P., & Grunstra, N.D.S. (2021). Biomechanical trade-offs in the pelvic floor constrain the evolution of the human birth canal. *PNAS, 118*(16), e2022159118. https://doi.org/10.1073/pnas.2022159118

Steckel, R.H. & Rose, J.C. (2002). *The Backbone of History: Health and Nutrition in the Western Hemisphere*. Cambridge: Cambridge University Press

Stevenson, P.H. (1929). On racial differences in stature long bone regression formulae, with special reference to stature reconstruction formulae for the Chinese. *Biometrika, 21*(1/4), 303-318. https://doi.org/10.2307/2332563

Stock, J.T. (2002). A test of two methods of radiographically deriving long bone cross-sectional properties compared to direct sectioning of the diaphysis. *International Journal of Osteoarchaeology*, *12*(5), 335-342. https://doi.org/10.1002/oa.629

Stock, J.T. & Pfeiffer, S. (2001). Linking structural variability in long bone diaphyses to habitual behaviors: Foragers from the southern African Later Stone Age and the Andaman Islands. *American Journal of Physical Anthropology, 115*(4), 337–348. https://doi.org/10.1002/ajpa.1090

Stock, J.T. & Pfeiffer, S. (2004). Long bone robusticity and subsistence behaviour among Later Stone Age foragers of the forest and fynbos biomes of South Africa. *Journal of Archaeological Science, 31*(7)*,* 999–1013. https://doi.org/10.1016/j.jas.2003.12.012

Stock, J.T. & Shaw, C.N. (2007). Which measures of diaphyseal robusticity are robust? A comparison of external methods of quantifying the strength of long bone diaphyses to cross-sectional geometric properties. *American Journal of Physical Anthropology*, *134*(3), 412-423. https://doi.org/10.1002/ajpa.20686

Stratovan Corporation (2018). *Stratovan Checkpoint [Software]*. Version 2018.08.07. URL: https://www.stratovan.com/products/checkpoint

Sundick, R. (1978). Human skeletal growth and age determination. *Homo, 29*(4)*,* 228-249.

Symchych, N. (2016). *An Ecogeographic Study of Body Proportion Development in the Sadlermiut Inuit of Southampton Island, Nunavut*. PhD Thesis, University of Toronto.

Tague, R.G. (1992). Sexual dimorphism in the human bony pelvis, with a consideration of the Neandertal pelvis from Kebara Cave, Israel. *American Journal of Physical Anthropology*, *88*(1), 1-21. https://doi.org/10.1002/ajpa.1330880102

Temple, D.H., Okazaki, K., & Cowgill, L.W. (2011). Ontogeny of limb proportions in late through final Jomon period foragers. *American Journal of Physical Anthropology, 145*(3), 415-425. https://doi.org/10.1002/ajpa.21515

The 1000 Genomes Project Consortium. (2012). An integrated map of genetic variation from 1,092 human genomes. *Nature, 491*(7422), 56-65. https://doi.org/10.1038/nature11632

Thomas, K. (1994). Thermoregulation in neonates. *Neonatal Network: NN, 13*(2), 15-22.

Tilkens, M.J., Wall-Scheffler, C.M., Weaver, T.D., & Steudel-Numbers, K. (2007). The effects of body proportions on thermoregulation: an experimental assessment of Allen's rule. *Journal of Human Evolution, 53*(3), 286-291. https://doi.org/10.1016/j.jhevol.2007.04.005

Tishkoff, S.A., Reed, F.A., Friedlaender, F.R., Ehret, C., Ranciaro, A., Froment, A., Hirbo, J.B., Awomoyi, A.A., Bodo, J-M., Doumbo, O., Ibrahim, M., Juma, A.T., Kotze, M.J., Lema, G., Moore, J.H., Mortensen, H., Nyambo, T.B., Omar, S.A., Powell, K., Pretorius, G.S., Smith, M.W., Thera, M.A., Wambebe, C., Weber, J.L., & Williams, S.M. (2009). The genetic structure and history of Africans and African Americans. *Science, 324*(5930), 1035-1044. https://doi.org/10.1126/science.1172257

Tishkoff, S.A. & Verrelli, B.C. (2003). Patterns of human genetic diversity: Implications for human evolutionary history and disease. *Annual Review of Genomics and Human Genetics, 4,* 293-340. https://doi.org/10.1146/annurev.genom.4.070802.110226

Trinkaus, E. & Ruff, C.B. (1989). Diaphyseal cross-sectional morphology and biomechanics of the Fond-de-Forêt 1 femur and the Spy 2 femur and tibia. *Anthropologie et Préhistoire*, *100*, 33-42.

Trotter, M. & Gleser, G.C. (1958). A re-evaluation of estimation of stature based on measurements of stature taken during life and of long bones after death. *American Journal of Physical Anthropology, 16*(1), 79-123. https://doi.org/10.1002/ajpa.1330160106

Truswell, A.S. & Hanson, J.D.L. (1976). Medical research among the !Kung. In R.B. Lee & I. DeVore (Eds.), *Kalahari Hunter-Gatherers*, (pp. 166-194). Cambridge, MA: Harvard University Press.

Tsutaya, T. & Yoneda, M. (2014). Reconstruction of breastfeeding and weaning practices using stable isotope and trace element analyses: A review. *Yearbook of Physical Anthropology, 156*(S59), 2-21. https://doi.org/10.1002/ajpa.22657

Ubelaker, D.H. & Volk, C.G. (2002). A test of the Phenice method for the estimation of sex. *Journal of Forensic Science*, *47*(1), 19-24. https://doi.org/10.1520/JFS15200J

Verbruggen, S.W. & Nowlan, N.C. (2017). Ontogeny of the human pelvis. *The Anatomical Record, 300*(4), 643–652. https://doi.org/10.1002/ar.23541

Waddington, C.H. (1942). Canalization of development and the inheritance of acquired characters. *Nature, 150*(3811), 563–565. https://doi.org/10.1038/150405d0

Wall-Scheffler, C.M. (2022). Women carry for less: body size, pelvis width, loading position, and energetics. *Evolutionary Human Sciences, 4,* e36. https://doi.org/10.1017/ehs.2022.35

Wall-Scheffler, C.M., Kurki, H.K., & Auerbach, B.M. (2020). *The Evolutionary Biology of the Human Pelvis: An Integrative Approach.* Cambridge Studies in Biological and Evolutionary Anthropology, Vol. 85. Cambridge, UK: Cambridge University Press.

Warrener, A.G., Lewton, K.L., Pontzer, H., & Lieberman, D.E. (2015). A wider pelvis does not increase locomotor cost in humans, with implications for the evolution of childbirth. *PLoS ONE, 10*(3), e0118903. https://doi.org/10.1371/journal.pone.0118903

Washburn, S.L. (1960). Tools and human evolution. *Scientific American*, *203*(3), 62-75. https://www.jstor.org/stable/24940615

WEA (Workshop of European Anthropologists) (1980). Reccomendations for age and sex diagnoses of skeletons, *Journal of Human Evolution, 9,* 517-549.

Weaver, T.D. & Hublin, J.-J. (2009). Neanderthal birth canal shape and the evolution of human childbirth. *PNAS, 106*(20), 8151-8156. https://doi.org/10.1073/pnas.0812554106

Webb, W.S. (1946). Indian Knoll, Site Oh 2, Ohio County, Kentucky. *The University of Kentucky Reports in Anthropology and Archaeology, 4*(3), Part I, 111-365. Lexington: Department of Anthropology.

Webb, W.S. (1974). *Indian Knoll.* Knoxville: University the Tennessee Press.

Wells, J.C.K. (2002). Thermal environment and human birth weight. *Journal of Theoretical Biology, 214*(3), 413-425. https://doi.org/10.1006/jtbi.2001.2465

Wells, J.C.K. (2015). Between Scylla and Charybdis: Renegotiating resolution of the "obstetric dilemma" in response to ecological change. *Philosophical Transactions of the Royal Society B, 370*, 20140067. https://doi.org/10.1098/rstb.2014.0067

Wells, J.C.K. (2017). The new "obstetrical dilemma": Stunting, obesity, and the risk of obstructed labour. *The Anatomical Record, 300*(4), 716-731. http://doi.wiley.com/10.1002/ar.23540

Wells, J.C.K., DeSilva, J.M., & Stock, J.T. (2012). The obstetric dilemma: An ancient game of Russian roulette, or a variable dilemma sensitive to ecology? *Yearbook of Physical Anthropology, 149*(S55), 40-71. https://doi.org/10.1002/ajpa.22160

Wells, J.C.K. & Stock, J. T. (2007). The biology of the colonizing ape. *Yearbook of Physical Anthropology, 134*(S45), 191-222. https://doi.org/10.1002/ajpa.20735

WHO. (1999). *Infant and Young Child Nutrition: The WHO Multicentre Growth Reference Study*. Geneva: WHO.

WHO Multicentre Growth Reference Study Group. (2006). Enrolment and baseline characteristics in the WHO Multicentre Growth Reference Study. *Acta Paediatrica,* 95(S450), 7-15. https://doi.org/10.1111/j.1651-2227.2006.tb02371.x

Wickham, H. (2016). *ggplot2: Elegant Graphics for Data Analysis*. Springer-Verlag: New York.

Wilson, L.A.B., Ives, R., Cardoso, H.F.V., & Humphrey, L.T. (2014). Shape, size, and maturity trajectories of the human ilium. *American Journal of Physical Anthropology*, *156*(1), 19–34. https://doi.org/10.1002/ajpa.22625

Wilson, L.A.B. & Humphrey, L.T. (2017). Voyaging into the third dimension: A perspective on virtual methods and their application to studies of juvenile sex estimation and the ontogeny of sexual dimorphism. *Forensic Science International, 278*, 32–46. https://doi.org/10.1016/j.forsciint.2017.06.016

Winters, H.D. (1974). Introduction to the New Edition. In W.S. Webb (author). *Indian Knoll*. Knoxville: University the Tennessee Press.

Wittman, A.B. & Wall, L.L. (2007). The evolutionary origins of obstructed labor: Bipedalism, encephalization, and the human obstetric dilemma. *Obstetrical and Gynecological Survey, 62*(11), 739-748. https://doi.org/10.1097/01.ogx.0000286584.04310.5c

Wood, B.A. & Chamberlain, A.T. (1986). The primate pelvis: Allometry or sexual dimorphism? *Journal of Human Evolution*, *15*(4), 257-263. https://doi.org/10.1016/S0047-2484(86)80053-7

Wood, J.W., Milner, G.R., Harpending, H.C., & Weiss, K.M. (1992). The osteological paradox: Problems of inferring prehistoric health from skeletal samples. *Current Anthropology, 33*(4), 343-370. https://doi.org/10.1086/204084

Yim, A.-D., Cowgill, L.W., Katz, D.C., & Roseman, C.C. (2023). Variation in ontogenetic trajectories of limb dimensions in humans is attributable to both climatic effects and neutral evolution. *Journal of Human Evolution, 179,* 103369. https://doi.org/10.1016/j.jhevol.2023.103369

Young, M., Richard, D., Grabowski, M., Auerbach, B.M., de Bakker, B.S., Hagoort, J., Muthuirulan, P., Kharkar, V., Kurki, H.K., Betti, L., Birkenstock, L., Lewton, K.L., & Capellini, T.D. (2022). The developmental impacts of natural selection on human pelvic morphology. *Science Advances, 8*(33), eabq4884. https://doi.org/10.1126/sciadv.abq4884

Zihlman, A.L. & Brunker, L. (1979). Hominid bipedalism: Then and now. *Yearbook of Physical Anthropology, 22*, 132-162.

APPENDIX A: Juvenile Individuals Included in the Study Sample

Table A.1 LATER STONE AGE SOUTHERN AFRICANS

Catalogue[1]	Age Estimate (years)	Age Method[2,3]	Mass Estimate (kg)	Mass Method[6,7]
ALB051	9.5	QMUL	19.43	RMA Log FHEB
ALB108	8.5	LBL	20.89	RMA Log FHEB
ALB116B	1.81	LBL	7.17	RMA Log FDMB
ALB120	14.5	QMUL	34.15	RMA Log FHEB
ALB132	7.5	QMUL	19.97	RMA Log FHEB
ALB133	8.5	QMUL	14.40	RMA Log FHEB
ALB135	1.5	QMUL	7.28	RMA Log FDMB
ALB137	3.5	QMUL	11.84	RMA Log FDMB
ALB138	4.5	QMUL	10.96	RMA Log FDMB
ALB139	16.5	QMUL	37.21	RMA Log FHEB
ALB151B	13.5	QMUL	26.05	RMA Log FHEB
ALB152	14.5	QMUL	25.31	RMA Log FHEB
ALB175	5.5	QMUL	15.17	RMA Log FDMB
ALB176	3.5	QMUL	14.65	RMA Log FDMB
ALB181	6.5	QMUL	18.09	RMA Log FHEB
ALB182	8.5	QMUL	27.33	Pred. FHEB from TML, TPML, HML
ALB183	6.5	QMUL	15.01	RMA Log FHEB
ALB193	3.5	QMUL	8.99	RMA Log FDMB
ALB198	15.5	QMUL	38.19	RMA Log FHEB
ALB199	13.5	QMUL	41.71	RMA Log FHEB
ALB200	17.5	QMUL	53.04	McHenry FHEB
ALB236	4.5	QMUL	8.83	RMA Log FDMB
ALB238	16.5	QMUL	27.05	RMA Log FHEB
ALB265	1.5	QMUL	6.48	RMA Log FDMB
ALB266	6.5	QMUL	14.84	RMA Log FHEB
ALB295	11.5	QMUL	20.09	RMA Log FHEB
ALB296	16.5	QMUL	46.95	RMA Log FHEB
ALB299	0.625	QMUL	6.72	RMA Log FDMB
ALB300	2.5	QMUL	8.60	RMA Log FDMB
ALB311	1.5	QMUL	8.18	RMA Log FDMB
ALB322	0.875	QMUL	6.29	RMA Log FDMB
ALB325	6.5	QMUL	14.44	RMA Log FDMB
ALB350	10.5	QMUL	18.36	RMA Log FHEB
ALB351	14.5	QMUL	33.84	RMA Log FHEB

MMK203	19.5	QMUL	42.12	Pred. McHenry FHEB from TPEW, TML, HML, FDEW
MMK214	3.5	QMUL	9.85	Pred. FDMB from TPMW, HDML
MMK222	15.5	QMUL	31.61	RMA Log FHEB
MMK223	4.5	QMUL	12.40	Pred. FDMB from TPMW
MMK228	23.5	QMUL	43.23	McHenry FHEB
MMK230	7.5	QMUL	21.75	RMA Log FHEB
MMK238	4.5	QMUL	13.09	RMA Log FDMB
MMK245	12.5	QMUL	18.30	RMA Log FHEB
MMK246	3.5	QMUL	6.65	RMA Log FDMB
MMK248	14.5	QMUL	27.80	RMA Log FHEB
MMK249	17.5	QMUL	49.53	McHenry FHEB
NMB.S4.26.3.6	-0.15	LBL	4.00	RMA Log FDMB
NMB.WiltonA	7.78	LBL	22.79	RMA Log FHEB
NMB.WiltonB	9.1	LBL	20.09	RMA Log FHEB
NMB.WSK1	-0.21	LBL	4.01	RMA Log FDMB
NMB1271	20.5	QMUL	41.11	McHenry FHEB
NMB1273	20.5	QMUL	41.68	McHenry FHEB
NMB1640	20.5	QMUL	41.87	McHenry FHEB
NMB1641	5.15	LBL	14.04	RMA Log FDMB
NMB1642	5.64	LBL	17.28	RMA Log FDMB
NMB1644	0.375	QMUL	3.00	RMA Log FDMB
NMBskeleton4	7.5	QMUL	19.48	RMA Log FHEB
SAM4207	5.5	QMUL	14.83	RMA Log FDMB
SAM4829	0.875	QMUL	8.17	RMA Log FDMB
SAM6052	4.5	QMUL	12.96	RMA Log FDMB
SAM6053	9.5	QMUL	26.82	RMA Log FHEB
SAM6054A	12.5	QMUL	17.31	RMA Log FHEB
SAM6054B	6.5	QMUL	18.19	RMA Log FHEB
SAM6054C	2.5	QMUL	6.93	RMA Log FDMB
SAM6348A	15.5	QMUL	31.77	RMA Log FHEB
UCT210	4.5	QMUL	13.43	RMA Log FDMB
UCT213	14.8	LBL	32.88	RMA Log FHEB
UCT213.Gr16.2	0.875	QMUL	7.99	RMA Log FDMB
UCT216J	0.375	QMUL	7.34	RMA Log FDMB
UCT217E	8.38	LBL	23.49	RMA Log FHEB
UCT247	8.5	QMUL	15.55	Pred. FHEB from TPMW, HML
UCT346	2.5	QMUL	10.85	RMA Log FDMB
UCT437	5.5	QMUL	13.65	RMA Log FDMB

Table A.2 INDIAN KNOLL

Catalogue	Age Estimate (years)	Age Method[2,4]	Mass Estimate (kg)	Mass Method[6,7]
IK008	0.125	QMUL	3.79	RMA Log FDMB
IK029	-0.21	QMUL	3.85	RMA Log FDMB
IK033	0	QMUL	3.38	RMA Log FDMB
IK047	14.5	QMUL	28.15	RMA Log FHEB
IK062	0.625	QMUL	6.75	RMA Log FDMB
IK089	0.375	QMUL	5.69	RMA Log FDMB
IK091	0.375	QMUL	3.54	RMA Log FDMB
IK114	0.375	QMUL	2.56	RMA Log FDMB
IK125	13.5	QMUL	30.07	RMA Log FHEB
IK127	15	QMUL	39.50	RMA Log FHEB
IK138	12.5	QMUL	19.94	RMA Log FHEB
IK139	2.5	QMUL	9.50	RMA Log FDMB
IK172	7.5	QMUL	22.97	RMA Log FHEB
IK184	16.5	QMUL	44.83	RMA Log FHEB
IK196	2.5	QMUL	10.23	RMA Log FDMB
IK215	23.5	QMUL	56.49	Grine FHEB
IK219	14.5	QMUL	29.85	RMA Log FHEB
IK225	3	QMUL	9.96	RMA Log FDMB
IK232	10.5	QMUL	21.39	RMA Log FHEB
IK244	8.5	QMUL	22.54	RMA Log FHEB
IK245	9.5	QMUL	24.73	RMA Log FHEB
IK265	0.875	QMUL	7.51	RMA Log FDMB
IK271	1	QMUL	7.68	RMA Log FDMB
IK286	3	QMUL	9.31	RMA Log FDMB
IK302	14.5	QMUL	37.00	RMA Log FHEB
IK350	14.5	QMUL	29.00	RMA Log FHEB
IK444	9.5	S/L&M	21.45	RMA Log FHEB
IK453	4.5	S/L&M	12.73	RMA Log FDMB
IK472	10.5	QMUL	28.35	RMA Log FHEB
IK515	4.5	QMUL	14.06	RMA Log FDMB
IK530	4.5	QMUL	9.83	RMA Log FDMB
IK571	7.5	QMUL	20.94	RMA Log FHEB
IK599	8.5	S/L&M	22.25	RMA Log FHEB
IK724	7.5	QMUL	19.75	RMA Log FHEB
IK770	7.5	QMUL	21.21	RMA Log FHEB
IK785	8.5	QMUL	21.12	RMA Log FHEB
IK826	9.5	QMUL	16.29	RMA Log FHEB
IK855	7.5	QMUL	20.48	RMA Log FHEB

Table A.3 SADLERMIUT

Catalogue	Age Estimate (years)	Age Method[2,5]	Mass Estimate (kg)	Mass Method[6,7]
XIV-C:075	12.5	QMUL	31.00	RMA Log FHEB
XIV-C:076	8.5	QMUL	28.63	RMA Log FHEB
XIV-C:077	1.5	QMUL	8.58	RMA Log FDMB
XIV-C:078	4.5	QMUL	13.98	RMA Log FDMB
XIV-C:079	1.5	QMUL	6.42	RMA Log FDMB
XIV-C:118	5.5	QMUL	16.06	RMA Log FDMB
XIV-C:119	0.875	QMUL	7.13	RMA Log FDMB
XIV-C:123	0.375	QMUL	4.56	RMA Log FDMB
XIV-C:124	9.5	QMUL	24.81	Pred. FHEB from FMD, TML, IL
XIV-C:135	1.5	FL, IB	6.63	RMA Log FDMB
XIV-C:146	19.5	QMUL	60.48	Grine FHEB
XIV-C:150	8.5	QMUL	26.50	Pred. FHEB from FMD, TML, IL
XIV-C:151	10.5	QMUL	37.29	RMA Log FHEB
XIV-C:158	20.5	QMUL	61.43	Grine FHEB
XIV-C:162-1	0.125	QMUL	4.27	RMA Log FDMB
XIV-C:163	0.375	QMUL	4.40	RMA Log FDMB
XIV-C:187	0.125	QMUL	3.42	RMA Log FDMB
XIV-C:193	23.5	QMUL	66.26	Grine FHEB
XIV-C:194	16.5	QMUL	39.81	RMA Log FHEB
XIV-C:198	12.5	QMUL	53.82	RMA Log FHEB
XIV-C:203	1.5	QMUL	7.77	RMA Log FDMB
XIV-C:204	0.5	FL, IB	4.70	RMA Log FDMB
XIV-C:205	0.5	FL, IB	5.55	RMA Log FDMB
XIV-C:206	0.625	QMUL	5.23	RMA Log FDMB
XIV-C:212	0.5	FL, IB	6.26	RMA Log FDMB
XIV-C:220	15.5	QMUL	34.85	RMA Log FHEB
XIV-C:222	1.5	QMUL	6.27	RMA Log FDMB
XIV-C:223	1.5	QMUL	8.40	RMA Log FDMB
XIV-C:231	10.5	QMUL	22.15	RMA Log FHEB
XIV-C:232	7.5	QMUL	22.24	RMA Log FHEB
XIV-C:238	6.5	QMUL	16.36	RMA Log FDMB
XIV-C:239	20.5	QMUL	51.34	Grine FHEB
XIV-C:245	19.5	IB	56.73	Pred. Grine FHEB from TML
XIV-C:249	16.5	QMUL	41.37	Pred. FHEB from FMD, TML, IL
XIV-C:250-3	11.5	FL	30.01	Pred. FHEB from FMD, TML, IL
XIV-C:250-5	5.5	IB	N/A	N/A
XIV-C:278	1.5	QMUL	6.83	RMA Log FDMB
XIV-C:279	1.5	QMUL	7.44	RMA Log FDMB

XIV-C:280	0.875	QMUL	5.26	RMA Log FDMB
XIV-C:281	0.125	QMUL	3.55	RMA Log FDMB
XIV-C:296	13.5	QMUL	N/A	N/A
XIV-C:300-1	11.5	QMUL	26.75	RMA Log FHEB
XIV-C:301	13.5	QMUL	38.74	Pred. FHEB from FMD, TML, IL
XIV-C:734	1.5	QMUL	7.43	RMA Log FDMB

Table A.4 POINT HOPE

Catalogue	**Age Estimate (years)**	**Age Method[2,4]**	**Mass Estimate (kg)**	**Mass Method[6,7]**
PH088	15.5	QMUL	42.11	RMA Log FHEB
PH092	14.5	QMUL	33.89	RMA Log FHEB
PH095	13.5	QMUL	53.22	RMA Log FHEB
PH304	16.5	QMUL	41.62	RMA Log FHEB
PH342	10.5	QMUL	22.11	RMA Log FHEB
PH343	11.5	QMUL	26.81	RMA Log FHEB
PH344	9.5	QMUL	31.26	RMA Log FHEB
PH354	12.5	QMUL	30.55	RMA Log FHEB
PH360	5.5	QMUL	16.89	RMA Log FDMB
PH361	16.5	QMUL	40.42	RMA Log FHEB
PH376	14.22	LBL	37.51	Pred. FHEB from TPMW, TML
PH385	6.5	QMUL	18.11	RMA Log FDMB
PH406	15.5	QMUL	32.74	RMA Log FHEB
PH419	11.5	QMUL	23.85	RMA Log FHEB
PH457	0	LBL	5.69	RMA Log FDMB

[1]LSA catalogue codes: ALB = Albany Museum; MMK = McGregor Museum; NMB = National Museum Bloemfontein; SAM = Iziko South African Museum; UCT = University of Cape Town

[2]QMUL = London Atlas of Human Tooth Development and Eruption (AlQahtani, 2010), assessed by Lesley Harrington; S/L&M = Smith (1991) and Liversidge & Molleson (2004), from Cowgill (2008). Where dental data wasn't available, age at death estimates were predicted from LBL = long bone lengths; FL = femur length; IB = ilium breadth.

[3]Age at death estimates made from long bones come from Harrington (2010).

[4]Age at death estimates from long bones come from Cowgill (2008).

[5]Age at death estimates from regression equations generated using either femur length or ilium breadth, based on Cardoso *et al.* (2014, 2017).

[6]Unless otherwise indicated, body mass estimation equations are from Ruff (2007) calculated using either the FDMB (femoral distal metaphyseal breadth) or FHEB (femoral head epiphyseal breadth).

[7]Where FDMB or FHEB weren't available, the measure was predicted using one of the following: FDEW = femoral distal epiphyseal width; FMD = femoral midshaft diameter; HDML = humeral diaphysis max length; HML = humerus max length; IL = ilium length; TML = tibia max length; TPEW = tibial proximal epiphyseal width; TPMW = tibia proximal epiphyseal width. Where multiple prediction methods are listed an average of the prediction results was used.

APPENDIX B: Adult Individuals Included in the Study Sample

Catalogue	Sample	Sex
ALB050	LSA	Male
ALB177	LSA	Female
ALB178	LSA	Female
ALB222	LSA	Male
ALB273	LSA	Male
ALB293	LSA	Female
ALB339	LSA	Female
MMK228	LSA	Female
MMK250	LSA	Female
NMB1275	LSA	Male
NMB1704	LSA	Female
SAM1145	LSA	Male
SAM1871	LSA	Female
SAM1878A	LSA	Male
SAM1879	LSA	Male
SAM1893	LSA	Male
SAM5075	LSA	Male
IK017	Indian Knoll	Female
IK022	Indian Knoll	Female
IK028	Indian Knoll	Male
IK126	Indian Knoll	Female
IK140	Indian Knoll	Female
IK142	Indian Knoll	Male
IK191	Indian Knoll	Female
IK205	Indian Knoll	Female
IK217	Indian Knoll	Male
IK270	Indian Knoll	Male
IK305	Indian Knoll	Male
IK338	Indian Knoll	Female
IK342	Indian Knoll	Male
IK347	Indian Knoll	Male
IK447	Indian Knoll	Male
IK454	Indian Knoll	Male
IK462	Indian Knoll	Male
IK476	Indian Knoll	Male
IK510	Indian Knoll	Female
IK522	Indian Knoll	Female
IK545	Indian Knoll	Female
IK555	Indian Knoll	Female
IK590	Indian Knoll	Female
IK850	Indian Knoll	Female
XIV-C:102	Sadlermiut	Male
XIV-C:112	Sadlermiut	Female
XIV-C:117	Sadlermiut	Male

Catalogue	Sample	Sex
XIV-C:126	Sadlermiut	Male
XIV-C:155	Sadlermiut	Female
XIV-C:164	Sadlermiut	Male
XIV-C:168	Sadlermiut	Male
XIV-C:179	Sadlermiut	Male
XIV-C:180	Sadlermiut	Female
XIV-C:182	Sadlermiut	Male
XIV-C:199	Sadlermiut	Male
XIV-C:219	Sadlermiut	Female
XIV-C:230	Sadlermiut	Male
XIV-C:233	Sadlermiut	Female
XIV-C:235	Sadlermiut	Female
XIV-C:241	Sadlermiut	Female
XIV-C:244	Sadlermiut	Female
XIV-C:246	Sadlermiut	Male
XIV-C:248	Sadlermiut	Female
XIV-C:743	Sadlermiut	Female
PH102	Point Hope	Female
PH103	Point Hope	Male
PH163	Point Hope	Male
PH166	Point Hope	Male
PH200	Point Hope	Female
PH228	Point Hope	Male
PH232	Point Hope	Female
PH277	Point Hope	Male
PH316	Point Hope	Female
PH336	Point Hope	Male
PH339	Point Hope	Male
PH346	Point Hope	Male
PH349	Point Hope	Male
PH353	Point Hope	Male
PH359	Point Hope	Female
PH371	Point Hope	Female
PH373	Point Hope	Male
PH377	Point Hope	Female
PH378	Point Hope	Female
PH381	Point Hope	Male
PH386	Point Hope	Male
PH392	Point Hope	Male
PH459	Point Hope	Female
PH464	Point Hope	Female
PH481	Point Hope	Male
PH485	Point Hope	Female
PH489	Point Hope	Female

APPENDIX C: LSA Site, Biome, and Date Information

Catalogue	Site	Biome	Date (BP)	Source
ALB050	Plettenberg Bay	Forest	2380 ± 45	Sealy, 2006
ALB051	Plettenberg Bay	Forest	3790 ± 60	Pfeiffer & Harrington, 2011
ALB108	Port Alfred golf course	Savanna	N/A	Morris, 1992
ALB116B	Wilton Large Rock Shelter	Savanna	4610 ± 70	Pfeiffer & Harrington, 2011
ALB120	Wilton Cave	Savanna	4630 ± 70	Pfeiffer & Harrington, 2011
ALB132	Spitzkop	Savanna	4720 ± 70	Pfeiffer & Harrington, 2011
ALB133	Spitzkop	Savanna	4860 ± 70	Pfeiffer & Harrington, 2011
ALB135	Spitzkop	Savanna	4900 ± 60	Pfeiffer & Harrington, 2011
ALB137	Spitzkop	Savanna	4750 ± 60	Pfeiffer & Harrington, 2011
ALB138	Spitzkop	Savanna	4800 ± 80	Pfeiffer & Harrington, 2011
ALB139	Spitzkop	Savanna	5100 ± 70	Pfeiffer & Harrington, 2011
ALB151B	Near Kabeljaawus	Savanna	4220 ± 70	Pfeiffer & Harrington, 2011
ALB152	Kabeljaauws River Cave B	Savanna	2990 ± 60	Pfeiffer & Harrington, 2011
ALB175	Kleinpoort	Savanna	N/A	Pfeiffer & Harrington, 2011
ALB176	Kleinpoort	Savanna	390 ± 50	Pfeiffer & Harrington, 2011
ALB177	Kleinpoort	Savanna	390 ± 40	Kurki, 2005 (Sealy pers com)
ALB178	Kleinpoort	Savanna	240 ± 45	Kurki, 2005 (Sealy pers com)
ALB181	Kleinpoort	Savanna	450 ± 50	Pfeiffer & Harrington, 2011
ALB182	Lakeside, Kleinpoort	Savanna	N/A	Morris, 1992
ALB183	Dunbrody	Savanna	220 ± 50	Pfeiffer & Harrington, 2011
ALB193	Kleinpoort	Savanna	230 ± 60	Pfeiffer & Harrington, 2011
ALB198	Middlekop Kloof	Savanna	5120 ± 70	Pfeiffer & Harrington, 2011
ALB199	Middlekop Kloof	Savanna	5100 ± 70	Pfeiffer & Harrington, 2011
ALB200	Middlekop Kloof	Savanna	5105 ± 20	Pfeiffer & Harrington, 2011
ALB222	Seal Point Cape St. Francis	Fynbos	2640 ± 60	Pfeiffer & Harrington, 2011
ALB236	Mitford Park	Savanna	2100 ± 60	Pfeiffer & Harrington, 2011
ALB238	Widcome	Savanna	5550 ± 70	Pfeiffer & Harrington, 2011
ALB265	New Gloucester, Cave 5	Savanna	5934 ± 33	Pfeiffer & Harrington, 2011
ALB266	Delamare Farm	Savanna	580 ± 50	Pfeiffer & Harrington, 2011
ALB273	Teasdale	Karoo	350 ± 50	Kurki, 2005 (Sealy pers com); Morris, 1992
ALB293	Cannon Rocks	Savanna	N/A	Morris, 1992
ALB295	Klasies River Mouth Cave 5	Fynbos	1860 ± 40	Pfeiffer & Harrington, 2011
ALB296	Klasies River Mouth Cave 5	Fynbos	2180 ± 50	Pfeiffer & Harrington, 2011
ALB299	Klasies River Mouth Cave 5	Fynbos	3210 ± 70	Pfeiffer & Harrington, 2011
ALB300	St. Francis Bay	Fynbos	805 ± 27	Pfeiffer & Harrington, 2011
ALB311	Welgeluk	Savanna	4694 ± 32	Pfeiffer & Harrington, 2011
ALB318	Kenton-on-Sea	Savanna	887 ± 27	Pfeiffer & Harrington, 2011
ALB319	Joubertina	Fynbos	2560 ± 60	Pfeiffer & Harrington, 2011
ALB322	Klasies River Mouth Cave 5	Fynbos	4340 ± 80	Pfeiffer & Harrington, 2011
ALB325	Loerie Forest Station	Savanna	830 ± 50	Pfeiffer & Harrington, 2011
ALB339	N/A	N/A	N/A	N/A
ALB350	Oyster Bay	Fynbos	2990 ± 60	Pfeiffer & Harrington, 2011
ALB351	Papiesfontein	Savanna	725 ± 28	Pfeiffer & Harrington, 2011
MMK203	Koffiefontein	Karoo	N/A	Humphreys, 1970
MMK214	Koffiefontein	Karoo	N/A	Humphreys, 1970
MMK222	Koffiefontein	Karoo	N/A	Humphreys, 1970
MMK223	Koffiefontein	Karoo	N/A	Humphreys, 1970
MMK228	Koffiefontein	Karoo	N/A	Humphreys, 1970
MMK230	Koffiefontein	Karoo	N/A	Humphreys, 1970

MMK238	Koffiefontein	Karoo	N/A	Humphreys, 1970
MMK245	Koffiefontein	Karoo	N/A	Humphreys, 1970
MMK246	Koffiefontein	Karoo	N/A	Humphreys, 1970
MMK248	Koffiefontein	Karoo	N/A	Humphreys, 1970
MMK249	Koffiefontein	Karoo	N/A	Humphreys, 1970
MMK250	Koffiefontein	Karoo	N/A	Humphreys, 1970
NMB.S4.26.3.6	Matjes River Cave	Forest	N/A	Pfeiffer & Harrington, 2011
NMB.WiltonA	Matjes River Cave	Forest	N/A	Pfeiffer & Harrington, 2011
NMB.WiltonB	Matjes River Cave	Forest	N/A	Pfeiffer & Harrington, 2011
NMB.WSK1	Matjes River Cave	Forest	N/A	Pfeiffer & Harrington, 2011
NMB1271	Matjes River Cave	Forest	3570 ± 50	Sealy & Pfeiffer, 2000
NMB1273	Matjes River Cave	Forest	3050 ± 60	Pfeiffer & Harrington, 2011
NMB1275	Matjes River Cave	Forest	4850 ± 60	Sealy, 2006
NMB1640	Robberg Cave	Forest	4120 ± 60	Sealy & Pfeiffer, 2000
NMB1641	Robberg Cave	Forest	N/A	Pfeiffer & Harrington, 2011
NMB1642	Robberg Cave	Forest	N/A	Pfeiffer & Harrington, 2011
NMB1644	Robberg Cave	Forest	N/A	Pfeiffer & Harrington, 2011
NMB1704	Plettengerg Bay	Forest	760 ± 50	Sealy, 2006
NMBskeleton4	Matjes River Cave	Forest	N/A	Pfeiffer & Harrington, 2011
SAM1145	Robberg Cave	Forest	3210 ± 70	Sealy, 2006
SAM1871	Robberg Cave D	Forest	3310 ± 60	Sealy, 2006
SAM1878A	Robberg Cave E	Forest	2170 ± 20	Sealy, 2006
SAM1893	Robberg Cave	Forest	2360 ± 20	Sealy, 2006
SAM4207	Drury's Cave	Forest	N/A	Pfeiffer & Harrington, 2011
SAM4829	Tucker's Cave	Forest	N/A	Pfeiffer & Harrington, 2011
SAM5075	Cape Point, Rooikrans	Fynbos	2530 ± 60	Pfeiffer & Sealy, 2006
SAM6052	Byneskranskop 3	Fynbos	1780 ± 50	Pfeiffer & Harrington, 2011
SAM6053	Byneskranskop 1	Fynbos	N/A	Pfeiffer & Harrington, 2011
SAM6054A	Modder River Mouth	Fynbos	2780 ± 45	Pfeiffer & Harrington, 2011
SAM6054B	Modder River Mouth	Fynbos	2530 ± 60	Pfeiffer & Harrington, 2011
SAM6054C	Modder River Mouth	Fynbos	ca. 2600	Pfeiffer & Harrington, 2011
SAM6348A	Melkbosstrand	Fynbos	2490 ± 50	Pfeiffer & Harrington, 2011
UCT210	Oakhurst Rock Shelter	Forest	4995 ± 215	Pfeiffer & Harrington, 2011
UCT213	Oakhurst Rock Shelter	Forest	9120 ± 90	Pfeiffer & Harrington, 2011
UCT213.Gr16.2	Oakhurst Rock Shelter	Forest	N/A	Pfeiffer & Harrington, 2011
UCT216J	Oakhurst Rock Shelter	Forest	2065 ± 105	Pfeiffer & Harrington, 2011
UCT217E	Oakhurst Rock Shelter	Forest	N/A	Pfeiffer & Harrington, 2011
UCT247	Klein Brakrivier	Fynbos	510 ± 40	Pfeiffer & Harrington, 2011
UCT346	Nelson Bay Cave	Forest	2500-3000	Pfeiffer & Harrington, 2011
UCT437	Kasteelberg	Fynbos	1310 ± 50	Pfeiffer & Harrington, 2011

APPENDIX D: Point Hope Cultural Periods

Catalogue	Age Estimate (years)	Time Period	Source
PH088	15.5	N/A	N/A
PH092	14.5	Ipiutak	Cowgill, pers com
PH095	13.5	Ipiutak	Cowgill, pers com
PH102	Adult	Ipiutak	Copes, 2012
PH103	Adult	Ipiutak	Copes, 2012
PH163	Adult	Ipiutak	Copes, 2012
PH166	Adult	Ipiutak	Copes, 2012
PH200	Adult	Ipiutak	Copes, 2012
PH228	Adult	Tigara	Copes, 2012
PH232	Adult	Tigara	Copes, 2012
PH277	Adult	Tigara	Copes, 2012
PH304	16.5	Tigara	Copes, 2012
PH316	Adult	Tigara	Cowgill, pers com
PH336	Adult	Tigara	Copes, 2012
PH339	Adult	Tigara	Copes, 2012
PH342	10.5	Tigara	Cowgill, pers com
PH343	11.5	Tigara	Cowgill, pers com
PH344	9.5	Tigara	Cowgill, pers com
PH346	Adult	Tigara	Copes, 2012
PH349	Adult	Tigara	Cowgill, pers com
PH353	Adult	Tigara	Cowgill, pers com
PH354	12.5	Tigara	Cowgill, pers com
PH359	Adult	Tigara	Cowgill, pers com
PH360	5.5	Tigara	Cowgill, pers com
PH361	16.5	Tigara	Cowgill, pers com
PH371	Adult	Tigara	Copes, 2012
PH373	Adult	Tigara	Copes, 2012
PH376	14.22	Tigara	Cowgill, pers com
PH377	Adult	Tigara	Copes, 2012
PH378	Adult	Tigara	Copes, 2012
PH381	Adult	Tigara	Copes, 2012
PH385	6.5	Tigara	Cowgill, pers com
PH386	Adult	N/A	N/A
PH392	Adult	N/A	N/A
PH406	15.5	Tigara	Cowgill, pers com
PH419	11.5	Tigara	Cowgill, pers com

PH457	0	Tigara	Cowgill, pers com
PH459	Adult	Tigara	Copes, 2012
PH464	Adult	Tigara	Copes, 2012
PH481	Adult	Tigara	Copes, 2012
PH485	Adult	Tigara	Copes, 2012
PH489	Adult	Tigara	Copes, 2012
PH517	Adult	Tigara	Copes, 2012
PH526	Adult	Tigara	Copes, 2012
PH546	Adult	Tigara	Copes, 2012

APPENDIX E: R Code for Sliding Semilandmarks, GPA, and PCA

```
# Slide semilandmarks on ilia, do Procrustes superimposition, run
PCA.

library(Morpho)
library(rgl)

MODEL_DIR <- "~/Documents/Thesis Data Collection/3D Models - All
Juvenile Ilia/"
LANDMARK_DIR <- "~/Documents/Thesis Data Collection/Landmarks -
All Juvenile Ilia/"

# import data    ================================

# get all data files
landmarkFileList <- list.files(path = LANDMARK_DIR);
modelFileList <- list.files(path = MODEL_DIR)

# get model ID
modelId <- lapply(landmarkFileList, substr, 1, 6)

# match landmark with model
getModelFile <- function(mId) {
  tmp <- grepl(mId, modelFileList, fixed=TRUE)
  return(modelFileList[tmp])
}

modelFiles <- lapply(modelId, getModelFile)

# remove model file extension
modelFiles = gsub(".ply", "", modelFiles)

# get full path to landmark files
landmarkPaths <- paste0(LANDMARK_DIR, landmarkFileList)

# import
lmData <- lapply(landmarkPaths, read.table, header=FALSE,
sep=",", skip=1)

# parse files   ================================
# extract only xyz columns
extractColumns <- function(x) {
  lmItem <- lmData[[x]]
  tmp <- as.matrix(lmItem[,4:6])
  return(tmp)
}
```

```
lmData <- lapply(1:length(lmData), extractColumns)

# convert to 3d array [npoints, ndimensions, nsamples]
arrayDim <- dim(lmData[[1]])
arrayDim <- c(arrayDim, length(lmData))

lmData = array(unlist(lmData), dim = arrayDim)
lmData <- lmData * 10;

# set dimnames to model files (used in Morpho slider3d fn)
dimnames(lmData)[[3]]<-modelFiles;

# slide stuff   ================================
fix <- c(1:11)
slider_indices <- list(
  #iliac crest (medial)
  c(1, 12:51, 2),
  #iliac crest (lateral) to iliac tubercle
  c(2, 52:58, 3),
  #rest of iliac crest (lateral)
  c(3, 59:95, 1),
  #greater sciatic notch
  c(11, 96:111, 5))

checkLM(lmData, path = MODEL_DIR)

slide <- slider3d(lmData, SMvector = fix, deselect = TRUE,
outlines = slider_indices, surp = NULL,
          sur.path = MODEL_DIR, iterations = 10, fullGPA = TRUE,
bending = TRUE, stepsize = 1, fixRepro = TRUE, mc.cores = 1)

toView <- 14
deformGrid3d(slide$dataslide[,,toView], lmData[,,toView], ngrid
=0)
spheres3d(slide$dataslide[fix,,toView],col=4,radius=1)

# Procrustes analysis of slid data
Proc <- procSym(slide$dataslide)

# Plot PCA results from procSym
pcaplot3d(Proc, pcshow = c(1:5))

# Variance explained
variance <- Proc$Variance
```

APPENDIX F: Equations for Age Estimation (Sadlermiut Sample)

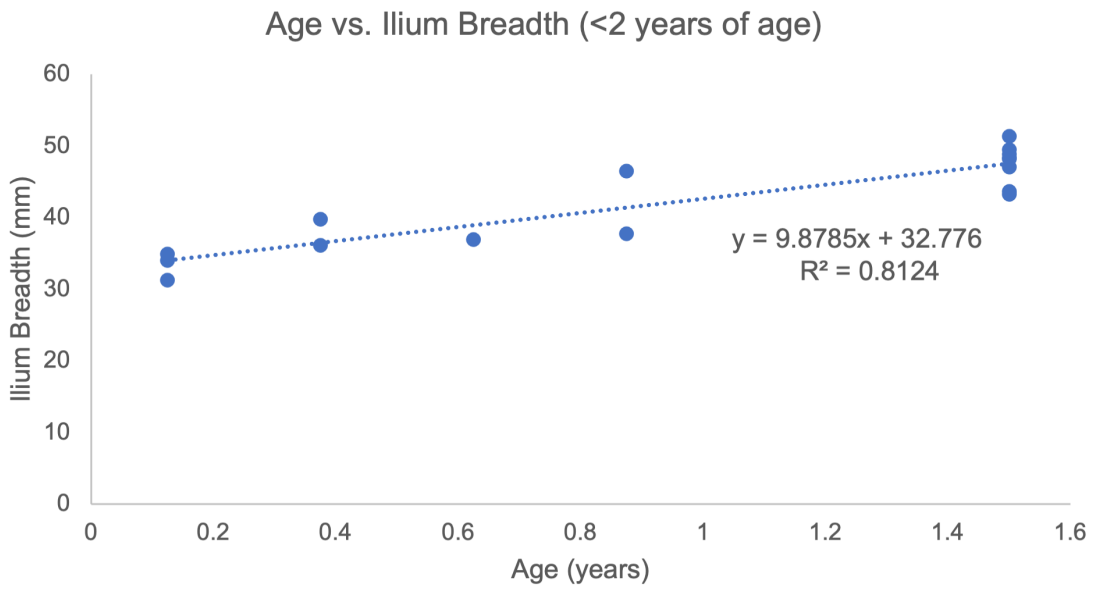

Inverse equation: $\text{Age} = \frac{\text{ilium breadth} - 32.776}{9.8785}$

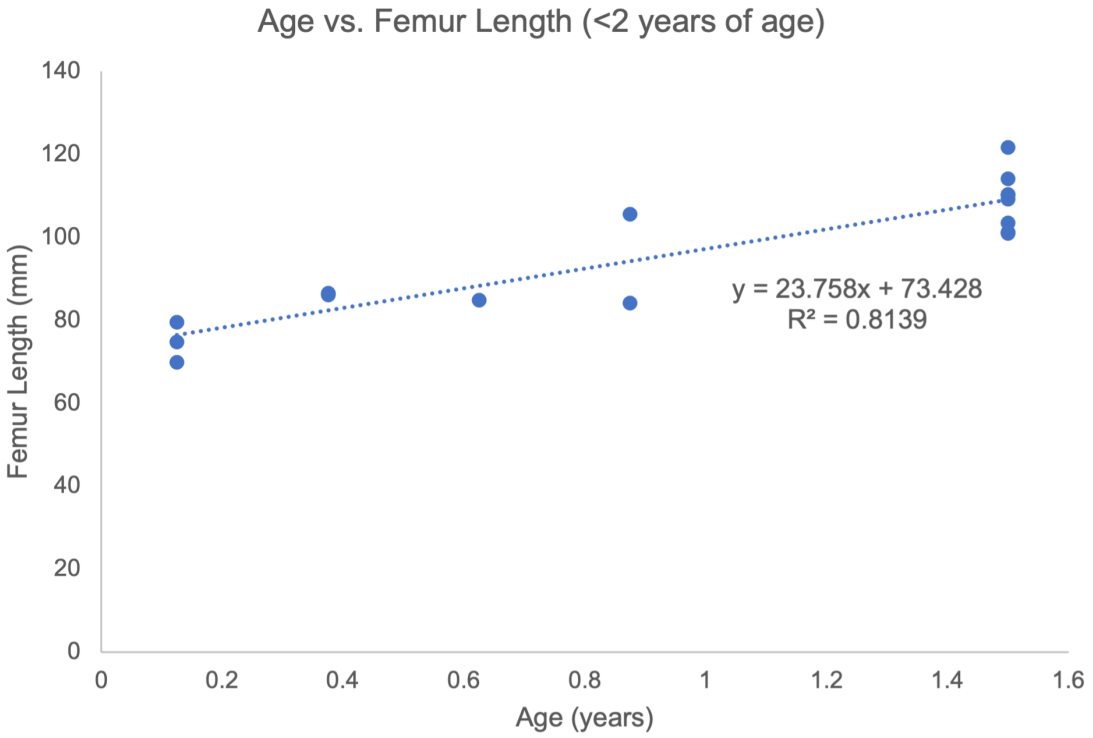

Inverse equation: $\text{Age} = \frac{\text{femur length} - 73.428}{23.758}$

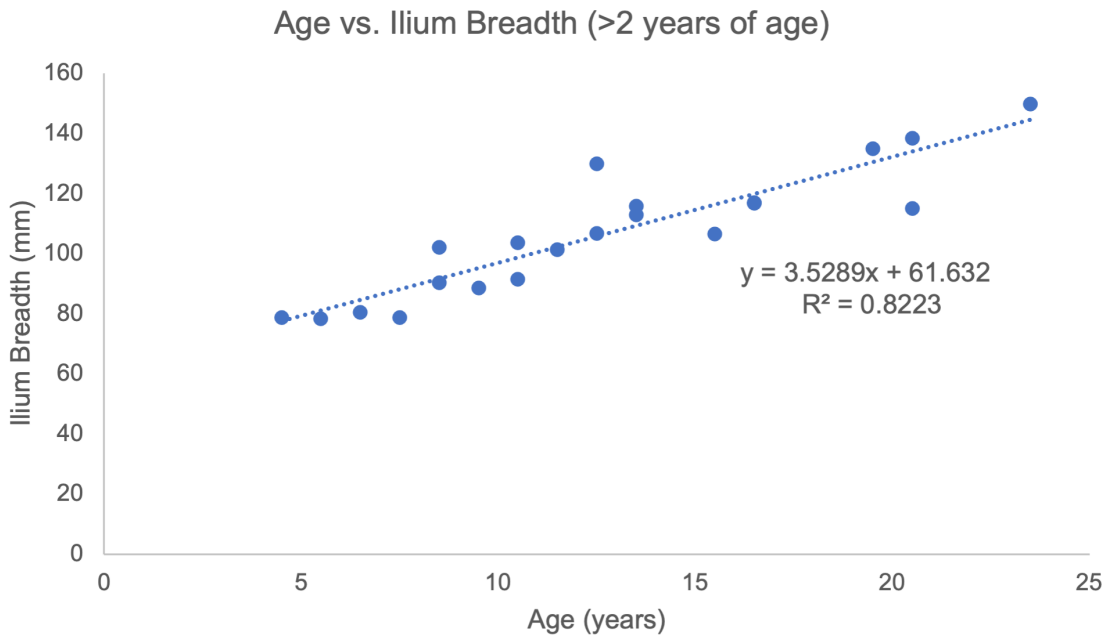

Inverse equation: $\text{Age} = \frac{\text{ilium breadth} - 61.632}{3.5289}$

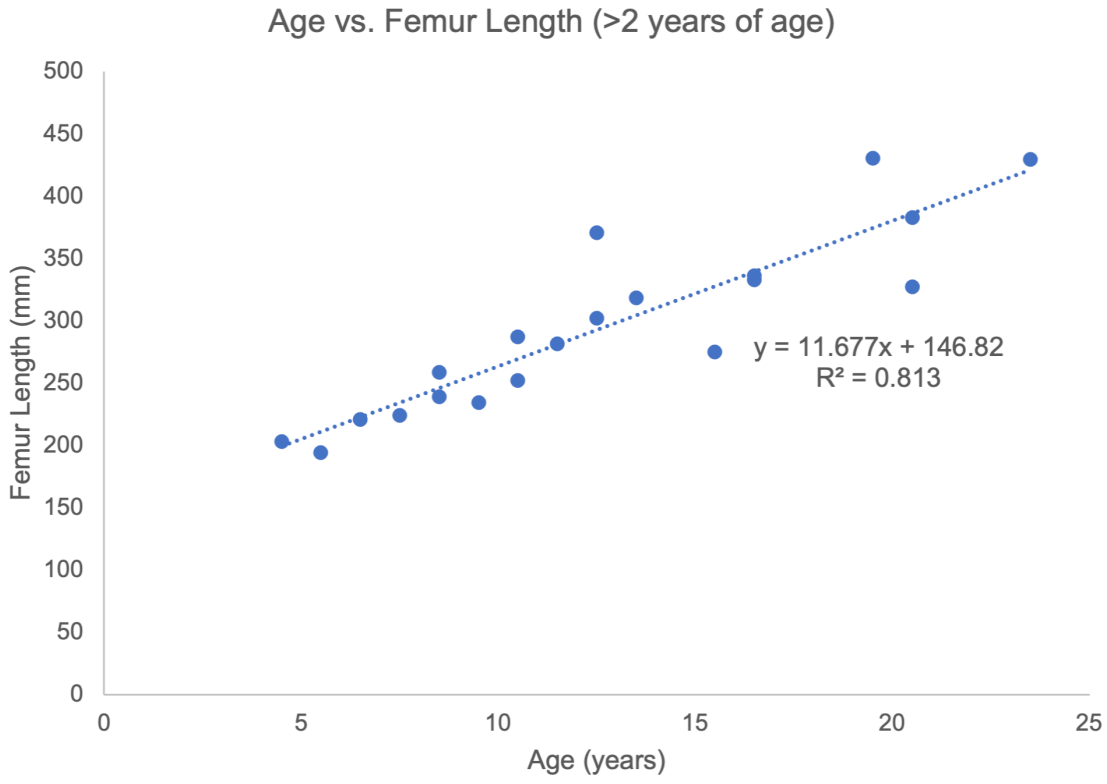

Inverse equation: $\text{Age} = \frac{\text{femur length} - 146.82}{11.677}$

APPENDIX G: R Code for Maturity Trajectories

```
# Maturity Trajectories - Indian Knoll Ilia

# import library files ----------------------------------------
library("geomorph")
library("ggplot2")
library("shapes")
library("RColorBrewer")

# define constants --------------------------------------------
# data files
DATA_DIRECTORY <- "."
JUVENILE_DATA_FILE <- "IKJuveniles.csv"
ADULT_DATA_FILE <- "IKAdults.csv"

# functional constants
NUM_METADATA_COLUMNS <- 2
AGE_COLUMN_INDEX <- 2

# import data -------------------------------------------------
# imports csv files into data frames
#   header = TRUE
#       means the first row of the csv contains the name of those
variables
#   row.names = 1
#       means column 1 contains the name of the observations
(individuals)
#
#   data can be selected as
#       juvenileDataRaw['IK724',]           gives one row of data
#       juvenileDataRaw['Population']       gives one column
#
# note(s) on data format
#   first 3 columns are metadata (catalogue, population, age)

juvenileDataRaw <- read.csv(
    file.path(DATA_DIRECTORY, JUVENILE_DATA_FILE),
    header = TRUE,
    row.names = 1
)
adultDataRaw <- read.csv(
    file.path(DATA_DIRECTORY, ADULT_DATA_FILE),
    header = TRUE,
    row.names = 1
)
```

```
# ============================================================
# ANALYSIS

# ================================================
# A.1   DEFINE HELPER FUNCTIONS
# ================================================

# processRawData
# import the spreadsheet data, convert the landmark data into a
3D array
processRawData <- function(
        rawData,
        nMetadataColumns,
        nDimensions = 3
) {
    # set up processing variables
    dataSize <- dim(rawData)
    dataStart <- nMetadataColumns + 1
    dataRange <- c(dataStart:dataSize[2])
    nIndividuals <- dataSize[1]

    # check data length makes sense
    nDataPoints <- length(dataRange)

    if (mod(nDataPoints, nDimensions) != 0) {
        stop('Calculated data points doesn\'t divide evenly by
number of dimensions.')
    }
    nLandmarks <- nDataPoints / nDimensions

    # store coordinates in a 3D array for geomorph (p x k x n)
    #   p = number of landmarks
    #   k = number of dimensions (2 or 3)
    #   n = number of individuals / specimens
    geomorphCoords <- arrayspecs(
        rawData[,dataRange],
        nLandmarks,
        nDimensions
    )

    individualNames = rownames(rawData)
    variableNames = colnames(rawData)

    output <- list()
    output$coords <- geomorphCoords;
    output$metadata <- rawData[,c(1:nMetadataColumns)]
    output$nIndividuals <- nIndividuals
    output$nLandmarks <- nLandmarks
```

```
    output$age <- as.vector(rawData[,AGE_COLUMN_INDEX])
    output$names <- rownames(rawData)

    return(output)
}

# runGpa
# runs the geomorph GPA on an input set of coordinates
# landmarkCoords = array
runGpa <- function(landmarkCoords) {
    # check coordinates are in the correct format for geomorph
    dataSize <- dim(landmarkCoords)
    if (length(dataSize) != 3) {
        stop('Landmark coords should be an array with 3
dimensions')
    }

    gpaResults <- gpagen(
        landmarkCoords,
        PrinAxes = TRUE,
        max.iter = NULL,
        ProcD = TRUE,
        Proj = TRUE,
        print.progress = TRUE
    )

    output <- list()

    output$gpaCoords <- gpaResults$coords
    output$centroidSize <- gpaResults$Csize
    output$meanShape <- gpaResults$consensus
    output$nIndividuals <- dim(landmarkCoords)[3]

    return(output)
}

getGeomorphCoordsForIndividuals <- function(processedData,
individualIds) {
    # assume processedData = the output of processDataRaw()

    return(processedData$coords[,,individualIds])
}

# create a dataset from a list of individuals given the ids that
go into the set
analyzeIndividuals <- function(dataset, idsToAnalyze = NULL) {

    # if no ids are used, assume the full dataset should be used
```

```
    if (is.null(idsToAnalyze)) {
        idsToAnalyze <- c(1:dataset$nIndividuals)
    }

    # get coordinates (rearranged for geomorph) for each
individual
    gpaCoords <- getGeomorphCoordsForIndividuals(dataset,
idsToAnalyze)

    # run GPA
    output <- runGpa(gpaCoords)

    # attach extra variable(s)
    output$age <- dataset$age[idsToAnalyze]
    output$meanAge <- mean(output$age)
    output$names <- dataset$names[idsToAnalyze]
    output$meanCentroidSize <- mean(output$centroidSize)

    return (output)
}

# ================================================
# A.2     INITIAL CALCULATIONS
# ================================================
# JUVENILE

# strip metadata and convert to 3D array [landmarks x dimension x
specimen]
juvenileData <- processRawData(juvenileDataRaw,
NUM_METADATA_COLUMNS)

# calculations for youngest 5 group
juvenileStartingPoint <- analyzeIndividuals(juvenileData, 1:5)

# calculations for the whole group
juvenileResults <- analyzeIndividuals(juvenileData)

# ADULT
adultData <- processRawData(adultDataRaw, NUM_METADATA_COLUMNS)
adultResults <- analyzeIndividuals(adultData)

# ================================================
# A.3     SHAPE MATURATION ANALYSIS
# ================================================

# calcProcrustesForGroup
# Calculates the Procrustes Distance (PD) for a group of
individididuals. The
```

```
# start + end shapes are required to get PD for the first and
last individuals.
#
# dataset = the output of runGpa()
#
# results will be dataset$procDist
# procDist[1] = procrustes distance from startingShape ->
individual 1
# procDist[2] = PD from individual 1 -> 2
#
# if you have 41 individuals then the last one
# procDist[41] = PD individual 40 -> 41
# procDist[42] = PD individual 41 -> endShape
calcProcrustesForGroup <- function(dataset, startingShape,
endShape) {

    # clear previous, if it exists
    nPoints <- dataset$nIndividuals
    dataset$procDist <- vector('numeric', nPoints + 1)

    dataset$procDist[1] <- procdist(
        startingShape,
        dataset$gpaCoords[,,1]
    )

    for (i in 2:(nPoints - 1)) {
        dataset$procDist[i] <- procdist(
            dataset$gpaCoords[,,i],
            dataset$gpaCoords[,,(i+1)]
        )
    }

    dataset$procDist[nPoints + 1] <- procdist(
        dataset$gpaCoords[,,nPoints],
        endShape
    )

    return(dataset)
}

# procrustes distance calculated for each individual to the next
# first individual uses the group of five youngest as a reference
# last individual is compared to mean juvenile shape
# additional value compares oldest juvenile with mean adult

# calculate juveniles
# inputs =
#   dataset (procrustes calculation will be added to it)
```

```
#   startingShape (to compare to individual 1)
#   endingShape (to compare to the last individual)
juvenileResults <- calcProcrustesForGroup(
    juvenileResults,
    juvenileStartingPoint$meanShape,
    adultResults$meanShape
)

# ================================================
# A.3.2     cumulative procrustes distance
# ================================================

# calculated as the sum of all proc dists up to the current
calcTotalProcDist <- function (dataset) {

    # get number of points to calculate
    nPoints <- length(dataset$procDist)
    dataset$totalProcDist <- vector('numeric', nPoints)

    # calculate for total[1] = PD[1]
    dataset$totalProcDist[1] <- dataset$procDist[1]

    # all other totals = partial sums
    for (i in 2:nPoints) {
        dataset$totalProcDist[i] <- dataset$totalProcDist[i-1] +
dataset$procDist[i]
    }

    return (dataset)
}

juvenileResults <- calcTotalProcDist(juvenileResults)

# cumulative distance is the last in the chain + PD (last ->
average adult)
# tail(<x>, 1) gets the last 1 element from a vector
cumulativeDistance <- tail(juvenileResults$totalProcDist, 1)

# ================================================
# A.3.3     groups
# ================================================

checkGroupParams <- function(dataLength, maxGroupSize = NULL,
maxOverlap = NULL) {

    if (length(maxGroupSize) == 2) {
        groupSizes <- c(maxGroupSize[1]:maxGroupSize[2])
    } else {
```

```
        groupSizes <- c(1:maxGroupSize)
    }

    if (length(maxOverlap) == 2) {
        overlaps <- c(maxOverlap[1]:maxOverlap[2])
    } else {
        overlaps <- c(1:maxOverlap)
    }

    validGroups <- NULL
    validOverlaps <- NULL

    for (i in 1:length(groupSizes)) {
        for (j in 1:length(overlaps)) {
            gs <- groupSizes[i]
            ol <- overlaps[j]

            if (ol >= gs) {
                next
            }

            if (mod((dataLength - gs), (gs - ol)) == 0) {
                validGroups <- append(validGroups, gs)
                validOverlaps <- append(validOverlaps, ol)
            }
        }
    }

    validCombos <- data.frame(
        validGroups,
        validOverlaps
    )

    return (validCombos)
}

calculateGroupAverages <- function(data, groupIndices) {

    output <- list();

    # calculate any group summary statistics here
    output$meanAge <- mean(data$age[groupIndices])
    output$meanTotalPd <- mean(data$totalProcDist[groupIndices])

    # add group data
    output$names <- data$names[groupIndices]

    return (output)
```

```
}

# groupData: calculate a moving average for a given dataset
#
# data      list    input data
# groupSize int     width of window
# overlap   int     overlap of windows

groupData <- function (data, groupSize, overlap) {
    nItems <- data$nIndividuals

    # get increment from params
    groupInc <- groupSize - overlap

    #groupStarts <- seq.int(1, nItems - groupSize + 1,
by=groupInc)
    groupStarts <- seq.int(1, nItems - groupInc, by=groupInc)
    nGroups <- length(groupStarts)

    # check numbers are valid
    # (total samples - group size) / (groupSize - overlap) must
have no remainder
    if (mod((nItems - groupSize), groupInc) != 0) {
        print(
            paste(
                'Warning: group params dont match sample size.
Last group will have size = ',
                (nItems - tail(groupStarts,1) + 1)
            )
        )
      #stop('Inputs invalid: group size/overlap don\'t fit into
sample size evenly')
    }

    # returned data
    groupSamples <- vector("character", nGroups)
    meanAge <- vector("numeric", nGroups)
    meanSize <- vector("numeric", nGroups)
    meanTotalPd <- vector("numeric", nGroups)

    for (i in 1:nGroups) {
        # calculate group indices for the i-th group
        groupEnd <- groupStarts[i] + groupSize - 1
        groupEnd = min(groupEnd, nItems)
        groupIndices <- c(groupStarts[i]:groupEnd)

        # store per-group calculations
```

```
        groupSamples[i] <- paste(data$names[groupIndices],
collapse = ", ")
        meanAge[i] <- mean(data$age[groupIndices])
        meanSize[i] <- mean(data$centroidSize[groupIndices])
        meanTotalPd[i] <- mean(data$totalProcDist[groupIndices])
    }

    # return data as a data frame
    output <- data.frame(
        groupSamples,
        meanAge,
        meanSize,
        meanTotalPd
    )

    return (output)
}

# group by size 5, windows 1
IKjuvenileGroups <- groupData(juvenileResults, 5, 3)

# ================================================
# trajectory time!
# ================================================

linearScale <- function(data, y0 = 0, yMax = NULL) {

    # if no max is specified, assume it's the max data value
(data scaled to 1)
    if (is.null(yMax)) {
        yMax = max(data)
    }

    yRange <- (yMax - y0)


    # shift to zero
    newData <- data - y0

    # scale to max
    newData <- newData / yRange
}

# get age + both scaled trajectories in %
IKAge <- IKjuvenileGroups$meanAge
IKSize <- linearScale(
    IKjuvenileGroups$meanSize,
    min(IKjuvenileGroups$meanSize),
```

```
    adultResults$meanCentroidSize
) * 100
IKShape <- linearScale(
    IKjuvenileGroups$meanTotalPd,
    0,
    cumulativeDistance
) * 100
```

APPENDIX H: Additional PCA Plots

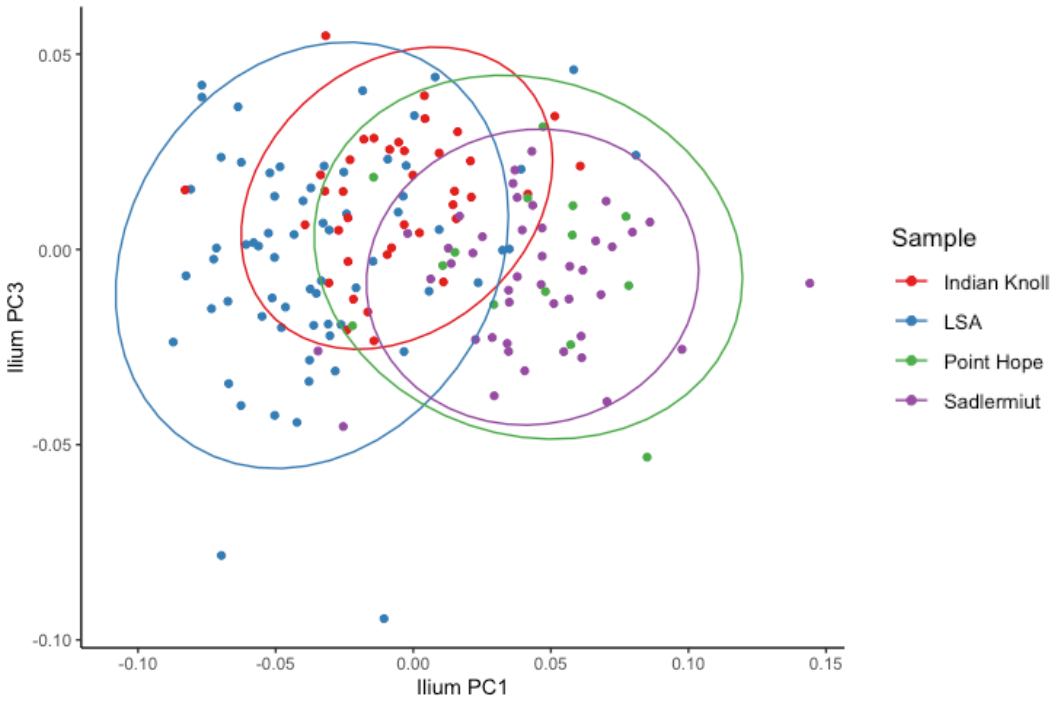

Figure H.1 PC3 of the combined-sample ilium data plotted on PC1.

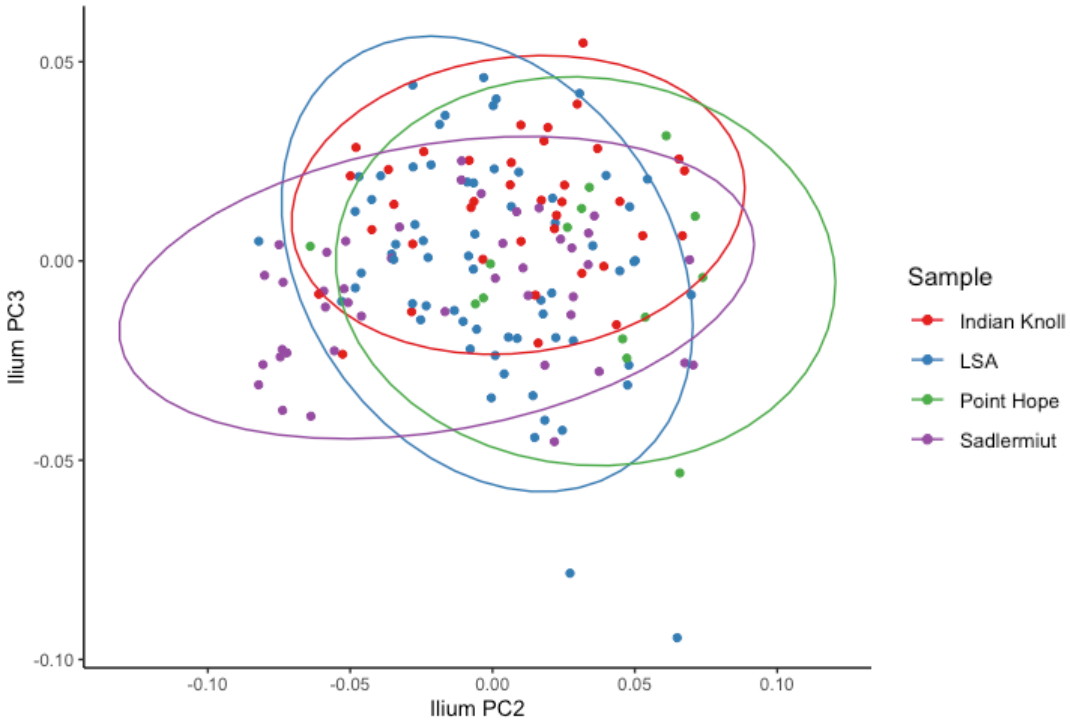

Figure H.2 PC3 of the combined-sample ilium data plotted on PC2.

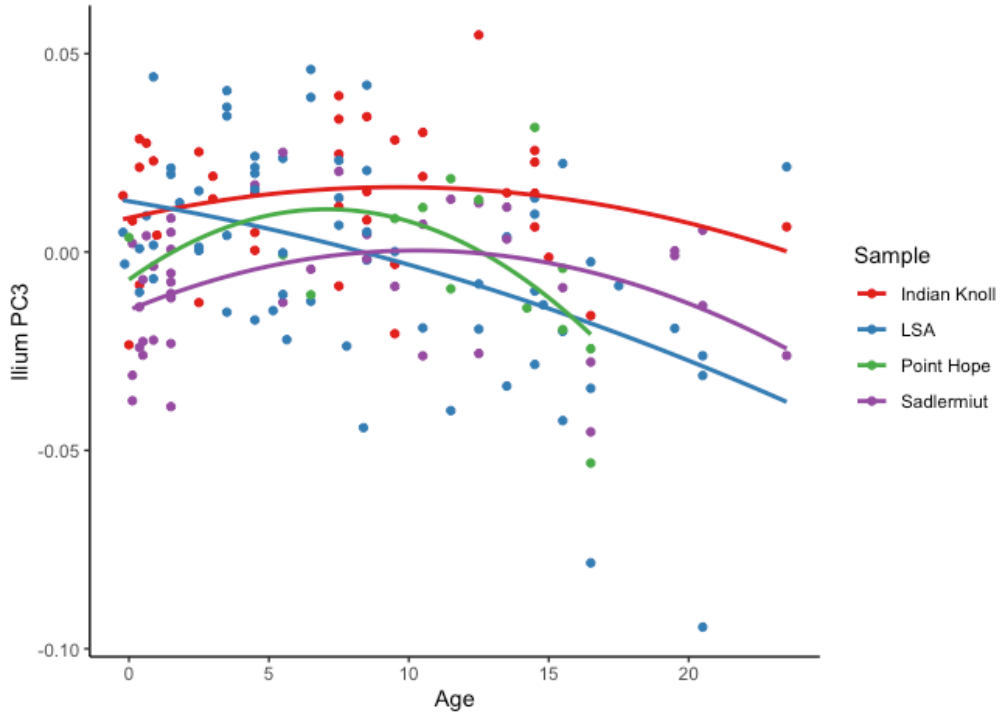

Figure H.3 Age vs. ilium PC3, fitted with quadratic regression lines.

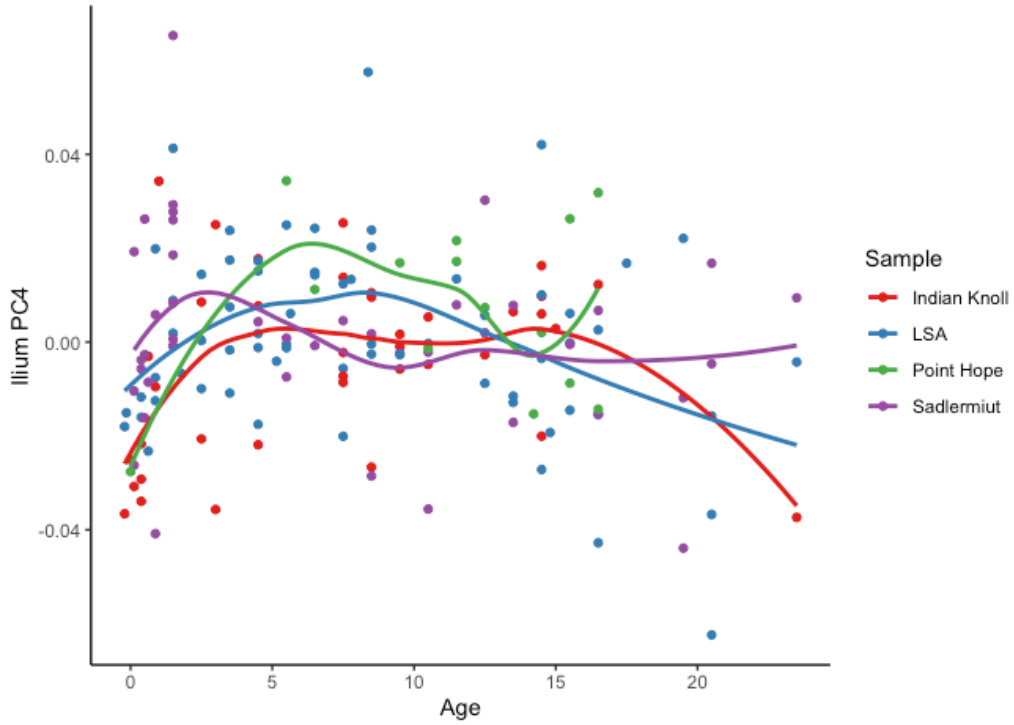

Figure H.4 Age vs. ilium PC4, fitted with LOESS curves.

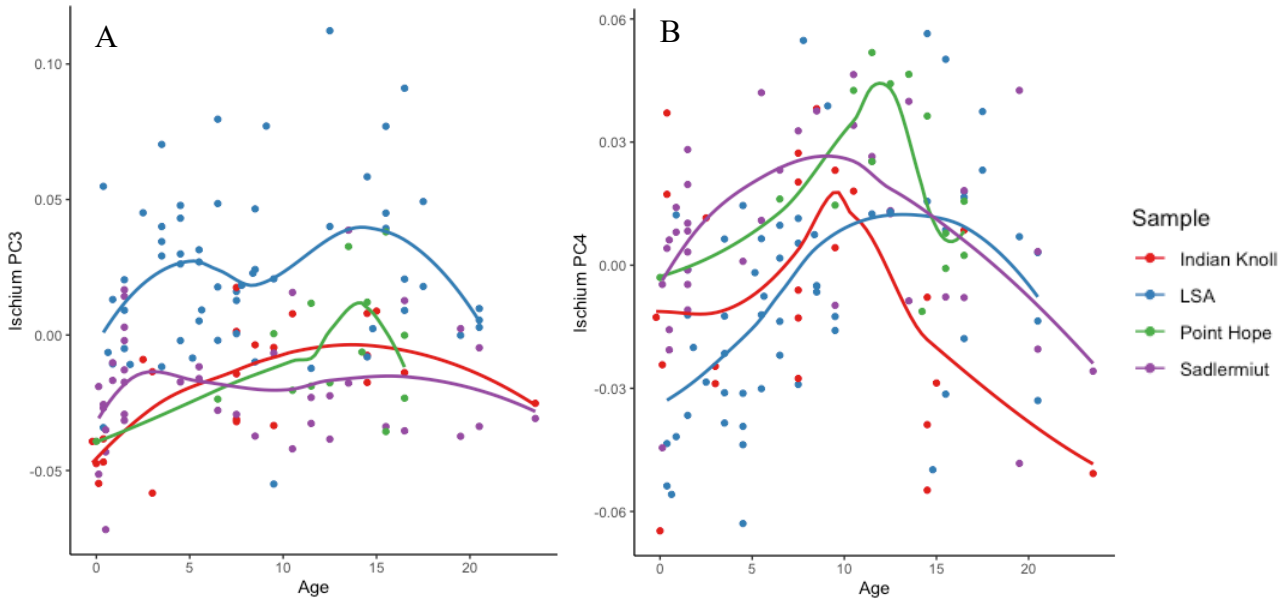

Figure H.5 Age vs. A) ischium PC3, and B) ischium PC4, fit with LOESS curves.

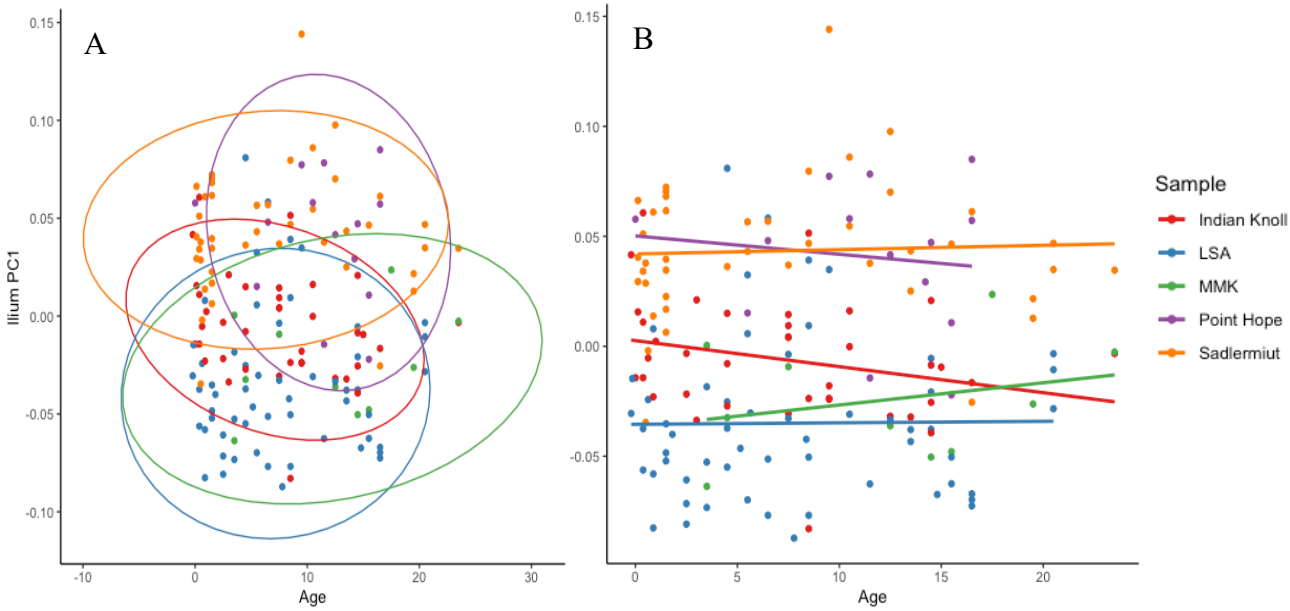

Figure H.6 Combined-sample ilium PC1 plotted on age, shown with A) 95% confidence ellipses, and B) lines of best fit, with the MMK group (green dots and line) separated out from the rest of the LSA sample.

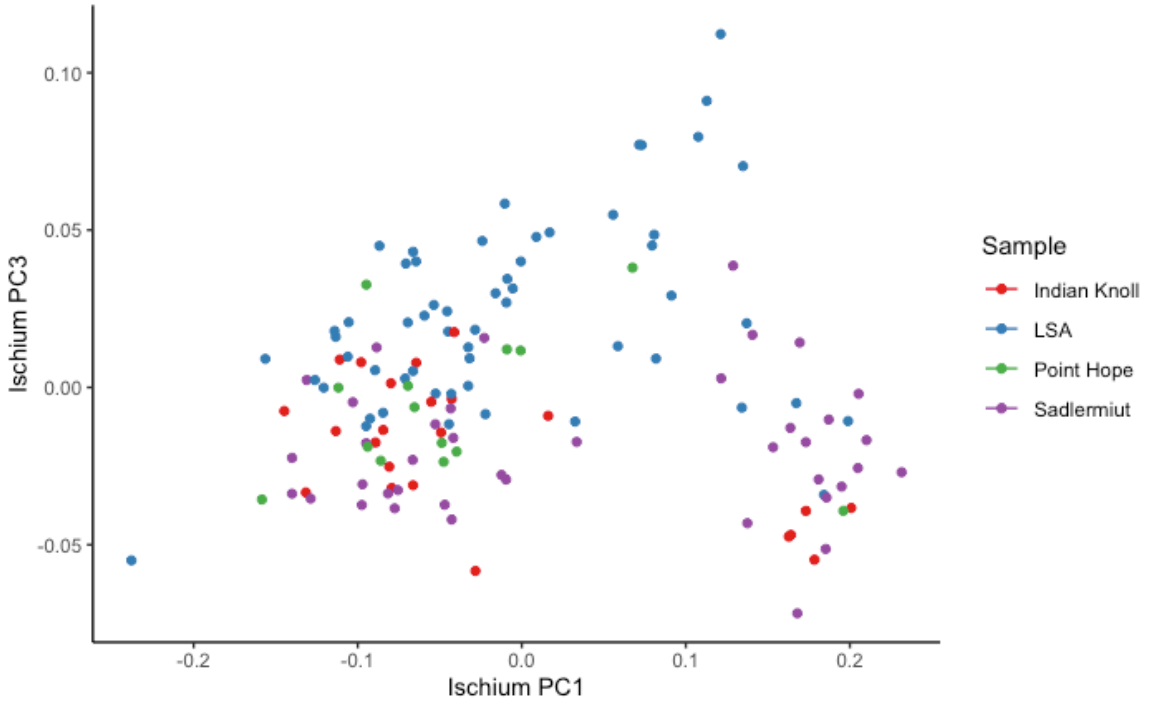

Figure H.7 PC3 of the combined-sample ischium data plotted on PC1.

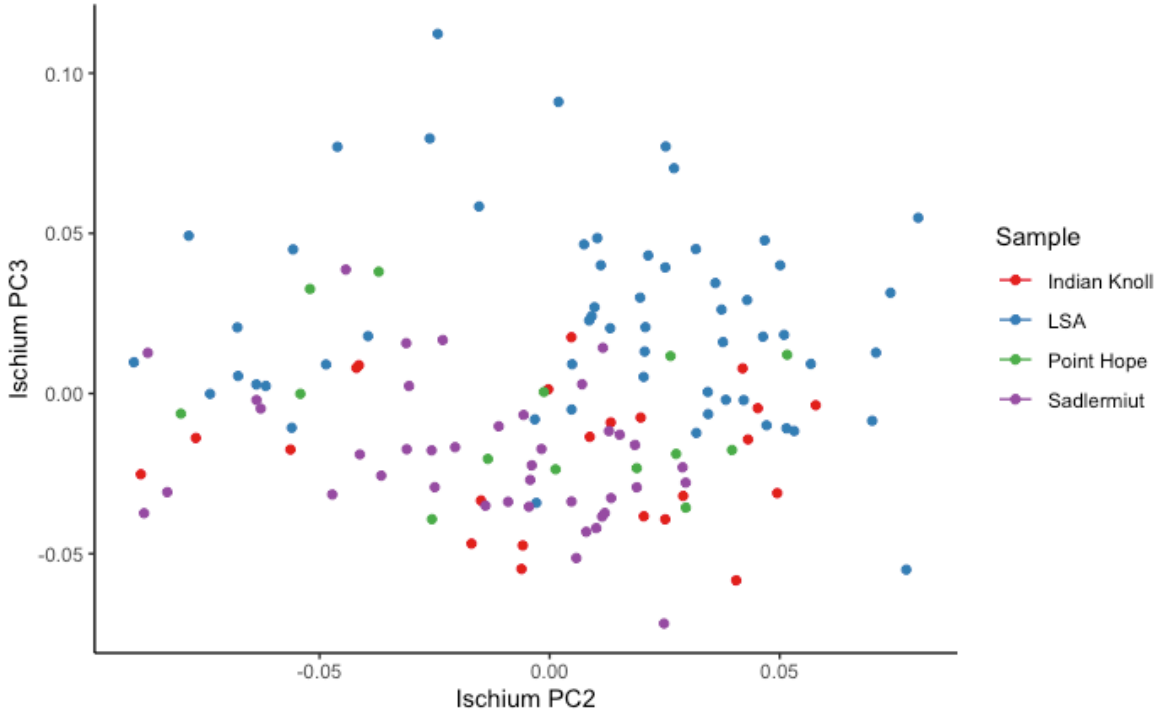

Figure H.8 PC3 of the combined-sample ischium data plotted on PC2.

APPENDIX I: Scale-Location Plots and Post-Hoc ANOVA Results

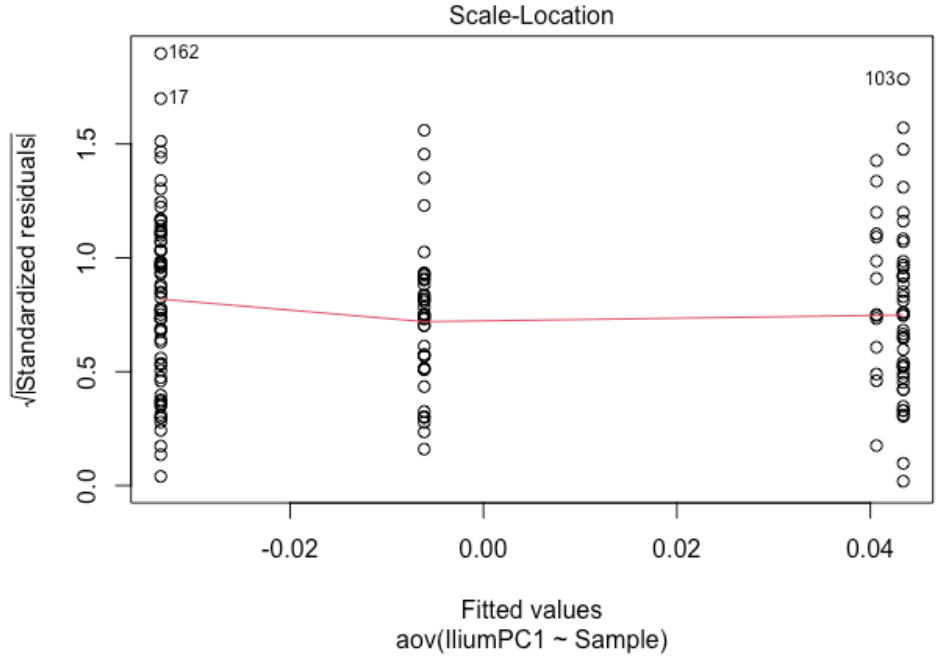

Figure I.1 Scale-location plot of the ilium PC1 data, showing that homogeneity of variances can be assumed.

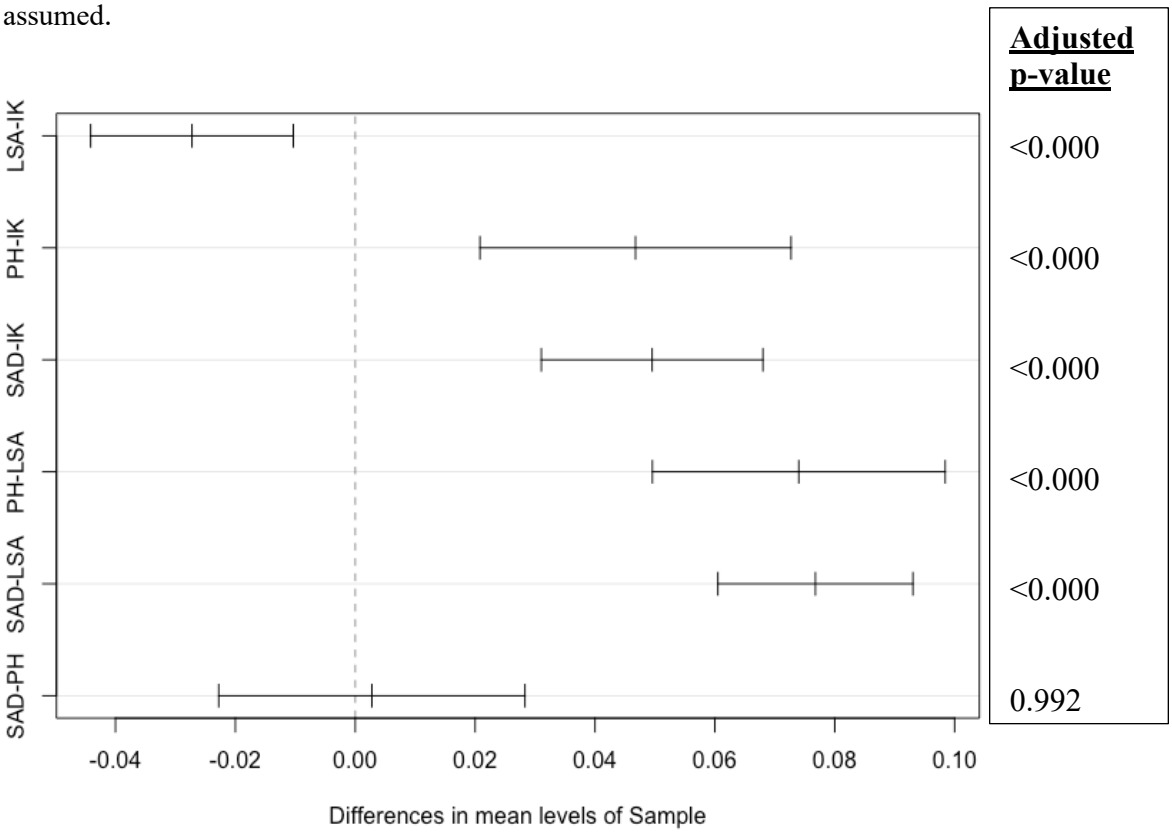

Figure I.2 Results of the ilium PC1 Tukey HSD test, showing the 95% family-wise confidence level with "sample" as the grouping factor.

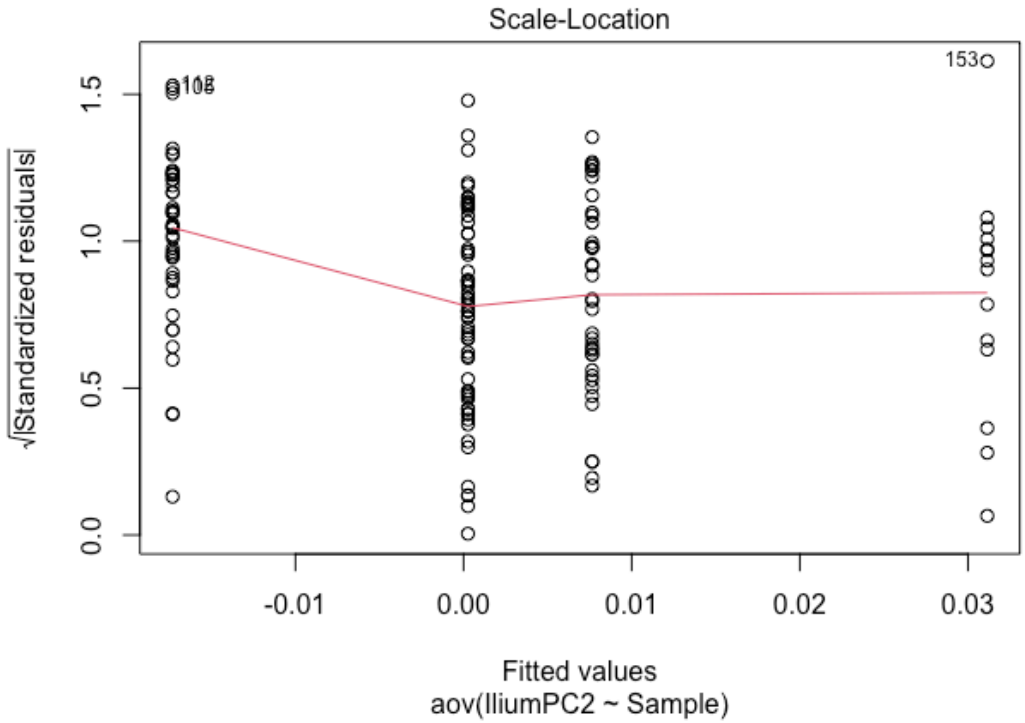

Figure I.3 Scale-location plot of the ilium PC2 data showing that homogeneity of variances cannot be assumed.

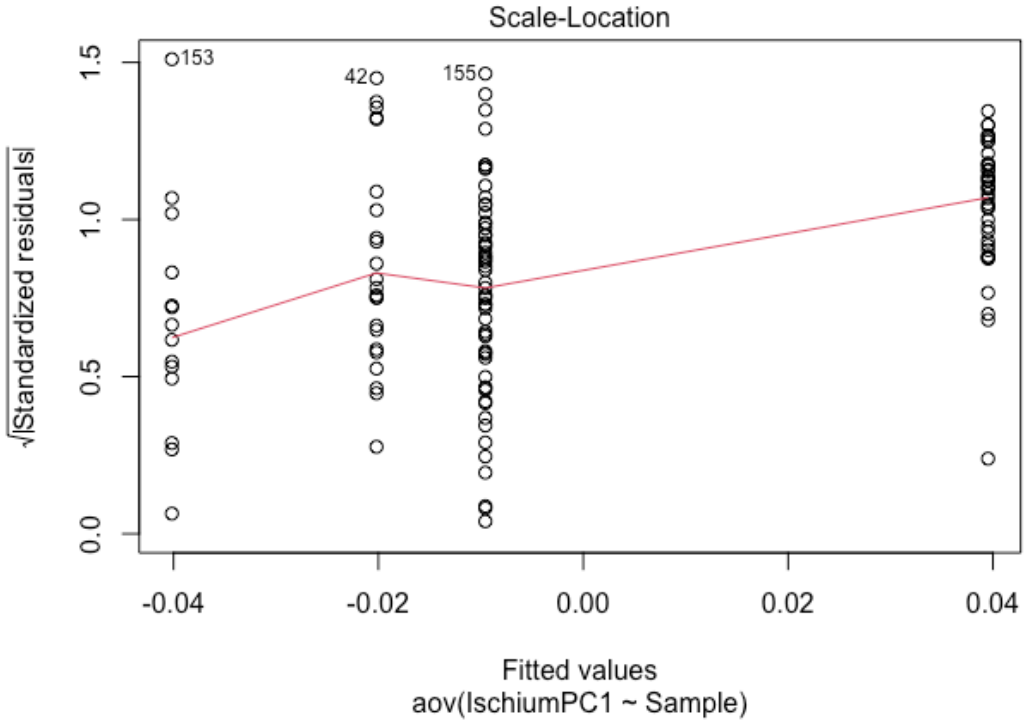

Figure I.4 Scale-location plot of the ischium PC1 data showing that homogeneity of variances cannot be assumed.

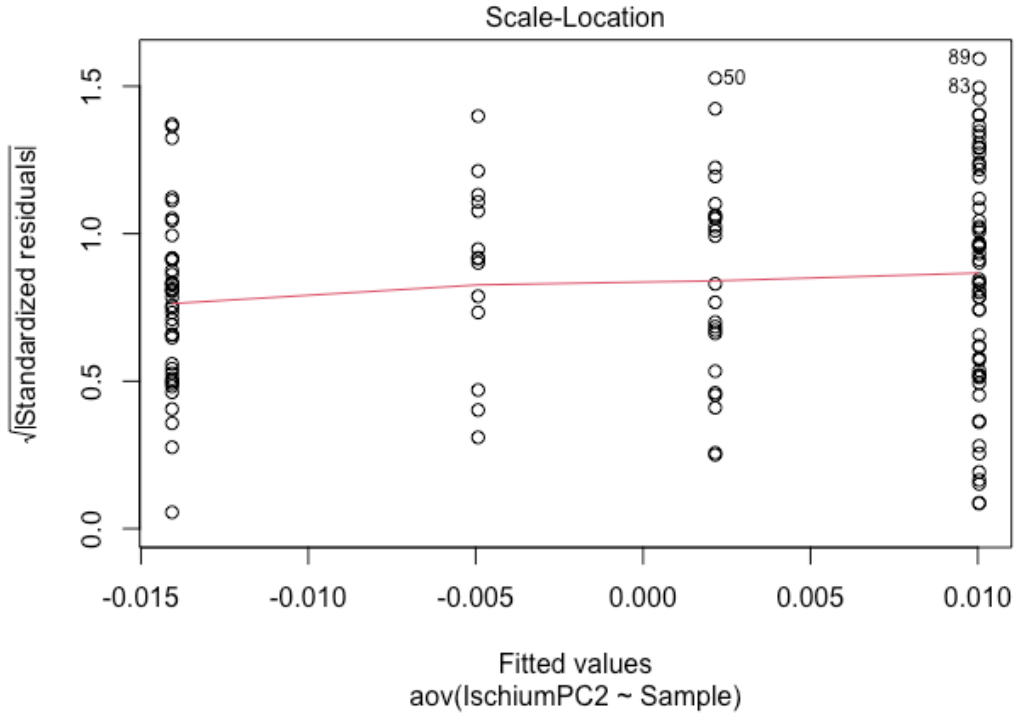

Figure I.5 Scale-location plot of the ischium PC2 data showing that homogeneity of variances can be assumed.

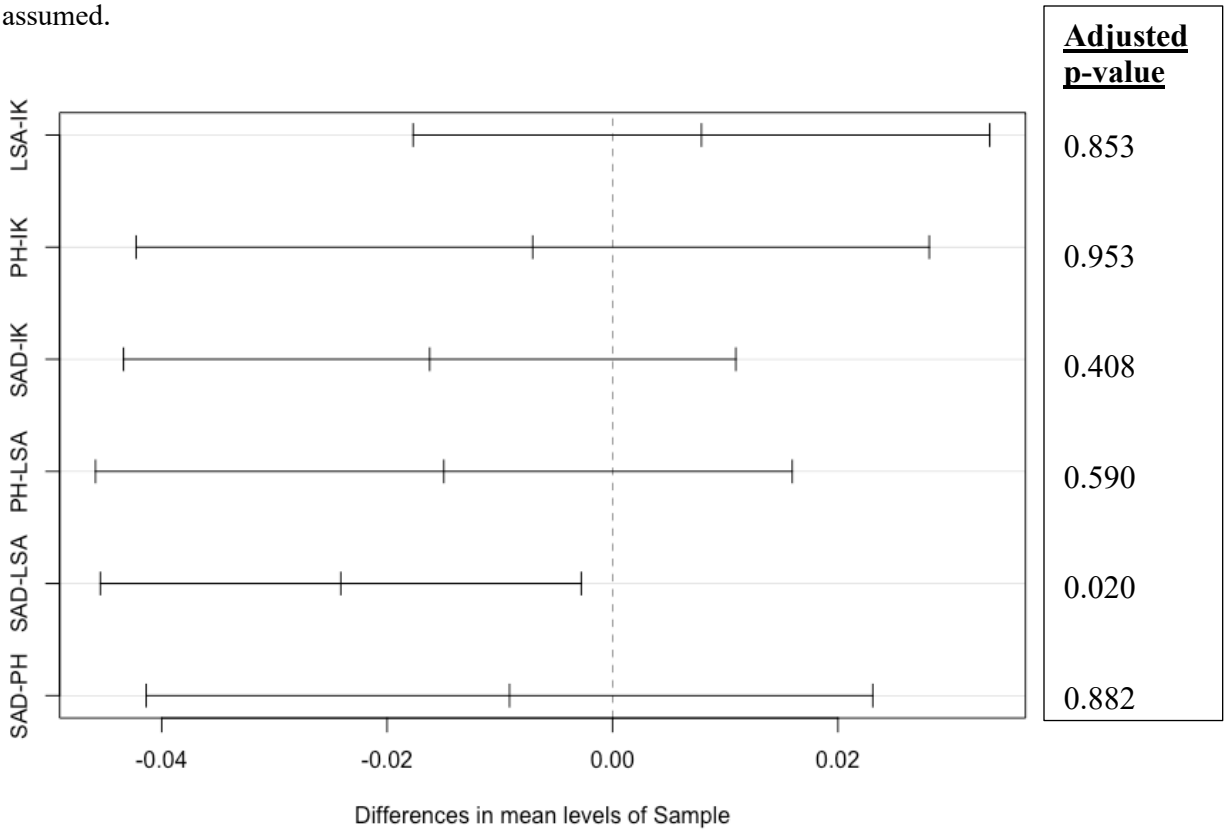

Figure I.6 Results of the ischium PC2 Tukey HSD test, showing the 95% family-wise confidence level with "sample" as the grouping factor.

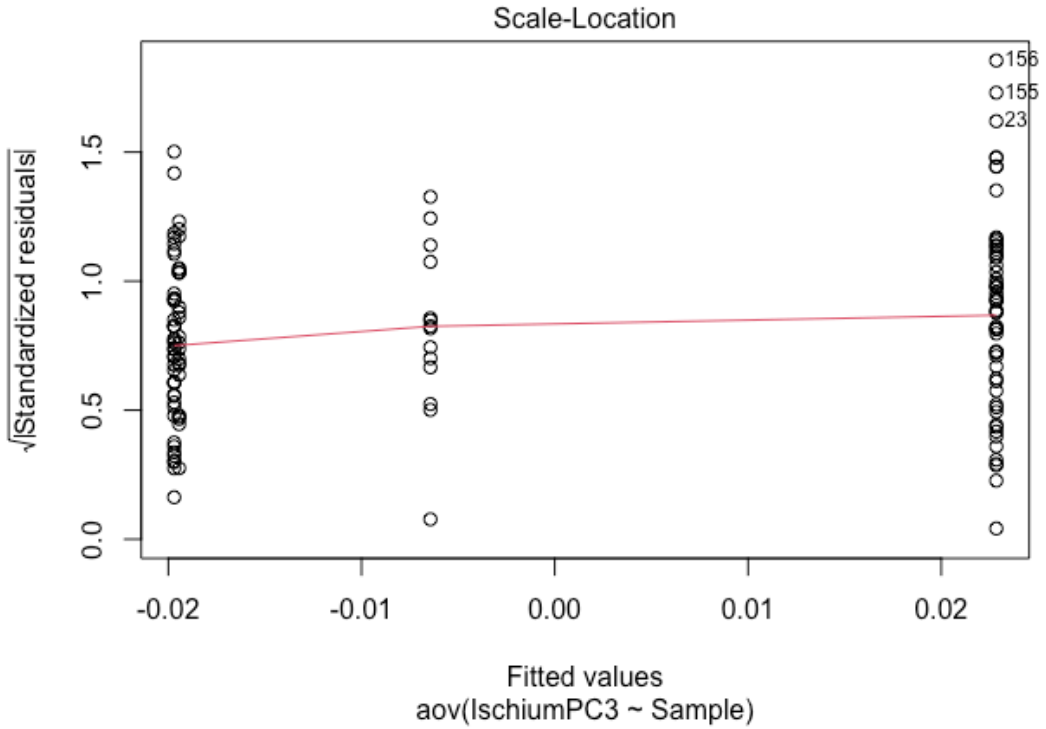

Figure I.7 Scale-location plot of the ischium PC3 data showing that homogeneity of variances can be assumed.

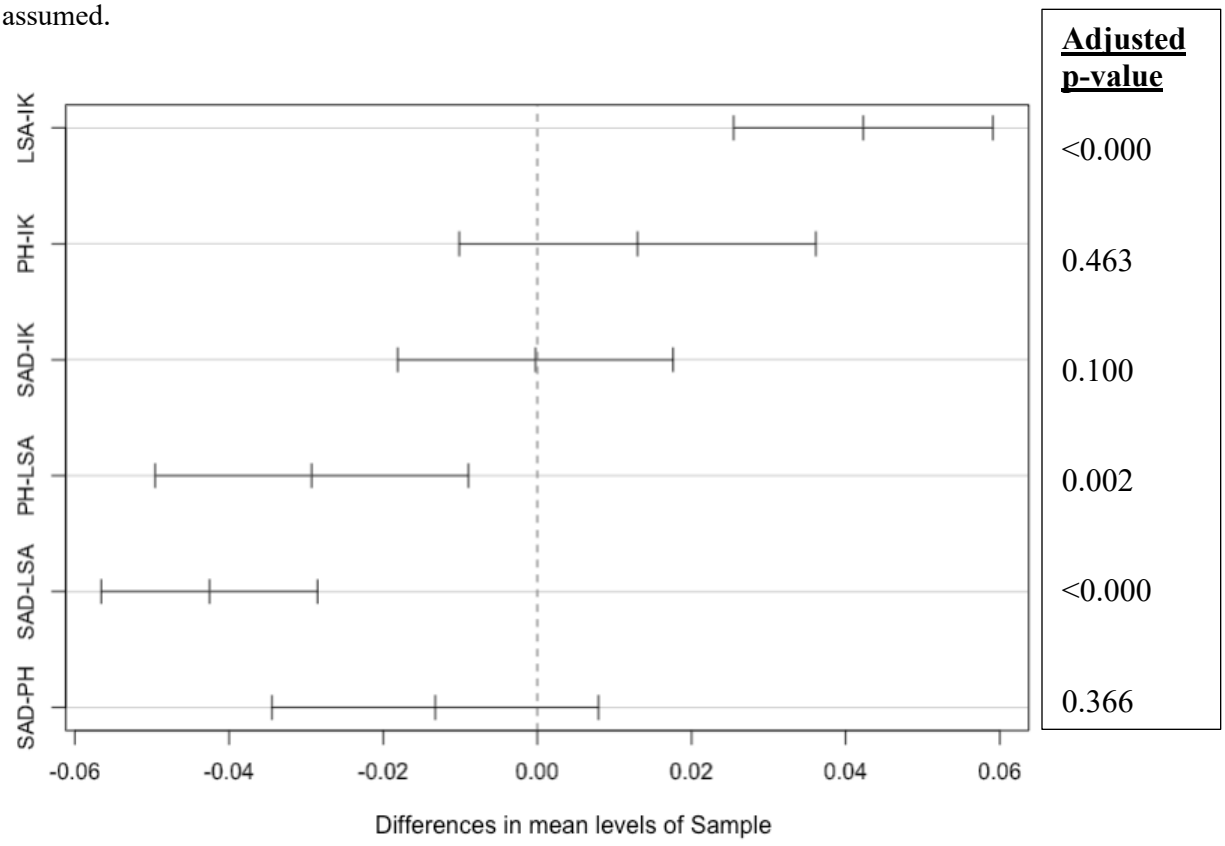

Figure I.8 Results of the ischium PC3 Tukey HSD test, showing the 95% family-wise confidence level with "sample" as the grouping factor.

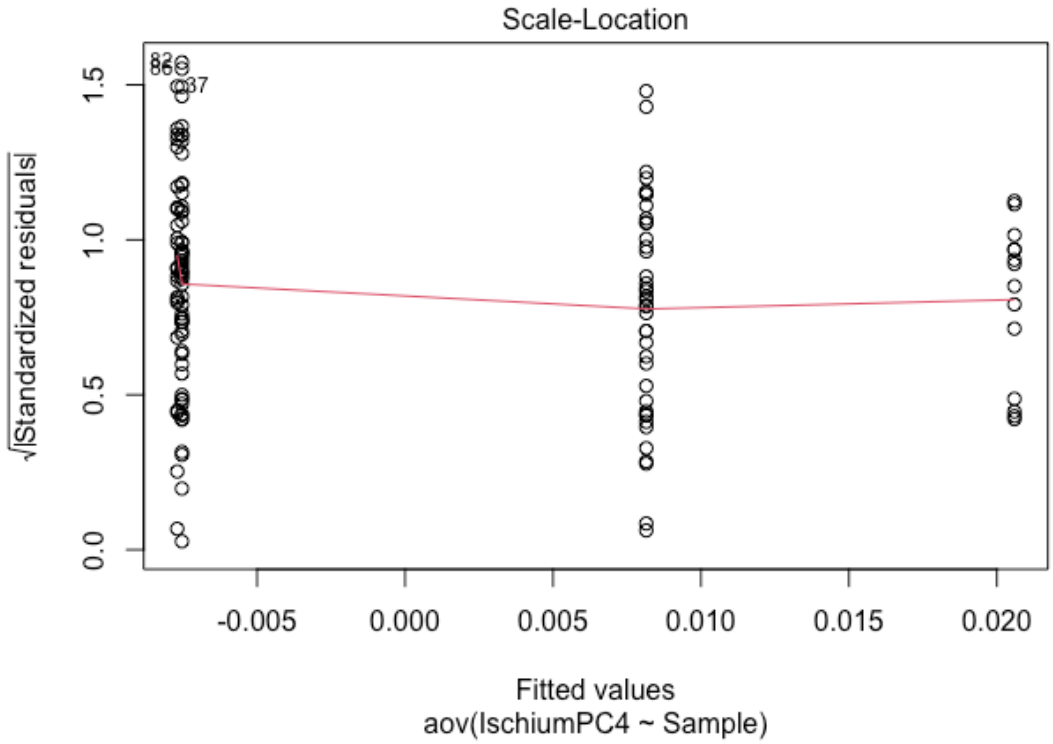

Figure I.9 Scale-location plot of the ischium PC4 data showing that homogeneity of variances can be assumed.

APPENDIX J: Individual Sample Centroid Sizes vs. PC2

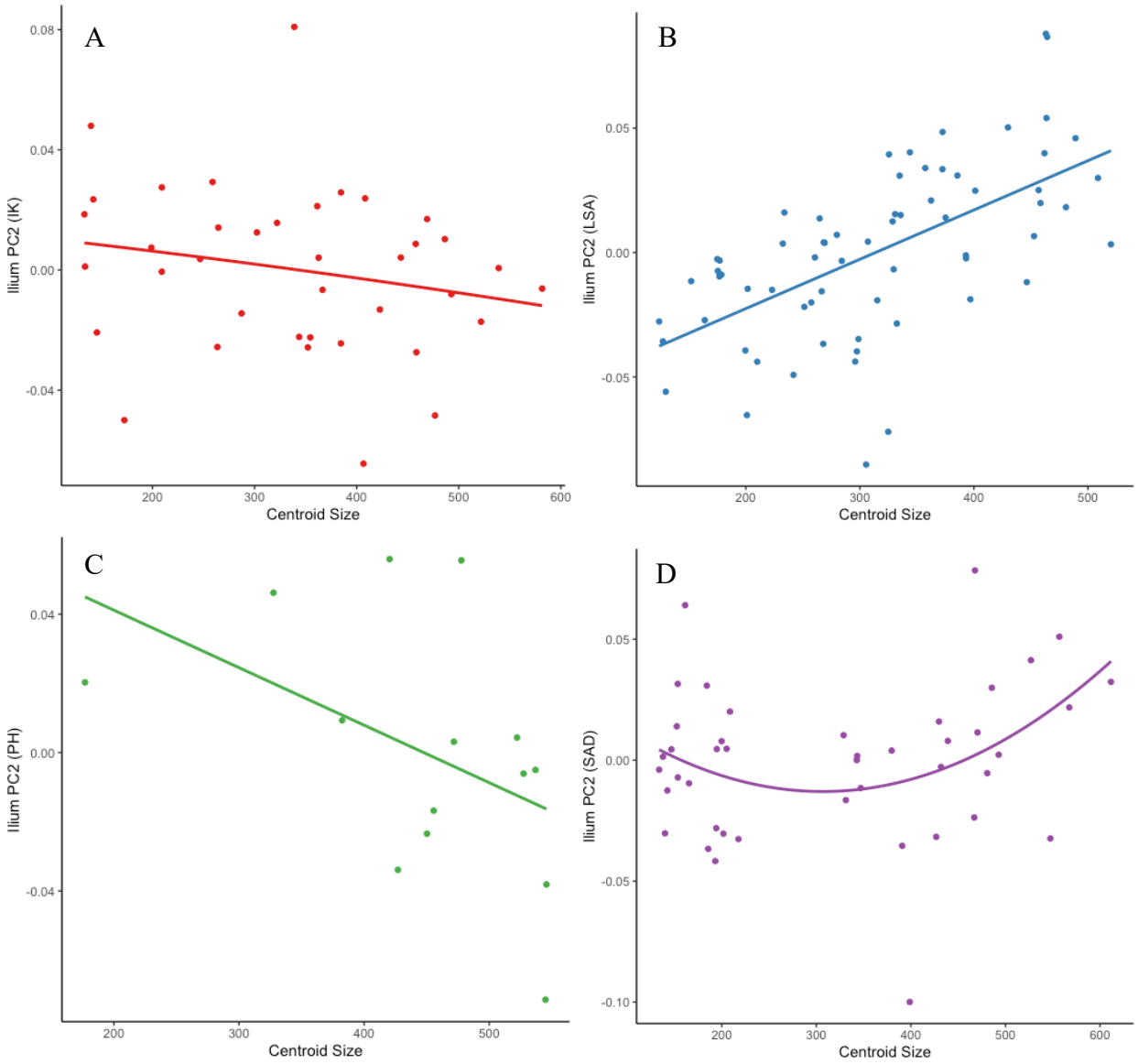

Figure J.1 Ilium centroid size vs PC2 from the individual sample PCAs for the A) Indian Knoll, B) LSA, C) Point Hope, and D) Sadlermiut samples, fitted with lines of best fit.

Table J.1 Regression results of the individual samples' ilium PC2 data plotted on centroid size.

Sample	**R^2**	**SEE**	**p-value**
Indian Knoll	0.044	0.027	0.208
Later Stone Age	0.365	0.028	<0.001
Point Hope	0.211	0.034	0.098
Sadlermiut	0.081	0.030	0.070

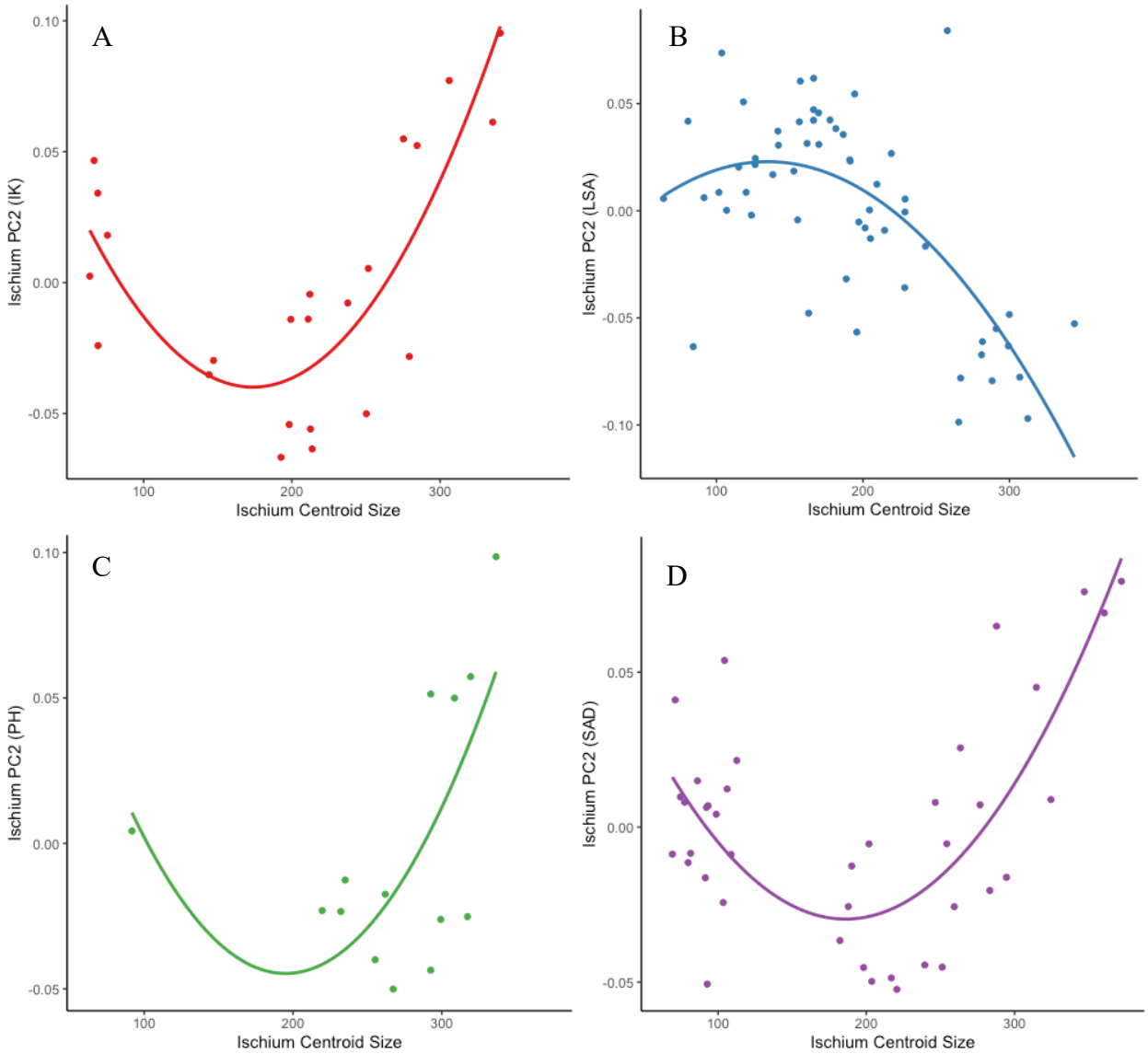

Figure J.2 Ischium centroid size vs PC2 from the individual sample PCAs for the A) Indian Knoll, B) LSA, C) Point Hope, and D) Sadlermiut samples, fitted with quadratic lines of best fit.

Table J.2 Regression results of the individual samples' ischium PC2 data plotted on centroid size.

Sample	**R^2**	**SEE**	**p-value**
Indian Knoll	0.644	0.028	<0.001
Later Stone Age	0.461	0.034	<0.001
Point Hope	0.365	0.036	0.033
Sadlermiut	0.514	0.025	<0.001

APPENDIX K: Additional CSG Data

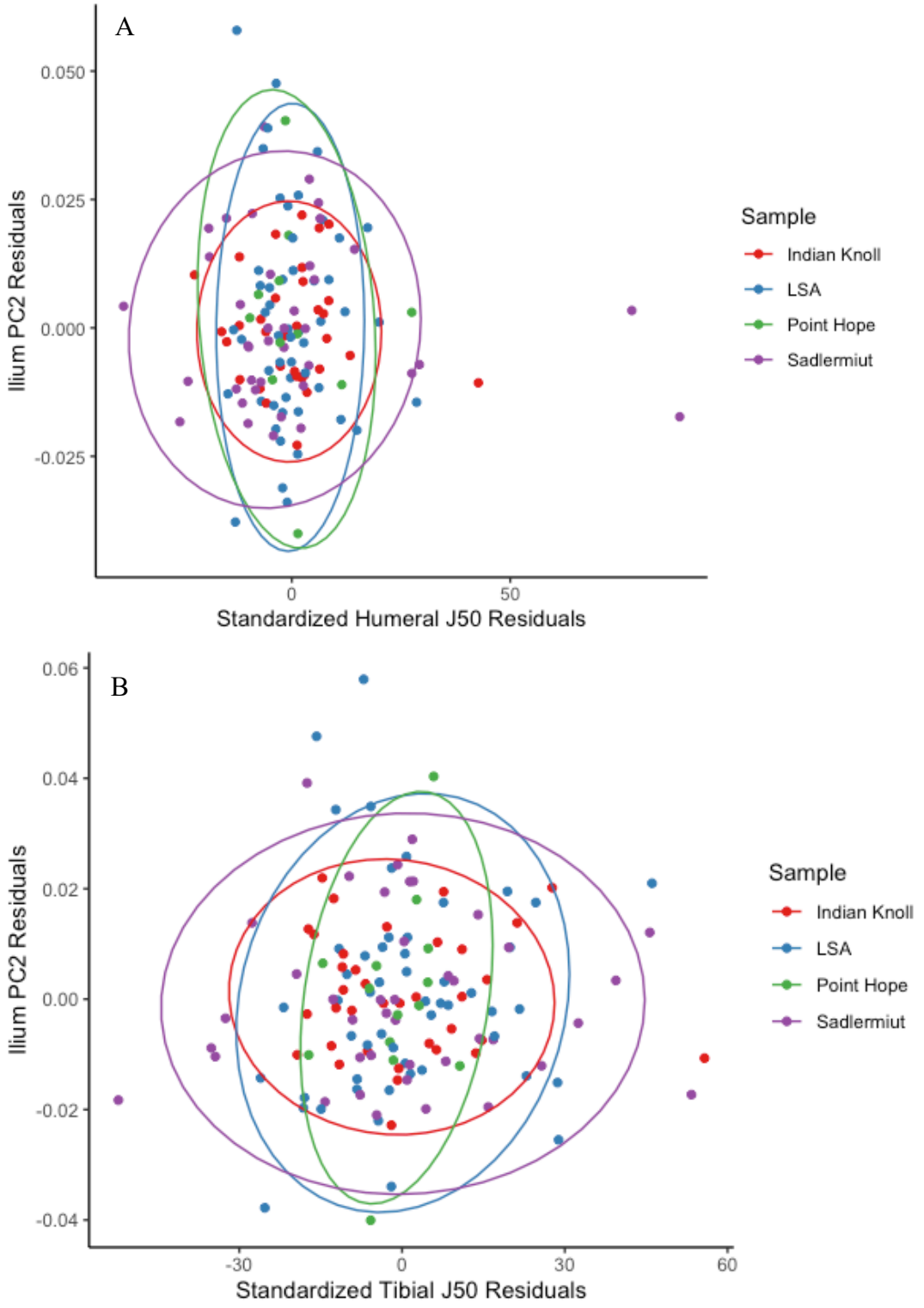

Figure K.1 Residuals from the quadratic regression of ilium PC2 data on age plotted on the residuals of the quadratic regression of A) standardized humeral J on age, and B) standardized femoral J on age, shown with 95% confidence ellipses.

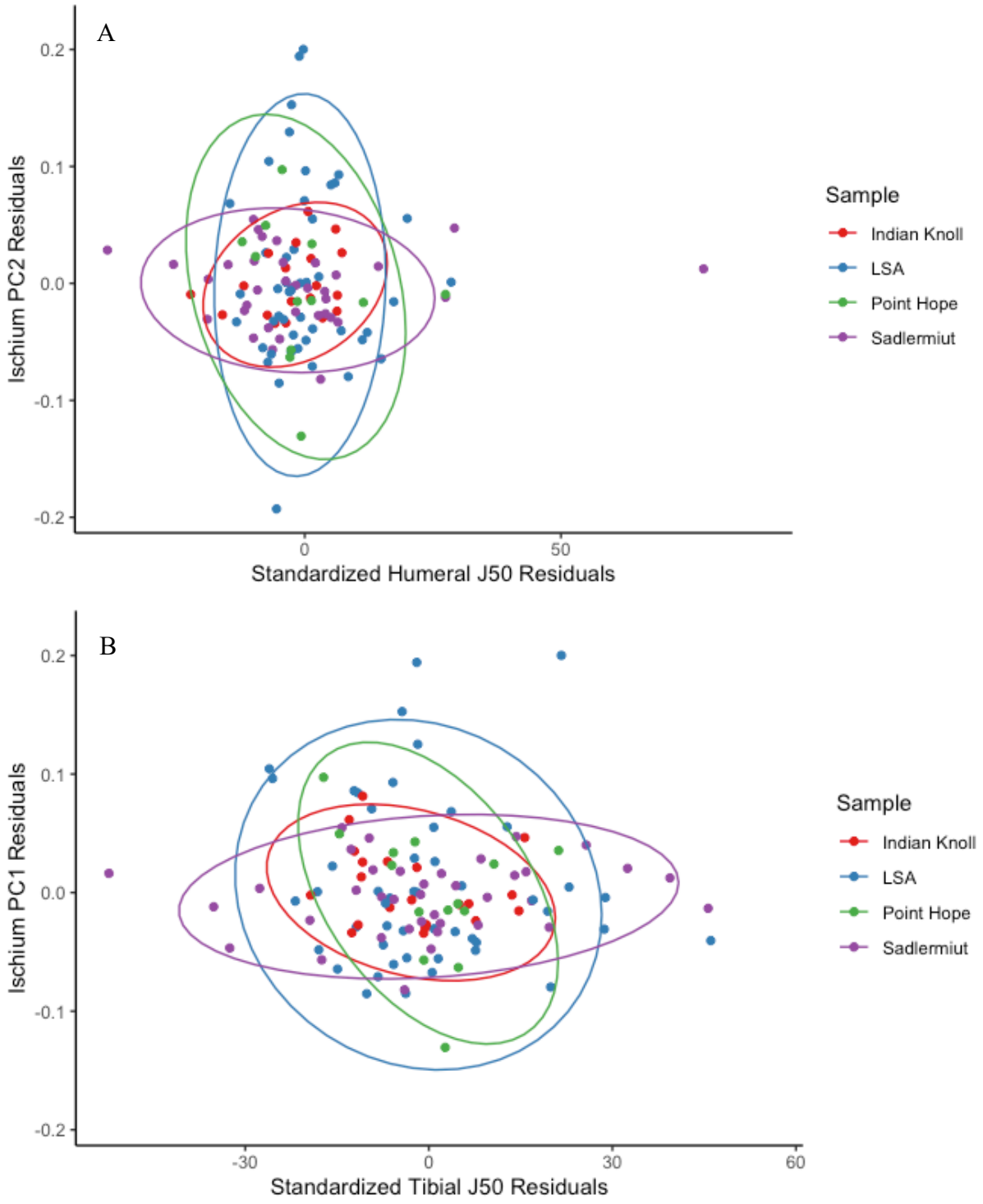

Figure K.2 Residuals from the quadratic regression of ischium PC1 data on age plotted on the residuals of the quadratic regression of A) standardized humeral J on age, and B) standardized femoral J on age, shown with 95% confidence ellipses.

Table K.1 Regression results of ilium PC scores on tibia J/humerus J ratio data.

Principal Component	Combined Sample R^2	Combined Sample SEE	Sample	R^2
PC1	0.120 (p = <0.001)	0.044	IK LSA PH SAD	0.000 0.003 0.043 0.025
PC2	0.138 (p = <0.001)	0.039	IK LSA PH SAD	0.206 0.301 0.276 0.305
PC3	0.005 (p = 0.411)	0.022	IK LSA PH SAD	0.023 0.154 0.007 0.030
PC4	0.001 (p = 0.793)	0.019	IK LSA PH SAD	0.061 0.022 0.056 0.028
PC5	0.008 (p = 0.316)	0.017	IK LSA PH SAD	0.054 0.009 0.254 0.030
PC6	0.002 (p = 0.583)	0.017	IK LSA PH SAD	0.008 0.043 0.054 0.072
PC7	0.066 (p = 0.003)	0.014	IK LSA PH SAD	0.025 0.041 0.023 0.003
PC8	0.001 (p = 0.687)	0.014	IK LSA PH SAD	0.171 0.031 0.000 0.035
PC9	0.015 (p = 0.157)	0.013	IK LSA PH SAD	0.012 0.052 0.163 0.020
PC10	0.002 (p = 0.659)	0.011	IK LSA PH SAD	0.035 0.009 0.091 0.000
PC11	0.050 (p = 0.009)	0.009	IK LSA PH SAD	0.003 0.164 0.001 0.082

PC12	0.008 (p = 0.313)	0.009	IK LSA PH SAD	0.085 0.001 0.213 0.197
PC13	0.000 (p = 0.850)	0.008	IK LSA PH SAD	0.018 0.014 0.150 0.008
PC14	0.001 (p = 0.765)	0.008	IK LSA PH SAD	0.017 0.003 0.027 0.006
PC15	0.001 (p = 0.769)	0.008	IK LSA PH SAD	0.015 0.001 0.092 0.020
PC16	0.018 (p = 0.115)	0.007	IK LSA PH SAD	0.007 0.006 0.149 0.002
PC17	0.006 (p = 0.354)	0.007	IK LSA PH SAD	0.080 0.012 0.152 0.052
PC18	0.033 (p = 0.034)	0.007	IK LSA PH SAD	0.090 0.053 0.078 0.021
PC19	0.048 (p = 0.011)	0.007	IK LSA PH SAD	0.002 0.095 0.096 0.007
PC20	0.009 (p = 0.267)	0.006	IK LSA PH SAD	0.002 0.058 0.048 0.001

Table K.2 Regression results of ischium PC scores on tibia J/humerus J ratio data.

Principal Component	Combined Sample R^2	Combined Sample SEE	Sample	R^2
PC1	0.121 (p = <0.001)	0.106	IK LSA PH SAD	0.136 0.179 0.067 0.357
PC2	0.011 (p = 0.273)	0.041	IK LSA PH SAD	0.063 0.034 0.039 0.010
PC3	0.216 (p = <0.001)	0.029	IK LSA PH SAD	0.145 0.045 0.507 0.000
PC4	0.002 (p = 0.672)	0.028	IK LSA PH SAD	0.073 0.093 0.228 0.014
PC5	0.001 (p = 0.692)	0.025	IK LSA PH SAD	0.052 0.021 0.369 0.021
PC6	0.014 (p = 0.212)	0.023	IK LSA PH SAD	0.027 0.033 0.299 0.103
PC7	0.000 (p = 0.902)	0.021	IK LSA PH SAD	0.007 0.004 0.287 0.004
PC8	0.075 (p = 0.003)	0.019	IK LSA PH SAD	0.026 0.196 0.016 0.016
PC9	0.000 (p = 0.887)	0.016	IK LSA PH SAD	0.027 0.000 0.011 0.067
PC10	0.019 (p = 0.136)	0.014	IK LSA PH SAD	0.055 0.003 0.001 0.016
PC11	0.000 (p = 0.946)	0.015	IK LSA PH SAD	0.136 0.000 0.007 0.000

PC12	0.008 (p = 0.339)	0.014	IK LSA PH SAD	0.012 0.075 0.541 0.009
PC13	0.004 (p = 0.497)	0.014	IK LSA PH SAD	0.073 0.037 0.000 0.001
PC14	0.020 (p = 0.130)	0.012	IK LSA PH SAD	0.024 0.091 0.287 0.014
PC15	0.001 (p = 0.709)	0.011	IK LSA PH SAD	0.001 0.004 0.101 0.059
PC16	0.003 (p = 0.542)	0.010	IK LSA PH SAD	0.011 0.028 0.309 0.000
PC17	0.000 (p = 0.877)	0.010	IK LSA PH SAD	0.011 0.001 0.027 0.045
PC18	0.003 (p = 0.597)	0.009	IK LSA PH SAD	0.120 0.065 0.104 0.001
PC19	0.006 (p = 0.411)	0.009	IK LSA PH SAD	0.003 0.067 0.002 0.013
PC20	0.002 (p = 0.658)	0.008	IK LSA PH SAD	0.101 0.009 0.352 0.002